UNIVERSITÉ DES SCIENCES ET TECHNIQUES DE LILLE



N° d'ordre 502



# THESE

*présentée à*

L'UNIVERSITÉ DES SCIENCES
ET TECHNIQUES DE LILLE

*pour obtenir le grade de*

DOCTEUR ES SCIENCES PHYSIQUES

*par*

*Bernard PINCHEMEL*

*

# STRUCTURE ELECTRONIQUE DES RADICAUX MnO, CuO et NiF

# SPECTROSCOPIE D'EXCITATION ET D'ABSORPTION SATUREE DE CaBr



*Soutenue le 18 décembre 1980 devant la Commission d'Examen*

| | | |
|---|---|---|
| M. | *WERTHEIMER* | *Président* |
| M. | *BACIS* | *Rapporteur* |
| M. | *BECART* | " |
| M. | *FIELD* | " |
| M. | *SCHAMPS* | " |
| Mme | *ROSTAS* | *Examinateur* |
| M. | *ENGELKE* | " |

U. E. R. DE PHYSIQUE FONDAMENTALE

# REMERCIEMENTS

Ce travail a été réalisé à l'Université de LILLE I, dans le Laboratoire de Spectroscopie des Molécules Diatomiques, Equipe de Recherche Associée au CNRS.

Les expériences de spectroscopie d'excitation et d'absorption saturée ont été faites dans le laboratoire de Monsieur le Professeur FIELD au M.I.T. en collaboration avec Peter BERNATH.

Il n'est pas possible de traduire ici le plaisir que j'ai eu à travailler avec eux, ni combien j'ai apprécié la qualité de leur accueil et l'efficacité de leurs méthodes de travail.

Je remercie les membres du Jury :

Monsieur le Professeur WERTHEIMER qui en a accepté la présidence.

Monsieur le Professeur BECART qui m'a accueilli dans son laboratoire.

Roger BACIS, Professeur à l'Université de LYON qui m'a fait profiter de son expérience concernant la cathode creuse à paroi composite.

Joël SCHAMPS, Professeur à l'Université de LILLE qui m'a apporté une aide efficace dans les différentes phases de ce travail.

Madame ROSTAS, Maître de Recherche au CNRS et Monsieur ENGELKE, Professeur à l'Université de BIELEFELD qui ont accepté de juger ce travail.

Je remercie aussi tous mes collègues du laboratoire et plus particulièrement Yannic LEFEBVRE.

Enfin je remercie tous ceux qui ont contribué à la réalisation matérielle de cette thèse, Mesdames PARSY et REAGAN, ainsi que Messieurs RAFFAUD, FAUQUEMBERGUE et VILAIN.

# INTRODUCTION

Ce travail comporte deux parties distinctes. La première est relative à l'étude des composés de trois éléments de transition : MnO, CuO et NiF. L'étude de ce type de molécules commencée dans notre équipe il y a quelques années doit permettre de mieux connaître le rôle des électrons d dans les liaisons moléculaires. Nous avons choisi d'aborder ce sujet simultanément sur le plan expérimental pour accroître le nombre de données susceptibles d'être confrontées à la théorie, et sur le plan théorique pour interprêter les structures électroniques des états rencontrés expérimentalement et essayer de dégager, de spectres apparemment complètement différents, les liens fondamentaux qui les unissent.

Cette thèse regroupe une partie des travaux réalisés jusqu'à présent mais il reste encore un travail important à faire puisque si l'étude de CuO semble assez complète, l'analyse de NiF n'en est qu'à ses débuts, surtout sur le plan théorique.

Les deux articles sur MnO reprennent en partie des résultats présentés dans notre thèse de spécialité mais l'article théorique est beaucoup plus complet.

Nous avons en effet pu affiner considérablement les résultats de l'interaction de configuration en prenant en compte des excitations électroniques que nous avions négligées dans un premier temps. Les nouveaux résultats nous ont conduit à étudier avec plus de précision un certain nombre de points.

Les travaux sur CuO et NiF nous ont amené à perfectionner nos techniques expérimentales de spectroscopie classique. Toutes les bandes analysées se caractérisent en effet par leur faible intensité et des recouvrements importants entre elles.

Une cathode creuse à paroi composite de type de celle mise au point à Lyon par Roger Bacis nous a donné des spectres de très bonne qualité. Elle a permis également de mettre en évidence des transitions d'intercombinaison entre deux états $^2\Pi$ dans la région verte du spectre de CuO.

La seconde partie, qui traîte de CaBr, fait appel à la spectroscopie laser pour résoudre la structure de cette molécule. En effet, la présence de deux isotopes d'égale importance associée à une structure de vibration très serrée avait rendu impossible toute analyse par les méthodes classiques. Commencée à Lille en spectroscopie de fluorescence, l'étude de CaBr que nous publions a été achevée au MIT, dans le laboratoire de Robert Field, en collaboration avec Peter Bernath. Nous avons analysé dans un premier temps la structure rotationnelle des transitions $A^2\Pi - X^2\Sigma^+$ et $B^2\Sigma^+ - X^2\Sigma^+$. Ce travail montre en particulier l'anomalie qui affecte les constantes de dédoublement $\Lambda$ et spin-rotation des états A et B remettant ainsi en cause le modèle ionique simple à orbitales localisées qui jusqu'ici semblait bien adapté à la description des fluorures d'alcalino-terreux, ce phénomène s'intensifiant lorsque l'on progresse dans la série des halogénures de calcium, de CaF vers CaI.

L'apport des mesures des raies de transitions micro-onde dans l'état fondamental, faites à Berlin par K. Möller et T. Törring, a permis d'obtenir des constantes très précises même dans les états supérieurs des transitions, dans la mesure où la corrélation entre constantes de même nature a pu ainsi être supprimée.

Ensuite nous avons entrepris l'analyse de la structure hyperfine de CaBr et de CaI. Cette étude confirme en particulier que la liaison chimique est complètement ionique dans tous les halogénures de calcium.

La majeure partie des résultats est présentée sous forme d'articles déjà publiés ou en voie de l'être. Cette présentation ne permet pas de développer de façon exhaustive les raisonnements et les calculs qui ont servi de base aux analyses. Cependant, nous

avons essayé de remédier à ce défaut en ajoutant des compléments aux articles, en particulier pour la dernière partie (CaBr et CaI) où nous avons détaillé les techniques expérimentales utilisées pour obtenir les spectres d'excitation et la structure hyperfine. On trouvera dans la thèse de Doctorat de Yannic Lefebvre tous les développements nécessaires à une bonne compréhension des articles sur CuO.

## COMMENTAIRES RELATIFS A L'ARTICLE I

## ETUDE DE LA TRANSITION $A^6\Sigma^+ - X^6\Sigma^+$ de MnO

Le but essentiel de l'analyse présentée dans cet article était de donner à nos calculs ab-initio (présentés dans l'article n° 2) une confirmation expérimentale en montrant que la transition intense de MnO mettait en jeu un état inférieur, selon toutes probabilités l'état fondamental, possédant la symétrie $^6\Sigma^+$. Ce but a été atteint en nous contentant d'analyser l'unique bande exploitable compte-tenu de la résolution dont nous disposions. Cependant, ainsi que nous le signalions à la page 433 de l'article, l'origine de la bande n'a pu être déterminée avec précision (c'est généralement le cas pour une transition $\Sigma$-$\Sigma$ incomplètement résolue telle que celle que nous avons étudiée). Il résulte une indétermination en ce qui concerne la numérotation exacte des raies en fonction du nombre quantique N. Le choix que nous avons adopté dans cet article (page 434) pour tenter de définir cette numérotation repose sur le calcul ab-initio dont la précision est assez faible en ce qui concerne les constantes de rotation. Un autre critère consistait à choisir une numérotation telle que l'ordre de grandeur de la constante de rotation B" qui en découle s'intègre normalement dans une évolution régulière des distances d'équilibre dans la série des oxydes d'élément de transition.

Nous avions d'ailleurs écrit dans notre thèse de 3ème Cycle "Nous constatons que ces résultats ne correspondent pas aux valeurs des constantes de rotation des oxydes des métaux de transition voisins, un spectre théorique réalisé pour $B_o^{"} = 0{,}517\ cm^{-1}$ et $B_i' = 0.473\ cm^{-1}$

correspond également très bien au spectre expérimental" (en ajoutant 2 unités aux valeurs de N).

Il s'avère aujourd'hui que c'est cette dernière hypothèse qui est la bonne. En effet R.M. Gordon et A.J. Merer (Can. J. Phys. 58 642 (1980) ) qui ont poursuivi avec succès l'étude du système A-X à plus haute résolution en utilisant une source de conception différente, sont parvenus à analyser les bandes 0-0 et 0-1 de la transition $^6\Sigma^+ - {}^6\Sigma^+$ de MnO.

Leur conclusion est que notre classement est correct quant à l'attribution des branches mais leur numérotation en N est plus élevée de deux unités par rapport à la notre et correspond donc à la seconde hypothèse que nous avions mentionnée.

Ils obtiennent les valeurs suivantes pour les niveaux

$v' = 1$ et $v'' = 0$

$B'_1 = 0{,}4597\ cm^{-1}$ $\qquad$ $\lambda'_1 = 0{,}43\ cm^{-1}$

$B''_0 = 0{,}50122\ cm^{-1}$ $\qquad$ $\lambda''_0 = 1{,}13\ cm^{-1}$

On remarque que l'écart $\Delta\lambda = -0{,}70\ cm^{-1}$ est voisin du notre ($-0{,}66\ cm^{-1}$).

La figure ci-dessous montre la position des têtes correspondant aux valeurs des constantes de rotation trouvées par Gordon et Merer.

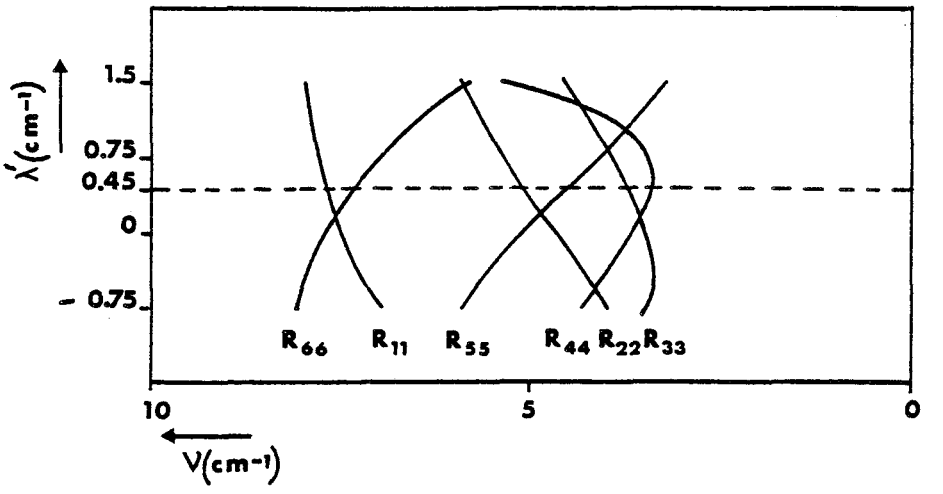


On constate que les valeurs des constantes d'interaction spin-spin donnant la position expérimentale des têtes sont voisines de $\lambda'_1 = 0,45\ cm^{-1}$ et de $\lambda''_0 = 1,12\ cm^{-1}$ en très bon accord avec Gordon et Merer. Il y a donc une forte corrélation entre les valeurs des paramètres $\lambda'$ et $\lambda''$ d'une part et celle des constantes de rotation B' et B" d'autre part.

L'influence des paramètres $\gamma$ sur la position des têtes et par conséquent sur les valeurs des paramètres $\lambda$ est négligeable, contrairement à l'hypothèse de Gordon et Merer qui suggèrent que se trouve là l'origine de l'erreur commise sur les valeurs individuelles de $\lambda'$ et $\lambda''$ dans notre analyse.

ARTICLE N° 1

# Etude de la transition $A^6\Sigma^+$–$X^6\Sigma^+$ de l'oxyde de manganèse MnO

B. PINCHEMEL ET J. SCHAMPS

*Laboratoire de Spectroscopie des Molécules Diatomiques, Equipe de recherche associée au C.N.R.S., Université de Lille I, Bâtiment P5, B.P. 36, 59650 Villeneuve D'Ascq, France*

Reçu le 1 août 1974[1]

Dans le but d'obtenir des renseignements sur la structure électronique de MnO, le système visible de cette molécule a été photographié à partir d'un arc à basse pression d'oxygène. De nouvelles bandes ont été observées. L'analyse rotationnelle de la bande 1–0 a montré que ce système provient d'une transition $A^6\Sigma^+$–$X^6\Sigma^+$ dont l'état inférieur est l'état fondamental de MnO. Les constantes de rotation et d'interaction spin–spin des deux états électroniques mis en jeu dans la transition ont été déterminées.

In order to obtain information relating to the electronic structure of MnO, the visible system of this molecule has been photographed from an arc at a low pressure of oxygen. New bands have been observed. The rotational analysis of the 1–0 band has shown that this system comes from a $A^6\Sigma^+$–$X^6\Sigma^+$ transition, the lower state of which is the ground state of MnO. The rotational and spin–spin constants of the two states involved in the transition have been determined.

Can. J. Phys., 53, 431 (1975)

Le spectre de l'oxyde de manganèse situé entre 4500 Å et 6650 Å a fait l'objet de plusieurs études toutes consacrées à la structure de vibration (Kayser 1910; Sen Gupta 1934; Das Sarma 1959) qui ont montré que les bandes observées correspondent à une transition unique $A$–$X$. Nous avons obtenu ce système au moyen d'un arc électrique à électrodes de manganèse plongées dans une atmosphère d'oxygène pur à une pression de 100 Torr. Par cette méthode se trouve éliminé le fond continu assez intense qui se superpose aux bandes situées au delà de 6650 Å lorsque l'arc est placé directement dans l'air. Un certain nombre de nouvelles bandes ont ainsi été mises en évidence. Elles appartiennent à:

(*i*) la fin de la séquence $\Delta v = -3$:

6–9: 6678 Å; 7–10: 6726 Å; 8–11: 6767 Å

(*ii*) la séquence $\Delta v = -4$:

1–5: 6850 Å; 2–6: 6880 Å;

3–7: 6910 Å; 4–8: 6944 Å;

5–9: 6983 Å; 6–10: 7028 Å; 7–11: 7068 Å

Trois autres séquences apparaissent vers 7160, 7570 et 7880 Å respectivement mais elles ne prennent pas place dans le tableau de Deslandres du système $A$–$X$. Ces séquences doivent donc appartenir à une nouvelle transition de MnO.

L'étude du système $A$–$X$ de MnO a été faite à l'aide d'un spectrographe de 4 m de distance focale dont la dispersion inverse est de 0.7 Å/mm et le pouvoir de résolution théorique d'environ 500 000 dans le second ordre.

Bien que le manganèse n'ait qu'un seul isotope naturel, la structure de rotation de MnO est très complexe; cette complexité doit donc être attribuée à la multiplicité élevée des états électroniques de la transition. Les fortes variations d'intensité des raies observées et la largeur anormale de beaucoup d'entre elles s'expliquent par le fait que celles-ci sont en réalité la superposition de plusieurs raies non résolues (jusqu'à 12 raies superposées en 1 seule dans certaines régions). En dépit du spin nucléaire assez élevé ($I = 5/2$), la structure hyperfine n'est pas décelable avec notre pouvoir de résolution, mais elle peut aussi contribuer à l'élargissement des raies.

Par suite de ces difficultés auxquelles s'ajoutent la proximité des têtes et le recouvrement des bandes successives, nous n'avons étudié que la bande 1–0, qui est la plus intense et la plus nette du spectre, dont une représentation est donnée dans la fig. 1.

[1]Revision reçue le 24 septembre 1974.

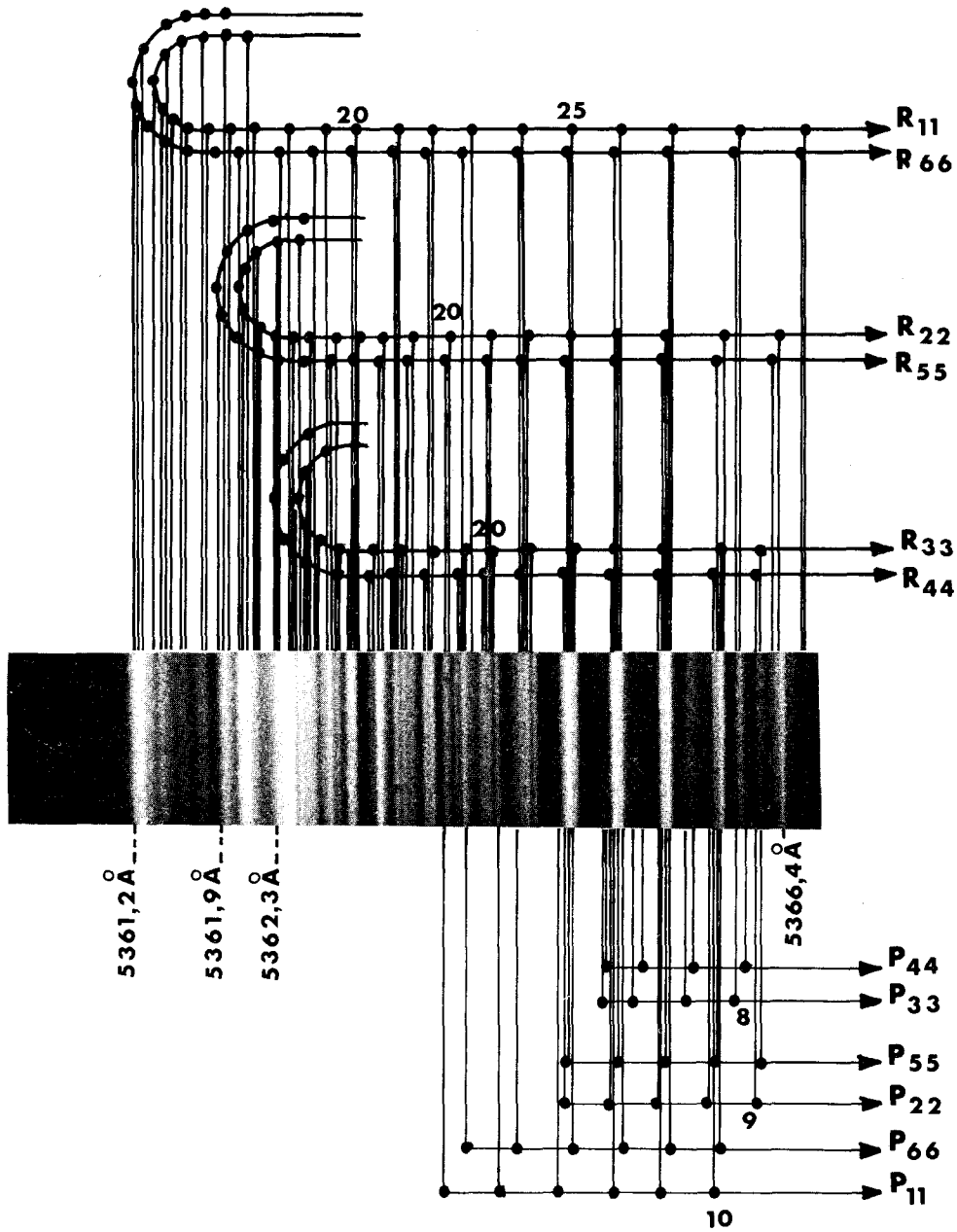


FIG. 1. Structure rotationnelle de la tête de la bande 1–0 du système $A^6\Sigma^+$–$X^6\Sigma^+$ de MnO.

Il ressort d'une étude théorique approfondie (Pinchemel, B. et Schamps, J., à paraître) fondée sur des calculs SCF–Cl que l'état fondamental de MnO est un état $^6\Sigma^+$ relevant du cas (*b*) de Hund. De plus l'analyse de rotation montre que la tête de la bande 1–0 comporte six sous-têtes groupées deux par deux (voir fig. 1). Cette structure est caractéristique d'une transition $^6\Sigma^+$–$^6\Sigma^+$. *

Nous n'avons pu déterminer que les paramètres $B$ (constante de rotation) et $\lambda$ (constante d'interaction spin–spin incluant les effets spin–orbite de second ordre) des états $^6\Sigma^+$ considérés. Il serait illusoire de tenter de déter-



* Voir appendice après cet article

miner les autres constantes (distorsion centrifuge, interaction spin–rotation) étant donné la faiblesse des valeurs atteintes pour le nombre quantique de rotation et surtout l'impossibilité de réaliser des pointés précis dans les très nombreux groupements de raies non résolus.

L'oxyde MnO étant une molécule relativement lourde, on peut s'attendre à ce que dans chaque état $^6\Sigma^+$, les constantes $B$ et $\lambda$ soient sensiblement du même ordre de grandeur, de sorte que les formules de Rao (1952) donnant les termes spectraux au premier ordre en $\lambda/B$ ne sont pas applicables. L'analyse rotationnelle de MnO doit donc se faire par combinaison directe des termes spectraux issus de la diagonalisation numérique exacte des matrices d'énergie des deux états $^6\Sigma^+$.

L'analyse de rotation de la bande 1–0 a permis de déterminer la valeur de la différence des constantes rotationnelles des deux états vibroniques:

$$B' - B'' = -0.045\ \text{cm}^{-1} \pm 0.001\ \text{cm}^{-1}$$

Avant d'essayer de déterminer $B'$ et $B''$ individuellement, nous avons déduit de la position des six sous-têtes de la bande 1–0 les valeurs des constantes d'interaction spin–spin $\lambda'$ et $\lambda''$. En effet, comme nous avons pu le vérifier sur une grande variété de spectres reconstitués sur ordinateur, il s'avère que les valeurs de ces deux paramètres ont une influence essentielle sur les écarts existant entre les six sous-têtes de la bande (la fig. 2 en est un exemple), alors que les constantes de rotation $B'$ et $B''$ n'ont d'influence sur ces écarts que dans la mesure où la loi de variation en $BN(N+1)$ des termes spectraux avec $N$ n'est que très approximative pour les basses valeurs de $N$ auxquelles correspondent les sous-têtes $R$ de la bande 1–0 de MnO (entre 8 et 14 environ selon les branches).

Il est donc possible de déterminer $\lambda'$ et $\lambda''$ en ne connaissant que l'ordre de grandeur de $B'$ et $B''$ (que l'on peut évaluer à $0.4\ \text{cm}^{-1}$ ou $0.5\ \text{cm}^{-1}$ par comparaison avec les oxydes voisins).

La fig. 2 montre que, pour une valeur donnée de la différence $\Delta\lambda = \lambda' - \lambda''$ des constantes d'interaction spin–spin, la position relative des têtes est très sensible à la variation de $\lambda'$ (et de $\lambda''$ qui en diffère de $\Delta\lambda$). D'autre part, nous avons constaté que si l'on fait varier $\Delta\lambda$, les schémas analogues à la fig. 2 se déduisent les uns des autres par une homothétie (dans le sens des

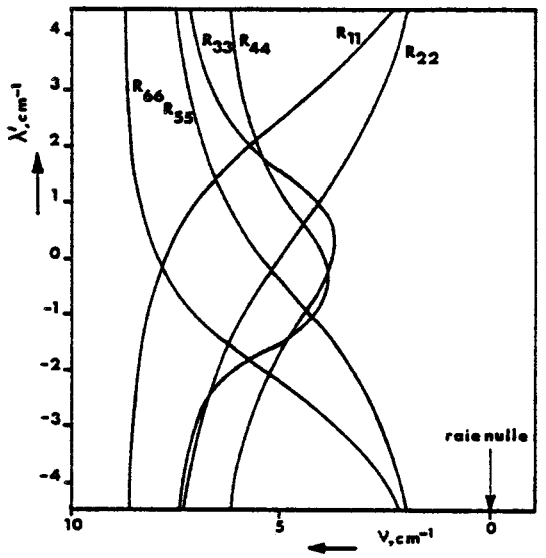


FIG. 2. Evolution de la position des sous-têtes d'une bande d'une transition $^6\Sigma^+$–$^6\Sigma^+$ en fonction de $\lambda'$ pour $B' = 0.390\ \text{cm}^{-1}$, $B'' = 0.435\ \text{cm}^{-1}$, $\lambda'-\lambda'' = -0.66\ \text{cm}^{-1}$.

nombres d'ondes) dont le rapport est proportionnel au quotient des $\Delta\lambda$. Appliquant ces remarques au spectre de MnO, nous trouvons que le groupement des six sous-têtes deux par deux est caractéristique d'une valeur de $\lambda'$ à peu près nulle et que, d'autre part, la valeur des écarts entre ces sous-têtes correspond à $\Delta\lambda = -0.66\ \text{cm}^{-1}$. En résumé, cette analyse nous fournit pour les constantes d'interaction spin–spin les valeurs:

$$\lambda' = 0.00\ \text{cm}^{-1} \pm 0.05\ \text{cm}^{-1}$$
$$\lambda'' = 0.66\ \text{cm}^{-1} \pm 0.05\ \text{cm}^{-1}$$

Comme nous avons été réduits à n'analyser qu'une seule bande, et que d'autre part nous ne sommes pas parvenus à localiser avec la précision désirée la position de l'origine (raie nulle), et par conséquent la numérotation exacte des raies de cette bande par suite de la présence de nombreux groupements de raies non résolues, nous ne pouvons pas déduire les valeurs de $B'$ et $B''$ par les méthodes habituelles (Herzberg 1950).

Nous avons pu cependant préciser ces constantes grâce au phénomène de battement qui apparaît dans la région $\lambda = 5365$ Å (voir fig. 1). Les valeurs de $B'$ (et de $B''$) déterminées pour chaque hypothèse de numérotation plau-

sible des raies varient par pas de 0.04 $cm^{-1}$ environ, c'est-à-dire, comme on pouvait s'y attendre, d'une quantité voisine de la différence $(B' - B'')$ précédemment déterminée. Afin de choisir parmi ces diverses possibilités, nous avons utilisé les résultats des calculs SCF déjà cités (Pinchemel, B. et Schamps, J., à paraître) qui donnent, pour l'état fondamental de MnO, une constante de rotation $B''$ égale à 0.45 $cm^{-1}$. Par analogie avec des calculs comparables effectués sur les molécules voisines ScO (Carlson *et al.* 1965), TiO (Carlson et Nesbet 1964) et VO (Carlson et Moser 1965) qui ont donné des valeurs des constantes de rotation en assez bon accord avec l'expérience quoique un peu trop grandes, nous proposons pour les constantes de rotation des états $X^6\Sigma^+$ et $A^6\Sigma^+$ les valeurs suivantes:

$$B'' = 0.435\ cm^{-1} \pm 0.005\ cm^{-1}$$

$$B' = 0.390\ cm^{-1} \pm 0.005\ cm^{-1}$$

Ces valeurs sont 10% à 20% plus basses que pour la plupart des autres oxydes de la quatrième période de la classification périodique; seules les molécules CaO, CuO et BrO ont des constantes de rotation du même ordre que celle de MnO.

Avec ces constantes $B$ et $\lambda$, toutes les raies du spectre de la tête 1–0 ont pu être attribuées aux six branches $R$ et aux six branches $P$ les plus intenses de la transition $A^6\Sigma^+$–$X^6\Sigma^+$ comme indiqué sur la fig. 1.

Il est intéressant de remarquer que de récentes expériences en matrice d'isolation réalisées par Thompson *et al.* (1973) ont montré que l'état inférieur de cette transition est l'état électronique fondamental de MnO. L'état électronique fondamental de MnO est donc de symétrie $^6\Sigma^+$. De ce point de vue, il faut remarquer la similitude qui existe entre la molécule MnO et l'atome neutre de manganèse: tous deux ont, dans leur état fondamental, une multiplicité de spin égale à six et une structure électronique totalement symétrique. Cette ressemblance donne à penser que la configuration de l'oxyde est analogue à celle de l'atome de manganèse, du moins en ce qui concerne la disposition de cinq électrons dans la couche 3*d*. Ceci confirme les conclusions générales de Cheetham et Barrow (1967) relatives aux composés des éléments de transition. Nous publierons d'ailleurs très prochainement une étude théorique concernant la structure de l'oxyde de manganèse où ce problème sera examiné en détail.


CARLSON, K. D. et MOSER, C. 1965. J. Chem. Phys. **44**, 3259.

CARLSON, K. D. et NESBET, R. K. 1964. J. Chem. Phys. **41**, 1051.

CARLSON, K. D., LUDENA, E. et MOSER, C. 1965. J. Chem. Phys. **43**, 2408.

CHEETHAM, C. J. et BARROW, R. F. 1967. Adv. High Temp. Chem. USA, **1**, 7.

DAS SARMA, J. M. 1959. Z. Phys. **157**, 98.

HERZBERG, G. 1950. Spectra of diatomic molecules (Van Nostrand, New York).

KAYSER, H. 1910. Handbuch der spektroskopie, Vol. V.S. (Hirzel, Leipzig) 768.

RAO, K. S. 1952. Indian J. Phys. **26**, 47.

SEN GUPTA, A. K. 1934. Z. Phys. **91**, 471.

THOMPSON, R. T., EASLEY, W. C. et KNIGHT, L. B. 1973. J. Phys. Chem. **77**, 49.

# APPENDICE I

## I - CALCUL DES ELEMENTS MATRICIELS D'UN ETAT $^6\Sigma^+$

Nous rappelons ici brièvement les principaux résultats relatifs à la structure d'un état $^6\Sigma^+$. L'étude détaillée précisant le calcul de tous les éléments de matrice est développé dans la référence 1.

Le hamiltonien total se décompose de la façon suivante :

$$H = H_{ev} + H_R + H_{SO} + H_{SS} + H_{SR} + H_D$$

$H_{ev}$ = Hamiltonien vibro-électronique

$H_R$ = " de rotation

$H_{SO}$ = " spin-orbite

$H_{SS}$ = " spin-spin

$H_{SR}$ = " spin-rotation

$H_D$ = " de distorsion centrifuge.

La projection $\Lambda$ sur l'axe internucléaire du moment orbital électronique étant nulle pour un état $\Sigma$, les nombres quantiques $\Sigma$ (projection sur l'axe du spin électronique) et $\Omega = \Lambda + \Sigma$ (projection du moment angulaire total) sont égaux.

Dans ces conditions les vecteurs de la base du cas a de Hund $|L,\Lambda,S,\Sigma;\Omega,J,M>$ peuvent être écrits sans ambiguité, pour chaque valeur de J,M, sous la forme réduite $|\Omega>$ ($\Omega$ prenant les 6 valeurs $\pm\frac{1}{2}$, $\pm\frac{3}{2}$, $\pm\frac{5}{2}$ ).

Une transformation de Kronig permet de décomposer la matrice en deux blocs notés e et f suivant la notation de Kopp et Hougen.

Les sous-états e correspondent aux vecteurs de base

$$|\Omega, + > = \frac{1}{\sqrt{2}} \left[ | + \Omega > + | - \Omega > \right].$$

Les sous-états f correspondent aux vecteurs de base

$$|\Omega, - > = \frac{1}{\sqrt{2}} \left[ | + \Omega > - | - \Omega > \right]$$

(Le hamiltonien vibro-électronique reste diagonal dans cette base).

Le hamiltonien de rotation est représenté dans cette base par la matrice.

| $\left\| \frac{1}{2}, \pm \right>$ | $\left\| \frac{3}{2}, \pm \right>$ | $\left\| \frac{5}{2}, \pm \right>$ |
|---|---|---|
| $Tev + B \left( J(J+1) - \frac{1}{4} + \frac{35}{4} - \frac{1}{4} \mp 3(J+\frac{1}{2}) \right)$ | $-2\sqrt{2}\ B \left[ J(J+1) - \frac{3}{4} \right]^{\frac{1}{2}}$ | |
| $-2\sqrt{2}\ B \left[ J(J+1) - \frac{3}{4} \right]^{\frac{1}{2}}$ | $Tev + B \left( J(J+1) - \frac{9}{4} + \frac{35}{4} - \frac{9}{4} \right)$ | $-\sqrt{5}\ B \left[ J(J+1) - \frac{15}{4} \right]^{\frac{1}{2}}$ |
| | $-\sqrt{5}\ B \left[ J(J+1) - \frac{15}{4} \right]^{\frac{1}{2}}$ | $Tev + B \left( J(J+1) - \frac{25}{4} + \frac{35}{4} - \frac{25}{4} \right)$ |

Le hamiltonien d'interaction spin-spin (2) ne donne que des termes diagonaux identiques pour les deux sous-matrices e et f

$$\langle \tfrac{1}{2}, \tfrac{+}{-} | H_{SS} | \tfrac{1}{2}, \tfrac{+}{-} \rangle = \frac{-16\lambda}{3}$$

$$\langle \tfrac{3}{2}, \pm | H_{SS} | \tfrac{3}{2}, \pm \rangle = \frac{-4\lambda}{3}$$

$$\langle \tfrac{5}{2}, \pm | H_{SS} | \tfrac{5}{2}, \pm \rangle = \frac{+20\lambda}{3}$$

Le hamiltonien spin-rotation (3) est représenté par la matrice

| $\lvert \frac{1}{2}, \frac{e}{f} \rangle$ | $\lvert \frac{3}{2}, \frac{e}{f} \rangle$ | $\lvert \frac{5}{2}, \frac{e}{f} \rangle$ |
|---|---|---|
| $-\frac{17}{2}\gamma'_{NS} \mp \gamma\,(J+\frac{1}{2})$ | $-\sqrt{2}\,\gamma'_{NS}\left[J(J+1) - \frac{3}{4}\right]^{\frac{1}{2}}$ | |
| $-\sqrt{2}\,\gamma'_{NS}\left[J(J+1) - \frac{3}{4}\right]^{\frac{1}{2}}$ | $-\frac{13}{2}\gamma'_{NS}$ | $-\frac{\sqrt{5}}{2}\gamma'_{NS}\left[J(J+1) - \frac{3}{4}\right]^{\frac{1}{2}}$ |
| | $-\frac{\sqrt{5}}{2}\gamma'_{NS}\left[J(J+1) - \frac{3}{4}\right]^{\frac{1}{2}}$ | $-\frac{5}{2}\gamma'_{NS}$ |

Seul le terme diagonal correspondant à $\Omega = \frac{1}{2}$ est différent dans les sous-matrices e et f.

La distorsion centrifuge (4) est traduite par les éléments de matrice suivants

$$\langle \tfrac{1}{2}\ {}^{e}_{f}\ |H_D|\ \tfrac{1}{2}\ {}^{e}_{f} \rangle = -D\left\{\left[J(J+1)+\tfrac{33}{4}\right]^2 + 17\left[J(J+1)-\tfrac{1}{4}\right]+\tfrac{1}{2} \mp 6\left[J(J+1)+\tfrac{33}{4}\right](J+\tfrac{1}{2})\right\}$$

$$\langle \tfrac{1}{2}\ {}^{e}_{f}\ |H_D|\ \tfrac{3}{2}\ {}^{e}_{f} \rangle = -2\sqrt{2}\ D\left(J(J+1)-\tfrac{3}{4}\right)^{1/2}\left[2J(J+1)+\tfrac{25}{2} \mp 3\left(J+\tfrac{1}{2}\right)\right]$$

$$\langle \tfrac{1}{2}, \text{ e ou f } |H_D| \tfrac{5}{2}, \text{e ou f} \rangle = -2\sqrt{10}\ D\left\{\left[J(J+1)-\tfrac{3}{4}\right]\left[J(J+1)-\tfrac{15}{4}\right]\right\}^{\frac{1}{2}}$$

$$\langle \tfrac{3}{2}, \text{ e ou f } |H_D| \tfrac{3}{2}, \text{e ou f} \rangle = -D\left\{\left[J(J+1)+\tfrac{17}{4}\right]^2 + 13\left[J(J+1)-\tfrac{9}{4}\right]+\tfrac{9}{2}\right\}$$

$$\langle \tfrac{5}{2}, \text{ e ou f } |H_D| \tfrac{5}{2}, \text{e ou f} \rangle = -D\left\{\left[J(J+1)-\tfrac{15}{4}\right]^2 + 5\left[J(J+1)-\tfrac{25}{4}\right]+\tfrac{25}{2}\right\}$$

$$\langle \tfrac{3}{2}, \text{ e ou f } |H_D| \tfrac{5}{2}, \text{e ou f} \rangle = -2\sqrt{5}\ D\left[J(J+1)+\tfrac{1}{4}\right]\left[J(J+1)-\tfrac{15}{4}\right]^{1/2}$$

Nous n'entrerons pas dans les détails de l'étude des interactions d'un état $^6\Sigma^+$ avec les états voisins. Ces interactions se traduisent par des éléments de couplage, entre les matrices des états, dûs au hamiltonien spin-orbite et au hamiltonien de rotation .

Si ces états ne sont pas trop proches de l'état $^6\Sigma^+$, on peut considérer ces effets d'interaction comme des perturbations et utiliser la transformation canonique de Van Vleck.

Nos calculs ont montré que tous ces éléments peuvent être inclus dans la matrice de l'état $^6\Sigma^+$ isolé en modifiant simplement la signification des paramètres B,D, $\lambda$ et $\gamma$ qui deviennent des paramètres effectifs incluant un nombre plus ou moins important de perturbations et qui ne gardent plus le caractère pur de rotation, de distorsion centrifuge et d'interaction spin-spin ou spin-rotation que nous leur avions attribué au départ.

On peut noter que le paramètre $\gamma$ peut voir son caractère de départ fortement modifié, dans la mesure où, pour les molécules lourdes, l'interaction spin-rotation pure est très faible (5). Elle est généralement négligeable

devant l' interaction du second ordre, introduite dans le paramètre $\gamma$ par la perturbation provenant des états $^6\Pi$ et $^6\Sigma^-$ voisins (voir complément de l'article 2).

## II - DIAGONALISATION

La diagonalisation de la matrice donne six niveaux d'énergie qui, si on ne conserve que la partie rotationnelle, peuvent se mettre sous la forme classique BN(N+1) propre au cas b de Hund.

N étant un nombre entier prenant successivement les valeurs

$J - \frac{1}{2}$ , $J + \frac{3}{2}$ , $J - \frac{5}{2}$ pour la matrice des états e

$J + \frac{1}{2}$ , $J - \frac{3}{2}$ , $J + \frac{5}{2}$ pour la matrice des états f.

Il y a des dégénérescence des six niveaux de même N, cette dégénérescence étant levée par l'interaction spin-spin principalement.

En général lorsque $\lambda$ est petit devant B comme c'est le cas pour les hydrures (Cr.H; $\frac{\lambda}{B} = 5\ 10^{-3}$ (6) ) il est possible comme l'a fait Rao (7) de développer au 1er ordre en $\lambda$ les niveaux d'énergie et de les écrire sous la forme

$$F_i(N) = B\ N\ (N+1) + K_i\ (N)\ \varepsilon \quad (i \text{ variant de } 1 \text{ à } 6)$$

cette approximation n'est plus valable lorsque le rapport $\frac{\lambda}{B}$ est supérieur à 1 puisqu'il n'est alors plus possible de négliger les termes d'ordre élevé qui deviennent même prépondérants.

Nous avons donc diagonalisé directement la matrice pour chaque valeur de J et nous avons regroupé les niveaux pour chaque valeur de N.

L'ordre des niveaux et leurs écarts relatifs (à un facteur multiplicatif B près) sont déterminés par la valeur $\frac{\lambda}{B}$ .

La figure A1 représente la variation de position realtive des sous-niveaux en fonction de N dans le cas $\frac{\lambda}{B} = 3$. La position absolue des sous-niveaux est obtenue en multipliant les ordonnées par B.

Pour N suffisamment grand, la figure 1 montre que les sous-niveaux ont une position relative pratiquement indépendante de N.

Dans la figure A2,nous représentons la variation des écarts $\frac{F_i(N) - BN(N+1)}{B}$ en fonction de $\frac{\lambda}{B}$ . Nous avons pris la valeur N = 20 du nombre quantique sans spin pour $0 < \frac{\lambda}{B} < 1,5$ ; ensuite, afin d'être sûr de nous trouver dans la région où la position des sous-niveaux (figure A1) est pratiquement indépendante de N, nous avons tracé le graphe, lorsque $\frac{\lambda}{B} > 1,5$ pour $N = 20 \times \frac{\lambda}{B}$ .

Cette figure met en évidence le fait que l'ordre des niveaux $F_i(N)$ pour les grandes valeurs de N dépend des valeurs relatives des constantes $\lambda$ et B, ce qui n'était pas le cas dans les calculs de Rao.

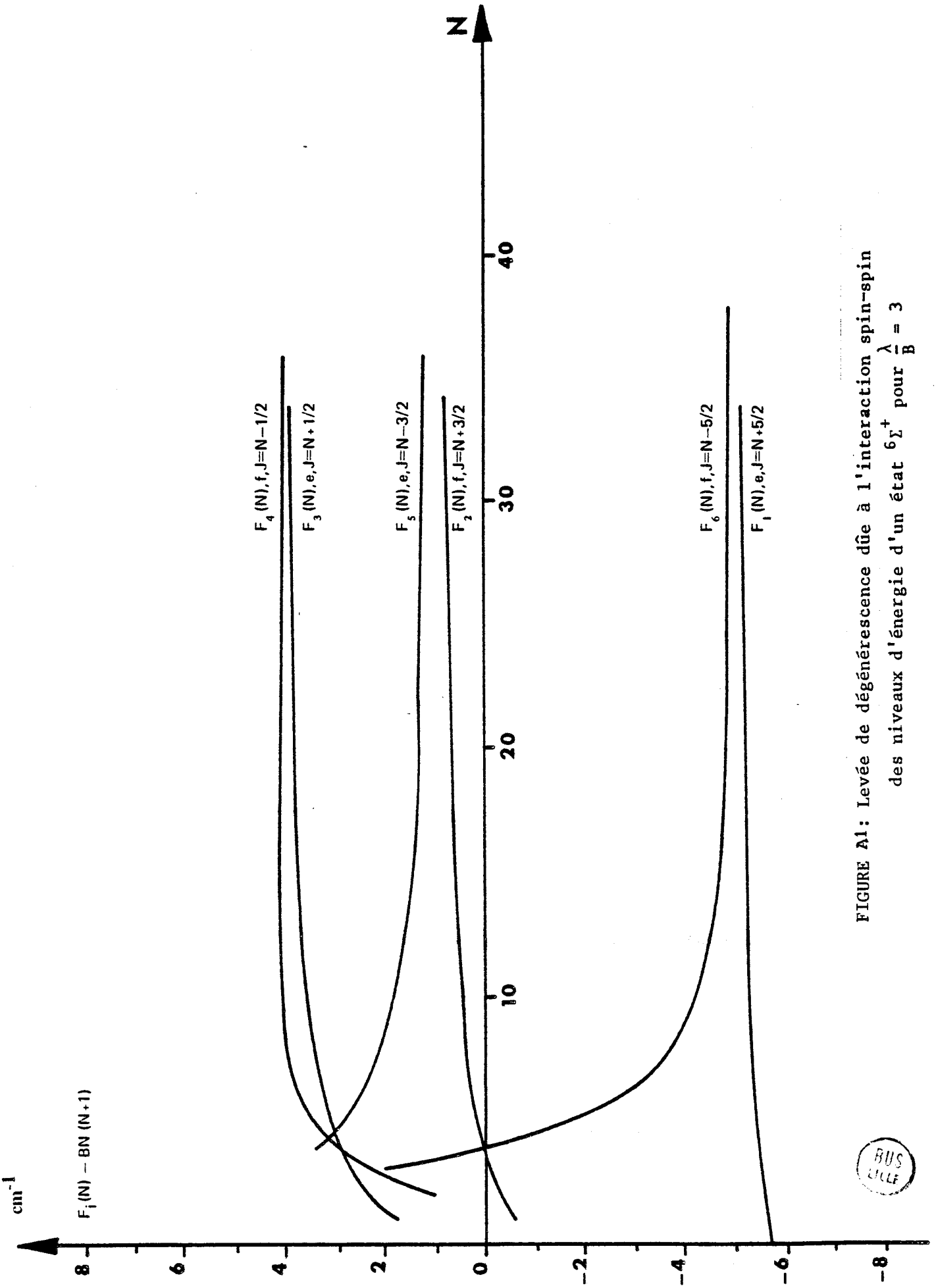


FIGURE A1: Levée de dégénérescence dûe à l'interaction spin-spin des niveaux d'énergie d'un état $^6\Sigma^+$ pour $\frac{\lambda}{B} = 3$

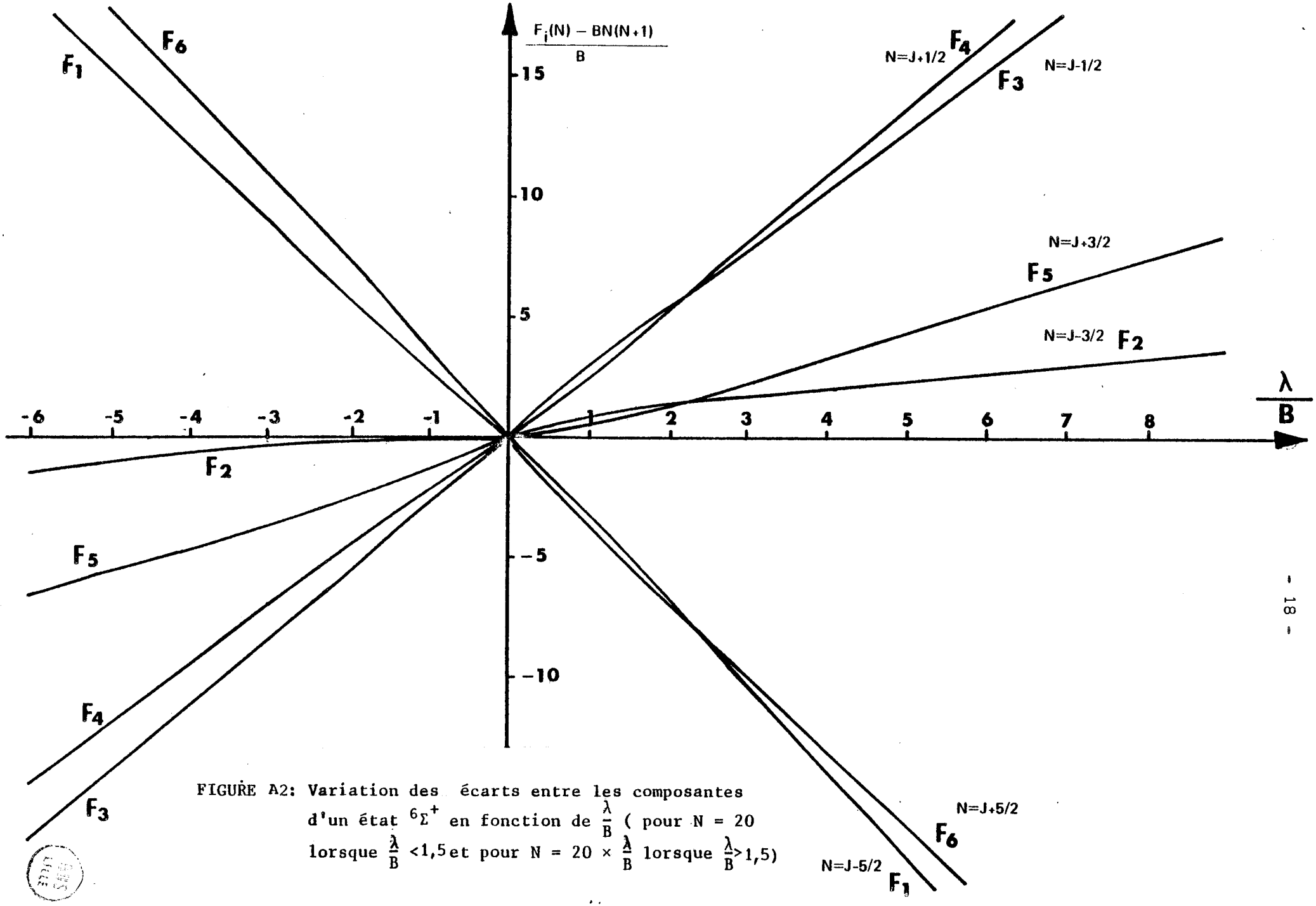


FIGURE A2: Variation des écarts entre les composantes d'un état $^6\Sigma^+$ en fonction de $\frac{\lambda}{B}$ ( pour N = 20 lorsque $\frac{\lambda}{B} < 1,5$ et pour N = 20 × $\frac{\lambda}{B}$ lorsque $\frac{\lambda}{B} > 1,5$)

1 - B. PINCHEMEL Thèse Doctorat de 3ème Cycle LILLE (1974)

2 - W. HEISENBERG et P. JORDAN Z. Phys. 37 268 (1926)

3 - J.H. VAN VLECK Rev. Mod. Phys. 23 213 (1951)

4 - I. KOVACS Rotational Structure in the Spectra of Diatomic Molecules
A. HILGER London (1969)

5 - J.H. VAN VLECK Phys. Rev. 33 467 (1969)

6 - B. KLEMAN et U. UHLER Can J. Phys. 37 537 (1959)

7 - K.S. Rao Indian J. Phys. 26 47 (1952)

Chemical Physics 18 (1976) 481–489


ARTICLE N° 2

# ELECTRONIC STRUCTURE OF MnO

B. PINCHEMEL and J. SCHAMPS
*Laboratoire de Spectroscopie des Molécules Diatomiques, Equipe de recherche associée au C.N.R.S., Université de Lille I, Bâtiment P. 5, B.P. 36, 59650 Villeneuve d'Ascq, France*
*and Centre de Mécanique Ondulatoire Appliquée, 23, rue du Maroc, 75 Paris XIXème, France*

Received 20 April 1976

SCF calculations have been performed in order to get information upon the ground and lowest excited states of manganese monoxide MnO and to study the bonding mechanism in this molecule. The ground state is found to be a $^6\Sigma^+$ state and configuration interaction calculations indicate that it is represented for more than 60% by the ($8\sigma^2\ 9\sigma\ 4\pi^2\ 1\delta^2$) configuration. In this energy level, the closed-shell $8\sigma$ orbital is the bonding orbital and the three open-shell orbitals are strongly localized on 3d(Mn). This open-shell structure on manganese 3d induces interesting analogies between the molecule and the manganese atom. SCF potential curves have been plotted in a diagram. The lowest excited states are found to be the observed $A^6\Sigma^+$ and a $^6\Pi$ state. The $A^6\Sigma^+$–$X^6\Sigma^+$ transition is the charge-transfer $8\sigma \leftarrow 10\sigma$ excitation. Rearrangements of orbitals in the excited states in order to maintain a $Mn^+(3d^5\ 4s) - O^-(2p^5)$ gross structure are pointed out. The results are compared to those of earlier semi-empirical studies and found to be essentially different.

## 1. Introduction

The detailed structure of molecular bonds involving transition elements is still imperfectly known, even in the simplest species such as diatomic compounds. On the basic of molecular orbital pictures, Jorgensen [1] then Cheetham and Barrow [2] discussed the possible nature of the ground states of these diatomic compounds but their arguments remained somewhat too empirical to be definitive so that more quantitative studies seemed to be desirable. In this connection, Hartree–Fock calculations have been performed on some hydrides [3], and in the field of transition element oxides, on ScO [4], TiO [5], VO [6] and FeO [7], the last work including configuration interaction. These works have shown the difficulty to obtain accurate relative locations of electronic states, in such molecules, which are heavy ones from the point of view of SCF calculations and for which the large number of valence electrons gives rise to a large number of low-lying configurations.

Table cI

We present here the results of an ab initio study of the MnO molecule originally undertaken in order to gather information upon its lowest-lying states so as to help us in the experimental analysis of the green system of the MnO electronic spectrum [8,9]. Furthermore, from the purely theoretical point of view, our study could be expected to contribute to elucidate the basic principles which govern the formation of valence orbitals in the bonds involving atoms with an open d-shell.

## 2. Calculations

The manganese monoxide molecule contains thirty-three electrons, twenty-two of which can be considered as core electrons belonging to a definite atom (Mn or O) and filling the $1\sigma$ to $7\sigma$ and $1\pi$, $2\pi$ molecular shells. The remaining eleven electrons are valence electrons to be shared out into the valence orbitals built from the 2p(O), 3d(Mn), 4s(Mn) and eventually 4p(Mn) atomic orbitals. Since all these orbitals have nearly equal energies [10], it is not easy to guess a priori the nature of the ground-state configuration of MnO. Exploratory SCF calculations were then performed using a single-

Table cII

les tables et les figures citées en marge font référence au complément placé à la fin de l'article.

Table 1
SCF energies of various MnO states (minimal basis set)

| Orbital occupancies | | | | | Calculated states | SCF energies (hartree) at $R$ = 3.0 bohr |
|---|---|---|---|---|---|---|
| $9\sigma$ | $4\pi$ | $1\delta$ | $10\sigma$ | $5\pi$ | | |
| 1 | 2 | 2 | | | $^6\Sigma^+$ | −1221.61233 |
| 2 | 1 | 2 | | | $^4\Pi$ | −1221.53638 |
| 2 | 2 | 1 | | | $^4\Delta$ | −1221.52004 |
| 1 | 2 | 1 | 1 | | $^6\Delta$ | −1221.47342 |
| 1 | 1 | 2 | 1 | | $^6\Pi$ | −1221.50178 |
| 1 | 1 | 2 | | 1 | $^6\Delta$ | −1221.43553 |
| | 2 | 2 | | 1 | $^6\Pi$ | −1221.42640 |
| 1 | 2 | 1 | | 1 | $^6\Phi$ | −1221.41990 |
| 1 | 1 | 3 | | | $^4\Phi$ | −1221.33228 |
| 1 | 3 | 1 | | | $^4\Phi$ | −1221.44708 |
| 2 | | 3 | | | $^2\Delta$ | −1221.39989 |
| 2 | 3 | | | | $^2\Pi$ | −1221.33634 |
| | 3 | 2 | | | $^4\Pi$ | −1221.31125 |
| | 2 | 3 | | | $^4\Delta$ | −1221.25228 |
| 1 | 4 | | | | $^2\Sigma^+$ | −1221.26736 |
| 1 | | 4 | | | $^2\Sigma^+$ | −1221.21029 |
| | 4 | 1 | | | $^2\Delta$ | −1221.21084 |
| | 1 | 4 | | | $^2\Pi$ | −1221.04040 |

zeta STO basis set, namely Clementi's and Raimondi's minimal basis set [11]. The ALCHEMY program [12] written by Bagus, Mc Lean, Yoshimine and Liu achieved the numerical minimizations of energies.

We first checked, on particular cases, that all the low-lying configurations of MnO should have completely occupied $8\sigma$ and $3\pi$ orbitals, the remaining five electrons having to be distributed into the $9\sigma$, $4\pi$ and $1\delta$ orbitals (or, exceptionally, in other low-lying orbitals such as $10\sigma$ and $5\pi$). SCF calculations were then performed with the minimal basis set to obtain the lowest-lying state (in practice, the state of highest spin-multiplicity and, for this multiplicity, of highest $\Lambda$-value) of every open-shell configuration of the type $(9\sigma^l\, 4\pi^m\, 1\delta^n)$ with $l + m + n = 5$. From these calculations (table 1), we deduced that the actual ground-state should belong, in the single-configuration representation, to one of the three following configurations:

$(9\sigma\ \ 4\pi^2\ 1\delta^2)$ giving a $^6\Sigma^+$ ground-state

$(9\sigma^2\ 4\pi\ \ 1\delta^2)$ giving a $^4\Pi$ ground-state

$(9\sigma^2\ 4\pi^2\ 1\delta)$ giving a $^4\Delta$ ground-state .

Other configurations still needed to be taken into consideration because they could yield low-lying excited states. Using the results of the calculations reported in table 1, we thus found that these states requiring further calculations were the $(9\sigma\ 4\pi^3\ 1\delta)\,^4\phi$ and $(9\sigma^2\ 1\delta^3)\,^2\Delta$ states and all the states (second group in table 1) obtained from the three possible ground-states determined above by exciting a valence electron into the low-lying $5\pi$ or $10\sigma$ orbitals (except for the $9\sigma \rightarrow 10\sigma$ excitation which will be taken into account later on, in the configuration interaction between $^6\Sigma^+$ states).

All these states were then submitted to a definitive second set of SCF calculations (table 2) using an improved STO basis set (called mixed basis set) obtained from the minimal basis set by replacing the single-zeta outer orbitals of Mn(4s,3d,4p) and O(2s,2p) by their double-zeta representations optimized by Clementi et al. [13,14], and keeping the exponents of the inner atomic orbitals unchanged. A number of tests have shown that, for our purpose of calculating energy differences between valence state, this mixed basis set formed a reasonable compromise between the too elementary minimal basis set of the first calculations and a refined but time-consuming completely double-zeta basis set. For instance, it has been checked that the energy-separation between the variational

Table 2
SCF energies (hartree) of MnO states (mixed basis set)

| States | 3.0 bohr | 3.2 bohr | 3.3 bohr | 3.4 bohr | 3.6 bohr | 3.8 bohr | 4.0 bohr |
|---|---|---|---|---|---|---|---|
| $(9\sigma\,4\pi^2\,1\delta^2)^6\Sigma^+$ | −1222.96956 | −1222.98687 | −1222.98993 | −1222.99042 | −1222.98671 | −1222.98004 | −1222.97242 |
| $(9\sigma^2\,4\pi\,1\delta^2)^4\Pi$ | −1222.82793 | −1222.83458 | −1222.83376 | −1222.83120 | −1222.82304 | −1222.81322 | −1222.80331 |
| $(9\sigma^2\,4\pi^2\,1\delta)^4\Delta$ | −1222.78022 | −1222.79265 | −1222.79400 | −1222.79323 | −1222.78775 | −1222.77967 | −1222.77082 |
| $(9\sigma\,4\pi^2\,1\delta\,10\sigma)^6\Delta$ | −1222.81262 | −1222.83719 | −1222.84418 | | −1222.85081 | −1222.84751 | −1222.84074 |
| $(9\sigma\,4\pi\,1\delta^2\,10\sigma)^6\Pi$ | −1222.86436 | −1222.88308 | | −1222.89110 | −1222.89131 | −1222.88646 | −1222.87853 |
| $(9\sigma\,4\pi\,1\delta^2\,5\pi)^6\Delta$ | −1222.73206 | −1222.75047 | −1222.75516 | −1222.75734 | −1222.75683 | −1222.75135 | −1222.74304 |
| $[(9\sigma)^0\,4\pi^2\,1\delta^2\,5\pi]^6\Pi$ | −1222.78070 | −1222.77907 | −1222.77425 | −1222.76792 | −1222.75288 | −1222.73696 | −1222.72166 |
| $(9\sigma\,4\pi^2\,1\delta\,5\pi)^6\Phi$ | −1222.68592 | −1222.70971 | −1222.71635 | −1222.72031 | −1222.72224 | −1222.71870 | −1222.71189 |
| $(9\sigma\,4\pi^3\,1\delta)^4\Phi$ | −1222.77927 | −1222.81259 | | −1222.82920 | −1222.83436 | −1222.83210 | −1222.82521 |
| $[9\sigma^2(4\pi)^0\,1\delta^3]^2\Delta$ | −1222.75616 | −1222.75854 | −1222.75573 | −1222.75123 | −1222.73959 | −1222.72715 | −1222.71548 |

Table cIII

$(9\sigma\,4\pi^2\,1\delta^2)^6\Sigma^+$ and $(9\sigma^2\,4\pi\,1\delta^2)^4\Pi$ states is practically the same in both calculations made with the mixed-basis set and the completely double-zeta set (deviation of less than 5%) whereas the calculations using the minimal basis set gave only about one half of these values. In atomic calculations on transition elements, Carlson [15] found that adding a third 3d(Mn) orbital to each symmetry block of the basis set significantly improved the $(3d^{n+1}\,4s) - (3d^n\,4s^2)$ term separation (by 0.04 hartree in manganese). This has not been done here but it has been checked on particular cases that such a modification of the basis produced only little changes (at most 0.01 hartree) in the mutual location of the states of fig. 1 (to be discussed later on).

The SCF calculations using the mixed basis set have been performed independently for each state at various internuclear distances between 3.0 and 4.0 bohr, region where the potential curves were found to reach their minimum. The energy results are given in table 2. The Fig c1
orbitals deduced from the minimization of the energy of the $(9\sigma\,4\pi^2\,1\delta^2)\,^6\Sigma^+$ state, found to be the Hartree–Fock ground-state, are reported in table 3.

## 3. Energy levels

As just stated, $(9\sigma\,4\pi^2\,1\delta^2)\,^6\Sigma^+$ is the fundamental state in the single-configuration approximation. This claim, however, is true under the condition that Hund's rule holds for the $(\sigma\,\pi^2\,\delta^2)$ configuration. This was checked by calculating the energies of the eighteen states of this configuration, using the orbitals deter- Table
mined from the SCF calculations on $^6\Sigma^+$. It was found cIV
that $^6\Sigma^+$ was indeed the lowest state of the $(9\sigma\,4\pi^2\,1\delta^2)$ configuration and that all the other states of this configuration were lying very much higher, the lowest being a $^4\Sigma^+$ level located 30 000 $cm^{-1}$ above $^6\Sigma^+$. Such large energy differences between the sextet $^6\Sigma^+$ state and the other states of the configuration must be ascribed to considerable exchange effects between the three open-shell orbitals which are centered on the same atomic orbital 3d(Mn) (see section 4).

Now the Hartree–Fock $^6\Sigma^+$ state also lies far below the states of any other low-lying configuration. Thus, the lowest of these states, namely $(9\sigma\,4\pi\,1\delta^2\,10\sigma)\,^6\Pi$, was calculated to be about 22 000 $cm^{-1}$ above $^6\Sigma^+$. Such energy differences are large enough to expect that inclusion of electronic correlation and relativistic

Table 3
SCF wavefunctions of the $(9\sigma\, 4\pi^2\, 1\delta^2)\, {}^6\Sigma^+$ state of MnO (mixed basis set) at $R$ = 3.4 au

| Basis orbitals | | ζ | 1σ | 2σ | 3σ | 4σ | 5σ | 6σ | 7σ | 8σ | 9σ |
|---|---|---|---|---|---|---|---|---|---|---|---|
| Mn | 1sσ | 24.3957 | 0.9985 | 0.3480 | 0.0009 | 0.0000 | 0.1367 | 0.0030 | −0.0086 | 0.0239 | −0.0145 |
| | 2sσ | 8.8969 | 0.0047 | −1.0749 | −0.0027 | −0.0001 | −0.4966 | −0.0113 | 0.0288 | −0.0841 | 0.0535 |
| | 3sσ | 4.3393 | −0.0011 | 0.0419 | 0.0001 | 0.0004 | 1.1020 | 0.0250 | −0.0882 | 0.2381 | −0.1379 |
| | 4sσ | 1.1029 | −0.0002 | 0.0084 | 0.0008 | 0.0021 | −0.0125 | 0.0047 | 0.0003 | −0.2453 | 0.1468 |
| | 4sσ | 2.0073 | 0.0005 | −0.0195 | 0.0027 | 0.0020 | 0.0465 | −0.0065 | 0.0352 | −0.2758 | 0.2306 |
| | 2pσ | 10.5420 | −0.0000 | 0.0025 | −0.9839 | −0.0000 | 0.0076 | −0.3393 | 0.0296 | −0.0212 | 0.0158 |
| | 3pσ | 4.0364 | −0.0000 | 0.0006 | −0.0520 | 0.0002 | −0.0222 | 1.0142 | −0.0982 | 0.0760 | −0.0522 |
| | 4pσ | 0.9000 | −0.0000 | 0.0009 | −0.0079 | 0.0018 | 0.0013 | −0.0260 | −0.0107 | 0.1100 | −0.0298 |
| | 4pσ | 1.7000 | 0.0001 | −0.0034 | 0.0197 | −0.0023 | −0.0033 | 0.0824 | 0.0073 | −0.0321 | 0.0679 |
| | 3dσ | 2.5044 | 0.0000 | −0.0013 | 0.0019 | 0.0009 | −0.0026 | −0.0149 | 0.0464 | −0.1574 | −0.6829 |
| | 3dσ | 5.7542 | −0.0000 | 0.0007 | −0.0004 | −0.0003 | −0.0010 | −0.0077 | 0.0195 | −0.0700 | −0.3718 |
| O | 1sσ | 7.6579 | −0.0000 | 0.0000 | −0.0001 | 0.9936 | −0.0012 | −0.0073 | −0.2443 | −0.0450 | −0.0124 |
| | 2sσ | 1.6270 | −0.0001 | 0.0034 | −0.0056 | −0.0200 | 0.0009 | 0.0010 | 0.4588 | 0.1423 | −0.0255 |
| | 2sσ | 2.6216 | 0.0000 | −0.0008 | 0.0006 | 0.0297 | 0.0015 | 0.0126 | 0.5821 | 0.1242 | 0.0395 |
| | 2pσ | 1.5413 | 0.0001 | −0.0045 | 0.0046 | 0.0029 | −0.0007 | −0.0097 | −0.0819 | 0.5825 | −0.0647 |
| | 2pσ | 3.6966 | −0.0000 | 0.0015 | −0.0011 | −0.0023 | −0.0014 | −0.0067 | −0.0181 | 0.2357 | −0.0180 |
| | ϵ(au) | | −240.6257 | −28.8298 | −24.7752 | −20.4096 | −3.7484 | −2.4876 | −1.0712 | −0.3255 | −0.5832 |

| Basis orbitals | | ζ | 1π | 2π | 3π | 4π |
|---|---|---|---|---|---|---|
| Mn | 2pπ | 10.5420 | 0.9841 | −0.3403 | −0.0225 | 0.0175 |
| | 3pπ | 4.0364 | 0.0516 | 1.0174 | 0.0758 | −0.0574 |
| | 4pπ | 0.9000 | 0.0074 | −0.0273 | −0.0894 | 0.0269 |
| | 4pπ | 1.7000 | −0.0156 | 0.0816 | −0.0964 | 0.0835 |
| | 3dπ | 2.5044 | −0.0002 | −0.0141 | −0.0975 | −0.7154 |
| | 3dπ | 5.7542 | −0.0003 | −0.0050 | −0.0363 | −0.3957 |
| O | 2pπ | 1.5413 | 0.0012 | −0.0008 | −0.7251 | 0.1189 |
| | 2pπ | 3.6966 | −0.0004 | 0.0021 | −0.2896 | 0.0495 |
| | ϵ(au) | | −24.7762 | −2.4889 | −0.3575 | −0.6268 |

| Basis orbitals | | ζ | 1δ |
|---|---|---|---|
| Mn | 3dδ | 2.5044 | 0.7262 |
| | 3dδ | 5.7542 | 0.3946 |
| | ϵ(au) | | −0.6531 |

Table 4
CI wavefunctions of the $X^6\Sigma^+$ and $A^6\Sigma^+$ states

| Excitations | Configurations | | | | | | CI weights | | | |
|---|---|---|---|---|---|---|---|---|---|---|
| | | | | | | | $X^6\Sigma^+$ | | $A^6\Sigma^+$ | |
| | | | | | | | $R$ = 3.4 bohr | $R$ = 3.8 bohr | $R$ = 3.4 bohr | $R$ = 3.8 bohr |
| ref. | $8\sigma^2$ | $3\pi^4$ | $9\sigma$ | $4\pi^2$ | $1\delta^2$ | | 0.644 | 0.622 | 0.106 | 0.128 |
| $8\sigma \rightarrow 9\sigma$ | $8\sigma$ | $3\pi^4$ | $9\sigma^2$ | $4\pi^2$ | $1\delta^2$ | | 0.003 | 0.004 | 0.105 | 0.047 |
| $8\sigma \rightarrow 10\sigma$ | $8\sigma$ | $3\pi^4$ | $9\sigma$ | $4\pi^2$ | $1\delta^2$ | $10\sigma$ | 0.189 | 0.172 | 0.621 | 0.705 |
| $8\sigma \rightarrow 11\sigma$ | $8\sigma$ | $3\pi^4$ | $9\sigma$ | $4\pi^2$ | $1\delta^2$ | $11\sigma$ | 0.027 | 0.021 | 0.056 | 0.049 |
| $9\sigma \rightarrow 10\sigma$ | $8\sigma^2$ | $3\pi^4$ | $4\pi^2$ | $1\delta^2$ | $10\sigma$ | | 0.031 | 0.004 | 0.045 | 0.015 |
| $9\sigma \rightarrow 11\sigma$ | $8\sigma^2$ | $3\pi^4$ | $4\pi^2$ | $1\delta^2$ | $11\sigma$ | | 0.004 | 0.000 | 0.004 | 0.001 |
| $3\pi \rightarrow 5\pi$ | $8\sigma^2$ | $3\pi^3$ | $9\sigma$ | $4\pi^2$ | $1\delta^2$ | $5\pi$ | 0.005 | 0.001 | 0.008 | 0.001 |
| $8\sigma^2 \rightarrow 10\sigma^2$ | $3\pi^4$ | $9\sigma$ | $4\pi^2$ | $1\delta^2$ | $10\sigma^2$ | | 0.062 | 0.135 | 0.024 | 0.033 |
| $8\sigma^2 \rightarrow 9\sigma 10\sigma$ | $3\pi^4$ | $9\sigma^2$ | $4\pi^2$ | $1\delta^2$ | $10\sigma$ | | 0.000 | 0.004 | 0.009 | 0.004 |
| $8\sigma^2 \rightarrow 10\sigma 11\sigma$ | $3\pi^4$ | $9\sigma$ | $4\pi^2$ | $1\delta^2$ | $10\sigma$ | $11\sigma$ | 0.016 | 0.029 | 0.004 | 0.009 |
| $8\sigma 9\sigma \rightarrow 10\sigma^2$ | $8\sigma$ | $3\pi^4$ | $4\pi^2$ | $1\delta^2$ | $10\sigma^2$ | | 0.004 | 0.002 | 0.005 | 0.002 |
| Other configurations | | | | | | | 0.015 | 0.006 | 0.013 | 0.006 |

Table 5
CI energies and spectroscopic constants of the $X^6\Sigma^+$ and $A^6\Sigma^+$ states of MnO

a) CI energies (au)

| $R$ (bohr) | $X^6\Sigma^+$ | $A^6\Sigma^+$ |
|---|---|---|
| 3.0 | −1223.02259 | −1222.93261 |
| 3.2 | −1223.03734 | −1222.96162 |
| 3.4 | −1223.04954 | −1222.99233 |
| 3.6 | −1223.05854 | −1223.01401 |
| 3.8 | −1223.05902 | −1223.02120 |
| 4.0 | −1223.05284 | −1223.01832 |

b) Spectroscopic constants

| | $X^6\Sigma^+$ | | $A^6\Sigma^+$ | |
|---|---|---|---|---|
| $T_e(cm^{-1})$ | HF | 0 (ref.) | HF | – |
| | CI | 0 (ref.) | CI | 8430 |
| | Exp | 0 (ref.) | Exp | 17949 |
| $\omega_e(cm^{-1})$ | HF | 641 | HF | – |
| | CI | 632 | CI | 709 |
| | Exp | 839.5 | Exp | 762.7 |
| $\omega_e x_e(cm^{-1})$ | HF | 7.9 | HF | – |
| | CI | 1.6 | CI | 5.6 |
| | Exp | 4.8 | Exp | 9.6 |
| $B_e(cm^{-1})$ | HF | 0.425 | HF | – |
| | CI | 0.353 | CI | 0.331 |
| $r_e(Å)$ | HF | 1.788 | HF | – |
| | CI | 1.964 | CI | 2.026 |

corrections in order to consider the actual situation in the MnO molecule would bot bring any state to be depressed below $^6\Sigma^+$. We then conclude that the ground state of MnO is a $^6\Sigma^+$ state.

In order to see to what extent the single configuration ($9\sigma\, 4\pi^2\, 1\delta^2$) was sufficient to approximate to the actual ground state wavefunction, a configuration interaction study has been achieved for the $^6\Sigma^+$ levels. In this CI process, we included the 191 $^6\Sigma^+$ states belonging to all the configurations deduced from ($9\sigma\, 4\pi^2\, 1\delta^2$) by either a monoexcitation or a diexcitation concerning electrons of the outer occupied or virtual $8\sigma$ to $11\sigma$, $3\pi$ to $5\pi$ and $1\delta$ orbitals. The weights (square of the coefficients) of the most important configurations participating in the CI wavefunction of the $^6\Sigma^+$ ground state are reported in table 4, the energies and spectroscopic constants in table 5. The ($9\sigma\, 4\pi^2\, 1\delta^2$) configuration contributes for more than 60% (for $R$ between 3 and 4 bohr) to the ground-state wavefunction so that the single-configuration approximation is not quite a good representation of the ground-state of MnO. Among the other determinants which complete the wavefunction, the $8\sigma \rightarrow 10\sigma$ and $8\sigma^2 \rightarrow 10\sigma^2$ excitations (with regard to the principal configuration) have the largest contributions. As for the spectroscopic constants, we note that the CI vibrational constants, $\omega_e$, is even worse than the Hartree–Fock one (see table 5); so, it is not possible to warrant that the other constants of interest ($B_e$ and $r_e$) deduced from configuration interaction are nearer from their experimental values than those calculated in the Hartree–Fock approximation.

In addition to the results obtained for the ground-

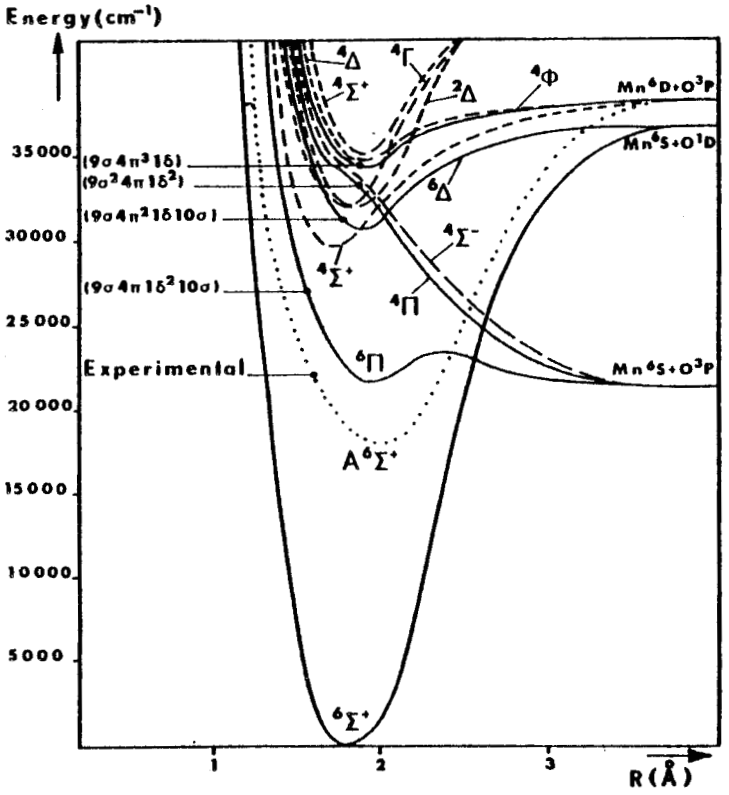


Fig. 1. Energy level diagram of MnO. Full lines: SCF states. Broken lines: states of the $(9\sigma\, 4\pi^2\, 1\delta^2)$ configuration. Dashed line: experimental $A^6\Sigma^+$.

Energy calculations have been performed between about 1.6 Å and 2.1 Å, that is to say the extreme bottom of the potential curves. For extrapolations, the energy positions of the atomic asymptotes have been obtained from a Birge–Sponer determination of the ground-state dissociation energy, using its experimental vibrational constants.

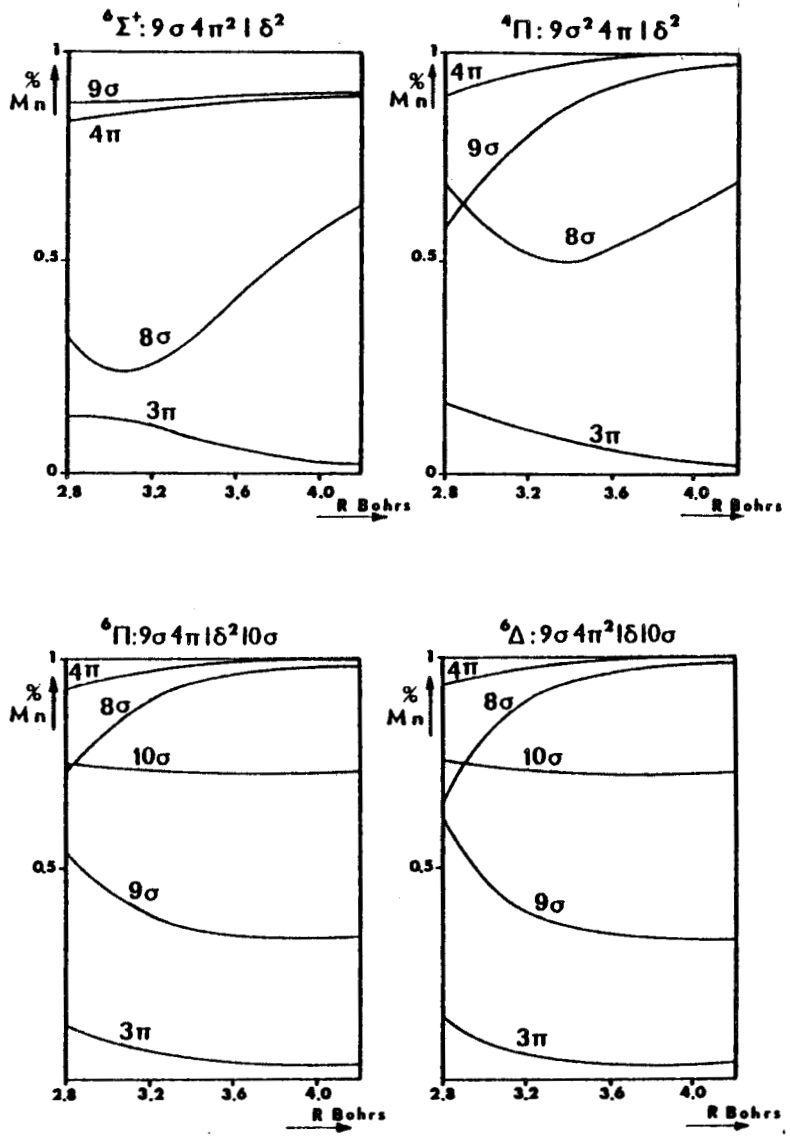


Fig. 2. Atomic population analysis in various SCF states of MnO.

state, our calculations gave much information about the nature of the low-lying excited states of MnO. We have gathered it in an energy level diagram up to about 40 000 $cm^{-1}$ above the ground state (fig. 1). This diagram contains the lowest of the SCF states calculated above (see table 1), the lowest ($^4\Sigma^+$, $^4\Sigma^-$, $^2\Delta$, $^4\Gamma$, $^4\Delta$, $^4\Sigma^+$) of the levels isoconfigurational to $X^6\Sigma^+$ (and assumed to have similar orbitals), and located at its experimental energy, the $A^6\Sigma^+$ upper state of the visible transition of MnO [9]. In this connection, the wavefunction of $A^6\Sigma^+$ has been determined from our $^6\Sigma^+$ configuration-interaction calculations, using the orbitals of the variational $(9\sigma\, 4\pi^2\, 1\delta^2)\,^6\Sigma^+$ state.

The conclusion is that the $A^6\Sigma^+$ state is mainly associated with the $(8\sigma\, 9\sigma\, 10\sigma\, 4\pi^2\, 1\delta^2)$ configuration and that the $A^6\Sigma^+ - X^6\Sigma^+$ transition must be ascribed to the charge-transfer excitation between the bonding $8\sigma$ and antibonding $10\sigma$ orbitals. The CI energy difference between the $A^6\Sigma^+$ and $X^6\Sigma^+$ states (8430 $cm^{-1}$) is smaller than the experimental one (17950 $cm^{-1}$): our CI basis set was too truncated to give reliable values of energy differences (and spectroscopic constants); it could be used only for determining approximate wavefunctions. Lastly, it must be emphasized that positions of the energy levels in fig. 1 are quite approximate in regard to their actual ones. However, considered with a spirit of criticism, fig. 1 may be helpful to future experimental spectroscopic studies of MnO because it gives a number of possible upper states of electronic transitions.

## 4. Structure of the molecular bond

From the SCF calculations, conclusions can be drawn relating to the structure of the molecular bond in MnO. In this connection, the results of atomic population analysis of the valence orbitals of various SCF states of MnO are presented in fig. 2. It follows from these diagrams that:

(i) the $3\pi$ closed shell is practically the atomic $2p\pi$ orbital of oxygen while the $4\pi$ and $1\delta$ orbitals are on 3d(Mn).

(ii) in the $X^6\Sigma^+$ ground state and in the $^4\Pi$ state, the $8\sigma$ orbital is the bonding orbital built on 4s(Mn) and 2p(O) while the $9\sigma$ orbital, as $4\pi$ and $1\delta$, is almost entirely located on 3d(Mn). However, when the $10\sigma$ orbital is occupied, that is in $^6\Pi$ and $^6\Delta$, the roles of $8\sigma$ and $9\sigma$ are exchanged, the open-shell $9\sigma$ orbital becoming the bonding combination of 4s(Mn) and 2p(O) while the closed-shell $8\sigma$ orbital becomes non-bonding, centered on 3d(Mn). In other words, this means that the order of filling the bonding 4s(Mn) + 2p(O) and the non-bonding 3d(Mn) $\sigma$ orbitals depends on whether $10\sigma$ is occupied or not.

(iii) the $10\sigma$ orbital is the antibonding 4s(Mn) − 2p(O) counterpart of the bonding $8\sigma$ (or $9\sigma$) orbital, with a slight 4p(Mn) contribution in addition.

So, in the ground state and in all the low-lying SCF states of MnO, the electronic structure of MnO is roughly $Mn^+(3d^5\,4s) + O^-(2p^5)$ at equilibrium separations. As just noticed exchanges in the order of filling orbitals may be required so as to maintain this structure when passing from one configuration to another. This makes elementary reasonings about excitations in the molecular orbital picture quite dangerous since the possibility of complete changes in the order or in the structure of the orbitals must be carefully taken into account. It was then quite essential to deal with excited states by applying the variational principle independently to at least one state of each low-lying configuration, which we did.

Another interesting consequence of the above atomic population analysis concerns the close relationship between the structure of the MnO molecule and that of the Mn atom. This comes from the fact that, in configurations of type $(9\sigma^l\, 4\pi^m\, 1\delta^n)$ with $l + m + n = 5$, the $9\sigma$, $4\pi$ and $1\delta$ molecular orbitals are practically the axially symmetric components of the 3d(Mn) atomic shell. Then these $(9\sigma^l\, 4\pi^m\, 1\delta^n)$ configurations can be considered as components of the $(3d^5)$ part of the configuration of the manganese atom (ionized or not). Under such conditions, Hund's rule which applies to the $(3d^5)$ *atomic* configuration, also applies to the whole group of *molecular* states arising from the $(9\sigma^l\, 4\pi^m\, 1\delta^n)$ configurations whatever particular molecular configuration they belong to. This implies that the ground state of MnO is the state among these configurations which has the highest number of parallel spins, that is $(8\sigma^2\, 9\sigma\, 4\pi^2\, 1\delta^2)\,^6\Sigma^+$, just as the ground state of MnI is $(3d^5\,4s^2)\,^6S$, that of MnII is $(3d^5\,4s)\,^7S$ and that of MnIII is $(3d^5)\,^6S$. For the other states of these configurations, the one-by-one correspondence between atomic and molecular states is however seldom possible to achieve since, in the SCF approximation, the molecular states often do not dissociate into pure

Table cV

Table cVI

atomic states. But when this is possible to achieve, this correspondence can give interesting information. Consider, for instance, the $^4\Gamma$ state of the $(9\sigma\, 4\pi^2\, 1\delta^2)$ configuration. It obviously corresponds to the $^4$G atomic levels [16] found at 25300 $cm^{-1}$ above the ground state in MnI, at 26800 $cm^{-1}$ in MnIII, and to the $[3d^5(^4G)4s]\,^5G$ level at 27500 $cm^{-1}$ in MnII. We thus expect to find $^4\Gamma$ between 25000 and 30000 $cm^{-1}$ in MnO and indeed our calculations of its energy from the SCF orbitals of the isoconfigurational $X^6\Sigma^+$ state, which are likely to amplify energy differences slightly, give $^4\Gamma$ et 31000 $cm^{-1}$ from $X^6\Sigma^+$. From this, we verify the usefulness of atomic data to locate approximately molecular states when the open-shell orbitals are non-bonding orbitals all centered on one of the atoms constituting the molecule.

In connection with the foregoing discussion, it is worthwhile to emphasize that the structure of MnO in its ground state is quite different from the ground state structure of the lighter transition element monoxides (ScO, TiO, VO) where the parts of the $3d\sigma$ and $4s\sigma$ atomic orbitals are exchanged with respect to MnO: in these three molecules, $3d\sigma$ is the orbital participating in the closed-shell bond while $4s\sigma$ constitutes the open-shell $9\sigma$ valence molecular orbital [4–6]. This has consequences on the magnitude of hyperfine structure. For instance, the large hyperfine effects in ScO, which must be ascribed to the Fermi-contact term due to the s-character of the $9\sigma$ orbital in this molecule [17], are not expected to be found in the ground state of MnO where the open-shell orbitals have a pure d-character.

## 5. Conclusion

The present calculations have shown that the ground state of MnO is a $^6\Sigma^+$ state. This result has been used somewhere else as a starting point to establish that the green system observed in the experimental spectrum of MnO is a $^6\Sigma^+ - {}^6\Sigma^+$ transition [9]. The $^6\Sigma^+$ symmetry of the ground state was already suspected in earlier semi-empirical studies (Jorgensen [1], Cheetham and Barrow [2]) where the authors hesitated between $^6\Sigma^+$ and $^4\Pi$. However, we do not agree with any of the possible configurations that they assumed for this $^6\Sigma^+$ ground state. Although they improved the simple crystal-field model of Berg and Sinanoğlu [18] by pointing out the importance of a $\sigma$ orbital (called either $\sigma^*$ or $\sigma_M$) in the stabilization of the molecule, they assumed this $\sigma$ orbital to be close to atomic 4s(Mn). Actually, our calculations show that this orbital is in fact the $8\sigma$ bonding mixing of 2p(O) and 4s(Mn). Moreover they postulated a $Mn^{++}O^{--}$ structure (five valence electrons on manganese) instead of the $Mn^+O^-$ structure revealed by our calculations. Therefore none of their $\sigma_M^2 d^3$, $\sigma_M^1 d^4$ or $\sigma_M^0 d^5$ configurations could be that of the ground state of MnO and we have found above that the actual ground state configurations is $(4s + 2p)^2\, \sigma_d\, \pi_d^2\, \delta_d^2$. We then conclude that, in MnO, the 2p electrons of oxygen contribute to the bond in the closed-shell $8\sigma$ orbital together with 4s electrons of manganese while the open-shell structure $9\sigma\, 4\pi^2\, 1\delta^2$ is essentially due to the five 3d electrons of manganese. Consequently, the open-shell structure is the same in the MnO molecule and in the Mn atom and this induces interesting analogies which have been studied in the previous section. Of course, it would be premature to directly extrapolate the present results obtained in the case of MnO to the other transition element compounds. We plan to study other molecules as TiO and CuO in order to draw general conclusions relating to the structure of the bond in transition element oxides. However, as it stands, this work allows some hypothesis to be made about molecules of the same type as MnO but heavier than MnO and consequently more difficult to treat theoretically by the SCF CI method. For instance, it is likely that MnS, MnSe, MnTe, ReO, and the chromium halides also have $^6\Sigma^+$ ground states. For some of these molecules, serious experimental support exists (chromium halides [19]) or begins to come out (Mns [20]) for such a ground-state symmetry.

## Acknowledgement

The authors wish to express their sincere thanks to Dr. H. Lefebvre-Brion for helpful comments and to Dr. A. Veillard for reading an early draft of the manuscript.

## References

[1] C.K. Jorgensen, Mol. Phys. 7 (1964) 417.
[2] C.J. Cheetham and R.F. Barrow, Adv. High Temp. Chem. USA 1 (1967) 7.
[3] P.S. Bagus and H.F. Schaefer III, J. Chem. Phys. 58 (1973) 1844;
P.R. Scott and W.G. Richards, J. Phys. B7 (1974) 1679.
[4] K.D. Carlson, E. Ludena and C. Moser, J. Chem. Phys. 43 (1965) 2408.
[5] K.D. Carlson and R.K. Nesbet, J. Chem. Phys. 41 (1964) 1051.
[6] K.D. Carlson and C. Moser, J. Chem. Phys. 44 (1966) 3259.
[7] P.S. Bagus and H.J.T.P. Preston, J. Chem. Phys. 59 (1973) 2986.
[8] J.M. Das Sarma, Z. Phys. 157 (1959) 98.
[9] B. Pinchemel and J. Schamps, Can. J. Phys. 53 (1975) 431.
[10] C. Froese-Fisher, Some Hartree–Fock results for the atoms helium to radon (Vancouver University, 1968).
[11] E. Clementi and D.L. Raimondi, J. Chem. Phys. 38 (x (1963) 2686.
[12] P.S. Bagus, B. Liu, A.D. Mc Lean and M. Yoshimine, ALCHEMY, IBM Research Lab., San Jose, California 95114 (USA).
[13] E. Clementi, IBM Res. Develop. S9 (1965) 2.
[14] E. Clementi, R. Matcha and A. Veillard, J. Chem. Phys. 47 (1967) 1865.
[15] C.R. Claydon and K.D. Carlson, J. Chem. Phys. 49 (1968) 1331.
[16] C.E. Moore, Atomic Energy levels, Nat. Bur. Std. (U.S), Circ. No 467 (1949).
[17] A. Adams, W. Klemperer and T.M. Dunn, Can. J. Phys. 46 (1968) 2213.
[18] R.A. Berg and O. Sinanoglu, J. Chem. Phys. 32 (1960) 1082.
[19] B. Rosen, Spectroscopic Data Relative to Diatomic Molecules (Pergamon Press, Oxford, 1970).
[20] B. Pinchemel and J. Schamps, in course of analysis.

| OXYDES | | | | HALOGENURES | | | |
|---|---|---|---|---|---|---|---|
| | Config. | Etat fond. | C=Calcul E=Expérience | | Config. | Etat fond. | C=Calcul E=Expérience |
| ScO | $\sigma$ | $^2\Sigma^+$ | C,E | CaF,CaCl | $\sigma$ | $^2\Sigma^+$ | E |
| TiO | $\sigma\delta$ | $^3\Delta$ | C,E | ScF,ScCl,YCl | $\sigma^2$ | $^1\Sigma^+$ | C,E |
| ZrO | $\sigma^2$ | $^1\Sigma^+$ | C,E | YF | $\sigma\delta$ | $^3\Delta$ | E |
| VO,NbO | $\sigma\delta^2$ | $^4\Sigma^-$ | C | TiF,TiCl ZrCl | $\sigma\delta^2$ | $^4\Sigma^-$ | E |
| | $\sigma^2\delta$ | $^2\Delta$ | E | | | | |
| CrO | $\sigma\pi\delta^2$ | $^5\Pi$ | E | VF | | | |
| MnO | $\sigma\pi^2\delta^2$ | $^6\Sigma^+$ | C,E | CrCl,CrF | $\sigma\delta^2\pi^2$ | $^6\Sigma^+$ | E |
| | $\sigma^2\pi\delta^2$ | $^4\Pi$ | | FeF | $\sigma\delta^3\pi^2\sigma'$ | $^6\Delta$ | C,E |

TABLE CI : Configurations probables des états fondamentaux des oxydes et halogénures des premiers éléments de transition

Orbitales de symétrie σ

| | | ZETA | | | ZETA |
|---|---|---|---|---|---|
| Mn: | 1sσ | 24,3957 | O: | 1sσ | 7,6579 |
| | 2sσ | 8,8969 | | 2sσ | 2,2458 |
| | 3sσ | 4,3393 | | 2pσ | 2,2266 |
| | 4sσ | 1,3208 | | | |
| | 2pσ | 10,5420 | | | |
| | 3pσ | 4,0364 | | | |
| | 4pσ | 1,0300 | | | |
| | 3dσ | 3,5094 | | | |

Orbitales de symétrie π

| | | ZETA | | | ZETA |
|---|---|---|---|---|---|
| Mn: | 2pπ | 10,5420 | O: | 2pπ | 2,2266 |
| | 3pπ | 4,0364 | | | |
| | 4pπ | 1,0300 | | | |
| | 3dπ | 3,5094 | | | |

Orbitale de symétrie δ

| | | ZETA |
|---|---|---|
| Mn: | 3dδ | 3,5094 |

Orbitales STO de la base minimale (21)

---

Orbitales de symétrie σ

| | | ZETA | | | ZETA |
|---|---|---|---|---|---|
| Mn: | 1sσ | 22,1654 | O: | 1sσ | 7,0600 |
| | | 27,9345 | | | 10,1100 |
| | 2sσ | 10,2186 | | 2sσ | 1,6270 |
| | | 13,5835 | | | 2,6216 |
| | 3sσ | 3,7964 | | 2pσ | 1,5413 |
| | | 5,2770 | | | 3,6966 |
| | 4sσ | 1,1029 | | 3dσ | 2,4200 |
| | | 2,0073 | | | |
| | 2pσ | 9,8608 | | | |
| | | 18,3004 | | | |
| | 3pσ | 5,5196 | | | |
| | | 3,4156 | | | |
| | 4pσ | 0,9000 | | | |
| | | 1,7000 | | | |
| | 3dσ | 2,5044 | | | |
| | | 5,7542 | | | |

Orbitales de symétrie π

| | | ZETA | | | ZETA |
|---|---|---|---|---|---|
| Mn: | 2pπ | 9,8608 | O: | 2pπ | 1,5413 |
| | | 18,3004 | | | 3,6966 |
| | 3pπ | 5,5196 | | 3dπ | 2,4200 |
| | | 3,4156 | | | |
| | 4pπ | 0,9000 | | | |
| | | 1,7000 | | | |
| | 3dπ | 2,5044 | | | |
| | | 5,7542 | | | |

Orbitales de symétrie δ

| | | ZETA | | | ZETA |
|---|---|---|---|---|---|
| Mn: | 3dδ | 2,5044 | O: | 3dδ | 2,4200 |
| | | 5,7542 | | | |

Orbitales STO de la base double zéta (23) (24)

---

Orbitales de symétrie σ

| | | ZETA | | | ZETA |
|---|---|---|---|---|---|
| Mn: | 1sσ | 24,3957 | O | 1sσ | 7,6579 |
| | 2sσ | 8,8969 | | 2sσ | 1,6270 |
| | 3sσ | 4,3393 | | | 2,6216 |
| | 4sσ | 1,1029 | | 2pσ | 1,5413 |
| | | 2,0073 | | | 3,6966 |
| | 2pσ | 10,5420 | | | |
| | 3pσ | 4,0364 | | | |
| | 4pσ | 0,9000 | | | |
| | | 1,7000 | | | |
| | 3dσ | 2,5044 | | | |
| | | 5,7542 | | | |

Orbitales de symétrie π

| | | ZETA | | | ZETA |
|---|---|---|---|---|---|
| Mn: | 2pπ | 10,5420 | O: | 2pπ | 1,5413 |
| | 3pπ | 4,0364 | | | 3,6966 |
| | 4pπ | 0,9000 | | | |
| | | 1,7000 | | | |
| | 3dπ | 2,5044 | | | |
| | | 5,7542 | | | |

Orbitales de symétrie δ

| | | ZETA |
|---|---|---|
| Mn: | 3dδ | 2,5044 |
| | | 5,7542 |

Orbitales STO de la base mixte

TABLE cII

BASE MIXTE

| Distance en Bohrs | Energie $^6\Sigma^+$ en Hartrees | Energie $^4\Pi$ en Hartrees | Différence d'énergie | |
|---|---|---|---|---|
| | | | en Hartrees | en $cm^{-1}$ |
| 2,8 | -1222,93574 | -1222,80283 | 0,13291 | 29170 |
| 3,0 | -1222,96956 | -1222,82793 | 0,14163 | 31084* |
| 3,2 | -1222,98687 | -1222,83458 | 0,15229 | 33424 |
| 3,4 | -1222,99042 | -1222,83120 | 0,15922 | 34945 |
| 4,0 | -1222,97242 | -1222,80331 | 0,16911 | 37115 |

ENERGIES

| | $^6\Sigma^+$ | $^4\Pi$ |
|---|---|---|
| Distance d'équilibre (Å) | 1,78 | 1,70 |
| $\omega_e$ ($cm^{-1}$) | 653,6 | 717,4 |
| $\omega_e x_e$ ($cm^{-1}$) | 15,70 | 10,24 |
| $B_e$ ($cm^{-1}$) | 0,43 | 0,47 |

Constantes moléculaires

BASE DOUBLE ZETA

| Distance en Bohrs | Energie $^6\Sigma^+$ | Energie $^4\Pi$ en Hartrees | Différence d'énergie | |
|---|---|---|---|---|
| | | | en Hartrees | en $cm^{-1}$ |
| 2,8 | -1224,53085 | | | |
| 3,0 | -1224,55442 | -1224,42024 | 0,13418 | 29449* |
| 3,2 | -1224,56514 | -1224,41870 | 0,14644 | 32140 |
| 3,4 | -1224,56423 | -1224,40945 | 0,15478 | 33970 |
| 4,0 | -1224,54007 | -1224,37337 | 0,16670 | 36586 |

ENERGIES

| | $^6\Sigma^+$ | $^4\Pi$ |
|---|---|---|
| Distance d'équilibre (Å) | 1,73 | 1,62 |
| $\omega_e$ ($cm^{-1}$) | 712,6 | 801,8 |
| $\omega_e x_e$ ($cm^{-1}$) | 10,00 | 8,24 |
| $B_e$ ($cm^{-1}$) | 0,45 | 0,52 |

Constantes moléculaires

* En base minimale la différence d'énergie entre les états $^6\Sigma^+$ et $^4\Pi$ à 3,0 Bohrs est de 16647 $cm^{-1}$

TABLE cIII: Comparaison des résultats SCF en bases mixte et double zéta

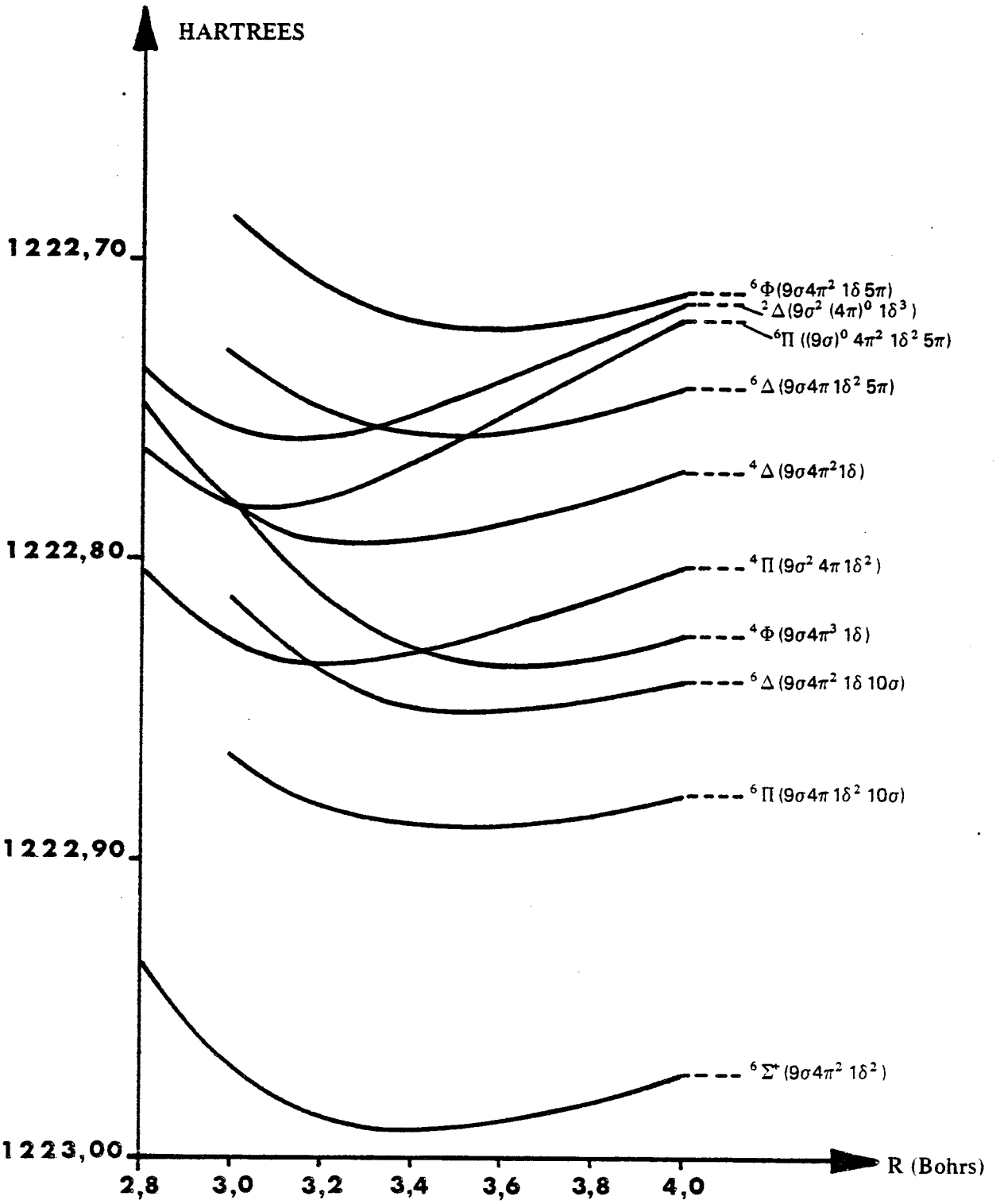


FIGURE c1: Courbes de potentiel des états calculés en base mixte

| | 3,0 Bohrs | 3,2 Bohrs | 3,4 Bohrs | 3,6 Bohrs | 3,8 Bohrs | 4,0 Bohrs |
|---|---|---|---|---|---|---|
| $^4\Sigma^-$ | 0,14799 | 0,16230 | 0,16527 | 0,16721 | 0,16834 | 0,16913 |
| | 0,22558 | 0,23515 | 0,24011 | 0,24346 | 0,24546 | 0,24661 |
| $^4\Sigma^+$ | 0,16168 | 0,16963 | 0,17454 | 0,17781 | 0,18002 | 0,18125 |
| | 0,11965 | 0,13183 | 0,13757 | 0,14112 | 0,14341 | 0,14476 |
| $^4\Delta$ | 0,14858 | 0,15383 | 0,15737 | 0,15974 | 0,16118 | 0,16201 |
| $^4\Gamma$ | 0,13487 | 0,13996 | 0,14276 | 0,14456 | 0,14566 | 0,14637 |
| $^2\Sigma^-$ | 0,22006 | 0,23170 | 0,23794 | 0,24196 | 0,24450 | 0,24621 |
| | 0,31419 | 0,33274 | 0,34332 | 0,35021 | 0,35463 | 0,35408 |
| $^2\Sigma^+$ | 0,17751 | 0,18546 | 0,19010 | 0,19072 | 0,19504 | 0,19597 |
| | 0,28899 | 0,30055 | 0,30742 | 0,31026 | 0,31474 | 0,31536 |
| | 0,23038 | 0,24372 | 0,25096 | 0,25968 | 0,25861 | 0,26009 |
| $^2\Delta$ | 0,31839 | 0,33093 | 0,33882 | 0,34411 | 0,34730 | 0,34965 |
| | 0,23176 | 0,24297 | 0,24942 | 0,25364 | 0,25628 | 0,25860 |
| | 0,13263 | 0,14028 | 0,14415 | 0,14660 | 0,14818 | 0,14936 |
| $^2\Gamma$ | 0,28078 | 0,29200 | 0,29903 | 0,30370 | 0,30654 | 0,30821 |
| | 0,19226 | 0,20341 | 0,20942 | 0,21330 | 0,21579 | 0,21740 |
| $^2I$ | 0,18788 | 0,19649 | 0,20152 | 0,20482 | 0,20686 | 0,20811 |

TABLE cIV: Distances en Hartrees entre les états de la configuration $9\sigma 4\pi^2 1\delta^2$ et l'état $^6\Sigma^+$

| Configuration | Désignation | Energie $cm^{-1}$ | Configuration | Désignation | Energie $cm^{-1}$ |
|---|---|---|---|---|---|
| $3d^5 4s^2$ | $a^6S$ | - | $3d^6 4s$ | $a^4H$ | 34300 |
| $3d^6 4s$ | $a^6D$ | 17450 | $3d^6 4s$ | $a^4F$ | 35041 |
| $3d^5 4s4p$ | $z^8P°$ | 18531 | $3d^5 4s4p$ | $y^6P°$ | 35725 |
| $3d^6 4s$ | $a^4D$ | 23550 | $3d^6 4s$ | $b^4G$ | 37630 |
| $3d^5 4s^4 p$ | $z^6P°$ | 24788 | $3d^6 4s$ | $a^2H$ | 38060 |
| $3d^5 4s^2$ | $a^4G$ | 25285 | $3d^6 4s$ | $a^2F$ | 38669 |
| $3d^5 4s^2$ | $a^4P$ | 27248 | $3d^5 4s5s$ | $e^8S$ | 39431 |
| $3d^5 4s^2$ | $b^4D$ | 30400 | $3d^5 4s5s$ | $e^6S$ | 41404 |
| $3d^5 4s4p$ | $z^4P°$ | 31076 | $3d^6 4p$ | $z^6D$ | 42053 |
| $3d^6 4s$ | $b^4P$ | 34463 | $3d^6 4p$ | $z^6F°$ | 43524 |

TABLE cV : Premiers niveaux d'énergie du manganèse neutre (23)

| Mn I | Mn II | Mn III |
|---|---|---|
| Configuration $3d^5 4s^2$ | Configuration $3d^5 4s$ | Configuration $3d^5$ |
| $^6S$ 0 | $^7S$ 0<br>$^5S$ 9473 | $^6S$ 0 |
| $^4G$ 25285 | $^3G$ 34900<br>$^5G$ 27570 | $^4G$ 26850 |
| $^4P$ 27248 | $^3P$ 36364<br>$^5P$ 29920 | $^4P$ 29200 |
| $^4D$ 30400 | $^3D$ 39813<br>$^5D$ 32836 | $^4D$ 32350 |
| $^4F$ ? | $^3F$ ?<br>$^5F$ 43395 | $^4F$ 43604 |

TABLE cVI : Energie des premiers états des configurations fondamentales des ions Mn I, Mn II et Mn III

COMPLEMENT A L'ARTICLE 2 : ELECTRONIC STRUCTURE OF MnO

EFFET SPIN-ROTATION DANS LES ETATS $X^6\Sigma^+$ ET $A^6\Sigma^+$

Gordon et Merer (Can J. Phys. 58, 642 (1980) ) ont pu déterminer la valeur du paramètre d'intéraction spin-rotation $\gamma$ dans les états $X^6\Sigma^+$ et $A^6\Sigma^+$ de MnO.

Ces valeurs sont relativement faibles ($\gamma''_o = -0{,}0019\ cm^{-1}$ et $\gamma'_1 = -0.0021\ cm^{-1}$).

Il est possible d'en donner une interprétation à partir des résultats obtenus sur la structure électronique de MnO.

La contribution prépondérante à ce paramètre est en effet due aux interactions du second ordre introduites par les perturbations provenant des états $^6\Pi$ et $^6\Sigma^-$ voisins qui seuls créent une dépendance en $(J + \frac{1}{2})$ du paramètre $\gamma$, les états de multiplicité supérieure ou inférieure n'introduisant que des termes constants dans l'énergie des niveaux.

En conséquence, l'expression de $\gamma$ pour un niveau v donné d'un état $^6\Sigma^+$ est :

$$\gamma_v = \gamma_{NS} - \sum_{i,v'} \frac{4\eta_{vv',i}(\xi_{vv',i} - \eta_{vv',i})}{E(^6\Pi_i,v') - E(^6\Sigma^+,v)} - \sum_{j,v'} \frac{^6B_{vv',j}\ \xi_{vv',j}}{E(^6\Sigma^-_{j,v'}) - E(^6\Sigma^+,v)}$$

où $\eta_{vv',i} = \frac{1}{2} < {}^6\Pi_{i,1/2,v'} \left| \sum_k B\ell_k^+ \right| {}^6\Sigma^+_{\frac{1}{2},v} >$

$\xi_{vv',i} = < {}^6\Pi_{i,1/2,v'} \left| \sum_k \frac{1}{2} a_k (\ell_k^+ s_k^- + \ell_k^- s_k^+) \right| {}^6\Sigma^+_{1/2,v} >$

$\xi_{vv',j} = < {}^6\Sigma^-_{j,1/2,v'} \left| \sum_k a_k \ell_{z_k} s_{z_k} \right| {}^6\Sigma^+_{1/2,v} >$

$B_{vv',j} = < {}^6\Sigma^-_{j,1/2,v'} \left| \frac{\hbar^2}{2\mu R^2} \right| {}^6\Sigma^+_{1/2,v} >$

Pour évaluer théoriquement $\gamma_v$, nous négligerons $\gamma_{NS}$ représentant la partie spin-rotation pure qui est faible pour les molécules lourdes.

En ce qui concerne le reste de la valeur du paramètre $\gamma$, c'est à dire les perturbations par les états ${}^6\Pi$ et ${}^6\Sigma^-$, nous nous limiterons aux termes les plus importants, ceux qui couplent la configuration prédominante de chacun des états $X^6\Sigma^+$ et $A^6\Sigma^+$ avec les configurations qui en diffèrent par une monoexcitation électronique. Les monoexcitations considérées correspondent à un saut d'un électron de valence vers les orbitales virtuelles les plus basses ou éventuellement, pour l'état $A^6\Sigma^+$, à une réorganisation interne de la distribution des électrons dans les orbitales occupées.

D'autre part il faut noter qu'on ne doit attendre d'interaction importante qu'entre états ne différant que par des orbitales moléculaires centrées, du moins partiellement sur la même orbitale atomique, à l'exclusion des orbitales s.

Considérons d'abord l'état fondamental $X^6\Sigma^+$ de configuration prédominante ($8\sigma^2\ 3\pi^4\ 9\sigma\ 4\pi^2\ 1\delta^2$). En se restreignant aux orbitales externes, les états $^6\Pi$ qui peuvent interagir avec l'état $X^6\Sigma^+$ proviennent soit d'une monoexcitation $8\sigma(2p_o + 4s_{Mn})$, $9\sigma(3d_{Mn})$ ou $1\delta(3d_{Mn})$ vers $5\pi(4p_{Mn})$, soit d'une monoexcitation $3\pi(2p_o)$ ou $4\pi(3d_{Mn})$ vers $10\sigma(4s_{Mn})$ ou $11\sigma(4p_{Mn})$. Les localisations atomiques précisées entre parenthèses montrent qu'aucune de ces interactions ne correspond à deux orbitales moléculaires centrées sur la même orbitale atomique et qu'en conséquence la contribution des états $^6\Pi$ à la valeur du paramètre $\gamma$ doit être faible*. De même, les états $^6\Sigma^-$ qui peuvent interagir avec l'état $X^6\Sigma^+$ proviennent soit de monoexcitations $8\sigma(2p_o + 4s_{Mn})$, $9\sigma(3d_{Mn})$ ou $1\delta(3d_{Mn})$ vers $10\sigma(4s_{Mn})$ ou $11\sigma(4p_{Mn})$ soit de monoexcitations $3\pi(2p_o)$ ou $4\pi(3d_{Mn})$ vers $5\pi(4p_{Mn})$. Là encore, on voit que la contribution des états $^6\Sigma^-$ à la valeur du paramètre $\gamma$ est faible.

Considérons maintenant l'état excité $A^6\Sigma^+$ de configuration ($8\sigma\ 3\pi^4\ 9\sigma\ \ 4\pi^2\ 1\delta^2\ 10\sigma$). Les monoexcitations à prendre en compte sont :

- d'une part les sauts d'une orbitale occupée vers une orbitale virtuelle (y compris $10\sigma$) ; nous venons de voir que les interactions correspondantes n'apportent pas de contribution significative à $\gamma(A^6\Sigma^+)$
- d'autre part les réorganisations de la distribution des électrons à l'intérieur des orbitales de valence. Dans ce cas, on peut obtenir des interactions fortes avec les états $^6\Pi$, dues en particulier à des excitations $9\sigma \rightarrow 4\pi$ $\ 4\pi \rightarrow 9\sigma$ $\ 4\pi \rightarrow 1\delta$ ou $1\delta \rightarrow 4\pi$ puisque toutes ces excitations mettent en jeu des composantes $\lambda$ de l'orbitale atomique $3d_{Mn}$. Cependant on peut

---

* Pour fixer les idées, dans le cas favorable d'une précession pure sur l'orbitale 3d entre deux états distants de 20 000 $cm^{-1}$, on peut estimer que le paramètre $\gamma$ vaudrait environ 0,04 $cm^{-1}$, c'est à dire vingt fois la valeur trouvée expérimentalement.

supposer que ces interactions vont se compenser deux par deux. En effet, puisque l'orbitale $9\sigma$ est légèrement moins stable que l'orbitale $4\pi$, les états de la configuration $(8\sigma 3\pi^4 (9\sigma)^0 4\pi^3 1\delta^2 10\sigma)$ provenant d'une monoexcitation $9\sigma \rightarrow 4\pi$ doivent être situés en dessous de la configuration de l'état $A^6\Sigma^+$. Par contre les états de la configuration $(8\sigma\ 3\pi^4\ 9\sigma^2\ 4\pi\ 1\delta^2\ 10\sigma)$ provenant d'une monoexcitation $4\pi \rightarrow 9\sigma$ seront situés au-dessus. Les effets répulsifs de perturbation agiront en sens inverse. On peut faire un raisonnement analogue pour les excitations $4\pi \rightarrow 1\delta$ et $1\delta \rightarrow 4\pi$.

Globalement, on peut donc s'attendre à ce que le paramètre $\gamma$ de l'état $A^6\Sigma^+$ soit lui aussi très faible.

Ce complément permet de justifier qualitativement pourquoi les valeurs de $\gamma$ obtenues expérimentalement par Gordon et Merer sont si faibles. Le fait qu'elles soient en plus, pratiquement égales peut être justifié en remarquant que les configurations prédominantes des états $X^6\Sigma^+$ et $A^6\Sigma^+$ étant très voisines (elles ne diffèrent en effet que par une excitation d'une orbitale liante $8\sigma$ vers sa contrepartie antiliante $10\sigma$) les diverses interactions avec des états $^6\Pi$ et $^6\Sigma^-$ doivent être pour la plupart analogues dans les deux états.

ARTICLE N° 3

JOURNAL OF MOLECULAR SPECTROSCOPY 68, 81–88 (1977)

# Rotational Analysis of a Red $A'\ ^2\Sigma^+$–$X\ ^2\Pi_i$ System of CuO

Y. LEFEBVRE, B. PINCHEMEL, AND J. SCHAMPS

*Laboratoire de Spectroscopie des molécules diatomiques, Equipe de Recherche associée au C.N.R.S. n° 303, U.E.R. de Physique Fondamentale, Université de Lille I, B.P. 36-59650 Villeneuve d'Ascq, France*

High dispersion rotational analysis of a red CuO band system has led to the identification of an $A'\ ^2\Sigma^+$–$X\ ^2\Pi_i$ transition. The anomalous appearance of the branches is due to a very large spin splitting of the $^2\Sigma$ upper state. The influence of centrifugal distortion effects on this spin splitting ($\gamma_D$ and $\gamma_H$ parameters) is essential for explaining the band structure. A reassignment of electronic symmetries of all the $^2\Sigma$ states of CuO is proposed.

## INTRODUCTION

The emission spectrum of copper monoxide in the visible region is made of many band systems. Due to their complex structures, various interpretations have been given in earlier studies (*1–3*). The most recent rotational analysis (*4–7*) seems to indicate that all of the observed electronic transitions are doublet–doublet transitions which involve as lower states the two components of an inverted $^2\Pi$ state presently considered as the ground state and labeled $X\ ^2\Pi_i$. This state exhibits a fairly large spin–orbit splitting ($A = -277\ cm^{-1}$) and its main spectroscopic constants have been determined accurately by Appelblad and Lagerqvist (*4*).

In 1945, using exploding-wire techniques, Lejeune and Rosen (*8*) reported the occurrence of two bandheads around 6500 Å which appeared to them as "wide and diffuse." Since this early work, no new investigation has been attempted to study these bands. By use of a nitrogen-cooled C.W.H.C. lamp (composite wall hollow cathode) (*9*) described elsewhere (*6*), we have photographed them in the second order of a plane-grating spectrograph (inverse dispersion at 6500 Å: 0.65 Å/mm, effective resolution: 300 000). In spite of the high luminosity of the source, the obtaining of sufficiently intense spectra requires long exposure times (up to 8 hr). The low temperature of the discharge allows one to obtain well-resolved bands and to avoid the troublesome band overlapping arising from high-temperature sources such as arc discharges. Thus it gives negligible intensity to the end of the $\Delta v = -1$ and $\Delta v = -2$ sequences of the orange $A\ ^2\Sigma$–$X\ ^2\Pi$ system which in other sources would superimpose the bands studied here.

## DESCRIPTION AND NATURE OF THE BANDS

The group of bands around 6500 Å is composed of numerous branches divided in two subsystems with red-shaded heads at 6429.7 and 6436.3 Å for the first subsystem





ISSN 0022-2852

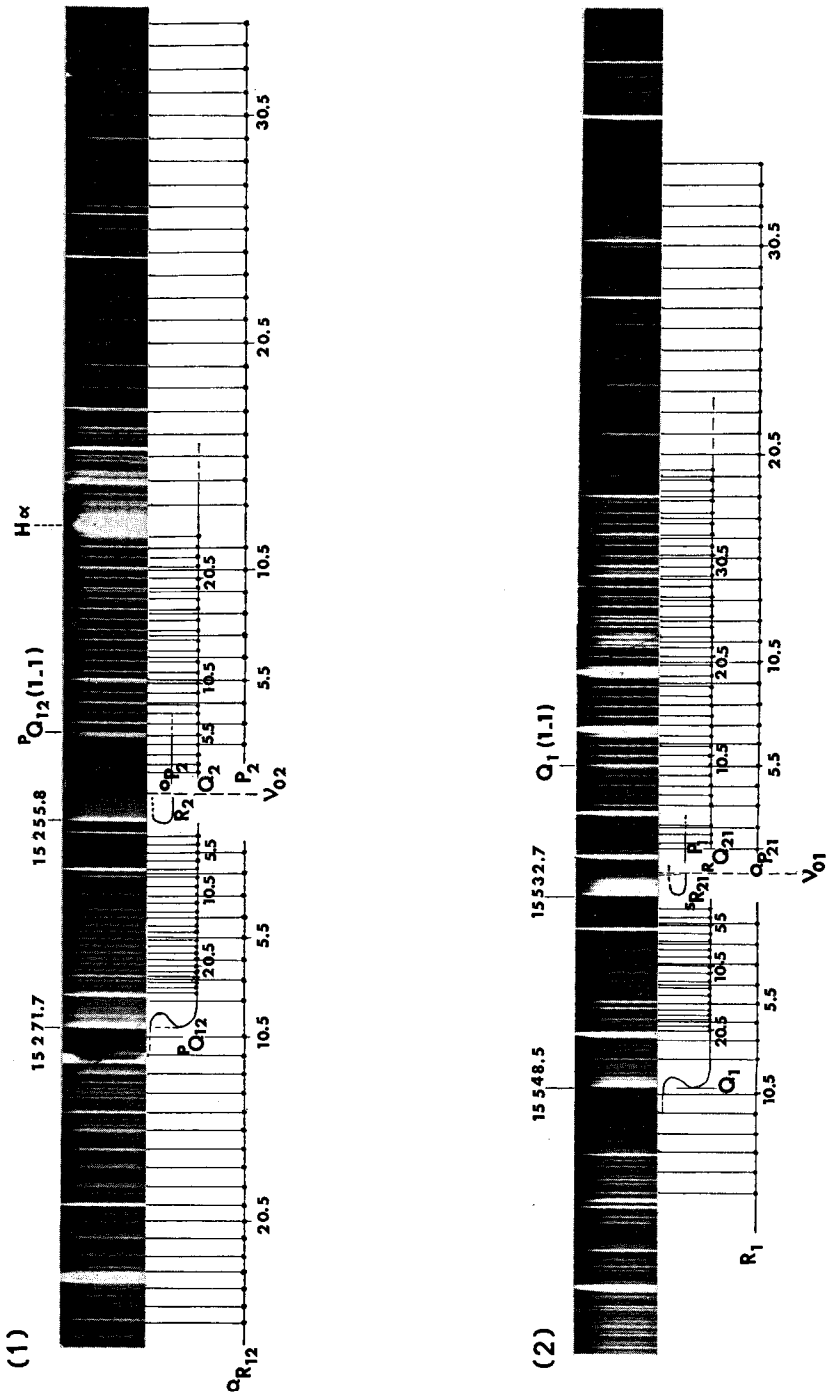


FIG. 1. Spectrogram of the 0–0 subbands of the new $A'\,^2\Sigma^+$–$X\,^2\Pi_i$ system of CuO. (1) $A'\,^2\Sigma^+$–$X\,^2\Pi_{\frac{1}{2}}$ transition. (2) $A'\,^2\Sigma^+$–$X\,^2\Pi_{\frac{3}{2}}$ transition.

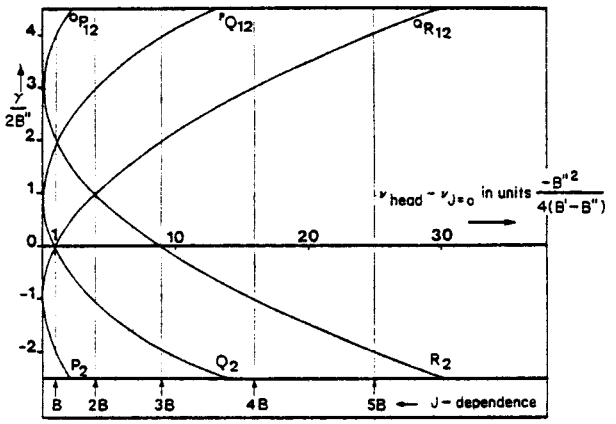


FIG. 2. Location of heads in a $^2\Sigma$–$^2\Pi_i$ transition as a function of spin splitting. Reduced units are used for sake of generality. At the bottom of the figure, the value of the $J$-coefficient is given for each branch whose head occurs at the vertical of the corresponding arrow (assuming that $B'$ and $B''$ have practically a common value, $B$).

and at 6546.3 and 6553.1 Å for the second one. This second subsystem lies close to the band observed at 6522.1 Å and was recently analyzed as a $^2\Delta_i$–$X^2\Pi_i$ transition (*10*). The structures of the two new subsystems appear to be very alike (Fig. 1). Corresponding heads are separated by 277 $cm^{-1}$, which is just the spin-orbit splitting of the $X^2\Pi_i$ ground state.

Therefore, we can a priori assume, and this will be confirmed later by the analysis, that the bands are the two subsystems of a $^2\Sigma(b)$–$X^2\Pi(a)$ transition. However, the appearance of the branches is somewhat anomalous. It is well known (*11*) that, in ordinary circumstances, the branches of a case ($b$)–case ($a$) transition have approximate $J$-dependences either proportional to $BJ$ or to 3 $BJ$. Here, the $J$-dependences of the branches are roughly proportional to zero $BJ$, 2 $BJ$, and 4 $BJ$. Such a behavior can be explained by assuming that the spin-splitting constant of the $^2\Sigma$ state is much larger than usual. Neglecting $J$-dependences of degree higher than 2 in the branches, we have plotted, in Fig. 2, a diagram showing the link between the value of $\gamma$ and the location of the bandheads of a $^2\Sigma$–$^2\Pi$ transition. From this diagram, the situation encountered here for the $J$-dependences of the branches can formally correspond to two possible values of $\gamma$, one positive ($\gamma$ of the order of 6 $B''$), the other negative ($|\gamma|$ of the order of 2 $B''$). Choosing the sign of $\gamma$ determines the labeling of branches. In the following, we shall arbitrarily adopt the labeling corresponding to a positive value of $\gamma$. This choice will be justified in the next section.

## ANALYSIS AND RESULTS

### (*a*) *Energy Levels*

The rotational energy levels of the $X^2\Pi$ state are given by Appelblad and Lagerqvist (*4*):

$$^2\Pi_i \begin{matrix} F_{1e}(J) \\ F_{1f}(J) \end{matrix} = B_i J(J+1) - D_i J^2(J+1)^2 \pm \tfrac{1}{2}a(J+\tfrac{1}{2})(J-\tfrac{1}{2})(J+\tfrac{3}{2}), \qquad (1)$$

$$^2\Pi_{\frac{1}{2}}\begin{matrix}F_{2e}(J)\\F_{2f}(J)\end{matrix} = B_{\frac{1}{2}}J(J+1) - D_{\frac{1}{2}}J^2(J+1)^2 \pm \tfrac{1}{2}[p + p_J J(J+1)](J+\tfrac{1}{2}), \quad (2)$$

where degenerate levels have the parity $(-1)^{J-\frac{1}{2}}$ for $e$ levels and $-(-1)^{J-\frac{1}{2}}$ for $f$ levels (*12*).[1]

Rotational energy levels of a case (*b*)–$^2\Sigma$ state are usually well fitted by using Van Vleck's expressions (*13*)

$$^2\Sigma\begin{matrix}F_1(N) = BN(N+1) - DN^2(N+1)^2 + \tfrac{1}{2}\gamma N & \text{with} \quad N = J - \tfrac{1}{2}, \quad (3)\\ F_2(N) = BN(N+1) - DN^2(N+1)^2 - \tfrac{1}{2}\gamma(N+1) & \text{with} \quad N = J + \tfrac{1}{2}, \quad (4)\end{matrix}$$

where parities are $F_{1e}$ and $F_{2f}$ for $^2\Sigma^+$ states and $F_{1f}$ and $F_{2e}$ for $^2\Sigma^-$ states.

However, the term values of the $^2\Sigma$ state involved as upper state in the present transition deviate strongly from these simple formulas. Such an anomaly has been found previously, yet to a much lower extent, in other molecules and explained as due both to the dependence of the energy difference between the interacting $^2\Sigma$ and $^2\Pi$ states on the rotational quantum number (*14*) and to the centrifugal distortion (*15*). In order to take these effects into account, one has to replace $\gamma$ in Eqs. (3) and (4) by a $J$-dependent parameter

$$\gamma_{eff} = \gamma + \gamma_D J(J+1) + \gamma_H J^2(J+1)^2. \quad (5)$$

This modification of Van Vleck's formulas proves to be essential for our analysis.

### (*b*) *Electronic Parity of the A'*$^2\Sigma$ *State*

Combination differences have been used to determine the line numbering of branches. Thus, the combination differences between the $Q_2(J)$ and $P_2(J+1)$ lines are equal to $(2B'' \pm p)(J+1)$, the sign before $p$ being minus for a $^2\Sigma^+$ upper state and plus for a $^2\Sigma^-$ one in the hypothesis when $\gamma$ is positive, the opposite if $\gamma$ is negative (in this case, names of branches are to be changed according to Fig. 2). Now, the value of $(2B'' \pm p)$ is experimentally found to be greater than $2B''$. Therefore if the ground-state $\Lambda$-doubling constant $p$ is positive (as assumed by Appelblad and Lagerqvist (*4*)), the upper state is a $\Sigma^+$ state if $\gamma$ is negative and a $\Sigma^-$ state if $\gamma$ is positive, the result being opposite if $p$ is negative. In other words, whatever the sign of $p$ could be, combination differences show that if $\gamma$ is negative the $^2\Sigma$ upper state of the presently studied transition has the same electronic symmetry as the upper state of the orange system (with the negative value of $-0.195$ cm$^{-1}$ for its $\gamma$ constant), whereas if $\gamma$ is positive, it has an opposite symmetry. This discussion is summarized in the first two rows of Table I (hypotheses a and b).

However, Appelblad and Lagerqvist's hypothesis of a positive sign for the $\Lambda$-doubling constant $p$ of $X\,^2\Pi_i$ is quite debatable since it only relied on the statement that the $A\,^2\Sigma$ state must be of $\Sigma^+$ electronic symmetry because $\Sigma^+$ states are more frequently observed than $\Sigma^-$ states. This justification no longer stands since another $\Sigma$ state of opposite

[1] Note that Appelblad and Lagerqvist's definition of the $p$-parameter is just the opposite of the common definition (*12*). However, we have come to the decision of using their definition throughout this work in order to remain in agreement with the previous studies on CuO.

TABLE I

Electronic Symmetry of $A\,^2\Sigma$ and $A'\,^2\Sigma$ States of CuO

| Sign of $p$ according to rel. (2) | $A\,^2\Sigma$ | | $A'\,^2\Sigma$ | |
|---|---|---|---|---|
| | Electronic symmetry | $\gamma$ Value ($cm^{-1}$) | Electronic symmetry | $\gamma$ Value ($cm^{-1}$) |
| $p > 0$ | $\Sigma^+$ | $-0.19$ | $\Sigma^+$ | $-0.68$ (a) |
| | | | $\Sigma^-$ | $+2.40$ (b) |
| $p < 0$ | $\Sigma^-$ | $-0.19$ | $\Sigma^-$ | $-0.68$ (c) |
| | | | $\Sigma^+$ | $+2.40$ (d) |
| $p > 0$ | $\Sigma^-$ | $+1.92$ | $\Sigma^+$ | $-0.68$ (e) |
| | | | $\Sigma^-$ | $+2.40$ (f) |
| $p < 0$ | $\Sigma^+$ | $+1.92$ | $\Sigma^-$ | $-0.68$ (g) |
| | | | $\Sigma^+$ | $+2.40$ (h) |

parity has been observed subsequently (*5*). Moreover, a negative sign of $p$ *defined* in Eq. (2) seems more adequate since the $(\pi^4\,\pi'^3\,\sigma^2)$ $X\,^2\Pi_i$ ground state is most likely in more or less pure precession with the higher-lying $(\pi^4\,\pi'^4\,\sigma)\,^2\Sigma^+$ state (as yet unobserved, however). Associated with the combination differences of both the $A$–$X$ and $A'$–$X$ systems, this new hypothesis ($p < 0$) leads to lines (c) and (d) of Table I. In this table we have also reported the possibility of the other (positive) value of $\gamma$ ($\gamma = 1.92$ $cm^{-1}$) which, according to Fig. 2, fits the lines of the orange system $A\,^2\Sigma$–$X\,^2\Pi$ as well as the negative value of $-0.195$ $cm^{-1}$. But so great a value of $\gamma$ would imply a significant value of $\gamma_D$ in this $A\,^2\Sigma$ state; this is not in agreement with the experimental situation (*4*).

Now, the $A\,^2\Sigma$ and $A'\,^2\Sigma$ states can be expected to belong to a single configuration, probably $(\pi^3\,\pi'^3\,\sigma^2\,\sigma')$ (*16*), and are likely to have opposite electronic symmetries. Moreover, the very high values of the centrifugal distortion constants, $\gamma_D$ and $\gamma_H$, lead one to think that, in absolute values, $\gamma$ is much greater in the $A'\,^2\Sigma$ state than in the other observed $A\,^2\Sigma$ state of CuO. From Table I, the solution which fulfills all these statements corresponds to hypothesis (d):

$p(X\,^2\Pi_{\frac{1}{2}}) = -0.0159$ $cm^{-1}$,

$\gamma(A\,^2\Sigma^-) = -0.1952$ $cm^{-1}$,

$\gamma(A'\,^2\Sigma^+)$ positive (its values given in Table I will be determined in the following).

(*c*) *Results*

On the basis of the term values given in Eqs. (1) to (5) (including terms up to the fifth power in $J$ in $A'\,^2\Sigma^+$) a least-squares fitting gives the following constants for the $A'\,^2\Sigma^+$ state (in $cm^{-1}$):

$$T_0 = 15531.90, \qquad \gamma = 2.400,$$

$$B_0 = 0.4382_8 \qquad \gamma_D = -2.36 \times 10^{-4},$$

$$D_0 = 1.38_4 \times 10^{-6}, \qquad \gamma_H = 4.28 \times 10^{-8}.$$

TABLE II

Lines of the 0–0 Bands of the $A'\,^2\Sigma^+$–$X\,^2\Pi_i$ Transition

| J | $R_1$ | $Q_1$ | $^SR_{21}$ | $P_1$ | $^RQ_{21}$ | $^QP_{21}$ | $^QR_{12}$ | $^PQ_{12}$ | $R_2$ | $^QP_{12}$ | $Q_2$ | $P_2$ |
|---|---|---|---|---|---|---|---|---|---|---|---|---|
| 1.5 | 15535.30 | | | | | | - | | | | 15252.22 | |
| | 536.90 | | | | 15528.55 | | - | | | | 251.43 | |
| | 538.47 | 15533.80 | | | 527.78 | 525.37 | 15261.43 | | | | 250.66 | 15248.24 |
| | 540.10 | 534.51 | | | 526.90 | 523.73 | 263.05 | 15257.42 | | | 249.85 | 246.60 |
| 5.5 | 541.70 | 535.20 | | | - | 522.05 | 264.60 | 258.10 | | | 249.09 | 244.93 |
| | 543.20 | 535.95 | | | 525.37 | 520.38 | 266.20 | 258.78 | | | 248.26 | 243.25 |
| | 544.72 | 536.54 | | | 524.54 | - | 267.74 | 259.46 | | | 247.49 | 241.51 |
| | 546.30 | 537.29 | | | 523.73 | 517.02 | 269.29 | 260.13 | | 15251.43 | 246.71 | 239.86 |
| | - | 537.88 | | | 522.94 | 515.30 | 270.81 | 260.78 | | 251.89 | 245.93 | 238.17 |
| 10.5 | 549.37 | 538.51 | | | 522.12 | 513.65 | 272.35 | 261.43 | | 251.71 | 245.12 | 236.48 |
| 11.5 | 550.89 | 539.14 | | | 521.33 | 511.96 | 273.86 | 262.02 | | 251.43 | 244.33 | 234.81 |
| | 552.30 | 539.80 | | | 520.50 | 510.29 | 275.37 | 262.61 | | 251.15 | 243.56 | - |
| | 553.80 | 540.38 | | | 519.68 | 508.58 | 276.85 | 263.21 | | 250.94 | 242.72 | 231.43 |
| | 555.30 | 540.97 | | | - | 506.86 | 278.33 | 263.83 | | 250.66 | 241.93 | - |
| 15.5 | 556.65 | 541.47 | | 15527.25 | 518.08 | 505.19 | 279.70 | 264.32 | | 250.40 | 241.15 | 228.05 |
| | 558.05 | 542.02 | | 526.90 | 517.26 | - | 281.15 | 264.90 | | - | 240.36 | 226.34 |
| | 559.45 | 542.49 | | 526.60 | 516.45 | | 282.53 | 265.45 | | 249.78 | 239.56 | 224.64 |
| | - | 543.05 | | - | 515.63 | 501.81 | 283.94 | 265.84 | | | 238.78 | - |
| | 562.10 | 543.56 | | - | 514.81 | 500.14 | - | 266.43 | | | 237.98 | 221.28 |
| 20.5 | 563.43 | - | | 525.45 | 514.03 | 498.40 | 286.65 | 266.86 | | | 237.18 | 219.59 |
| 21.5 | 564.70 | | | - | 513.22 | 496.73 | 287.90 | 267.29 | | | 236.42 | 217.91 |
| | 565.98 | | | 524.80 | 512.41 | 495.05 | 289.20 | 267.74 | | | 235.61 | 216.22 |
| | 567.25 | | | 524.10 | 511.60 | 493.30 | - | 268.13 | | | 234.81 | 214.53 |
| | 568.50 | | | 523.80 | 510.75 | | 291.75 | 268.54 | | | 233.99 | 212.85 |
| 25.5 | 569.63 | | | 523.16 | 509.98 | | 293.03 | - | | | | 211.16 |
| | | | | | 509.14 | | 294.25 | - | | | 232.44 | 209.48 |
| | | | | | 508.32 | | 295.40 | 269.59 | | | 231.62 | 207.80 |
| | | | | | 507.49 | | 296.57 | | | | 230.83 | 206.11 |
| | | | | | 506.65 | | 297.64 | | | | 229.99 | 204.43 |
| 30.5 | | | | | 505.83 | | 298.82 | | | | 229.20 | 202.73 |
| 31.5 | | | | | 505.00 | | 299.90 | | | | 228.41 | 201.04 |
| | | | | | 504.13 | | 300.99 | | | | 227.57 | 199.33 |
| | | | | | 503.27 | | 302.00 | | | | 226.78 | 197.65 |
| | | | head | | 502.41 | | 302.98 | | head | | 225.98 | |
| | | | 15532.7 | | 501.53 | | 303.98 | | 15255.8 | | 225.06 | |
| | | | | | 500.65 | | 304.96 | | | | 224.21 | |

With these constants all lines are fitted to an accuracy better than 0.05 $cm^{-1}$ (Table II). The spin-doubling constants are several orders of magnitude larger than in standard cases. By itself, this fact is sufficient to explain the unusual appearance of the spectrum. Thus, it was already noticed above that the large value of $\gamma$ was responsible for the anomalous $J$-dependences in zero $B$, $2B$, and $4B$ of the branches instead of $B$ and $3B$.

Other consequences affect the higher-order dependences of the branches. Thus, although the $(B' - B'')$ difference represents the largest part of the $J^2$-coefficients, it is worthwhile noting that, because of its unusually large value, $\gamma_D$ also contributes appreciably to these coefficients. Since this contribution is not the same in each branch, this yields the strange result that the $J^2$-coefficients are fairly different from one branch to the other (extreme values in $cm^{-1}$: $-0.00303$ in $R_2$ and $-0.00407$ in $^QR_{12}$). In the same way, the $J^4$-coefficients of the branches are also widely different because of the nonnegligible value of $\gamma_H$ compared to the $(D' - D'')$ difference of the centrifugal distortion rotational constants.

The $B_0$ rotational constant of $A'\,^2\Sigma^+$ is quite close to the corresponding constant of

the ground state so that all the $J^2$-coefficients are fairly small. This explains why, at least for the lowest $J$-values, several branches such as $Q_2$, $P_2$, $^RQ_{21}$ and $^QP_{21}$ appear to have a linear-in-$J$ evolution.

We can also notice that, for higher values of $J$ than those observed with our low-excitation source, extra heads are expected to occur in the $^PQ_{12}$ and $Q_1$ branches. Likewise, the centrifugal distortion of the spin-doubling constant prevents the $^QR_{12}$ and $R_1$ branches from forming heads, as would be expected in more traditional spectra.

*(d) Vibrational Assignments*

The separation between the origins of the two subsystems has been found here to be equal to 277.10 $cm^{-1}$. This is to be compared to the separation of 277.04 $cm^{-1}$ between the $v = 0$ levels of the two spin–orbit components of the $X\,^2\Pi_i$ ground state given by Appelblad and Lagerqvist (*4*). This rather good agreement confirms that all the bands studied here involve the $v = 0$ levels of the ground state. The observation of the weak isotopic shifts between the lines of $^{63}Cu\,^{16}O$ and $^{65}Cu\,^{16}O$ (abundance ratio: 69.1%) proves that the transitions are $\Delta v = 0$ transitions so that the vibrational level of $A'\,^2\Sigma^+$ implied here is also a $v = 0$ level.

The 0–0 band that we have analyzed overlaps other weak heads which also belong to the $\Delta v = 0$ sequence of the $A'\,^2\Sigma^+$–$X\,^2\Pi_i$ transition. These heads [$^PQ_{12}(1\text{–}1)$:15 249.1 $cm^{-1}$; $^PQ_{12}(2\text{–}2)$:15 226.2 $cm^{-1}$; $Q_1(1\text{–}1)$:15 532.7 $cm^{-1}$] are more visible in our spectra but the rotational analysis of the associated band is quite impossible. From this we deduce the following approximate vibrational constants for $A'\,^2\Sigma^+$:

$$\omega_e' = 614.0\ cm^{-1} \qquad \omega_e'x_e' = 4.5\ cm^{-1}.$$

Using this value of $\omega_e$ and the value of $B_0$ determined above, and assuming a Morse potential for the $A'\,^2\Sigma^+$ state, one can expect a value of $D_0 = 0.89 \times 10^{-6}$ $cm^{-1}$ for the centrifugal distortion constant of this state. The experimental value is fairly large ($D_0 = 1.38 \times 10^{-6}$ $cm^{-1}$) and it is likely that it represents an effective parameter including not only centrifugal distortion effects but also an effect due to the probable proximity of the interacting $^2\Pi$ levels from $A'\,^2\Sigma^+$ as discussed by Kovacs (*14*) from a general point of view.

## CONCLUSION

The coherence of the present analysis can be considered as a gratifying test of the correctness of the model for representing the term values [Eqs. (1) to (5)], especially as for the rotational dependence of the $\gamma_D$ and $\gamma_H$ spin-doubling constants.

The high value obtained for the $\gamma$ parameter suggests that the $A'\,^2\Sigma^+$ state strongly interacts with a nearby $^2\Pi_i$ state. Therefore, it could be more suitable to use Hund's case-$c$ notation for describing the $A'$ state and to call it simply a $\Omega = \frac{1}{2}$ electronic state rather than a $^2\Sigma^+$ state. Anyway, this distinction has no impact on the phenomenological formulas describing the energy structure of the $A'$ state but, as pointed out by Veseth (*17*, *18*), it may be important for understanding the real meaning of the effective spin-doubling parameters or for comparing branch intensities. These problems will be the subject of further studies.

RECEIVED: April 5, 1977

## REFERENCES


1. A. GUNTSCH, *Ark. Mat. Astron. Fys. A* 33, No. 2 (1946).
2. A. ANTIC-JOVANOVIC, D. S. PESIC, AND G. GAYDON, *Proc. Roy. Soc. London Ser. A* 307, 399 (1968).
3. A. LAGERQVIST AND U. UHLER, *Z. Naturforsch. B* 22, 551 (1967).
4. O. APPELBLAD AND A. LAGERQVIST, *Phys. Scrip.* 10, 307 (1974).
5. O. APPELBLAD AND A. LAGERQVIST, *Canad. J. Phys.* 53, 2221 (1975).
6. Y. LEFEBVRE, B. PINCHEMEL, AND R. BACIS, *Canad. J. Phys.* 54, 735 (1976).
7. O. APPELBLAD AND A. LAGERQVIST, *Phys. Scrip.* 13, 274 (1976).
8. J. M. LEJEUNE AND B. ROSEN, *Bull. Soc. Roy. Sci. Liege* 14, 81 (1945).
9. R. BACIS, *J. Phys. E* 9, 1081 (1976).
10. B. PINCHEMEL, Y. LEFEBVRE, AND J. SCHAMPS, to appear.
11. G. HERZBERG, "Spectra of Diatomic Molecules," Van Nostrand, New York, 1950.
12. I. KOPP AND J. T. HOUGEN, *Canad. J. Phys.* 45, 2581 (1967).
13. J. H. VAN VLECK, *Phys. Rev.* 33, 467 (1929).
14. I. KOVACS, *Bull. Sci. Chim. Ind. Bologna* 21, 44 (1963).
15. L. VESETH, *J. Phys. B* 3, 1677 (1970).
16. J. SCHAMPS, B. PINCHEMEL, AND Y. LEFEBVRE, to appear.
17. L. VESETH, *J. Mol. Spectrosc.* 44, 251 (1972).
18. L. VESETH, *J. Phys. B* 6, 1484 (1973).

ARTICLE N° 4

J. Phys. B: Atom. Molec. Phys., Vol. 10, No. 16, 1977. Printed in Great Britain. 

# Spectrum of CuO: a red $^2\Delta$–x $^2\Pi_i$ transition

B Pinchemel, Y Lefebvre and J Schamps

Laboratoire de Spectroscopie des Molécules Diatomiques, Equipe de Recherche associée au CNRS No 303, Université de Lille I, Bâtiment P5, BP36, 59650 Villeneuve d'Ascq, France

Received 4 March 1977, in final form 14 June 1977

**Abstract.** A new band of CuO with head at 6522·1 Å has been analysed and interpreted as a $^2\Delta_{5/2}$–x $^2\Pi_{3/2}$ transition. The constants derived for the new $^2\Delta_{5/2}$ state are (in cm$^{-1}$): $T_0 = 15317{\cdot}24$, $B_0 = 0{\cdot}4253_6$, $D_0 = 0{\cdot}84_5 \times 10^{-6}$.

The red part of the emission spectrum of CuO has been reinvestigated using a composite-wall hollow cathode (CWHC) previously described elsewhere (Bacis 1976, Lefebvre *et al* 1976). Spectra were photographed in the second order of a 4 m plane-grating spectrograph with an aperture of *f*/20 (inverse dispersion at 6500 Å: 0·65 Å mm$^{-1}$; effective resolution: 300000).

Among the numerous heads occurring between 6450 and 6550 Å, one red-degraded band with a head at 6522·1 Å, exhibits a remarkably regular structure and cannot be associated with any other band analysed in the region. This band has very low intensity and has not been observed before: exposures of 15 hours were necessary to produce workable spectrograms such as that of figure 1 (plate).

The appearance of a Q branch and the higher intensity of the R branch compared to the P branch suggest that the transition corresponds to $\Delta\Lambda = +1$. The $R(J-1) - Q(J)$ combination differences establish the line numbering (table 1) and indicate that the lower state is the $v = 0$ level of the x $^2\Pi_i$ ground state whose spectroscopic constants were given by Appelblad and Lagerqvist (1974, 1976). No $\Lambda$-type doubling is visible; the band is therefore assigned to the transition $^2\Delta_{5/2}$–x $^2\Pi_{3/2}$. In such a transition the x $^2\Pi_{3/2}$ $\Lambda$-type splitting, which would be the largest cause of $\Lambda$-type doubling for the band, is negligible (it is about 0·013 cm$^{-1}$ at $J = 40{\cdot}5$), far below the resolving power of the spectrograph. Consequently the term values in each transition state can be approximated by the classical case (a) formula (Herzberg 1950):

$$T(J) = T_0 + BJ(J+1) - DJ^2(J+1)^2.$$

Least-squares fitting yields the following constants for the $^2\Delta_{5/2}$ state:

$$T_0(^2\Delta_{5/2}) = 15317{\cdot}24 \text{ cm}^{-1}$$
$$B = 0{\cdot}4253_6 \text{ cm}^{-1}$$
$$D = 0{\cdot}84_5 \times 10^{-6} \text{ cm}^{-1}.$$



A.M.P.(B). 10/16—D

**Table 1.** Lines of the 0–0 band of the $^2\Delta_{5/2}$–$X\ ^2\Pi_{3/2}$ system.

| $J$ | $R_1$ | $Q_1$ | $P_1$ |
|---|---|---|---|
| 1·5 | 15319·28 | | |
| | 20·10 | | |
| | 20·75 | | |
| | 21·52 | | |
| | 22·12 | | |
| 6·5 | 22·77 | 15316·41 | |
| | 23·40 | 16·16 | 15309·79 |
| | 23·91 | 15·87 | 8·60 |
| | 24·49 | 15·57 | 7·50 |
| | 24·97 | 15·20 | 6·25 |
| 11·5 | 25·42 | 14·81 | 5·01 |
| | 25·86 | 14·40 | 3·74 |
| | 26·25 | 13·94 | 2·45 |
| | 26·60 | 13·45 | 1·05 |
| | 26·91 | 12·91 | 15299·70 |
| 16·5 | 27·21 | 12·36 | 98·35 |
| | 27·47 | 11·75 | 96·90 |
| | 27·69 | 11·10 | 95·40 |
| | 27·89 | 10·47 | |
| | 28·04 | 9·79 | |
| 21·5 | | 9·05 | |
| | | 8·30 | |
| | | 7·50 | |
| | head 28·30 | 6·66 | |
| | | 5·79 | |
| 26·5 | | 4·96 | |
| | | 4·05 | |
| | 28·04 | 2·99 | |
| | 27·89 | 2·01 | |
| | 27·70 | 0·99 | |
| 31·5 | 27·47 | 299·93 | |
| | 27·21 | 98·82 | |
| | 26·91 | 97·74 | |
| | 26·60 | 96·57 | |
| | 26·24 | 95·32 | |
| 36·5 | 25·85 | 94·09 | |
| | 25·42 | 92·82 | |
| | 24·97 | | |
| | 24·45 | 90·19 | |
| | 23·88 | 88·84 | |
| 41·5 | 23·35 | — | |
| | | 85·96 | |
| | | 84·51 | |

The accuracy of the wavenumbers is about 0·03 $cm^{-1}$. Isotopic shifts between the $^{63}Cu^{16}O$ and $^{65}Cu^{16}O$ molecules (respective abundances 70% and 30%) confirm that the system is a $v' = 0 \rightarrow v'' = 0$ transition.

The enhancement of intensity of the lines beyond the Q(27·5) line is probably due to the R head of the $v' = 1 \rightarrow v'' = 1$ transition but the intensity of this head

J. Phys. B: Atom. Molec. Phys., Vol. 10, No. 16. © 1977—*B Pinchemel et al*

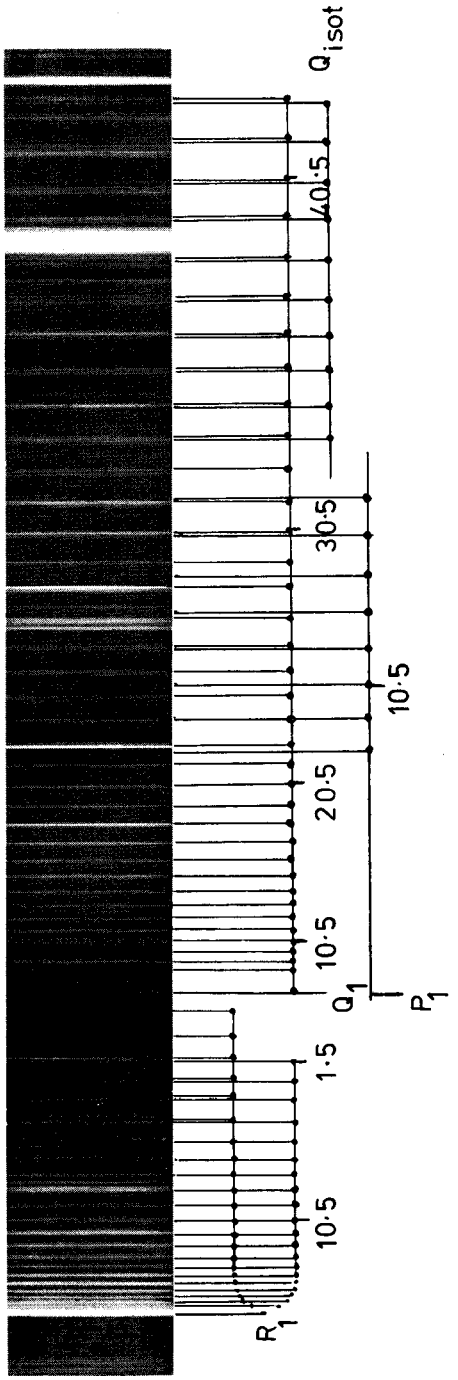


**Figure 1.** 0–0 band of the red $^2\Delta_{5/2}$–X $^2\Pi_{3/2}$ transition of CuO.

[facing page 3216]

observed at 6532·3 Å is too weak to allow any rotational analysis which would confirm this assignment. Anyway, this would give $\Delta G'(\frac{1}{2}) = 607{\cdot}3\ \text{cm}^{-1}$ for the $^2\Delta_{5/2}$ state.

An unresolved weak band lying at 6493·4 Å shows R and Q branches similar to the 6522 Å band. Although rotational analysis is not possible, it is not out of the question that this band may be the 0–0 band of the $^2\Delta_{3/2}$–X $^2\Pi_{1/2}$ sub-system. Under these circumstances, the distance between the $Q_1$ and $Q_2$ heads should be about 69·9 $\text{cm}^{-1}$ corresponding to a spin–orbit splitting of about $-347\ \text{cm}^{-1}$ for the $^2\Delta$ state of inverted character. This character is confirmed by the normal intensity distribution of branches whereas a $^2\Delta_r \rightarrow {}^2\Pi_i$ transition would give an abnormal intensity distribution (Douglas and Routly 1955).

## References

Appelblad O and Lagerqvist A 1974 *Phys. Scr.* **10** 307
——1976 *Phys. Scr.* **13** 275
Bacis R 1976 *J. Phys. E: Sci. Instrum.* **9** 1081
Douglas A E and Routly P M 1955 *Astrophys. J. Suppl.* **1** 295
Herzberg G 1950 *Spectra of Diatomic Molecules* (New York: Van Nostrand)
Lefebvre Y, Pinchemel B and Bacis R 1976 *Can. J. Phys.* **54** 735

Physica Scripta Vol. 18, 125–136, 1978

# The Spectrum of CuO: Rotational Analysis of Some Green Bands

O. Appelblad and A. Lagerqvist

Institute of Physics, University of Stockholm, Vanadisvägen 9, S-113 46 Stockholm, Sweden

and

Y. Lefebvre, B. Pinchemel and J. Schamps

Laboratoire de Spectroscopie des Molécules Diatomiques, Equipe de Recherche associée au CNRS No 303 Université de Lille I, Bâtiment P5, BP 36, 59650 Villeneuve d'Ascq, France

*Received March 17, 1978*

## Abstract

*The spectrum of CuO: Rotational analysis of some green bands.* O. Appelblad and A. Lagerqvist (Institute of Physics, University of Stockholm, Stockholm, Sweden) and Y. Lefebvre, B. Pinchemel and J. Schamps (Laboratoire de Spectroscopie des Molécules Diatomiques, Université de Lille I, France).
*Physica Scripta (Sweden) 18*, 125–136, 1978.

Two band systems of the emission spectrum of CuO in the green region have been rotationally analyzed, nameley the $C\,^2\Pi_i$–$X\,^2\Pi_i$ and $D\,^2\Delta_i$–$X\,^2\Pi_i$ systems. Molecular constants of the states are given.

## 1. Introduction

Until rather recently, the spectrum of the CuO molecule was only poorly known. During the last few years several rotational analyses have been made [1–8] leading to the knowledge of many electronic states. All experiments have been performed in emission. The systems analyzed up to now are located in the visible spectral region, from about 4200 Å to about 6600 Å.

Figure 5 in paper [6] represents an energy level diagram showing all electronic states of CuO analyzed at that time together with their molecular constants. In this diagram the transition $C\,^2\Pi_i$–$X\,^2\Pi_i$ is marked. The 0–0 bands of the $C\,^2\Pi_{3/2}$–$X\,^2\Pi_{3/2}$ and $C\,^2\Pi_{1/2}$–$X\,^2\Pi_{1/2}$ transitions are situated at 5312 and 5345 Å respectively. These two bands were rotationally analyzed [5]. The analysis of the 5345 Å band is not completely correct in all details. In the present paper we report analyses of these bands and other bands belonging to the $C$–$X$ system. It is of interest that also bands from the intercombination subsystems $C\,^2\Pi_{3/2}$–$X\,^2\Pi_{1/2}$ and $C\,^2\Pi_{1/2}$–$X\,^2\Pi_{3/2}$ have been observed and analyzed. In addition to the $C$–$X$ system another system in the green region has been found and analyzed, namely the $D\,^2\Delta_i$–$X\,^2\Pi_i$ system. The 0–0 bands of the $D\,^2\Delta_{5/2}$–$X\,^2\Pi_{3/2}$ and $D\,^2\Delta_{3/2}$–$X\,^2\Pi_{1/2}$ subsystems are located at 5236 and 5274 Å respectively. The $C$–$X$ and $D$–$X$ bands treated here are situated in the green spectral region from about 5100 Å to about 5650 Å.

## 2. Experimental

The emission spectrum of CuO in the green region has been obtained by using an arc between copper electrodes in an oxygen atmosphere, a conventional hollow cathode described in paper [3] and a liquid nitrogen cooled CWHC (Composite Wall Hollow Cathode) similar to the one described by Bacis [9] in 1976. Employing the latter, the discharge current was 100 mA and the pressure 1.0 torr with neon as carrier gas. In order to avoid strong overlapping atomic neon lines, argon at a pressure of 0.5 torr was occasionally used as carrier gas instead of neon. The liquid nitrogen cooled CWHC provides an excellent method for obtaining emission spectra at low rotational temperatures. This can be seen in Fig. 1 where the spectrum produced by the CWHC is compared with that produced in an arc in the same spectral region.

The spectrum was photographed in the 10th and 11th orders of a Jarrel Ash 5 m Fastie plane grating spectrograph with linear dispersions between 3.2 mm Å$^{-1}$ and 4.8 mm Å$^{-1}$ in the actual orders. All the bands were recorded on Kodak 103a–F plates with exposure times between 5 h and 20 h.

Lines from a thorium hollow cathode were used for calibration. The wave length standards were obtained from a table of interferometrically measured lines collected by Kopp et al. [10].

The plates were measured in a modified Abbe comparator as described in [3]. Third and fourth order polynomials were used to determine the dispersion curve from the reference lines and the standard errors of fit varied between 0.001 Å and 0.002 Å. The wave numbers of the analyzed lines are listed in the Appendix. Many of the lines are overlapped but, due to the way of producing the tables, such lines have not been marked.

## 3. Description of the bands

As mentioned in the introduction, this work deals with two electronic systems of CuO located in the green spectral region. From an $^{18}O$ study we could unambiguously decide the vibrational numbering. For a transition having $\Delta v = +1$ or $\Delta v = -1$, the isotopic shift, $\nu(\mathrm{Cu}\,^{16}\mathrm{O})$–$\nu(\mathrm{Cu}\,^{18}\mathrm{O})$, is of the magnitude $+25$ cm$^{-1}$ or $-25$ cm$^{-1}$ respectively while, for a transition $\Delta v = 0$, the isotopic shift is rather small, at most a couple cm$^{-1}$. Table I gives the isotopic shifts for some bandheads belonging to the $C$–$X$ and $D$–$X$ systems.

### 3.1. *The* $C\,^2\Pi_i$–$X\,^2\Pi_i$ system

The $C$–$X$ bands constitute a rather intense system in the CuO spectrum. About 30 bandheads belonging to this system are collected in Table II. The predominating heads are those at 5312 Å, 5345 Å and 5391 Å. These are the 0–0 bands of the transitions $C\,^2\Pi_{3/2}$–$X\,^2\Pi_{3/2}$, $C\,^2\Pi_{1/2}$–$X\,^2\Pi_{1/2}$ and $C\,^2\Pi_{3/2}$–$X\,^2\Pi_{1/2}$. The appearance of the 5391 Å band shows that the $C$ state belongs to a coupling case between Hund's cases ($a$) and ($c$).

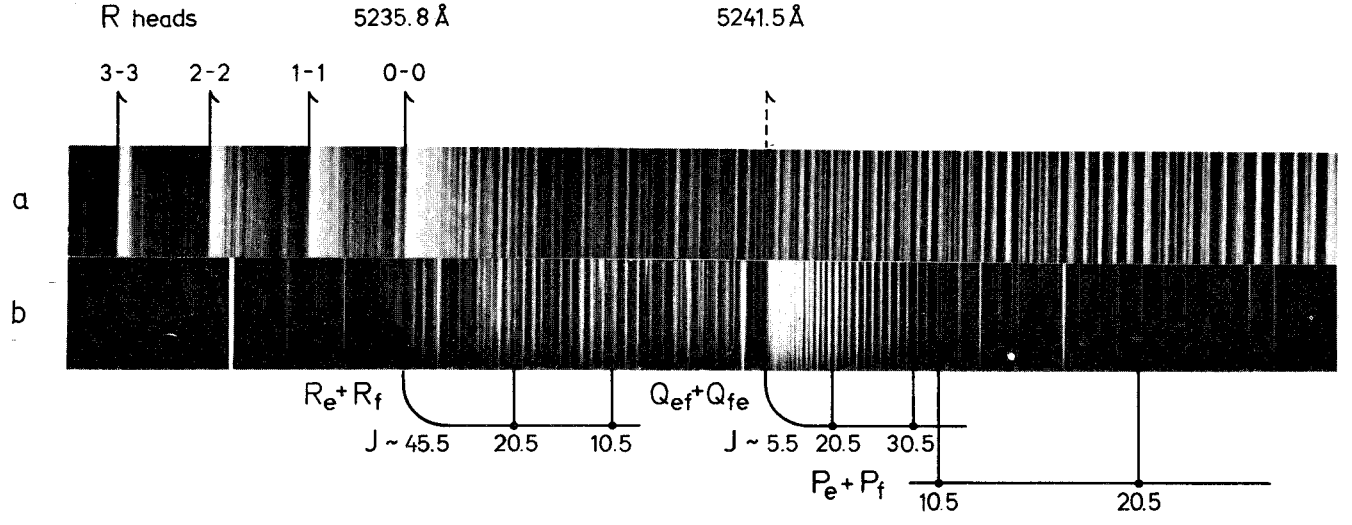


*Fig. 1.* Spectrogram of the $D\ ^2\Delta_{5/2}-X\ ^2\Pi_{3/2}$ subsystem at different temperatures. (a) Arc spectrum, $T \sim 3000$ K. (b) Hollow cathode spectrum, $T \sim 300$ K.

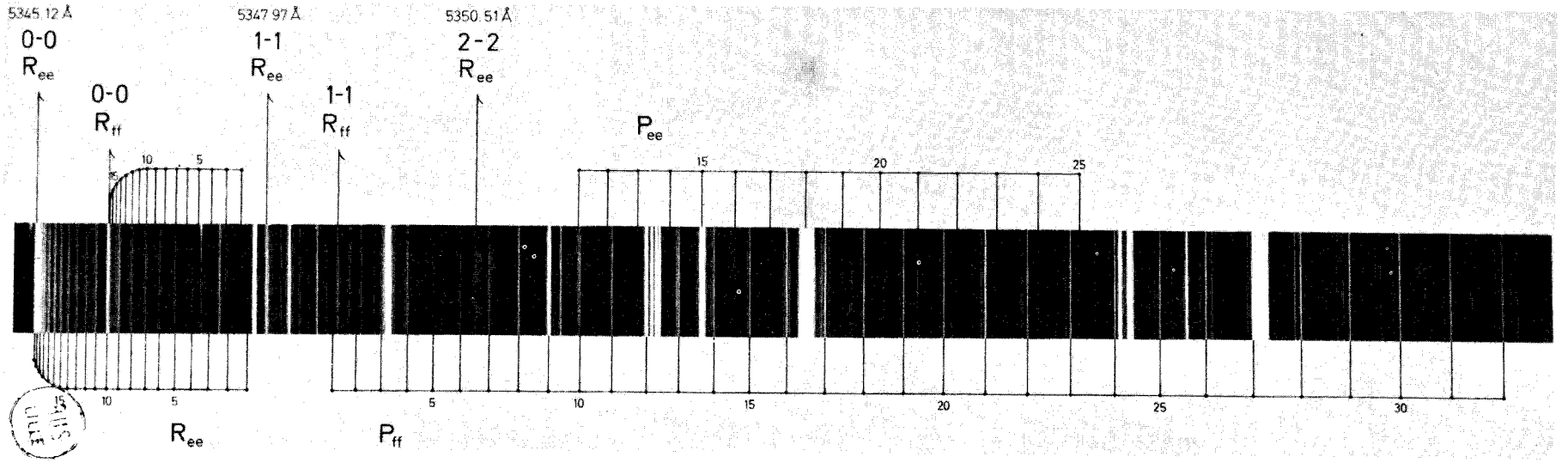


*Fig. 2.* Spectrogram of the 0–0 band of the $C\ ^2\Pi_{1/2}-X\ ^2\Pi_{1/2}$ subsystem at 5345 Å. The $(J-\frac{1}{2})$ numbers are indicated in the branches.

Table I. *Isotopic shifts of some of the green bands*

| Transition | $v'$–$v''$ | Branch | λ(Å)Cu $^{16}$O | $\nu$(Cu $^{16}$O)–$\nu$(Cu $^{18}$O) cm$^{-1}$ |
|---|---|---|---|---|
| $C^2\Pi_{3/2}$–$X^2\Pi_{3/2}$ | 0–0 | $R_{ee}+R_{ff}$ | 5312.13 | + 0.6 |
| $C^2\Pi_{1/2}$–$X^2\Pi_{1/2}$ | 0–0 | $R_{ee}$ | 5345.15 | + 0.9 |
| $C^2\Pi_{3/2}$–$X^2\Pi_{1/2}$ | 0–0 | $R_{ff}$ | 5391.43 | + 0.6 |
| $D^2\Delta_{5/2}$–$X^2\Pi_{3/2}$ | 0–0 | $Q_{ef}+Q_{fe}$ | 5241.50 | − 0.1 |
| | 1–1 | $Q_{ef}+Q_{fe}$ | 5239.98 | − 1.8 |
| | 0–0 | $R_{ee}+R_{ff}$ | 5235.75 | + 2.6 |
| $D^2\Delta_{3/2}$–$X^2\Pi_{1/2}$ | 0–0 | $R_{ff}$ | 5273.99 | + 2.9 |
| | 1–1 | $R_{ff}$ | 5278.85 | + 4.2 |
| | 2–2 | $R_{ff}$ | 5282.75 | + 4.5 |
| | 3–3 | $R_{ff}$ | 5285.78 | + 5.2 |

Also the 0–0 band of the $C^2\Pi_{1/2}$–$X^2\Pi_{3/2}$ transition is present, although much weaker than the 5391 Å band. A weak $Q$ head of this band appears at 5270 Å.

3.1.1. *The $C^2\Pi_{3/2}$–$X^2\Pi_{3/2}$ subsystem.* Heads belonging to three sequences have been observed, $\Delta v = +1, 0$ and $-1$ (see Table II). The sequences $\Delta v = 0$ and $-1$ are degraded to the violet although the bands are shaded to the red. For the $\Delta v = +1$ sequence the heads coincide heavily. This appearance is due to the magnitudes of the molecular constants of the upper and lower states.

Table II. *Heads of the C–X bands*

| Transition | $v'$–$v''$ | Branch | λ (Å) | $\nu$ (cm$^{-1}$) |
|---|---|---|---|---|
| $C^2\Pi_{3/2}$–$X^2\Pi_{3/2}$ | 1–0[a] | $R_{ee}+R_{ff}$ | 5135.42 | 19467.2 |
| | 0–0 | $R_{ee}+R_{ff}$ | 5312.13 | 18819.6 |
| | 1–1 | $R_{ee}+R_{ff}$ | 5307.80 | 18835.0 |
| | 2–2 | $R_{ee}+R_{ff}$ | 5304.66 | 18846.1 |
| | 3–3[a] | $R_{ee}+R_{ff}$ | 5302.23 | 18854.8 |
| | 0–1 | $R_{ee}+R_{ff}$ | 5495.92 | 18190.3 |
| | 1–2 | $R_{ee}+R_{ff}$ | 5488.58 | 18214.6 |
| | 2–3 | $R_{ee}+R_{ff}$ | 5482.57 | 18234.5 |
| | 3–4 | $R_{ee}+R_{ff}$ | 5477.47 | 18251.5 |
| | 4–5[a] | $R_{ee}+R_{ff}$ | 5473.02 | 18266.4 |
| | 5–6[a] | $R_{ee}+R_{ff}$ | 5469.15 | 18279.3 |
| | 6–7[b] | $R_{ee}+R_{ff}$ | 5465.86 | 18290.3 |
| | 1–3[b] | $R_{ee}+R_{ff}$ | 5678.78 | 17604.5 |
| | 2–4[b] | $R_{ee}+R_{ff}$ | 5669.76 | 17632.5 |
| | 3–5[b] | $R_{ee}+R_{ff}$ | 5661.43 | 17658.5 |
| | 4–6[b] | $R_{ee}+R_{ff}$ | 5654.01 | 17681.7 |
| | 5–7[b] | $R_{ee}+R_{ff}$ | 5647.50 | 17702.0 |
| | 6–8[b] | $R_{ee}+R_{ff}$ | 5641.47 | 17721.0 |
| | 7–9[b] | $R_{ee}+R_{ff}$ | 5635.96 | 17738.3 |
| $C^2\Pi_{1/2}$–$X^2\Pi_{1/2}$ | 1–0 | $R_{ee}$ | 5174.89 | 19318.7 |
| | 2–1 | $R_{ee}$ | 5179.64 | 19301.0 |
| | 3–2[a] | $R_{ee}$ | 5184.16 | 19284.2 |
| | 0–0 | $R_{ee}$ | 5345.15 | 18703.3 |
| | 0–0 | $R_{ff}$ | 5346.03 | 18700.3 |
| | 1–1 | $R_{ee}$ | 5347.97 | 18693.5 |
| | 1–1 | $R_{ff}$ | 5348.84 | 18690.4 |
| | 2–2[a] | $R_{ee}$ | 5350.51 | 18684.6 |
| | 0–1 | $R_{ee}$ | 5529.66 | 18079.3 |
| | 1–2 | $R_{ee}$ | 5529.92 | 18078.4 |
| | 2–3 | $R_{ee}$ | 5529.80 | 18078.8 |
| $C^2\Pi_{3/2}$–$X^2\Pi_{1/2}$ | 0–0 | $R_{ff}$ | 5391.43 | 18542.8 |
| | 0–0 | $R_{ee}$ | 5391.49 | 18542.6 |
| | 1–1[a] | $R_{ff}$ | 5385.84 | 18562.0 |
| | 1–1[a] | $R_{ee}$ | 5385.91 | 18561.8 |
| | 2–2[a] | $R_{ff}$ | 5381.56 | 18576.8 |
| | 2–2[a] | $R_{ee}$ | 5381.62 | 18576.6 |
| $C^2\Pi_{1/2}$–$X^2\Pi_{3/2}$ | 0–0 | $Q_{ef}+Q_{fe}$ | 5270.26 | 18969.1 |

[a] Not rotationally analyzed.
[b] Obtained using an arc as light source and not rotationally analyzed.

The 0–0 band at 5312 Å has an appearance typical for a $^2\Pi_{3/2}$ (case *a*)–$^2\Pi_{3/2}$ (case *a*) transition. Thus it has two $R$ and two $P$ branches. The split of the branches is only observable at high $J$ values since the Λ type doubling of both states is rather small, being least for the ground state. Figure 1 in paper [5] shows a spectrogram of this band although the doubling of the branches is not resolved there.

The 1–1, 2–2, 0–1, 1–2, 2–3, and 3–4 bands are also rotationally analyzed.

3.1.2. *The $C^2\Pi_{1/2}$–$X^2\Pi_{1/2}$ subsystem.* The 0–0 band of this subsystem has its head at 5345 Å. The band has two $R$ and two $P$ branches. The branch intensities are very anomalous, the $R_e$ and $P_f$ lines being strong, while the $R_f$ and $P_e$ lines are very weak, considerably weaker than the $R_e$ and $P_f$ lines of the less abundant isotopic molecule $^{65}$CuO. In paper [5] the weak $R_f$ and $P_e$ lines were not reported and the $J$ numbering of the observed branches was incorrect. Apart from the anomalous branch intensities, the appearance of the 5345 Å band resembles that of a $^2\Pi_{1/2}$–$^2\Pi_{1/2}$ transition. The Λ type doubling of the upper state is typical for a $^2\Pi_{1/2}$ state (see Section 4.2). Figure 2 shows a spectrogram of this band.

Besides the 0–0 band, also the 1–1, 0–1, 1–2, 2–3, 1–0, and 2–1 bands have been analyzed.

3.1.3. *The $C^2\Pi_{3/2}$–$X^2\Pi_{1/2}$ subsystem.* The 5391 Å bands constitute the 0–0 transition of the intercombination $C^2\Pi_{3/2}$–$X^2\Pi_{1/2}$ system. This band has two $R$, two $Q$ and two $P$ branches. Figure 3 shows a spectrogram of this band. A characteristic feature is two fairly intense $Q$ branches where the Λ type doubling, mainly in the $X^2\Pi_{1/2}$ state, can be clearly seen. The $R$ lines are broadened since the two $R$ branches overlap each other heavily. This broadening is also caused by isotopic lines.

The unexpectedly high intensity of the 5391 Å band might be explained by an interaction between the upper state and an adjacent state also having $\Omega = 3/2$ (see Section 5).

3.1.4. *The $C^2\Pi_{1/2}$–$X^2\Pi_{3/2}$ subsystem.* A very weak band is situated just in front of the rather intense 5274 Å band. It consists of two discernible $Q$ branches which form a head at 5270 Å. Some of the $P$ lines have also been traced while no $R$ lines have been found on our plates. In the Appendix, only the $Q$ lines are given. The band has turned out to be the 0–0 transition of the $C^2\Pi_{1/2}$–$X^2\Pi_{3/2}$ subsystem.

Figure 4 shows a spectrogram of the 5270 Å band.

### 3.2. *The $D^2\Delta_i$–$X^2\Pi_i$ system*

Only two sequences of the $D$–$X$ system have been found. These are the $\Delta v = 0$ sequences of the $D^2\Delta_{5/2}$–$X^2\Pi_{3/2}$ and $D^2\Delta_{3/2}$–$X^2\Pi_{1/2}$ transitions. The $R$ heads of the 0–0 bands are located at 5236 Å and 5274 Å. The 5236 Å band is con-

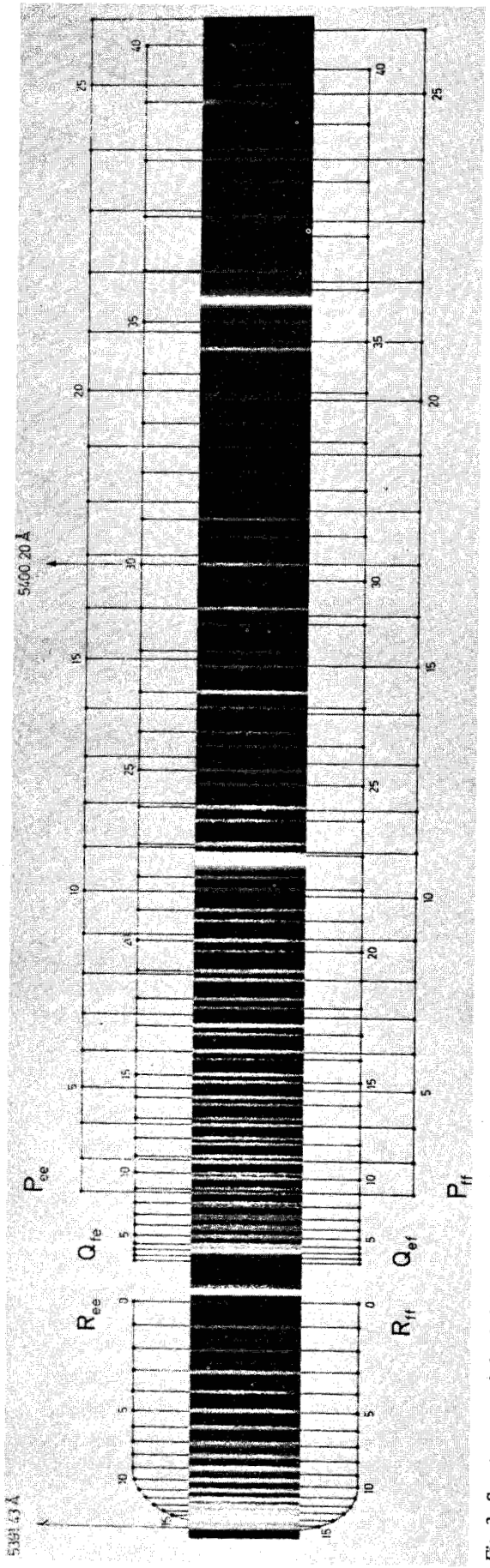


*Fig. 3.* Spectrogram of the 0–0 band of the $C\,^2\Pi_{3/2} - X\,^2\Pi_{1/2}$ subsystem at 5391 Å. The $(J-\frac{1}{2})$ numbers are indicated in the branches.

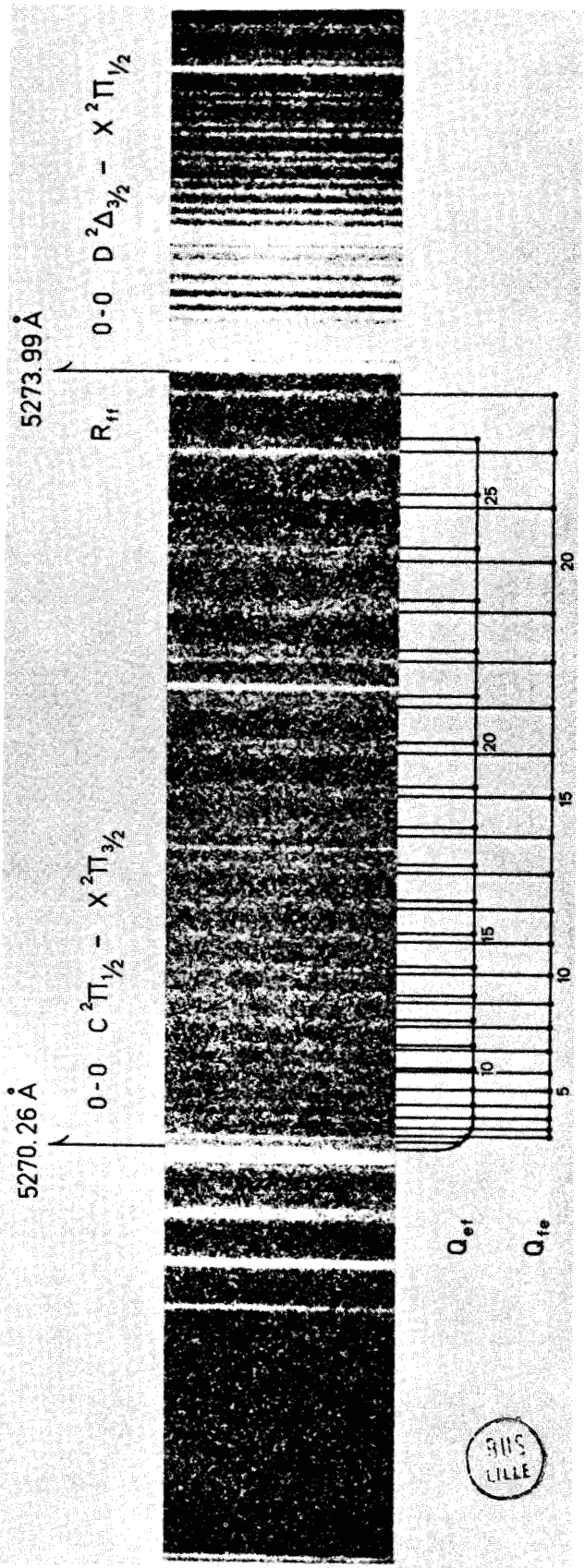


*Fig. 4.* Spectrogram of the very faint 0–0 band of the $C\,^2\Pi_{1/2} - X\,^2\Pi_{3/2}$ subsystem at 5270 Å. The $(J-\frac{1}{2})$ numbers are indicated in the branches.

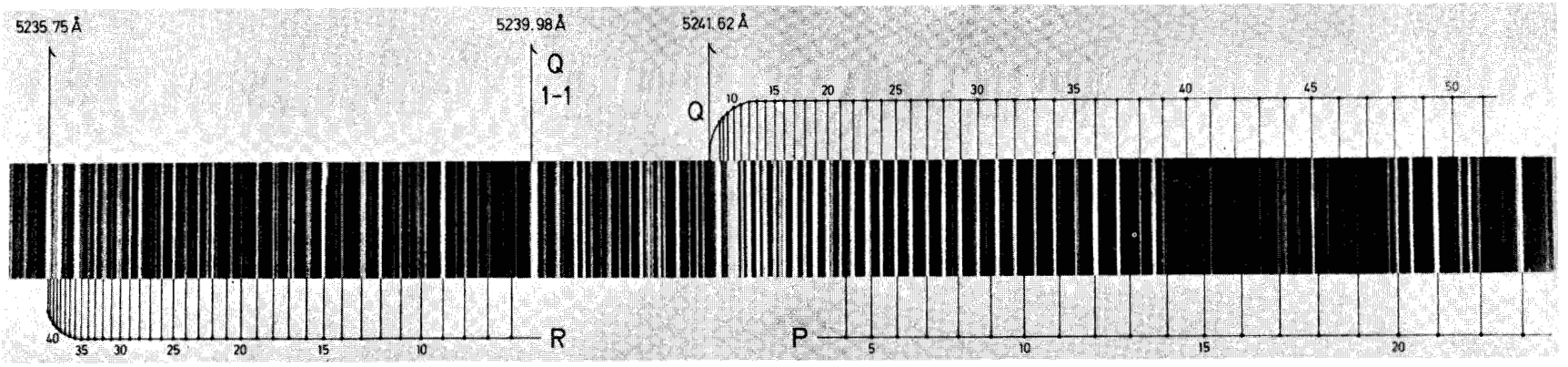


*Fig. 5.* Spectrogram of the 0–0 band of the $D\,^2\Delta_{5/2}$–$X\,^2\Pi_{3/2}$ subsystem at 5236 Å. The $(J-\frac{1}{2})$ numbers are indicated in the branches.

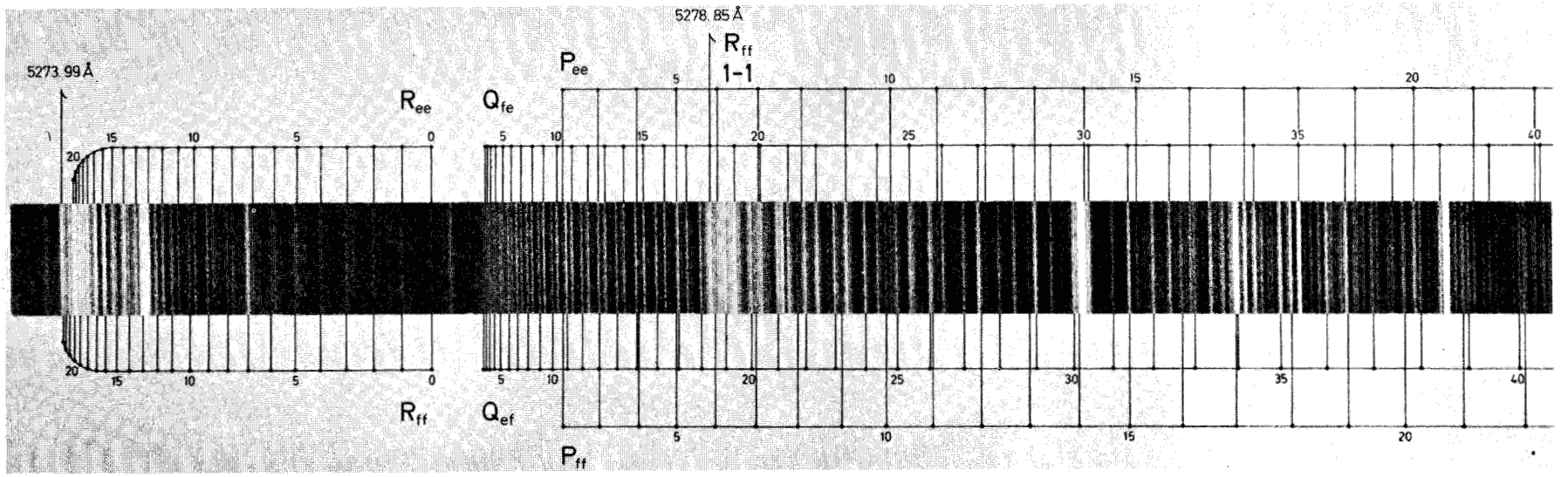


*Fig. 6.* Spectrogram of the 0–0 band of the $D\,^2\Delta_{3/2}$–$X\,^2\Pi_{1/2}$ subsystem at 5274 Å. The $(J-\frac{1}{2})$ numbers are indicated in the branches.

Table III. *Heads of the D–X bands*

| Transition | $v'$–$v''$ | Branch | λ (Å) | $\nu$ (cm$^{-1}$) |
|---|---|---|---|---|
| $D\,^2\Delta_{5/2}$–$X\,^2\Pi_{3/2}$ | 0–0 | $R_{ee}+R_{ff}$ | 5235.75 | 19094.1 |
| | 0–0 | $Q_{ef}+Q_{fe}$ | 5241.50 | 19073.2 |
| | 1–1 | $R_{ee}+R_{ff}$ | 5234.20 | 19099.8 |
| | 1–1 | $Q_{ef}+Q_{fe}$ | 5239.98 | 19078.7 |
| | 2–2[a] | $R_{ee}+R_{ff}$ | 5232.73 | 19105.2 |
| | 3–3[a] | $R_{ee}+R_{ff}$ | 5231.29 | 19110.4 |
| | 4–4[a] | $R_{ee}+R_{ff}$ | 5229.78 | 19115.9 |
| $D\,^2\Delta_{3/2}$–$X\,^2\Pi_{1/2}$ | 0–0 | $R_{ff}$ | 5273.99 | 18955.7 |
| | 0–0 | $R_{ee}$ | 5274.08 | 18955.4 |
| | 1–1[a] | $R_{ff}$ | 5278.85 | 18938.3 |
| | 2–2[a] | $R_{ff}$ | 5282.75 | 18924.3 |
| | 3–3[a] | $R_{ff}$ | 5285.78 | 18913.4 |

[a] Not rotationally analyzed.

siderably stronger than the 5274 Å band. The band-heads of this system are listed in Table III.

No intercombination transitions have been observed.

3.2.1. *The $D\,^2\Delta_{5/2}$–$X\,^2\Pi_{3/2}$ subsystem.* The 0–0 band at 5236 Å is the strongest band in the sequence observed. The band has the typical appearance of a $^2\Delta_{5/2}$–$^2\Pi_{3/2}$ transition where the Λ type doubling is very small in both states. Thus we can only observe one $R$, one $Q$ and one $P$ branch. Figure 5 shows a spectrogram of this band.

The 1–1 band has also been analyzed.

3.2.2. *The $D\,^2\Delta_{3/2}$–$X\,^2\Pi_{1/2}$ subsystem.* Of this system, only the 0–0 band has been rotationally analyzed. The band has two $R$, two $Q$ and two $P$ branches. Figure 6 shows a spectrogram of this band. As can be seen from the figure the branches have been followed to their lowest $J$ values.

## 4. Evaluation of the molecular constants

### 4.1. *Determination of term values*

Some years ago Åslund [11] reported a method for the simultaneous determination of term values and molecular constants. In this case the term values of the involved states have been determined from all the band lines where the term values of the ground state were simultaneously fitted to formula (1). The molecular constants of the ground states are obtained by means of the method of least squares.

$$T_v(J) = T_e + G(v) + F_v(J) \pm \tfrac{1}{2}\,\Delta\nu_{ef} \qquad (1)$$

where

$$G(v) = \omega_e(v+\tfrac{1}{2}) - \omega_e x_e(v+\tfrac{1}{2})^2 + \omega_e y_e(v+\tfrac{1}{2})^3$$

and

$$F_v(J) = B_v J(J+1) - D_v J^2(J+1)^2$$

with

$$B_v = B_e - \alpha_e(v+\tfrac{1}{2}) + \delta_e(v+\tfrac{1}{2})^2$$

and

$$D_v = D_e + \beta_e(v+\tfrac{1}{2})$$

Finally the Λ type doubling $\Delta\nu_{ef}$ can be written

$$\Delta\nu_{ef} = T_e(J) - T_f(J) = \begin{cases} a(J-\tfrac{1}{2})(J+\tfrac{1}{2})(J+\tfrac{3}{2}) & \text{for } ^2\Pi_{3/2} \\ -[p + p_J J(J+1)]\,(J+\tfrac{1}{2}) & \text{for } ^2\Pi_{1/2} \end{cases}$$

It should be pointed out that, in the earlier papers [3, 4, 6], the definition of the Λ type doubling of the $^2\Pi_{1/2}$ state was given with the opposite sign.

The molecular constants for the ground state determined in this way are given in Table VI. No significant values were obtained for the $\beta_e$ constants. These constants were therefore put equal to zero. The values calculated for $p_J$ were also not significant which is most likely due to the fact that only term values with $J \leqslant 50.5$ could be reached from the band lines. For this reason $p_J$ was put equal to zero. The following $p$ values in cm$^{-1}$, not given in Table VI, were derived:

$$p_0 = -0.0137\,(1) \quad p_1 = -0.0143\,(3)$$

$$p_2 = -0.0136\,(4) \quad p_3 = -0.0144\,(7)$$

In paper [3] the constants $D_e$ and $a$ were determined by use of term values of much higher $J$. For this reason these constants have, in these calculations, been given the values derived in paper [3].

### 4.2. *Molecular constants for the excited states*

The molecular constants for the four substates have been calculated for all vibrational levels analyzed. For the $^2\Pi_{3/2}$ and $^2\Delta_{3/2}$ levels the following formula has been chosen:

$$\left.\begin{matrix} T_e(J) \\ T_f(J) \end{matrix}\right\} = T_v(J=0) + B_v J(J+1) - D_v J^2(J+1)^2 \pm \tfrac{1}{2}\,a(J-\tfrac{1}{2})(J+\tfrac{1}{2})(J+\tfrac{3}{2}), \qquad (2)$$

and for the $^2\Pi_{1/2}$ level:

$$\left.\begin{matrix} T_e(J) \\ T_f(J) \end{matrix}\right\} = T_v(J=0) + B_v J(J+1) - D_v J^2(J+1)^2 \mp \tfrac{1}{2}\,[p + p_J J(J+1)]\,(J+\tfrac{1}{2}) \qquad (3)$$

Table IV. *Molecular constants in cm$^{-1}$ of the $C\,^2\Pi$ and $D\,^2\Delta$ states calculated from formulas (2) and (3)*

| State | $v$ | $T_v$ | $B_v$ | $D_v \times 10^6$ | $a \times 10^5$ | $p$ | $p_J \times 10^5$ | RMS |
|---|---|---|---|---|---|---|---|---|
| $C\,^2\Pi_{3/2}$ | 0 | 18811.540(4) | 0.41938(1) | 0.725(5) | 0.28(1) | – | – | 0.020 |
| | 1 | 19457.937(5) | 0.41593(1) | 0.72(3) | – | – | – | 0.027 |
| | 2 | 20091.492(6) | 0.41196(2) | 0.75(5) | – | – | – | 0.025 |
| | 3 | 20713.785(6) | 0.4078(1) | 0.7(2) | – | – | – | 0.024 |
| $C\,^2\Pi_{1/2}$ | 0 | 18969.118(3) | 0.42270(1) | 0.821(4) | – | −0.1503(3) | 0.62(2) | 0.016 |
| | 1 | 19586.196(3) | 0.41951(1) | 0.819(6) | – | −0.1412(4) | 0.37(4) | 0.015 |
| | 2 | 20195.573(6) | 0.41638(2) | 0.84(2) | – | −0.1317(6) | 0.17(8) | 0.018 |
| $D\,^2\Delta_{5/2}$ | 0 | 19073.379(3) | 0.43316(1) | 0.826(3) | – | – | – | 0.014 |
| | 1 | 19710.083(5) | 0.42888(1) | 0.828(6) | – | – | – | 0.014 |
| $D\,^2\Delta_{3/2}$ | 0 | 19221.471(3) | 0.42501(1) | 0.703(5) | – | – | – | 0.016 |

Table V. *Molecular constants in cm$^{-1}$ of the C $^2\Pi$ and D $^2\Delta$ states calculated from formula (4)*

| State | $v$ | $T_v$ | $B_v$ | $D_v \times 10^6$ | $A_v$ | $A_J \times 10^3$ | $p$ | $q \times 10^3$ | RMS |
|---|---|---|---|---|---|---|---|---|---|
| $C\ ^2\Pi$ | 0 | 18890.647(3) | 0.42102(1) | 0.762(4) | −156.758(5) | −0.977(5) | −0.1480(3) | 0.41(2) | 0.024 |
| | 1 | 19522.386(4) | 0.41769(1) | 0.748(7) | −127.437(7) | −0.81(1) | −0.1397(2) | – | 0.024 |
| | 2 | 20143.841(5) | 0.41418(2) | 0.80(2) | −103.252(8) | −1.16(2) | −0.1321(3) | – | 0.022 |
| $D\ ^2\Delta$ | 0 | 19149.036(3) | 0.42906(1) | 0.752(3) | −73.184(2) | 5.350(2) | – | – | 0.018 |

For the $^2\Delta_{5/2}$ component, no Λ type doubling correction has been taken into account since it is expected to be negligible. It should be noted that, in the rotational expression here, the part $[J(J+1)]$ has been used instead of $[(J+\frac{1}{2})^2 - \Lambda^2]$.

The molecular constants derived are collected in Table IV. The Λ type doubling in the $C\ ^2\Pi_{3/2}$ levels has only been observed for $v=0$ because, for this level, the term values could be followed to much higher $J$ than for the levels $v=1$, 2 and 3. The RMS errors of fit given in Table IV are those of the differences between calculated term values and term values obtained from the method described in Section 4.1.

### 4.3. *Calculation of the spin–orbit constants*

In order to determine the spin–orbit constant $A$, the following energy expressions given by James [12] and modified by Klynning et al. [13] have been used:

$$\left.\begin{matrix} T_{1e}(J) \\ T_{1f}(J) \\ T_{2e}(J) \\ T_{2f}(J) \end{matrix}\right\} = T(X=0) + BX - DX^2 \mp (Z \mp \tfrac{1}{2}\Delta\nu_{ef}) \qquad (4)$$

where

$$Z = [\tfrac{1}{4}(A^* - 2B^*)^2 \Lambda^2 + B^{*2} X]^{1/2}$$

$$X = (J+\tfrac{1}{2})^2 - \Lambda^2$$

$$A^* = A + A_J J(J+1)$$

$$B^* = B - 2DX - \tfrac{1}{2}\gamma .$$

For the $D\ ^2\Delta$ state the Λ type doubling, $\Delta\nu_{ef}$, has not been observed and therefore, in this case, $\Delta\nu_{ef}$ was put equal to zero in the calculations. For $^2\Pi$ states, Mulliken and Christy [14] have given an expression for the Λ type doubling. Introducing the definitions of the $A$ and $B$ parameters given above we have:

$$\Delta\nu_{ef} = \left[\left(\pm 1 - \frac{A^* - 2B^*}{2Z}\right)(\tfrac{1}{2}p^* + q^*) + \frac{q^* BX}{Z}\right](J+\tfrac{1}{2}),$$

where

$$p^* = p\left(1 - \frac{2D}{B}X\right) \quad \text{and} \quad q^* = q\left(1 - \frac{4D}{B}X\right).$$

For a $^2\Pi_i$ state the plus sign gives the Λ type doubling of the $^2\Pi_{1/2}$ substate and the minus sign that of the $^2\Pi_{3/2}$ substate while the contrary applies for a $^2\Pi_r$ state.

Table V gives values for the spin–orbit constant $A$ and the other molecular constants in formula (4). As can be seen from Table V, the spin–orbit constant $A$ is $-157$ cm$^{-1}$ for $v=0$ of the $C$ state and $-73$ cm$^{-1}$ for $v=0$ of the $D$ state.

### 4.4. *Equilibrium constants*

The equilibrium constants for the $X$, $C$ and $D$ states are collected in Table VI.

It is surprising that the $\omega_e x_e$ value of the $C\ ^2\Pi_{3/2}$ and $C\ ^2\Pi_{1/2}$ states are so different, viz. 6.1 and 3.9 cm$^{-1}$ respectively. Also the $\omega_e$ values are different, viz. 658.3 and 624.8 cm$^{-1}$. It is noteworthy that the same thing applied for the $D$ sublevels. From head measurements we have estimated the following values (in cm$^{-1}$) for the vibrational constants:

| State | $\omega_e$ | $\omega_e x_e$ |
|---|---|---|
| $D\ ^2\Delta_{5/2}$ | 645.9 | 4.5 |
| $D\ ^2\Delta_{3/2}$ | 615.3 | 2.7 |

## 5. Discussion

Most of the CuO bands observed in the green region have now been analyzed. The assignations of the bands are made on the assumption that the observed bands emanate from the two electronic states $C\ ^2\Pi_i$ and $D\ ^2\Delta_i$. The differences, however, between the vibrational constants of the sublevels (see Section 4.4) indicate that this assumption could be discussed. It is not out of the question that we have four separate excited electronic states. It seems very likely that the states have some tendency to case (c) and that the labelling should be given using the Ω values instead of the Λ values.

Table VI. *Equilibrium constants of the X $^2\Pi$, C $^2\Pi$ and D $^2\Delta$ states*[a]

| State | $T_0$ | $\omega_e$[b] | $\omega_e x_e$ | $\omega_e y_e$ | $B_e$[c] | $\alpha_e \times 10^3$ | $\delta_e \times 10^5$ | $D_e \times 10^6$[d] | $r_e \times 10^8$ (cm)[e] |
|---|---|---|---|---|---|---|---|---|---|
| $D\ ^2\Delta_{3/2}$ | 19221.47 | – | – | – | (0.42501) | – | – | (0.70) | (1.763) |
| $D\ ^2\Delta_{5/2}$ | 19073.38 | (636.7) | – | – | 0.4353 | 4.3 | – | 0.83 | 1.742 |
| $C\ ^2\Pi_{1/2}$ | 18969.12 | 624.8 | 3.9 | – | 0.4243 | 3.2 | – | 0.82 | 1.765 |
| $C\ ^2\Pi_{3/2}$ | 18811.54 | 658.3 | 6.1 | – | 0.4213 | 3.6 | – | 0.72 | 1.771 |
| $X\ ^2\Pi_{1/2}$ | 277.05 | 636.24(2) | 4.45(1) | 0.028(2) | 0.44417(2) | 4.55(1) | 2.2(4) | 0.84 | 1.7247 |
| $X\ ^2\Pi_{3/2}$ | 0.00 | 640.23(1) | 4.52(1) | 0.025(1) | 0.44454(2) | 4.60(2) | 1.9(5) | 0.85 | 1.7240 |

[a] All quantities, except when noted, are in cm$^{-1}$.
[b] $(\omega_e) = \Delta G(\frac{1}{2})$. [c] $(B_e) = B_0$. [d] $(D_e) = D_0$. [e] $(r_e) = r_0$.
The molecular constants of the $X\ ^2\Pi_{3/2}$ and $X\ ^2\Pi_{1/2}$ substates are obtained by fitting the term values to formula (1). Figures in parentheses are the RMS errors of fit.

The strong intensity of the intercombination band at 5391 Å, labelled as the 0–0 band of the $C\,^2\Pi_{3/2}-X\,^2\Pi_{1/2}$ transition, might be explained as being due to an interaction between the $v=0$ levels of $C\,^2\Pi_{3/2}$ and $D\,^2\Delta_{3/2}$. This interpretation is supported by the fact that the 0–0 band of $D\,^2\Delta_{3/2}-X\,^2\Pi_{1/2}$ at 5274 Å is weak (weaker than the 0–0 band at 5236 Å of $D\,^2\Pi_{5/2}-X\,^2\Pi_{3/2}$) and that the 0–0 band of $C\,^2\Pi_{3/2}-X\,^2\Pi_{3/2}$ at 5312 Å is stronger than the 0–0 band of $C\,^2\Pi_{1/2}-X\,^2\Pi_{1/2}$ at 5345 Å.

## References

1. Lagerqvist, A. and Uhler, U., Z. Naturforsch. **22B**, 551 (1967).
2. Appelblad, O. and Lagerqvist, A., J. Molecular Spectr. **68**, 81 (1973).
3. Appelblad, O. and Lagerqvist, A., Physica Scripta **10**, 307 (1974).
4. Appelblad, O. and Lagerqvist, A., Can. J. Phys. **53**, 2221 (1975).
5. Lefebvre, Y., Pinchemel, B. and Bacis, R., Can. J. Phys. **54**, 735 (1976).
6. Appelblad, O. and Lagerqvist, A., Physica Scripta, **13**, 275 (1976).
7. Lefebvre, Y., Pinchemel, B. and Schamps, J., J. Molecular Spectr. **68**, 81 (1977).
8. Pinchemel, B., Lefebvre, Y. and Schamps, J., J. Phys. B: Atom. Molec. Phys. **10**, 3215 (1977).
9. Bacis, R., J. Phys. E: Sci. Instrum. **9**, 1081 (1976).
10. Kopp, I. and Rydh, B., Tables of Compiled Th Reference Lines (to be published).
11. Aslund, N., J. Moleculare Spectr. **50**, 424 (1974).
12. James, T. C., J. Chem. Phys. **41**, 631 (1964).
13. Klynning, L., Lindgren, B. and Aslund, N., Arkiv Fysik **30**, 141 (1965).
14. Mulliken, R. S. and Christy, A., Phys. Rev. **38**, 87 (1931).

*Institute of Physics*
*University of Stockholm*
*Vanadisvägen 9*
*S-113 46 Stockholm*
*Sweden*

## Appendix

Wave numbers of CuO lines.

The 0–0, 0–1, 1–1, 1–2, 2–2, 2–3, and 3–4 bands of the $C\,^2\Pi_{3/2}$–$X\,^2\Pi_{3/2}$ transition.

| J | 0 - 0 | | | | 0 - 1 | | 1 - 1 | | 1 - 2 | | 2 - 2 | | 2 - 3 | | 3 - 4 | |
|---|---|---|---|---|---|---|---|---|---|---|---|---|---|---|---|---|
| | $R_e$ | $R_f$ | $P_e$ | $P_f$ | $R_e+R_f$ | $P_e+P_f$ | $R_e+R_f$ | $P_e+P_f$ | $R_e+R_f$ | $P_e+P_f$ | $R_e+R_f$ | $P_e+P_f$ | $R_e+R_f$ | $P_e+P_f$ | $R_e+R_f$ | $P_e+P_f$ |
| 1.5 | 18813.51 | 18813.51 | | | 18182.17 | | | | | | | | | | | |
| 2.5 | 814.21 | 814.21 | 18809.12 | 18809.12 | 182.98 | | | | 18206.90 | | | | 18226.73 | | 18243.67 | |
| 3.5 | 814.87 | 814.87 | 808.16 | 808.16 | 183.68 | 18176.93 | 18830.03 | | 207.65 | | | | 227.39 | | 244.34 | |
| 4.5 | 815.52 | 815.43 | 807.13 | 807.13 | 184.36 | 175.99 | 830.70 | 18822.34 | 208.32 | 18199.95 | | | 227.99 | 18219.83 | 245.02 | 18236.92 |
| 5.5 | 816.10 | 816.10 | 806.05 | 806.05 | 185.01 | 174.94 | 831.25 | 821.24 | 208.95 | 198.98 | | | 228.67 | 218.78 | 245.67 | 235.89 |
| 6.5 | 816.65 | 816.65 | 804.92 | 804.92 | 185.61 | 173.88 | 831.82 | 820.19 | 209.54 | 197.91 | | | 229.25 | 217.68 | 246.27 | 234.79 |
| 7.5 | 817.14 | 817.14 | 803.74 | 803.74 | 186.17 | 172.77 | 832.32 | 818.94 | 210.13 | 196.83 | 18843.34 | | 229.87 | 216.68 | 246.83 | 233.77 |
| 8.5 | 817.58 | 817.58 | 802.51 | 802.51 | 186.69 | 171.63 | 832.77 | 817.88 | 210.66 | 195.69 | 843.82 | | 230.41 | 215.56 | 247.37 | 232.72 |
| 9.5 | 817.98 | 817.98 | 801.24 | 801.24 | 187.20 | 170.43 | 833.19 | 816.53 | 211.17 | 194.54 | 844.24 | 18827.74 | 230.91 | 214.45 | 247.88 | 231.56 |
| 10.5 | 818.34 | 818.34 | 799.92 | 799.92 | 187.64 | 169.21 | 833.55 | 815.33 | 211.65 | 193.37 | 844.59 | 826.55 | 231.39 | 213.28 | 248.34 | 230.41 |
| 11.5 | 818.65 | 818.65 | 798.55 | 798.55 | 188.05 | 167.94 | 833.90 | 813.98 | 212.08 | 192.12 | 844.96 | 825.19 | 231.82 | 212.08 | 248.78 | 229.21 |
| 12.5 | 818.93 | 818.93 | 797.14 | 797.14 | 188.45 | 166.67 | 834.17 | 812.55 | 212.47 | 190.86 | 845.24 | 823.78 | 232.22 | 210.82 | 249.20 | 227.99 |
| 13.5 | 819.15 | 819.15 | 795.68 | 795.69 | 188.78 | 165.33 | 834.43 | 811.14 | 212.83 | 189.57 | 845.49 | 822.41 | 232.60 | 209.54 | 249.57 | 226.73 |
| 14.5 | 819.33 | 819.33 | 794.19 | 794.19 | 189.10 | 163.97 | 834.61 | 809.67 | 213.16 | 188.22 | 845.70 | 821.01 | 232.92 | 208.24 | 249.90 | 225.44 |
| 15.5 | 819.50 | 819.50 | 792.65 | 792.65 | 189.38 | 162.55 | 834.83 | 808.19 | 213.46 | 186.88 | 845.88 | | 233.24 | 206.90 | 250.19 | 224.13 |
| 16.5 | 819.59 | 819.59 | 791.06 | 791.06 | 189.61 | 161.11 | 834.96 | 806.63 | 213.70 | 185.49 | 846.01 | | 233.52 | 205.53 | 250.47 | 222.76 |
| 17.5 | 819.59 | 819.59 | 789.42 | 789.42 | 189.80 | 159.64 | 834.96 | 805.06 | 213.95 | 184.04 | 846.10 | | 233.77 | 204.14 | 250.71 | - |
| 18.5 | 819.59 | 819.59 | 787.74 | 787.74 | 189.96 | 158.12 | 834.96 | 803.40 | 214.15 | 182.56 | 846.10 | | 233.96 | 202.71 | 250.94 | 219.98 |
| 19.5 | 819.56 | 819.56 | 786.02 | 786.02 | 190.09 | 156.62 | 834.96 | 801.74 | 214.28 | 181.07 | 846.01 | | 234.15 | 201.21 | 251.14 | 218.53 |
| 20.5 | 819.47 | 819.47 | 784.26 | 784.26 | 190.21 | 155.02 | 834.83 | 800.00 | 214.44 | 179.52 | | | 234.29 | 199.72 | 251.21 | 217.07 |
| 21.5 | 819.29 | 819.29 | 782.44 | 782.44 | 190.26 | 153.38 | 834.74 | 798.25 | 214.53 | 177.96 | | | 234.42 | 198.19 | | 215.56 |
| 22.5 | 819.10 | 819.10 | 780.58 | 780.58 | 190.26 | 151.73 | 834.61 | 796.45 | 214.57 | 176.38 | | | 234.49 | 196.61 | | 213.94 |
| 23.5 | 818.87 | 818.87 | 778.68 | 778.68 | 190.26 | 150.02 | 834.43 | 794.60 | 214.57 | 174.75 | | | 234.49 | 195.01 | | |
| 24.5 | 818.59 | 818.59 | 776.74 | 776.74 | 190.21 | 148.29 | 834.19 | 792.68 | 214.57 | 173.08 | | | 234.42 | 193.37 | | |
| 25.5 | 818.26 | 818.26 | 774.76 | 774.76 | 190.09 | 146.56 | 833.90 | 790.76 | 214.57 | 171.38 | | | | 191.68 | | |
| 26.5 | 817.89 | 817.89 | 772.70 | 772.70 | 189.96 | 144.83 | 833.60 | 788.79 | | 169.66 | | | | 189.96 | | |
| 27.5 | 817.47 | 817.47 | 770.63 | 770.63 | 189.80 | 142.96 | 833.26 | 786.79 | | 167.94 | | | | | | |
| 28.5 | 817.00 | 817.00 | 768.51 | 768.51 | 189.57 | 141.10 | 832.85 | 784.73 | | | | | | | | |
| 29.5 | 816.50 | 816.46 | 766.34 | 766.34 | 189.38 | 139.16 | 832.43 | 782.64 | | | | | | | | |
| 30.5 | 815.95 | 815.90 | 764.13 | 764.13 | 189.01 | 137.19 | 831.93 | 780.47 | | | | | | | | |
| 31.5 | 815.37 | 815.28 | 761.86 | 761.86 | 188.68 | 135.24 | 831.34 | 778.36 | | | | | | | | |
| 32.5 | 814.71 | 814.65 | 759.66 | 759.58 | | 133.22 | 830.84 | 776.17 | | | | | | | | |
| 33.5 | 814.05 | 813.94 | 757.32 | 757.24 | | 131.24 | 830.31 | 773.90 | | | | | | | | |
| 34.5 | 813.30 | 813.22 | 754.91 | 754.82 | | | 829.58 | 771.63 | | | | | | | | |
| 35.5 | 812.52 | 812.44 | 752.50 | 752.38 | | | 828.91 | 769.27 | | | | | | | | |
| 36.5 | 811.72 | 811.62 | 750.02 | 749.87 | | | | 766.91 | | | | | | | | |
| 37.5 | 810.91 | 810.78 | 747.49 | 747.34 | | | | 764.48 | | | | | | | | |
| 38.5 | 810.04 | 809.87 | 744.95 | 744.79 | | | | | | | | | | | | |
| 39.5 | 809.12 | 808.91 | 742.38 | 742.17 | | | | | | | | | | | | |
| 40.5 | 808.16 | 807.94 | 739.77 | 739.53 | | | | | | | | | | | | |
| 41.5 | 807.13 | 806.87 | 737.04 | 736.82 | | | | | | | | | | | | |
| 42.5 | 806.05 | 805.80 | 734.38 | 734.10 | | | | | | | | | | | | |
| 43.5 | 804.92 | 804.67 | 731.55 | 731.29 | | | | | | | | | | | | |
| 44.5 | 803.74 | 803.52 | 728.78 | 728.50 | | | | | | | | | | | | |
| 45.5 | 802.51 | 802.26 | 725.90 | 725.66 | | | | | | | | | | | | |
| 46.5 | 801.24 | 800.90 | 723.00 | 722.74 | | | | | | | | | | | | |
| 47.5 | | | 720.04 | 719.81 | | | | | | | | | | | | |
| 48.5 | | | 717.08 | 716.76 | | | | | | | | | | | | |
| 49.5 | | | | | | | | | | | | | | | | |
| 50.5 | | | | | | | | | | | | | | | | |

The 0–0, 0–1, 1–0, 1–1, 1–2, 2–1, and 2–3 band of the $C\,^2\Pi_{1/2}$–$X\,^2\Pi_{1/2}$ transition.

| J | 0 - 0 | | | | 0 - 1 | | 1 - 0 | | 1 - 1 | | | 1 - 2 | | 2 - 1 | | 2 - 3 | |
|---|---|---|---|---|---|---|---|---|---|---|---|---|---|---|---|---|---|
| | $R_e$ | $R_f$ | $P_e$ | $P_f$ | $R_e$ | $P_f$ | $R_e$ | $P_f$ | $R_e$ | $P_e$ | $P_f$ | $R_e$ | $P_f$ | $R_e$ | $P_f$ | $R_e$ | $P_f$ |
| 1.5 | 18694.31 | | | 18690.63 | 18066.91 | 18063.19 | | | | | | | | | | | |
| 2.5 | 695.11 | 18694.57 | | 689.65 | 067.76 | 062.28 | | | | | | | | | | | |
| 3.5 | 695.90 | 695.19 | | 688.51 | 068.53 | 061.25 | | | 18685.53 | | 18678.28 | 19066.79 | | | | | |
| 4.5 | 696.65 | 695.90 | | 687.49 | 069.29 | 060.22 | | | 686.27 | | 677.19 | 067.59 | 18058.48 | | | | |
| 5.5 | 697.36 | 696.38 | | 686.41 | 070.06 | 059.12 | 19314.26 | 19303.44 | 686.97 | | 676.13 | 068.34 | 057.51 | 19296.19 | 19285.47 | 18067.37 | 18056.48 |
| 6.5 | 698.02 | 696.91 | | 685.25 | 070.82 | 058.01 | 314.89 | 302.25 | 687.62 | 18675.73 | 674.99 | 069.08 | 056.49 | 296.79 | 284.31 | 068.12 | 055.65 |
| 7.5 | 698.64 | 697.36 | | 684.04 | 071.50 | 056.89 | 315.46 | 300.99 | 688.25 | 674.67 | 673.85 | 069.78 | 055.34 | 297.34 | 283.12 | 068.86 | 054.55 |
| 8.5 | 699.23 | 697.96 | | 682.80 | 072.16 | 055.73 | 315.96 | 299.70 | 688.89 | 673.67 | 672.65 | 070.45 | 054.21 | 297.89 | 281.85 | 069.49 | 053.49 |
| 9.5 | 699.77 | 698.26 | | 681.50 | 072.79 | 054.54 | 316.43 | 298.39 | 689.45 | 672.51 | 671.40 | 071.09 | 053.06 | 298.40 | 280.57 | 070.20 | 052.28 |
| 10.5 | 700.26 | 698.64 | | 680.21 | 073.37 | 053.34 | 316.88 | 296.99 | 689.95 | 671.40 | 670.12 | 071.73 | 051.87 | 298.85 | 279.25 | 070.82 | 051.21 |
| 11.5 | 700.75 | 698.98 | 18680.28 | 678.85 | 073.96 | 052.08 | 317.24 | 295.56 | 690.45 | 670.22 | 668.82 | 072.34 | 050.66 | 299.28 | 277.86 | 071.50 | 050.01 |
| 12.5 | 701.17 | 699.23 | 679.04 | 677.42 | 074.53 | 050.81 | 317.56 | 294.13 | 690.50 | 669.02 | 667.47 | 072.95 | 049.43 | 299.63 | 276.44 | 072.02 | 048.87 |
| 13.5 | 701.57 | 699.55 | 677.76 | 676.03 | 075.01 | 049.48 | 317.88 | 292.64 | 691.32 | 667.72 | 666.08 | 073.42 | 048.17 | 299.91 | 274.99 | 072.59 | 047.65 |
| 14.5 | 701.93 | 699.77 | 676.43 | 674.57 | 075.47 | 048.17 | 318.12 | 291.07 | 691.70 | 666.41 | 664.67 | 073.96 | 046.88 | 300.21 | 273.47 | 073.14 | 046.41 |
| 15.5 | 702.24 | 699.94 | 675.07 | 673.06 | 075.96 | 046.78 | 318.34 | 289.51 | 692.06 | 665.13 | 663.24 | 074.44 | 045.57 | 300.41 | 271.91 | 073.60 | 045.12 |
| 16.5 | 702.51 | 700.10 | 673.67 | 671.52 | 076.37 | 045.41 | 318.49 | 287.84 | 692.35 | 663.74 | 661.73 | 074.86 | 044.23 | 300.64 | 270.38 | 074.13 | 043.85 |
| 17.5 | 702.76 | 700.27 | 672.20 | 669.94 | 076.79 | 043.97 | 318.63 | 286.17 | 692.64 | 662.32 | 660.21 | 075.27 | 042.84 | 300.76 | 268.74 | 074.53 | 042.53 |
| 18.5 | 702.97 | 700.27 | 670.73 | 668.32 | 077.14 | 042.53 | 318.68 | 284.45 | 692.85 | 660.88 | 658.65 | 075.67 | 041.47 | 300.85 | 267.06 | 075.01 | 041.20 |
| 19.5 | 703.13 | 700.27 | 669.22 | 666.67 | 077.52 | 041.06 | 318.68 | 282.68 | 693.06 | 659.46 | 657.06 | 076.03 | 040.05 | 300.95 | 265.39 | 075.40 | 039.85 |
| 20.5 | 703.23 | 700.27 | 667.63 | 664.97 | 077.78 | 039.53 | 318.68 | 280.86 | 693.21 | | 655.42 | 076.37 | 038.60 | 300.99 | 263.63 | 075.79 | 038.45 |
| 21.5 | 703.30 | | 666.09 | 663.24 | 078.06 | 038.00 | 318.63 | 279.00 | 693.36 | | 653.77 | 076.71 | 037.12 | 300.99 | 261.85 | 076.22 | 037.04 |
| 22.5 | 703.35 | | 664.42 | 661.48 | 078.29 | 036.43 | 318.49 | 277.10 | 693.49 | | 652.07 | 077.04 | 035.63 | 300.95 | 259.99 | 076.53 | 035.53 |
| 23.5 | 703.35 | | 662.74 | 659.67 | 078.55 | 034.84 | 318.34 | 275.15 | 693.49 | | 650.33 | 077.34 | 034.06 | 300.85 | 258.13 | 076.82 | 034.16 |
| 24.5 | 703.30 | | 661.02 | 657.82 | 078.69 | 033.21 | 318.12 | 273.18 | 693.49 | | 648.57 | 077.56 | 032.57 | | 256.23 | 077.09 | 032.69 |
| 25.5 | 703.23 | | 659.30 | 655.95 | 078.85 | 031.57 | 317.88 | 271.14 | 693.49 | | 646.76 | 077.78 | 030.98 | | 254.28 | 077.34 | 031.18 |
| 26.5 | 703.13 | | | 654.03 | | 029.87 | 317.56 | 269.03 | 693.49 | | 644.91 | 077.93 | 029.37 | | 252.27 | 077.62 | 029.66 |
| 27.5 | 702.97 | | | 652.07 | | 028.17 | 317.24 | 266.93 | 693.36 | | 643.04 | 078.06 | 027.75 | | 250.25 | 077.84 | 028.11 |
| 28.5 | 702.76 | | | 650.08 | | 026.45 | 316.88 | 264.72 | 693.21 | | 641.14 | 078.21 | 026.10 | | 248.17 | 078.02 | 026.52 |
| 29.5 | 702.51 | | | 648.05 | | 024.68 | 316.43 | 262.54 | 693.06 | | 639.19 | 078.29 | 024.41 | | 246.01 | 078.21 | 024.94 |
| 30.5 | 702.24 | | | 645.99 | | 022.89 | 315.96 | 260.31 | 692.85 | | 637.19 | 078.37 | 022.72 | | | 078.37 | 023.33 |
| 31.5 | 701.93 | | | 643.88 | | 021.07 | 315.46 | 257.97 | 692.64 | | 635.20 | 078.42 | 020.98 | | | | 021.68 |
| 32.5 | 701.57 | | | 641.75 | | 019.22 | 314.89 | 255.67 | 692.35 | | 633.15 | 078.42 | 019.22 | | | | 020.01 |
| 33.5 | 701.17 | | | 639.57 | | 017.33 | 314.26 | 253.32 | 692.06 | | 631.08 | 078.42 | 017.44 | | | | 018.32 |
| 34.5 | 700.75 | | | 637.36 | | 015.45 | 313.64 | 250.93 | 691.70 | | 628.97 | 078.37 | 015.63 | | | | 016.61 |
| 35.5 | 700.26 | | | 635.10 | | 013.52 | 312.94 | 248.35 | 691.22 | | 626.81 | | 013.80 | | | | 014.89 |
| 36.5 | 699.77 | | | 632.82 | | 011.56 | 312.16 | 245.87 | 690.90 | | 624.64 | | 011.96 | | | | 013.11 |
| 37.5 | 699.23 | | | 630.49 | | 009.57 | | | | | 622.41 | | 010.08 | | | | 011.33 |
| 38.5 | 698.64 | | | 628.12 | | 007.56 | | | | | 620.17 | | 008.15 | | | | 009.51 |
| 39.5 | 698.02 | | | 625.73 | | 005.52 | | | | | 617.87 | | 006.14 | | | | |
| 40.5 | 697.36 | | | 623.30 | | 003.45 | | | | | 615.56 | | 004.24 | | | | |
| 41.5 | 696.65 | | | 620.83 | | 001.36 | | | | | 613.20 | | | | | | |
| 42.5 | 695.90 | | | 618.32 | | 17999.26 | | | | | 610.80 | | | | | | |
| 43.5 | | | | 615.78 | | | | | | | 608.41 | | | | | | |
| 44.5 | | | | 613.20 | | | | | | | 605.92 | | | | | | |
| 45.5 | | | | 610.59 | | | | | | | 603.44 | | | | | | |
| 46.5 | | | | 607.94 | | | | | | | 600.91 | | | | | | |
| 47.5 | | | | 605.25 | | | | | | | 598.39 | | | | | | |
| 48.5 | | | | 602.55 | | | | | | | 595.77 | | | | | | |
| 49.5 | | | | 599.77 | | | | | | | | | | | | | |
| 50.5 | | | | 596.99 | | | | | | | | | | | | | |
| 51.5 | | | | 594.15 | | | | | | | | | | | | | |

The 0–0 bands of the $C\,^2\Pi_{3/2}$–$X\,^2\Pi_{1/2}$ and $C\,^2\Pi_{1/2}$–$X\,^2\Pi_{3/2}$ transitions.

| J | 0 - 0 | | | | | | 0 - 0 | |
|---|---|---|---|---|---|---|---|---|
| | $R_f$ | $R_e$ | $Q_{ef}$ | $Q_{fe}$ | $P_f$ | $P_e$ | $Q_{ef}$ | $Q_{fe}$ |
| 0.5 | 18535.70 | 18535.70 | | | | | | |
| 1.5 | 536.48 | 536.48 | 18534.44 | 18534.44 | | | | 18968.80 |
| 2.5 | 537.20 | 537.20 | 534.30 | 534.30 | 18532.18 | 18532.18 | 18969.11 | 968.64 |
| 3.5 | 537.90 | 537.90 | 534.12 | 534.12 | 531.18 | 531.18 | - | 968.43 |
| 4.5 | 538.54 | 538.54 | 533.98 | 533.92 | 530.19 | 530.19 | 968.96 | 968.19 |
| 5.5 | 539.16 | 539.11 | 533.73 | 533.66 | 529.08 | 529.05 | 968.80 | 967.82 |
| 6.5 | 539.71 | 539.64 | 533.45 | 533.35 | 527.94 | 527.89 | 968.64 | 967.58 |
| 7.5 | 540.24 | 540.13 | 533.12 | 533.01 | 526.83 | 526.72 | 968.43 | 967.27 |
| 8.5 | 540.70 | 540.58 | 532.75 | 532.62 | 525.61 | 525.47 | 968.19 | 966.83 |
| 9.5 | 541.12 | 540.92 | 532.33 | 532.18 | 524.35 | 524.22 | 967.82 | 966.39 |
| 10.5 | 541.49 | 541.33 | 531.85 | 531.70 | 523.05 | 522.90 | 967.46 | 965.88 |
| 11.5 | 541.89 | 541.66 | 531.35 | 531.18 | 521.69 | 521.51 | 967.14 | 965.35 |
| 12.5 | 542.12 | 541.94 | 530.79 | 530.61 | 520.28 | 520.13 | 966.75 | 964.81 |
| 13.5 | 542.31 | 542.14 | 530.19 | 530.00 | 518.87 | 518.68 | 966.27 | 964.22 |
| 14.5 | 542.58 | 542.31 | 529.55 | 529.33 | 517.39 | 517.17 | 965.76 | 963.60 |
| 15.5 | 542.75 | 542.47 | 528.86 | 528.63 | 515.87 | 515.65 | 965.29 | 962.89 |
| 16.5 | 542.80 | 542.58 | 528.13 | 527.88 | 514.28 | 514.07 | 964.70 | 962.19 |
| 17.5 | 542.80 | 542.58 | 527.36 | 527.09 | 512.70 | 512.43 | 964.07 | 961.41 |
| 18.5 | 542.80 | 542.58 | 526.53 | 526.26 | 511.00 | 510.77 | 963.45 | 960.66 |
| 19.5 | 542.80 | 542.58 | 525.66 | 525.37 | 509.31 | 509.05 | 962.76 | 959.81 |
| 20.5 | 542.75 | 542.47 | 524.75 | 524.43 | 507.56 | 507.28 | 962.05 | 958.94 |
| 21.5 | 542.58 | 542.31 | 523.79 | 523.46 | 505.78 | 505.47 | 961.27 | 958.01 |
| 22.5 | 542.47 | 542.14 | 522.79 | 522.45 | 503.94 | 503.61 | 960.47 | 957.07 |
| 23.5 | 542.25 | 541.89 | 521.75 | 521.39 | 502.05 | 501.73 | 959.64 | 956.12 |
| 24.5 | 541.94 | 541.61 | 520.66 | 520.28 | 500.15 | 499.83 | 958.75 | |
| 25.5 | 541.66 | 541.28 | 519.53 | 519.12 | 498.15 | 497.84 | | |
| 26.5 | 541.33 | 540.97 | 518.37 | 517.93 | 496.08 | 495.81 | | |
| 27.5 | 540.92 | 540.52 | 517.17 | 516.70 | 494.02 | 493.74 | | |
| 28.5 | 540.52 | 540.13 | 515.87 | 515.40 | 491.95 | 491.62 | | |
| 29.5 | 540.04 | 539.64 | 514.56 | 514.07 | 489.94 | 489.48 | | |
| 30.5 | 539.45 | 539.11 | 513.21 | 512.70 | 487.61 | 487.27 | | |
| 31.5 | 538.88 | 538.54 | 511.82 | 511.29 | 485.41 | 485.04 | | |
| 32.5 | 538.28 | 537.91 | 510.38 | 509.82 | 483.17 | 482.78 | | |
| 33.5 | 537.62 | 537.25 | 508.88 | 508.31 | 480.84 | 480.43 | | |
| 34.5 | 536.90 | 536.53 | 507.36 | 506.78 | 478.47 | 478.07 | | |
| 35.5 | 536.18 | 535.77 | 505.78 | 505.16 | 476.05 | 475.67 | | |
| 36.5 | | 535.00 | 504.19 | 503.55 | 473.57 | 473.22 | | |
| 37.5 | | 534.13 | 502.55 | 501.90 | 471.14 | 470.72 | | |
| 38.5 | | | 500.86 | 500.15 | 468.65 | 468.20 | | |
| 39.5 | | | 499.08 | 498.39 | 466.02 | 465.65 | | |
| 40.5 | | | 497.39 | 496.61 | 463.34 | 462.96 | | |

The 0–0 and 1–1 bands of the $D\ ^2\Delta_{5/2}-X\ ^2\Pi_{3/2}$ transition and the 0–0 band of the $D\ ^2\Delta_{3/2}-X\ ^2\Pi_{1/2}$ transition.

| J | 0 - 0 | | | 1 - 1 | | | 0 - 0 | | | | | |
|---|---|---|---|---|---|---|---|---|---|---|---|---|
| | $R_e+R_f$ | $Q_{ef}+Q_{fe}$ | $P_e+P_f$ | $R_e+R_f$ | $Q_{ef}+Q_{fe}$ | $P_e+P_f$ | $R_f$ | $R_e$ | $Q_{ef}$ | $Q_{fe}$ | $P_f$ | $P_e$ |
| 0.5 | | | | | | | 18945.67 | 18945.67 | | | | |
| 1.5 | | | | | | | 946.49 | 946.49 | 18944.33 | 18944.33 | | |
| 2.5 | | | | | | | 947.24 | 947.24 | 944.27 | 944.27 | 18942.17 | 18942.17 |
| 3.5 | | | | | | | 947.99 | 947.95 | 944.13 | 944.13 | 941.22 | 941.22 |
| 4.5 | | | | | | | 948.70 | 948.63 | 944.02 | 943.97 | 940.19 | 940.19 |
| 5.5 | | | | | | | 949.35 | 949.30 | 943.85 | 943.77 | 939.15 | 939.09 |
| 6.5 | 19079.34 | 19072.90 | | | | | 950.00 | 949.91 | 943.63 | 943.54 | 938.10 | 938.01 |
| 7.5 | 080.09 | 072.73 | 19066.20 | | | | 950.65 | 950.59 | 943.40 | 943.28 | 937.02 | 936.95 |
| 8.5 | 080.82 | 072.59 | 065.24 | | | | 951.19 | 951.06 | 943.12 | 942.99 | 935.90 | 935.76 |
| 9.5 | 081.50 | 072.43 | 064.21 | 19096.90 | | | 951.72 | 951.57 | 942.79 | 942.68 | 934.74 | 934.59 |
| 10.5 | 082.19 | 072.22 | 063.17 | 087.55 | 19077.69 | | 952.22 | 952.07 | 942.45 | 942.31 | 933.52 | 933.38 |
| 11.5 | 082.84 | 072.03 | 062.07 | 088.24 | 077.48 | 19067.65 | 952.69 | 952.52 | 942.07 | 941.92 | 932.29 | 932.20 |
| 12.5 | 083.50 | 071.80 | 061.00 | 088.83 | 077.29 | 066.54 | 953.12 | 952.94 | 941.66 | 941.48 | 931.00 | 930.85 |
| 13.5 | 084.09 | 071.54 | 059.87 | 089.45 | 077.03 | 065.42 | 953.52 | 953.32 | 941.22 | 941.07 | 929.74 | 929.55 |
| 14.5 | 084.70 | 071.27 | 058.73 | 090.08 | 076.79 | 064.35 | 953.89 | 953.69 | 940.73 | 940.52 | 928.39 | 928.30 |
| 15.5 | 085.29 | 071.00 | 057.60 | 090.65 | 076.49 | 063.29 | 954.21 | 954.05 | 940.22 | 939.99 | 927.04 | 926.83 |
| 16.5 | 085.83 | 070.69 | 056.43 | 091.19 | 076.20 | 062.07 | 954.55 | 954.32 | 939.67 | 939.43 | 925.65 | 925.41 |
| 17.5 | 086.40 | 070.38 | 055.25 | 091.77 | 075.90 | 060.94 | 954.78 | 954.55 | 939.09 | 938.84 | 924.18 | 923.96 |
| 18.5 | 086.90 | 070.04 | 054.04 | 092.27 | 075.57 | 059.70 | 955.01 | 954.78 | 938.47 | 938.24 | 922.75 | 922.52 |
| 19.5 | 087.42 | 069.69 | 052.82 | 092.81 | 075.22 | 058.55 | 955.22 | 955.01 | 937.82 | 937.57 | 921.29 | 921.07 |
| 20.5 | 087.91 | 069.31 | 051.59 | 093.25 | 074.87 | 057.37 | 955.37 | 955.11 | 937.14 | 936.86 | 919.77 | 919.48 |
| 21.5 | 088.38 | 068.93 | 050.33 | 093.73 | 074.49 | 056.09 | 955.51 | 955.22 | 936.43 | 936.13 | 918.19 | 917.89 |
| 22.5 | 088.82 | 068.52 | 049.07 | 094.17 | 074.08 | 054.84 | 955.60 | 955.30 | 935.69 | 935.35 | 916.59 | 916.28 |
| 23.5 | 089.29 | 068.09 | 047.79 | 094.65 | 073.68 | 053.57 | 955.70 | 955.37 | 934.91 | 934.58 | 914.96 | 914.69 |
| 24.5 | 089.69 | 067.65 | 046.47 | 095.08 | 073.25 | 052.29 | 955.70 | 955.37 | 934.09 | 933.75 | 913.30 | 913.01 |
| 25.5 | 090.09 | 067.18 | 045.15 | 095.46 | 072.80 | 050.99 | 955.70 | 955.37 | 933.25 | 932.89 | 911.64 | 911.21 |
| 26.5 | 090.46 | 066.71 | 043.82 | 095.86 | 072.34 | 049.66 | 955.70 | 955.30 | 932.36 | 931.99 | 909.99 | 909.47 |
| 27.5 | 090.82 | 066.20 | 042.46 | 096.23 | 071.84 | 048.34 | 955.60 | 955.22 | 931.46 | 931.06 | 908.12 | 907.74 |
| 28.5 | 091.19 | 065.69 | 041.08 | 096.57 | 071.35 | 046.99 | 955.51 | 955.11 | 930.52 | 930.12 | 906.35 | 905.95 |
| 29.5 | 091.49 | 065.16 | 039.69 | 096.91 | 070.84 | 045.62 | 955.37 | 955.01 | 929.55 | 929.13 | 904.53 | 904.11 |
| 30.5 | 091.77 | 064.61 | 038.28 | 097.21 | 070.32 | 044.28 | 955.22 | 954.78 | 928.52 | 928.11 | 902.67 | 902.26 |
| 31.5 | 092.07 | 064.04 | 036.85 | 097.50 | 069.75 | 042.90 | 955.01 | 954.55 | 927.49 | 927.04 | 900.80 | 900.36 |
| 32.5 | 092.32 | 063.45 | 035.41 | 097.82 | 069.19 | 041.42 | 954.78 | 954.32 | 926.41 | 925.95 | 898.87 | 898.44 |
| 33.5 | 092.60 | 062.85 | 033.95 | 098.11 | 068.59 | 040.00 | 954.55 | 954.05 | 925.31 | 924.85 | 896.95 | 896.47 |
| 34.5 | 092.81 | 062.21 | 032.46 | 098.35 | 067.99 | 038.56 | 954.21 | 953.76 | 924.18 | 923.70 | 894.96 | 894.48 |
| 35.5 | 093.04 | 061.58 | 030.97 | 098.58 | 067.38 | 037.02 | 953.89 | 953.44 | 923.02 | 922.52 | 892.97 | |
| 36.5 | 093.25 | 060.94 | 029.47 | 098.81 | 066.71 | 035.59 | 953.52 | 952.99 | 921.80 | 921.29 | | |
| 37.5 | 093.39 | 060.25 | 027.92 | 098.99 | 066.08 | 034.12 | 953.20 | 952.69 | 920.59 | 920.06 | | |
| 38.5 | 093.56 | 059.56 | 026.37 | | 065.42 | 032.56 | 952.80 | 952.32 | 919.34 | 919.80 | | |
| 39.5 | 093.73 | 058.95 | 024.83 | | 064.71 | 031.04 | 952.33 | 951.72 | 918.05 | 917.48 | | |
| 40.5 | 093.83 | 058.12 | 023.23 | | 064.04 | 029.47 | 951.86 | 951.19 | 916.71 | 916.14 | | |
| 41.5 | 093.91 | 057.37 | 021.64 | | 063.28 | 027.92 | 951.19 | 950.65 | 915.34 | 914.81 | | |
| 42.5 | 094.03 | 056.60 | 020.02 | | 062.54 | 026.37 | 950.65 | 950.10 | 913.95 | 913.41 | | |
| 43.5 | 094.13 | 055.83 | 018.39 | | 061.78 | | 950.10 | 949.49 | 912.54 | 911.94 | | |
| 44.5 | | 055.03 | 016.74 | | 061.00 | | 949.49 | 948.98 | 911.09 | 910.52 | | |
| 45.5 | | 054.20 | 015.07 | | | | | | 909.58 | 909.01 | | |
| 46.5 | | 053.36 | 013.41 | | | | | | | | | |
| 47.5 | | 052.51 | 011.70 | | | | | | | | | |
| 48.5 | | 051.66 | | | | | | | | | | |
| 49.5 | | 050.76 | | | | | | | | | | |
| 50.5 | | 049.32 | | | | | | | | | | |
| 51.5 | | 048.91 | | | | | | | | | | |

ARTICLE N° 6

JOURNAL OF MOLECULAR SPECTROSCOPY 77, 29–35 (1979)

# Rotational Analysis of a $^2\Delta$–$^2\Pi$ System of NiF

B. PINCHEMEL, Y. LEFEBVRE, AND J. SCHAMPS

*Laboratoire de Spectroscopie des Molécules Diatomiques, Equipe de Recherche Associée au CNRS No. 303, Université de Lille I–bâtiment P5–B.P. 36, 59650–Villeneuve d'Ascq, France*

A $^2\Delta$–$^2\Pi$ system of NiF has been obtained in emission from a "composite wall hollow cathode" in the blue region. High-dispersion rotational analysis has led to the following constants (in $cm^{-1}$):

| | $^2\Pi_{1/2}$ | $^2\Pi_{3/2}$ | $^2\Delta_{3/2}$ | $^2\Delta_{5/2}$ |
|---|---|---|---|---|
| $B$ | 0.3861 | 0.3886 | 0.3772 | 0.3792 |
| $D \times 10^6$ | 0.46 | 0.35 | 0.40 | 0.37 |
| $p$ | 0.154 | | | |
| $p_J$ | $-3.8 \times 10^{-6}$ | | | |


## INTRODUCTION

Electronic spectra of diatomic molecules involving an atom with an open *d* shell have been extensively studied in recent years. However, the spectra of some transition metal compounds, such as NiF, are still poorly known. Moreover, NiF is isoelectronic with CuO (*1–3*), which is now experimentally fairly well known. A comparison between these two molecules could be expected to help elucidate some basic principles which govern the formation of valence orbitals in bonds involving atoms with an open *d* shell.

NiF was first discovered, at low resolution, by Krishnamurty (*4*), using high-intensity discharge techniques. He reported the occurrence of three groups of red-shaded intense bandheads. He suggested that these groups were the $\Delta v = 0$, $\Delta v = -1$, and $\Delta v = -2$ sequences of a $^2\Pi$–$^2\Sigma$ transition. But he did not carry out rotational analyses. Some difficulty was experienced in the use of high-intensity discharge techniques: Free fluorine liberated during the exposure reacts with the wall of the discharge tube and emits silicon fluoride bands in the spectral region of NiF.

## EXPERIMENTAL DETAILS AND DESCRIPTION OF THE BANDS

The composite wall hollow-cathode (CWHC) lamp (*5*) used for obtaining spectra of NiF fulfills two important requirements: First, this source avoids the emission of the SiF spectra which were so troublesome in Krishnamurty's high-intensity excitation; second, it simplifies spectral analysis of the complex and compact structure of NiF bands owing to its ability to emit at very low temperature.

Spectra have been photographed in the third order of a plane grating spectro-



0022-2852/79/080029-07$02.00/0

graph (inverse dispersion at 4600 Å: 0.4 Å/mm, effective resolution: 400 000). Thorium lines were used as standards.

However, some strong emission lines of atomic nickel lie in the same spectral region as NiF bands and impede the observation of NiF bands. We have been able to subdue these lines by adjusting the pressure of the carrier gas, which was argon. Unfortunately, some atomic lines of Ar also occurred in the spectrum. Trying to replace argon by neon has sometimes been advantageous, but this carrier gas also emits atomic lines in the same region and slightly intensifies the emission lines of the cathode metal Ni (*5*).

In the 4500- to 4750-Å region the observed bands occur in four separate groups, three of which (4515, 4675, 4700 Å) have been seen by Krishnamurty; the fourth lies at about 4550 Å. However, we have not found the group which, according to Krishnamurty, should lie at about 4850 Å.

The structures of the two groups lying at 4550 and 4675 Å appear very difficult to explain; for example, some branches do not form a head. The analyses of these bands do not seem to be simple. The present work is only concerned with rotational analyses for the two groups situated at 4515 and 4700 Å.

In spite of the high dispersion, the structure is very compact because the rotational constants of the two states are quite similar, as will be confirmed later by the analysis. The study of the isotopic shifts $^{58}$NiF (68%) and $^{60}$NiF (26%) with $\rho = \mu^{1/2}/\mu_i^{1/2} = 0.99587$ shows that the transitions correspond to $\Delta v = 0$.

To obtain workable spectra of the 0–0 bands, it has been necessary to subdue the 1–1 and 2–2 vibrational bands by working with a very low intensity for the CWHC lamp (40 mA).

## ROTATIONAL ANALYSIS OF THE 4515- AND 4700-Å BANDS

The 4515- and 4700-Å bands show $Q$ branches which are characteristic of a transition between two states belonging to Hund's case (*a*) or eventually case (*c*) coupling. The $R$ and $P$ branches are weaker than the $Q$ branches. The higher intensity of the $R$ branch compared to the $P$ branch suggests that the transitions correspond to $\Delta\Lambda = +1$ (*6*).

The $Q$ branch of the band lying at 4700 Å consists of double lines because of the existence of two subbranches, $Q_{ef}$ and $Q_{fe}$. This band has also two $R$ heads, $R_{ee}$ and $R_{ff}$, separated by 6 cm$^{-1}$. This can be explained as due to a large $\Lambda$-type doubling in at least one of the states of the transition, which is therefore interpreted as a state with $\Omega = \frac{1}{2}$. Consequently, we can asume that the bands belong to the two subsystems of a $^2\Delta$–$^2\Pi$ transition; the 4515-Å band (where no doubling is observed) is the $^2\Delta_{5/2}$–$^2\Pi_{3/2}$ subband, while the other, at 4700 Å (with large doubling effects), is the $^2\Delta_{3/2}$–$^2\Pi_{1/2}$ subband.

In Hund's case (*a*) coupling, the term values of a $^2\Pi$ state are given by

$$^2\Pi_{3/2}{}^{F_1(J)}_{F_2(J)} = T_{ev}(^2\Pi_{3/2}) + B_{3/2}J(J+1) - D_{3/2}J^2(J+1)^2 \mp a(J+\tfrac{1}{2})(J-\tfrac{1}{2})(J+\tfrac{3}{2}); \quad (1)$$

$$^2\Pi_{1/2}{}^{F_2(J)}_{F_1(J)} = T_{ev}(^2\Pi_{1/2}) + B_{1/2}J(J+1) - D_{1/2}J^2(J+1) \mp \tfrac{1}{2}[p + p_jJ(J+1)](J+\tfrac{1}{2}), \quad (2)$$

where nearly degenerate levels have the parity $(-1)^{(J-1/2)}$ for $e$ levels and $-(-1)^{(J-1/2)}$ for $f$ levels [Kopp's and Hougen's notation (*7*)].

Rotational energy levels of both $\Omega = 3/2$ and $5/2$ components of a $^2\Delta$ state can be approximated by the classical case ($a$) formula (*8*)

$$^2\Delta_{3/2 \text{ or } 5/2}F(J) = T_{ev}(^2\Delta_{3/2 \text{ or } 5/2}) + BJ(J+1) - DJ^2(J+1)^2, \quad (3)$$

where $\Lambda$-type doubling has been neglected since $\Omega$ differs from 1/2.

On the basis of the term values given in Eqs. (1) to (3) a least-squares fitting gives the following constants for the two states (in $cm^{-1}$):

| | | | |
|---|---|---|---|
| Upper state $^2\Delta$: | $B'_{5/2}$ : 0.3792 | $D'_{5/2}$ : $0.37 \times 10^{-6}$ |
| | $B'_{3/2}$ : 0.3772 | $D'_{3/2}$ : $0.40 \times 10^{-6}$ |
| Lower state $^2\Pi$: | $B''_{3/2}$ : 0.3886 | $D''_{3/2}$ : $0.35 \times 10^{-6}$ |
| | $B''_{1/2}$ : 0.3861 | $D''_{1/2}$ : $0.46 \times 10^{-6}$ |
| | $p''$ : 0.1540 | $p''_j$ : $-3.8 \times 10^{-6}$ |

$$T'_{5/2} - T''_{3/2} = 22125.66$$

$$T'_{3/2} - T''_{1/2} = 21274.76$$

The choice of the positive sign for the $\Lambda$-doubling constant $p$ of the $^2\Pi$ state is arbitrary because it is not possible to assign the $e$ or $f$ nature of rotational levels, but with a positive sign of $p$, the sign of $p_j$ must be negative to give correct fittings.

With these constants, all lines are fitted to an accuracy better than 0.05 $cm^{-1}$ (Tables Ia, Ib). Photographs of the two systems including line assignments are given in Fig. 1.

It may be mentioned that in the $^2\Delta_{3/2}$–$^2\Pi_{1/2}$ subsystem a fit of the measured lines using the fourth-order equation in $J$ containing $D$ and $p_j$ terms was not satisfactory because of lack of data for high $J$ values. Therefore, the $D$ and $p_j$ values are not very accurate. Moreover, $\Lambda$-type doubling effects are not observed in the $^2\Delta_{5/2}$–$^2\Pi_{3/2}$ transition, so that the $a$ parameter appearing in formula (1) is negligible.

## VIBRATIONAL ASSIGNMENT

The two 0–0 bands that we have analyzed overlap other weak bands which also belong to the $\Delta v = 0$ sequences of the two $^2\Delta$–$^2\Pi$ subsystems. The weak isotopic shifts between heads of the $^{58}$NiF and $^{60}$NiF 1–1 and 2–2 bands give evidence of this assignment. These bands are compiled in Table II. In this table we can see that the heads of the 0–0 bands of the 5/2–3/2 transitions are at longer wavelengths than those of the 1–1 bands. This indicates that $G'_{5/2}(v)$ is larger than $G''_{3/2}(v)$, whereas it is just the opposite for $G'_{3/2}$ and $G''_{1/2}$ in the $\Omega = 3/2 \rightarrow \Omega = 1/2$ transition.

Krishnamurty (*4*) noted that the third group of bands (4675-Å system) is just 740 $cm^{-1}$ away from the $^2\Delta_{5/2}$–$^2\Pi_{3/2}$ $\Delta v = 0$ sequence (4515 Å system), which is the expected order of magnitude for the separation between two neighboring sequences of a single electronic transition in such halides. But the difference of rotational structures and the observation of isotopic shifts characteristic of a

TABLE Ia

The 0–0 Band of the $^2\Delta_{5/2}$–$^2\Pi_{3/2}$ System of NiF

| J | Q | R | P |
|---|---|---|---|
| | | | 22121.97 |
| | | | 121.15 |
| | | | 120.29 |
| | 22125.01 | | 119.37 |
| | 124.94 | 22132.07 | 118.35 |
| | 124.72 | 132.73 | - |
| 10.5 | 124.57 | 133.30 | - |
| | 124.29 | 133.87 | 115.59 |
| | 124.16 | 134.31 | 114.64 |
| | 123.81 | 134.80 | 113.61 |
| | 123.55 | 135.27 | 112.56 |
| 15.5 | 123.29 | 135.72 | 111.52 |
| | 122.95 | 136.13 | 110.52 |
| | 122.66 | 136.72 | 109.36 |
| | 122.30 | 137.11 | 108.30 |
| | 121.97 | 137.44 | 107.16 |
| 20.5 | 121.53 | 137.76 | - |
| | 121.15 | 138.15 | 104.85 |
| | 120.72 | 138.59 | 103.65 |
| | 120.29 | 138.82 | 102.45 |
| | 119.83 | 139.14 | 101.28 |
| 25.5 | 119.39 | 139.39 | 100.05 |
| | 118.87 | 139.70 | 98.79 |
| | 118.35 | 139.93 | 97.54 |
| | 117.74 | 140.07 | 96.24 |
| | 117.28 | 140.33 | 94.93 |
| 30.5 | 116.68 | - | 93.60 |
| | 116.13 | - | 92.26 |
| | 115.59 | - | 90.92 |
| | 114.93 | - | 89.53 |
| | 114.26 | - | 88.13 |
| 35.5 | 113.61 | - | 86.71 |
| | 112.88 | - | 85.30 |
| | 112.19 | - | 83.82 |
| | 111.52 | - | 82.41 |
| | 110.79 | 141.30 (Head) | 80.88 |
| 40.5 | 109.98 | | 79.33 |
| | 109.26 | | 77.87 |
| | 108.49 | | 76.29 |
| | 107.63 | | 74.79 |
| | - | | 73.22 |
| 45.5 | - | | 71.63 |
| | 105.09 | | 70.01 |
| | 104.26 | | 68.41 |
| | 103.37 | | 66.73 |
| | 102.45 | | 65.01 |
| 50.5 | 101.47 | | |
| | 100.54 | | |
| | 99.59 | | |
| | 98.61 | | |

$\Delta v = 0$ sequence for the 4675-Å system indicates that this system is a new electronic transition of NiF and not the $\Delta v = -1$ sequence of the $^2\Delta_{5/2}$–$^2\Pi_{3/2}$ system, as initially suggested by Krishnamurty.

## CONCLUSION

Owing to the use of our low-temperature hollow-cathode source, it has been possible to analyze two groups of bands of NiF as the subsystems corresponding to a transition between a $^2\Delta$ state and a $^2\Pi$ state. It is not definitely established

TABLE Ib

The 0–0 Band of the $^2\Delta_{3/2}$–$^2\Pi_{1/2}$ System of NiF

| J | $Q_{ef}$ | $Q_{fe}$ | $R_{ee}$ | $R_{ff}$ | $P_{ee}$ | $P_{ff}$ |
|---|---|---|---|---|---|---|
| | 21274.16 | | | | | |
| 5.5 | 273.95 | | | | | |
| | 273.78 | | | | | |
| | 273.56 | | | | | |
| | 273.36 | 21274.73 | | | | |
| | 273.12 | 274.65 | 21282.58 | | | |
| 10.5 | 272.85 | 274.55 | 283.22 | 21281.53 | | |
| | 272.57 | 274.40 | 283.32 | 282.00 | | |
| | 272.26 | - | 284.47 | 282.44 | | |
| | - | 274.12 | 285.04 | 282.88 | | |
| | 271.61 | 273.94 | 285.59 | 283.32 | | |
| 15.5 | 271.26 | 273.75 | 286.17 | - | | |
| | 270.90 | 273.52 | 286.70 | - | | |
| | 270.54 | - | 287.17 | 284.47 | | |
| | 270.08 | 273.03 | 287.72 | 284.78 | | |
| | 269.71 | 272.75 | 288.20 | | | |
| 20.5 | 269.26 | 272.46 | 288.66 | | | |
| | 268.83 | 272.14 | 289.08 | | | |
| | 268.31 | 271.83 | - | | | 21251.38 |
| | 267.82 | 271.49 | 289.92 | | | 250.10 |
| | 267.33 | 271.15 | 290.33 | | | 248.90 |
| 25.5 | 266.82 | 270.72 | 290.89 | | 21251.51 | 247.60 |
| | 266.25 | 270.36 | 291.04 | | 250.35 | 246.35 |
| | 265.66 | 269.95 | | | 249.20 | |
| | | 269.50 | | | 248.00 | |
| | | 269.08 | | | 246.80 | |
| 30.5 | | 268.58 | | | - | |
| | | 268.13 | | | 244.38 | |
| | | 267.63 | 294.47 | 288.17 | 243.14 | |
| | | 267.11 | (Head J=46.5) | (Head J=38.5) | | |
| | | 266.57 | | | | |
| 35.5 | | 266.02 | | | | |
| | | 265.43 | | | | |

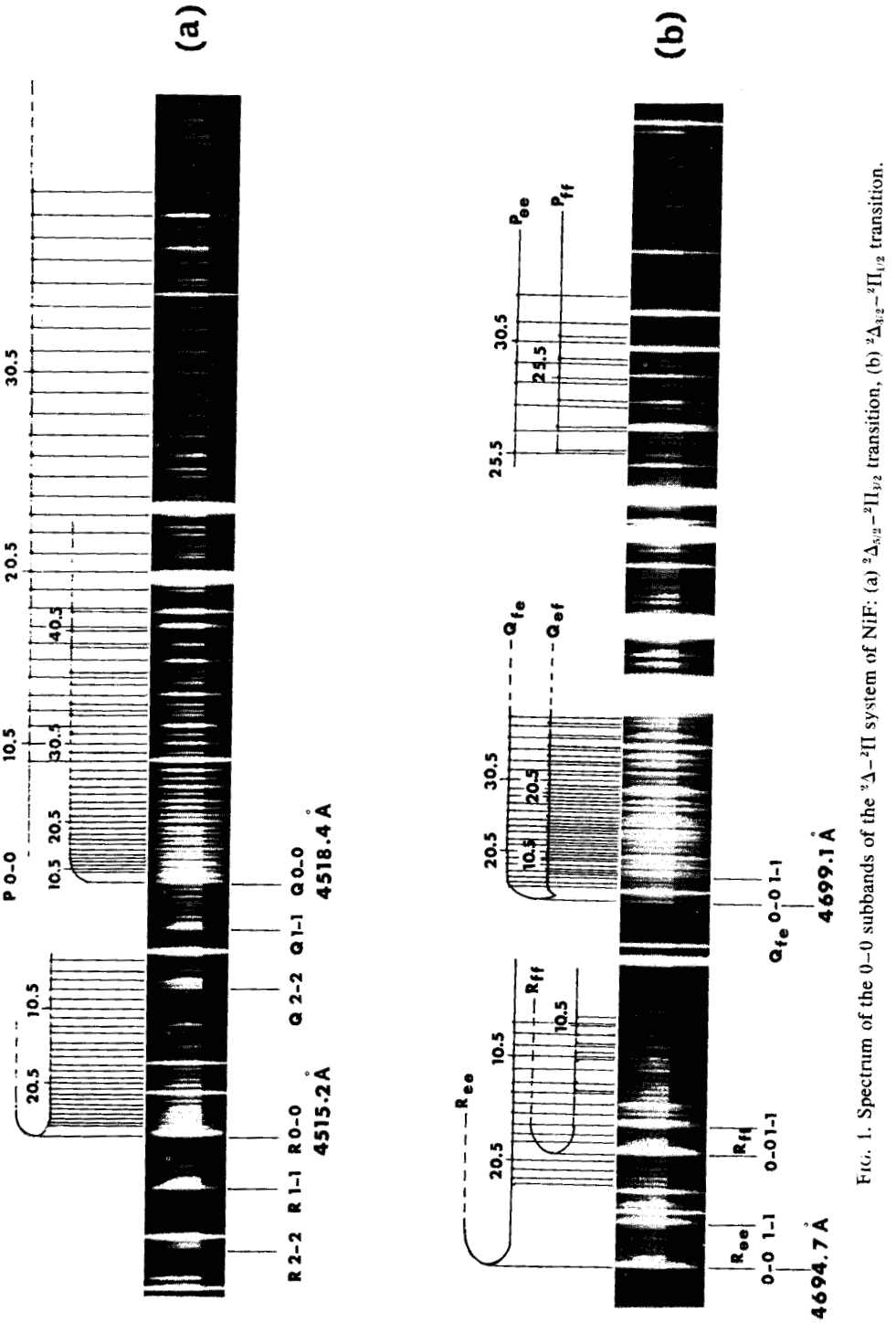


FIG. 1. Spectrum of the 0–0 subbands of the $^2\Delta$–$^2\Pi$ system of NiF: (a) $^2\Delta_{5/2}$–$^2\Pi_{3/2}$ transition, (b) $^2\Delta_{3/2}$–$^2\Pi_{1/2}$ transition.

TABLE II

Heads of the $^2\Delta$–$^2\Pi$ Bands of the NiF Molecule

| Transition | v' – v" | Branch | λ (Å) | ν(cm$^{-1}$) |
|---|---|---|---|---|
| $^2\Delta_{5/2}$ – $^2\Pi_{3/2}$ | 2 – 2 | $R_{ee}$ + $R_{ff}$ | 4513.73 | 22148.40 |
| | 1 – 1 | " | 4514.50 | 22144.63 |
| | 0 – 0 | " | 4515.18 | 22141.30 |
| | 2 – 2 | $Q_{ef}$ + $Q_{fe}$ | 4517.07 | 22132.00 |
| | 1 – 1 | " | 4517.80 | 22128.50 |
| | 0 – 0 | " | 4518.38 | 22125.61 |
| $^2\Delta_{3/2}$ – $^2\Pi_{1/2}$ | 0 – 0 | $R_{ee}$ | 4694.74 | 21294.47 |
| | 1 – 1 | " | 4695.33 | 21291.79 |
| | 0 – 0 | $R_{ff}$ | 4696.12 | 21288.17 |
| | 1 – 1 | " | 4696.45 | 21286.70 |
| | 0 – 0 | $Q_{fe}$ | 4699.10 | 21274.73 |
| | 1 – 1 | " | 4699.35 | 21273.56 |

which of these states is the lower, since both $^2\Pi$–$^2\Delta$ and $^2\Delta$–$^2\Pi$ transitions lead to practically similar line patterns. However, intensity considerations seem to indicate that the $^2\Pi$ state is the lower state of the transition. Another proof would be to look at the origin locations of the *R* branches which differ by *p* for $^2\Delta$–$^2\Pi$ and $^2\Pi$–$^2\Delta$ transitions. But the few *R* lines observed did not lead to positive conclusions at this point.

It is probably too early to attempt a firm configuration assignment for the two observed states. We hope that the analysis of the two other groups of bands will be feasible so that we have more information to use in order to interpret at least the electronic structure of the ground state of the NiF molecule. At the present time, it is not known whether the transition analyzed here involves the ground state or some other low-lying state of the molecule.

RECEIVED: June 28, 1978

REFERENCES


1. O. APPELBLAD AND A. LAGERQVIST, *Phys. Scrip.* 13, 275–288 (1976).
2. Y. LEFEBVRE, B. PINCHEMEL, AND J. SCHAMPS, *J. Mol. Spectrosc.* **68**, 81–88 (1977).
3. O. APPELBLAD, A. LAGERQVIST, Y. LEFEBVRE, B. PINCHEMEL, AND J. SCHAMPS, *Phys. Scrip.* **18**, 125–136 (1978).
4. V. G. KRISHNAMURTY, *Indian J. Phys.* **27**, 354–358 (1953).
5. R. BACIS, *J. Phys. E* **9**, 1081–1086 (1976).
6. I. KOVACS, "Rotational Structure in the Spectra of Diatomic Molecules", Hilger, London, 1969.
7. I. KOPP AND J. T. HOUGEN, *Canad. J. Phys.* **45**, 2581–2596 (1967).
8. G. HERZBERG, "Spectra of Diatomic Molecules," Van Nostrand, New York, 1950.

COMPLEMENT A L'ARTICLE N° 6

ROTATIONAL ANALYSIS OF $a^2\Delta - {}^2\Pi$ SYSTEM of NiF

## I - INTRODUCTION

Dans l'article qui précède nous avions noté la présence de bandes de NiF situées à 4675 Å et 4550 Å .

Elles se caractérisent par leur faible intensité et par un recouvrement important entre les bandes de la séquence située à 4675 Å .

Pour améliorer la qualité des spectres nous avons fait fonctionner une cathode creuse à parois composites (Ni + $NiF_2$) sous un courant d'intensité très faible (25 mA), afin de limiter au maximum l'excitation des niveaux de vibration élevés. Des poses de dix-huit heures ont été nécessaires pour obtenir des spectres exploitables. Toutes les autres conditions expérimentales sont identiques à celles décrites dans l'article précédent.

Cette technique a donné de bons résultats dans la zone 4675 Å (figure c1), la bande située à 4550 Å reste très confuse, on observe en effet deux séries de raies mais l'absence de têtes nettes et le manque de structure résolue dans la région que l'on peut supposer proche de l'origine rend illusoire toute tentative d'analyse.

## II - ANALYSE DE LA BANDE SITUEE A 4675 Å

La bande située à 4675 Å présente deux branches très serrées

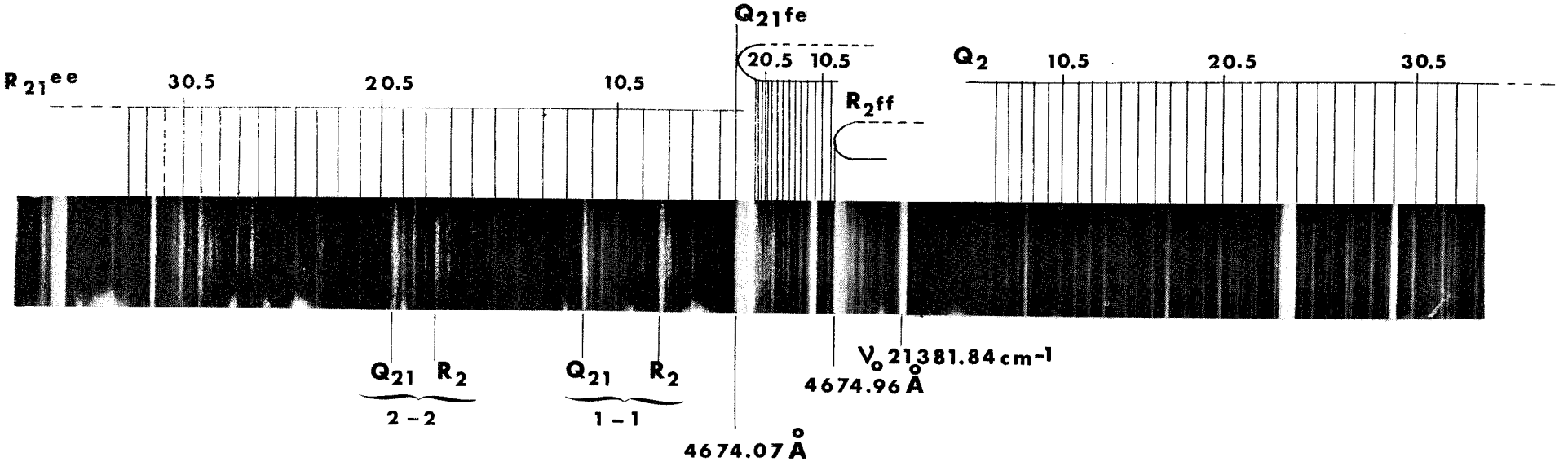


Figure cI : transition $^2\Pi_{3/2}$ - $^2\Sigma^+$ de NiF, séquence principale

dégradées vers le rouge et formant chacune une tête. L'une d'elle n'est pas résolue.

Deux autres branches sont visibles de part et d'autre de ces deux têtes. La branche se développant vers le bleu devrait former une tête, mais son évolution quasi linéaire place cette tête à une valeur de J élevée, non observable dans les conditions de fonctionnement de la cathode creuse.

L'absence de dédoublement isotopique des têtes permet d'affirmer que nous sommes bien en présence d'une bande O-O.

Cette structure est caractéristique d'une transition $^2\Pi - {}^2\Sigma$ ou $^2\Sigma - {}^2\Pi$. En fait chaque bande d'une telle transition comporte normalement six branches dans chacun des deux sous-systèmes mais quatre seulement sont nettement visibles ici.

Les branches de structure serrée sont des branches de type 1/2 dans la notation de Mulliken (1), c'est à dire des branches dont le coefficient de dépendance linéaire en J est de l'ordre de B (constante de rotation). Par contre, la branche présentant une évolution très lente est du type 3/2, c'est à dire dont le coefficient en J dans son équation est de l'ordre de 3B.

On peut noter également que la valeur de la constante $\gamma$ d'interaction spin-rotation de l'état $^2\Sigma$ doit être assez grande car l'écart entre les deux têtes est important (4 $cm^{-1}$).

A moins de pouvoir observer les tout premiers niveaux de rotation il n'est pas possible de déterminer si la transition est du type $^2\Pi - {}^2\Sigma$ ou $^2\Sigma - {}^2\Pi$.

En effet comme le montre la Table cI,on peut toujours, dans les deux cas, trouver un jeu de trois equations associant les branches de la transition deux par deux.

Notre hypothèse de départ a été d'envisager une transition $^2\Sigma - {}^2\Pi$ mettant en jeu l'état $^2\Pi$ déjà observé.

Les équations des niveaux d'énergie obtenus par diagonalisation des hamiltoniens effectifs des états $^2\Sigma$ et $^2\Pi$ (formules de Hill et Van Vleck (2) ) sont bien connues, celles de l'état $^2\Sigma$ se trouvent par exemple dans l'article numéro 3 relatif à CuO, celle du $^2\Pi$ dans l'article précédent.

Le paramètre $\gamma$ dans l'état $^2\Sigma$ traduit à la fois le dédoublement spin-rotation propre à l'état lui-même mais contient aussi, pour une part généralement largement prépondérante, l'effet des interactions de second ordre avec les niveaux vibrationnels des états $^2\Pi$ voisins.

En adoptant l'hypothèse (et par conséquent les notations) d'une transition $^2\Sigma - {}^2\Pi_{1/2}$ les trois branches résolues sont : la branche $R_{2ff}$ de type 3/2, la branche $Q_{2fe}$ résolue et formant tête (type 1/2), enfin la branche $^PQ_{12ef}$ (type 1/2). Il existe une relation de combinaison intéressante entre les branches $R_2$ et $Q_2$,elles proviennent d'un même niveau f de l'état $^2\Sigma$ supérieur et la relation de combinaison ne fait donc intervenir que des paramètres de l'état inférieur :

$R_2$ (J) - $Q_2$ (J+1) = (2B"-p) (J+1), nous trouvons par cette relation une valeur moyenne de B" - $\frac{p}{2}$ égale à 0,3787 $cm^{-1}$ ce qui ne correspond ni à la valeur trouvée pour l'état $^2\Pi_{1/2}$ (0,3091 $cm^{-1}$) déjà connu, ni à celle de l'état $^2\Pi_{3/2}$ (0,3886 $cm^{-1}$) correspondant ; rappelons que dans ce dernier cas la relation de combinaison reste valable puisque seuls changent le nom des branches (avec conservation des parités) et le résultat puisqu'en l'absence de p on obtient directement la valeur de B".

Il n'est donc pas possible que l'état $^2\Pi$ soit commun aux deux transitions. Comme il est peu vraissemblable, compte-tenu des configurations électroniques possibles pour NiF, qu'un second état $^2\Pi$, autre que celui déjà connu, se trouve dans la région des basses énergies, nous avons alors envisagé l'hypothèse d'une transition $^2\Pi$ - $^2\Sigma$ pour ce nouveau système (la figure c1 donne les noms des branches correspondant à une transition $^2\Pi_{3/2}$ - $^2\Sigma$).

L'analyse numérique a été faite en deux temps. Nous avons d'abord associé aux relations de combinaison un calcul de moindre carré linéaire classique effectué sur les branches afin de déterminer la numérotation absolue des raies. Cette détermination est facilitée par l'évolution très différente des branches du spectre. En effet un décalage d'une unité de la valeur de J modifie la position de l'origine de la branche $R_{21}$ (d'allure 3B) de 1,2 $cm^{-1}$ alors que les branches $Q_{21}$ et $R_2$ (d'allure B) ne sont décalées que de 0,4 $cm^{-1}$. La position des deux têtes des branches $Q_4$ et $R_2$ est donc un critère très précis qui permet de définir la numérotation exacte des raies.

Table CI: Equation des branches d'une transition $^2\Pi - {}^2\Sigma$ ou $^2\Sigma - {}^2\Pi$, les signes supérieurs sont relatifs à une transition $^2\Pi - {}^2\Sigma$, les signes inférieurs à une transition $^2\Sigma - {}^2\Pi$

Nomenclature

| $^2\Pi_{1/2} - {}^2\Sigma_{1/2}$ | $^2\Pi_{3/2} - {}^2\Sigma_{1/2}$ | $^2\Sigma - {}^2\Pi_{1/2}$ | $^2\Sigma - {}^2\Pi_{3/2}$ | |
|---|---|---|---|---|
| $^{R}1_{ee}$ | $^{S}R_{21_{ee}}$ | $^{R}2_{ff}$ | $^{S}R_{21_{ff}}$ | $\nu = \nu_o \mp \left[\frac{3}{4}(B_\Sigma - \gamma) + \frac{1}{4}p\right] + (2B_\Sigma + B_\Pi - \frac{\gamma}{2} - \frac{p}{2})m \mp (B_\Sigma - B_\Pi)m^2$ |
| $(m = J + 1)$ | | $(m = J + 1)$ | | |
| $^{O}P_{12_{ff}}$ | $^{P}2_{ff}$ | $^{O}P_{12_{ee}}$ | $^{P}1_{ee}$ | |
| $(m = -J)$ | | $(m = -J)$ | | |
| $^{Q}1_{fe}$ | $^{R}Q_{21_{fe}}$ | $^{Q}2_{fe}$ | $^{R}Q_{21_{fe}}$ | $\nu = \nu_o \mp \left[\frac{3}{4}(B_\Sigma - \gamma) + \frac{1}{4}p\right] + (2B_\Sigma - B_\Pi - \frac{\gamma}{2} + \frac{p}{2})m \mp (B_\Sigma - B_\Pi)m^2$ |
| $(m = J + 1)$ | | $(m = J)$ | | |
| $^{P}Q_{12_{ef}}$ | $^{Q}2_{ef}$ | $^{P}Q_{12_{ef}}$ | $^{Q}1_{fe}$ | |
| $(m = -J)$ | | $(m = -J - 1)$ | | |
| $^{Q}R_{12_{ff}}$ | $^{R}2_{ff}$ | $^{Q}R_{12_{ee}}$ | $^{R}1_{ee}$ | $\nu = \nu_o \mp \left[\frac{3}{4}(B_\Sigma + \frac{1}{3}\gamma) + \frac{1}{4}p\right] + (2B_\Sigma - B_\Pi + \frac{\gamma}{2} + \frac{p}{2})m \mp (B_\Sigma - B_\Pi)m^2$ |
| $(m = +J+2)$ | | $(m = J)$ | | |
| $^{P}1_{ee}$ | $^{Q}P_{21_{ee}}$ | $^{P}2_{ff}$ | $^{Q}P_{21_{ff}}$ | |
| $(m = -J+1)$ | | $(m = -J-1)$ | | |

Le calcul de moindre carré éffectué branche par branche présente l'inconvénient de produire plusieurs jeux de paramètres possibles. De plus la précision des résultats n'est pas optimum puisque nous ne pouvons pas introduire toutes les données expérimentales dans le même calcul.

Nous avons donc utilisé, dans un deuxième temps, un programme de moindre carré non linéaire qui permet d'analyser une transition par diagonalisation directe des matrices des états mis en jeu en utilisant de ce fait toutes les raies de la transition simultanément.

Ce programme mis au point par R.C. Stern a fait l'objet de plusieurs modifications dues notamment à T.H. Bergeman et R.A. Gottscho (3).

Dans le cas de NiF nous n'avons pas utilisé la possibilité offerte de calculer les éléments de matrice correspondant aux interactions avec d'autres états électroniques. Ces interactions sont prises en compte globalement sous forme de paramètres effectifs (coefficient $\gamma$ par exemple) introduits par une transformation de Van Vleck dans la matrice de chacun des états .

Le programme permet en outre d'attribuer un poids statistique à chaque raie et donc de tenir compte de la précision du pointé qui est fonction par exemple de l'élargissement ou du recouvrement des raies.

Un premier calcul utilisant les trois branches les plus intenses a donné un jeu de paramètres qui nous a permis d'identifier les premières raies des branches $^{Q}P_{21}$ et $P_2$ que nous avons ensuite introduites dans le calcul final.

La Table cII regroupe les nombres d'onde des raies des cinq branches, le nombre entre parenthèse représentant l'écart multiplié par 100 entre la valeur mesurée et la valeur calculée.

Les paramètres obtenus sont en $cm^{-1}$ :

| | $Te_{o-o}$ | $B_o$ | $\gamma_o$ | $D_o \times 10^7$ |
|---|---|---|---|---|
| $^2\Pi_{3/2}$ | 21381,840 (4) | 0,37880 (10) | - | 4,9 (4) |
| $^2\Sigma^+$ | 0 | 0,38567 (10) | - 0,1494 (3) | 4,9 (4) |

(l'incertitude représente une fois la déviation standard sur le dernier chiffre significatif)

Il n'a pas été possible de calculer le paramètre $\gamma_j$ qui traduit la distortion centrifuge sur $\gamma$ car la déviation standard sur ce paramètre est très élevée. Un calcul fait en incluant $\gamma_j$ donne par exemple $\gamma_j = - 0,67 \times 10^{-6} \pm 0,78 \times 10^{-6}$ $cm^{-1}$, nous avons donc préféré ne pas tenir compte de ce paramètre.

Table cII Nombres d'onde des raies de la bande O-O de la transition

$^2\Pi_{3/2} - {}^2\Sigma^+$

| J | $Q_{2ef}$ | $R_{Q_{21fe}}$ | $^{\Omega}P_{21ee}$ | $R_{2ff}$ | $S_{R_{21ee}}$ | $P_{2ff}$ |
|---|---|---|---|---|---|---|
| | | | | | 21 386.14 (-1) | |
| | | | | | 87.29 (-1) | |
| 5.5 | 21 378.03 ( 3) | 21 383.54 ( 2) | | | 88.48 ( 3) | 21 373.86 ( 3) |
| | 77.41 (-4) | 83.90 ( 1) | | | 89.57 ( 0) | 72.55 ( 2) |
| | 76.87 (-2) | - | | | 90.69 ( 0) | 71.21 ( 1) |
| | 76.32 ( 1) | - | | | 91.75 (-4) | - |
| | 75.71 (-1) | 84.90 (-2) | | | - | - |
| 10.5 | 75.09 (-2) | 85.22 (-2) | 21 377.31 ( 3) | | 93.96 ( 1) | 67.17 ( 1) |
| | 74.48 (-1) | - | 76.86 (-3) | | 95.02 ( 1) | 65.76 (-2) |
| | 73.87 ( 1) | 85.83 ( 0) | 76.33 (-2) | | 96.05 ( 0) | 64.40 ( 0) |
| | 73.24 ( 2) | 86.11 ( 1) | 75.86 (-2) | | 97.08 ( 0) | 62.97 (-2) |
| | 72.55 (-1) | 86.36 ( 0) | - | | 98.11 ( 1) | - |
| 15.5 | 71.89 ( 0) | 86.63 ( 2) | - | | 99.10 ( 0) | 60.13 (-2) |
| | 71.20 ( 0) | 86.83 (-1) | - | | 400.09 ( 0) | |
| | 70.50 ( 0) | 87.07 ( 1) | - | | 1.05 (-1) | |
| | 69.80 ( 1) | 87.29 ( 1) | 73.24 (-2) | | 2.02 ( 0) | |
| | 69.05 (-1) | 87.46 ( 0) | 72.68 (-1) | | 2.97 ( 0) | |
| | | | | Head | | |
| 20.5 | 68.32 ( 0) | 87.62 (-1) | 72.12 ( 0) | 21 384.56 (-3) | 3.90 ( 0) | |
| | 67.57 ( 1) | 87.80 ( 0) | 71.50 (-3) | | 4.82 ( 0) | |
| | 66.80 ( 1) | 87.97 ( 2) | 70.91 (-1) | | 5.71 (-1) | |
| | 65.99 (-2) | | 70.29 (-1) | | 6.61 ( 0) | |
| | 65.20 (-2) | | - | | 7.51 ( 2) | |
| 25.5 | 64.40 (-1) | | 69.05 (-2) | | 8.38 ( 3) | |
| | 63.59 ( 1) | | 68.34 (-3) | | 9.21 ( 3) | |
| | 62.75 ( 0) | | 67.73 ( 4) | | 10.04 ( 1) | |
| | 61.91 ( 1) | | 66.78 (-3) | | 10.84 (-1) | |
| | 61.01 (-2) | | - | | 11.62 (-3) | |
| 30.5 | 60.13 (-2) | | - | | 12.42 (-2) | |
| | 59.28 ( 2) | Head | 64.85 (-2) | | - | |
| | 58.36 ( 2) | 88.66 (-2) | 64.11 (-2) | | 13.97 (-1) | |
| | 57.44 ( 0) | | 63.39 ( 2) | | 14.75 ( 2) | |
| | 56.51 ( 0) | | 62.62 ( 1) | | - | |
| 35.5 | 55.59 ( 3) | | | | 16.14 (-4) | |
| | - | | | | - | |
| | 53.63 ( 0) | | | | 17.60 ( 3) | |
| | - | | | | - | |
| | 51.63 (-1) | | | | 18.93 ( 3) | |
| 40.5 | | | | | 19.58 ( 3) | |
| | | | | | - | |
| | | | | | - | |
| | | | | | - | |
| 45.5 | | | | | 21.98 ( 0) | |
| | | | | | 22.52 (-3) | |

La formule empirique de Kratzer (4) $\omega_e = (4B_e^3/D_e)^{1/2}$ donne pour l'état inférieur $\omega_e = 684\ cm^{-1}$ (en utilisant les valeurs $B_o$ et $D_o$). Cette valeur est bien de l'ordre de grandeur attendu en se fondant sur une comparaison avec les molécules du même type (par exemple 640 $cm^{-1}$ dans CuO).

## III - DISCUSSION

L'absence de coefficient p montre que l'état supérieur de la transition est une composante $^2\Pi_{3/2}$. Pour les mêmes raisons que pour $\gamma_j$ il n'est pas possible de calculer le coefficient q qui caractérise le dédoublement $\Lambda$ dans l'état $^2\Pi_{3/2}$. Dans les deux cas il faudrait pouvoir disposer de raies mettant en jeu des niveaux de rotation de valeur de J élevées pour déterminer avec précision ces paramètres.

Nous remarquons la similitude des valeurs absolues de $p_o$ ( = 0,154$cm^{-1}$) dans l'état $^2\Pi$ de la transition $^2\Delta$ - $^2\Pi$ et de $\gamma_o$ ( = 0,149 $cm^{-1}$) dans l'état $^2\Sigma$. Rappelons que le choix du signe positif de p est arbitraire puisque nous ne connaissons pas la position de l'état $^2\Sigma^+$ responsable du dédoublement $\Lambda$ de l'état $^2\Pi$. Nous pouvons donc penser que ces deux états forment un couple de perturbants mutuels (5). Ceci confirme le choix que nous avons fait concernant la nature des états inférieurs des deux transitions analysées.

Avant de tenter d'établir une relation avec la structure électronique de NiF. nous pouvons faire quelques hypothèses sur la position des états $^2\Pi$ et $^2\Sigma$. Nous verrons que l'état $^2\Sigma$ doit être de symétrie

positive. Par conséquent, la valeur négative trouvée pour $\gamma$ et le fait que l'état $^2\Pi$ soit inversé supposent que l'état $^2\Sigma^+$ se trouve au-dessous de l'état $^2\Pi$ (2). Il faut donc changer le signe de p dans l'état $^2\Pi$ de la transition $^2\Delta$ - $^2\Pi$ et permuter en conséquence les dénominations e et f indiquées dans l'article concernant cette transition.

Comme dans la plupart des composés fluorés la forte électronégativité du fluor a pour conséquence que le spectre moléculaire de NiF provient de l'association des ions $Ni^+$ et $F^-$ plutôt que des atomes neutres.

L'association des états fondamentaux de ces deux ions donne naissance aux trois états moléculaires suivants :

$^2\Sigma^+$ de configuration $3d^9_{Ni^+}\ (\sigma\pi^4\delta^4) + 2p^6_{F^-}\ (\pi^4\sigma^2)$

$^2\Pi_i$ de configuration $3d^9_{Ni^+}\ (\sigma^2\pi^3\delta^4) + 2p^6_{F^-}(\pi^4\sigma^2)$

$^2\Delta_i$ de configuration $3d^9_{Ni^+}\ (\sigma^2\pi^4\delta^3) + 2p^6_{F^-}(\pi^4\sigma^2)$

Si l'on ne tient pas compte des effets de polarisation entre les orbitales centrées sur le nickel et des interactions possibles avec d'autres configurations électroniques, l'orbitale $\delta$ est plus basse en énergie que l'orbitale $\pi$ , elle-même plus basse que l'orbitale $\sigma$ . Par conséquent l'état $^2\Sigma^+$ avec ses couches $\pi$ et $\delta$ totalement occupées doit être plus bas en énergie que l'état $^2\Pi$ , lui-même plus bas que l'état $^2\Delta$.

Il est difficile d'apprécier les écarts d'énergie sans calculs ab initio, mais, par comparaison avec FeF(6), la levée de dégénérescence entre les composantes $\lambda$ provenant de la couche 3d du nickel doit donner un écart de l'ordre de 4 000 $cm^{-1}$ entre les états $^2\Sigma^+$ et $^2\Pi_i$ et 2 000 $cm^{-1}$ entre les états $^2\Pi_i$ et $^2\Delta_i$.

L'écart entre les composantes $^2D_{5/2}$ et $^2D_{3/2}$ de $Ni^+$ (7) permet de calculer le paramètre d'interaction atomique de l'ion : $A_{at} = 603\ cm^{-1}$. On peut montrer facilement que le paramètre spin-orbite caractéristique de la couche 3d, noté $\zeta_{3d}$ est égal à $A_{at}$. Par conséquent, nous prendrons $\zeta_{3d} = 600\ cm^{-1}$, valeur assez bien confirmée d'ailleurs par Froese-Fisher qui, calculant ce paramètre à partir d'orbitales SCF, obtient $\zeta_{3d} = 662\ cm^{-1}$ (8). Pour un état $^2\Pi$, l'écart entre les composantes $^2\Pi_{1/2}$ et $^2\Pi_{3/2}$ est égal à la constante spin-orbite moléculaire $A_{mol}$. Dans le cas a de Hund, cette constante est, elle aussi, égale au paramètre $\zeta_{3d}$ si, comme on peut le supposer, la couche ouverte est de caractère $3d\pi$ pur.

Ainsi l'écart entre les composantes $^2\Pi_{1/2}$ et $^2\Pi_{3/2}$ devrait être de l'ordre de $600\ cm^{-1}$.

Les résultats expérimentaux et en particulier le signe de $\gamma(^2\Sigma^+)$ indiquent que l'état $^2\Sigma^+$ est plus bas que l'état $^2\Pi_i$, en accord avec nos considérations théoriques élémentaires. En utilisant la formule (5) valable en pure précession,

$$p = \frac{2\ A\ B\ \ell(\ell+1)}{E_\Pi - E_\Sigma}$$

on peut mesurer le degré d'éxactitude de nos calculs en prenant $E_\Pi - E_\Sigma = 4000\ cm^{-1}$. On trouve A voisin de $-\ 400\ cm^{-1}$, cette valeur diffère assez fortement des $-\ 600\ cm^{-1}$ trouvés précédemment, mais il est difficile de dire si l'erreur provient d'une mauvaise appréciation de $E_\Pi - E_\Sigma$, ou de A, ou encore d'une tendance de l'état $^2\Pi$ à tendre vers une structure de type cas c de Hund, due à une forte interaction avec les états $^2\Sigma^+$ et $^2\Delta$ de structure $3d^9_{Ni^+}\ 2p^6_{F^-}$, comme c'est le cas dans la situation correspondante de CuO.

En ce qui concerne les états supérieurs nous pouvons penser qu'ils proviennent de la configuration $3d^{8}_{Ni^+}\ 4s_{Ni^+} + 2p^{6}_{F^+}$ par analogie avec les transitions électroniques observées dans CuO.

A ce stade il est délicat d'essayer de tirer des conclusions plus quantitatives en ce qui concerne la structure électronique de NiF. Nous avons émis quelques hypothèses sur l'état fondamental qui permettent de rendre compte simplement de l'ordre de grandeur des écarts entre les états inférieurs $^2\Pi$ et $^2\Sigma^+$ des transitions observées et du paramètre d'interaction spin-orbite A de l'état $^2\Pi$ inférieur.

Des calculs ab-initio sont en projet, ils devraient permettre de comprendre plus clairement la structure électronique de NiF.

1 - R.S. Mulliken, Rev. Mod. Phys. 3, 89 (1931)

2 - E.L. Hill et J.H. Van Vleck Phys Rev 32 , 250 (1928)

3 - R.A. Gottscho Ph D, M.I.T. Cambridge Mass (1979)

4 - G. Herzberg. Spectra of diatomic molecules,Van Nostrand,New-York (1950)

5 - R.N. Zare, A.L. Schmeltekopf, W.J. Harrop et D.L. Albritton
J. Mol. Spectr. 46 37 (1973)

6 - B. Pouilly, J. Schamps, D.J.W. Lumley et R.F. Barrow
J. Phys B : Atom. Molec. Phys. 11 2289 (1978)

7 - C.E. Moore, Atomic energy levels National Bureau of Standards (U.S.) circ. N° 467 (1952)

8 - C. Froese-Fisher, Some Hartree-Fock results for the atoms helium to radon (Vancouver University 1968)

# Laser Spectroscopy of CaBr:

# $A^2\Pi$-$X^2\Sigma^+$ and $B^2\Sigma^+$-$X^2\Sigma^+$ Systems

P. F. Bernath[1] and R. W. Field
Spectroscopy Laboratory and Department of Chemistry
Massachusetts Institute of Technology
Cambridge, Massachusetts 02139

and

B. Pinchemel[2], Y. Lefebvre, and J. Schamps
Laboratoire de Spectroscopie des Molécules Diatomiques
E.R.A. 303
Université des Sciences et Techniques de Lille
Bât. P5
59655 Villeneuve d'Ascq, FRANCE

15 Pages

8 Tables

2 Figures

1. Present address, Herzberg Institute of Astrophysics, National Research Council of Canada, Ottawa K1A OR6, CANADA.

2. Visiting scientist at M.I.T.

Abstract

Laser excitation spectra have been recorded for $Ca^{79}Br$ and $Ca^{81}Br$ in the spectral region 600-630 nm. The use of a 1 meter monochromator as a narrow band pass filter (1-2 $cm^{-1}$) has allowed rotational analysis of the 0-0, 1-1 and 2-2 bands of the $B^2\Sigma^+$-$X^2\Sigma^+$ transition and the 0-0 and 1-1 bands of the $A^2\Pi$-$X^2\Sigma^+$ transition. A few additional lines of the 0-1, 1-2, 1-0 and 2-1 bands of the B-X system were used to obtain band origins for vibrational analysis. The main constants for $Ca^{79}Br$ were (in $cm^{-1}$):

| | $X^2\Sigma^+$ | $A^2\Pi$ | $B^2\Sigma^+$ |
|---|---|---|---|
| $T_e$ | 0 | 15 958.41 (10) | 16 383.137 (6) |
| $\omega_e$ | 285.732 (9) | 288.56 (20) | 285.746 (9) |
| $\omega_e x_e$ | 0.840 (4) | - | 0.954 (4) |
| $B_e$ | 0.094467266 (30) | 0.0957343 (20) | 0.0965151 (20) |
| $\alpha_e$ | 0.000406251 (40) | 0.0004327 (20) | 0.0004483 (15) |
| $\gamma_e$(spin-rot.) | 0.00301484 (50) | - | 0.068767 (79) |
| $p_e$ | - | -0.066834 (64) | - |
| $A_e$ | - | 59.175 (1) | - |

(all uncertainties are 1σ)

The usual isotope relations between the constants for $Ca^{79}Br$ and $Ca^{81}Br$ are satisfied to within 3σ. The A and B states form a unique perturber pair with $\ell_{eff} = 1.17$

## I. Introduction

The first CaBr spectra were observed by Walters and Barratt in 1928 (1). The vibrational assignments appearing in Rosen's tables (2) were made by Harrington (3) in 1942. The potential curves of the X, A, and B states are very similar, causing the spectra to be extremely congested and overlapped. In addition, there are two isotopes of bromine ($^{79}Br$, 50.5%; $^{81}Br$, 49.5%) of approximately equal abundance. Consequently, no rotational analysis of the $A^2\Pi$-$X^2\Sigma^+$ and $B^2\Sigma^+$-$X^2\Sigma^+$ transitions has been previously performed. The use here of a tunable single-mode, cw dye laser, coupled with selective, narrow band pass fluorescence detection, has allowed us to assign more than 2000 lines belonging to these two transitions. The A-X and B-X transitions were simultaneously fit using a "direct" approach (4). In addition, some X state microwave transitions, provided by Möller and Törring (5), were included in the final fits.

## II. Experiment

A preliminary study of the A-X and B-X systems was performed in Lille. The CaBr radical was generated from $CaBr_2$ solid, in a King furnace at 1500-2000 K. Fluorescence was excited using a broad band (1 $cm^{-1}$) CR 590 Rhodamine 6G dye laser. Rotational assignments were made using laser induced fluorescence spectra recorded with a Jobin-Yvon THR 1500 spectrometer and calibrated against Thorium lines. This technique has rather limited resolution, $\sim$0.05 $cm^{-1}$, but the lines recorded and assigned in this way served as a guide for our Doppler-limited laser excitation experiments at MIT.

The excitation spectra were recorded using a Coherent model CR 599-21 dye laser pumped with 4W from the 5145Å line of a Coherent CR 10 $Ar^+$ laser.

We obtained single mode powers (<1 MHz bandwidth) of about 30 mW at 6290Å and 150 mW at 6000Å using Rhodamine 6G dye. Ten percent of the dye laser output power was divided between an $I_2$ cell, a 300 MHz semi-confocal Fabry-Perot and a 1.5 GHz spectrum analyser. The $I_2$ fluorescence and Fabry-Perot peaks were recorded as calibration at the same time as CaBr excitation spectra. The $I_2$ lines were assigned using the $I_2$ atlas of Gerstenkorn and Luc (6). The absolute accuracy of the lines is $\pm$ 0.003 $cm^{-1}$, except for blended lines. The line positions and band origins given in this paper have not been corrected by subtraction of 0.0056 $cm^{-1}$ as suggested by Gerstenkorn and Luc (7).

The CaBr molecule was made in a Broida-type flow system (8) by the reaction of Ca metal with $CH_3Br$. The pressure was typically 0.5 torr of argon carrier gas (with less than 1% $CH_3Br$).

The total laser induced fluorescence was monitored, through a Corning color glass filter (chosen to eliminate scattered laser light), by a Hamamatsu R212 photomultiplier. A typical excitation spectrum of one of the most uncluttered regions of the $B^2\Sigma^+$-$X^2\Sigma^+$ system is shown as the lower trace of Figure 1. Even with Doppler-limited resolution there is no clear pattern in this badly overlapped spectrum.

Intermodulated fluorescence spectra (9, 10) were recorded in order to increase the resolution. This technique is not very useful in this case because, although the lines were better resolved, the pattern of overlapped sequence bands and branches was no clearer. The one exception was in the $P_1$ branch of the 0-1 band of the $B^2\Sigma^+$-$X^2\Sigma^+$ transition of $Ca^{79}Br$. The low N and the returning high N lines near the $P_1$ head were clearly resolved using intermodulated fluorescence. Hyperfine structure was observed and will be the subject of a future paper (11).

The problem in the CaBr A-X and B-X systems is that branches from two isotopes and many sequence bands occur in the same spectral region. However, fluorescence arising from simultaneous laser excitation of overlapped lines often occurs in different spectral regions, as shown in Figure 2. Thus, by using a monochromator as a narrow band filter, it is possible to select only the fluorescence from a particular branch of a chosen band. The excitation spectrum is then greatly simplified, as shown by the top trace of Figure 1. In this figure four branches are recorded simultaneously (the $R_1$ branch of 0-0 and 1-1 bands, for both isotopes) but the pattern is quite clear. By tuning the monochromator from one fluorescence feature to another it is possible to separately record all of the branches occurring in a selected region of the spectrum. This technique has been previously applied to CaF (12), CaCl (13), $NO_2$ (14) and YO (15).

A 1-meter monochromator with 1200 grooves/mm grating was used, in first order, as a filter. The band pass of the monochromator was set at 1-2 $cm^{-1}$. A cooled RCA C31034 photomultiplier with photon counting electronics was used to detect the filtered fluorescence.

## III. Results

The lines of the 0-0 and 1-1 bands of the $A^2\Pi$-$X^2\Sigma^+$ transition and the 0-0, 1-1 and 2-2 bands of the $B^2\Sigma^+$-$X^2\Sigma^+$ transition of $Ca^{79}Br$ are listed in Table I. The corresponding lines of $Ca^{81}Br$ are in Table II. The assignments were made using standard combination difference relations. Initially, mainly ground state differences were used since, by analogy with CaF and CaCl, the spin-rotation parameter, $\gamma$, was expected to be small.

Lines were fit using a weighted (reciprocal, squared uncertainty), non-linear, least-squares approach ("direct approach") (4). The model Hamiltonian includes standard $^2\Pi$ and $^2\Sigma$ matrix elements (17). Lambda doubling and spin-rotation effects were accounted for in each state with the usual second order perturbation theory expressions (4). The uncertainties of well resolved and blended lines are taken at 0.005 $cm^{-1}$ and 0.01 $cm^{-1}$, respectively. For each isotope, the v=0 levels of B, A and X states were fit simultaneously. Similar fits were made for v=1. The 2-2 band of the B-X system of $Ca^{79}Br$ was fit alone with $\gamma_D'$ fixed at the value obtained for the v=0 level. For the B-X 2-2 band of $Ca^{81}Br$, D" and $\gamma$" were fixed at values linearly extrapolated from v"=0 and 1 levels.

After our optical analysis was complete, Möller and Törring provided 40 microwave transitions for $X^2\Sigma^+$ v" = 0, 1, and 2 of both isotopes. These data include high N ($\sim$50) and low N ($\sim$15) transitions of about 40 kHz ($1.3 \times 10^{-6} cm^{-1}$) accuracy. These transitions were included in our final fits. The microwave transitions greatly improved the ground state constants and broke the correlation between ground and excited state constants.

The spectroscopic constants obtained from these fits are given in Table III. One extra digit is retained so that the constants will reproduce the original data.

In order to perform a vibrational analysis of the $B^2\Sigma^+$-$X^2\Sigma^+$ system, we recorded a few lines from bands of $\Delta v = \pm 1$ sequences. These lines are listed in Table IV. The assignments were made by calculating spectra using the constants of Table III and estimated band origins obtained from the band heads given in Table V. These lines were then used to determine the band origins of Table VI.

Table VII contains the equilibrium constants of X, A and B states for

both isotopes. For the A state we used the Pekeris relationship (18) to obtain the $\omega_e x_e$. All Franck-Condon factors greater than 0.001 for vibrational levels less than 5 for the A-X and B-X transitions appear in Table VIII. They were calculated using standard RKR (19) and FCF (20) programs from $Ca^{79}Br$ equilibrium constants.

## IV. Discussion

In the calcium halides, the $X^2\Sigma^+$ state is derived from the slightly antibonding 4sσ molecular orbital centered on $Ca^+$. The $A^2\Pi$ and $B^2\Sigma^+$ states seem to form a 4p-complex, split by the ligand field of the halide. Thus the A-X and B-X transitions are the molecular analogues of the atomic resonance lines of a one valence electron atom. By analogy with CaF (12, 21) and CaCl (13, 22), the A and B states are expected to form a unique perturber pair (4) with $\ell$ slightly greater than 1. Using $\ell = 1$, the pure precession relationship (23) predicts $\gamma_0 \approx p_0 = -0.0529\ cm^{-1}$. As can be seen from Table III, $\gamma_0 \approx p_0$ but both are 27% larger than this value. This implies an $\ell_{eff} = 1.17$ for the expression $\frac{2AB\ell_{eff}(\ell_{eff}+1)}{\Delta\nu_{\Sigma-\Pi_{1/2}}}$. The simplest explanation of this is that the p complex contains some 3d character which increases the $\ell$ value towards 2. There is a trend in the calcium halides for an increase in $\ell_{eff}$ from 1.03 in CaF (12), 1.08 in CaCl (13) to 1.28 in CaI (24).

The Franck-Condon factors for the A-X and B-X systems (Table VIII) are similar to those for the other calcium halides. The vibrational structure of the transitions, particularly for low v, is very diagonal. The $\Delta v \neq 0$ CaBr

Franck-Condon factors are, respectively, larger and smaller than those for CaF (12) and CaI (24). As for the other calcium halides, the $v \neq 0$ sequences of CaBr become significantly stronger at high v.

Rotation-vibration analysis for two isotopes of CaBr allows a test of the usual isotopic relationships between parameters (16). The agreement between our experimental isotopic parameter ratios and those predicted from the reduced masses is satisfactory ($<3\sigma$).

Brown and Watson (25 and 26) showed that it is possible to separate $A_D$ (effective) into "true" $\gamma$ and $A_D$, provided that isotopic data are available.[4] In our case, the isotopic $A_D$ values differ so slightly that this procedure is unlikely to give reliable values. The values of $\gamma_0$ (true) and $A_D$ obtained from isotopic data are:

$$\gamma_0 = 0.057 \text{ cm}^{-1}$$

$$A_{D_0} = 4.1 \times 10^{-5} \text{ cm}^{-1}.$$

The pure precession estimate of $\gamma_0$ (true) is

$$\gamma_0 = -p/2 = 0.034 \text{ cm}^{-1}.$$

In order to check the significance of some of our small parameters, we have used the customary Pekeris and Kratzer relations (16). The values are included in the table of equilibrium constants (Table VII) and the agreement is 10% for $\omega_e x_e$ and <1% for $D_e$.

In addition, the program of Albritton et al. (27) was used (along with the RKR curve) in order to calculate $D_v$ values. The agreement is excellent ($\pm$ 0.1%) even in the excited states. For example, calculated values for the v = 0 levels of $Ca^{79}Br$ are $D_0 = 4.128 \times 10^{-8}$ cm$^{-1}$ ($X^2\Sigma^+$), $4.220 \times 10^{-8}$cm$^{-1}$ ($A^2\Pi$), and $4.404 \times 10^{-8}$cm$^{-1}$ ($B^2\Sigma^+$). The calculated values were fit to extract $D_e$ and $\beta_e$ and these values are included in Table VII.

Veseth (28) has derived a formula for estimating $\gamma_{D_v}$:

$$\gamma_{D_v} = \gamma_v \left[ \frac{A_{D_v}}{A_v} - \frac{2D_v}{B_v} - \frac{B_\Pi - B_\Sigma}{\Delta\nu_{\Pi\Sigma}} \right]$$

For $\gamma_{D_0}$ of $Ca^{79}Br$, this equation gives $2.25 \times 10^{-7} cm^{-1}$, which is close to the experimental value, $2.58 \times 10^{-7}$ $cm^{-1}$. A similar expression for $p_{D_v}$ gives $p_{D_0} = 2.16 \times 10^{-7} cm^{-1}$. The unique perturber model requires $p_D \approx \gamma_D$. The $\gamma_D$ and $p_D$ values predicted by Veseth's equations are in reasonable agreement with each other and fall between the respective experimental values. However, our phenomenological $A_D$ is a factor of 7 larger than the value predicted by Merer's relationship (29).

## V. Summary

The spectrum of CaBr is typical of alkaline earth halides and, more generally, transitions involving non-bonding electrons. Laser excitation spectroscopy with narrow band detection allows the dense and badly overlapped spectrum to be analyzed. Narrow band detection allows the experimenter to select the branches and bands of greatest interest from the jumble of overlapped lines in the spectrum. The use of a continuously tunable single-mode, dye laser provides very high quality data ($\pm$ .003 $cm^{-1}$ accuracy).

Simultaneous fitting of the A-X, B-X and microwave data reduces correlations in the molecular constants. The combined fit molecular constants obey the expected isotopic relations. The molecular constants allow accurate Franck-Condon factors to be calculated. These Franck-Condon factors are required for the conversion of laser induced fluorescence intensities into molecular populations in monitored chemical reactions. The molecular constants, particularly lambda doubling and spin-rotation parameters, provide some insight into the orbital structure of CaBr. The A and B states form a unique perturber pair with $\ell_{eff} = 1.17$, suggestive of 3d character in these states.

## Acknowledgments

We are greatly indebted to K. Möller and Professor T. Törring for providing us with their microwave data in advance of publication. P. F. Bernath was supported, in part, by a Natural Sciences and Engineering Research Council of Canada postgraduate fellowship. The MIT portion of this research was supported by the following grants: AFOSR-76-3056, NSF CHE-78-18427, and CHE-78-10178, NATO 1177.

References


1. O. H. Walters and S. Barratt, Proc. Roy. Soc. Sev. A G.B. 118, 120-137 (1928).

2. B. Rosen, Spectroscopic Data Relative to Diatomic Molecules, in "International Tables of Selected Constants", Pergamon, New York, 1970.

3. R. E. Harrington, Ph.D. thesis, Berkeley, 1942.

4. R. N. Zare, A. L. Schmeltekopf, W. J. Harrop, and D. L. Albritton, J. Mol. Spectrosc. 46, 37-66 (1973). The fitting routines used were generated by R. C. Stern and revised by T. H. Bergeman, R. A. Gottscho, and A. J. Kotlar.

5. K. Möller and T. Törring, private communication.

6. S. Gerstenkorn and P. Luc, Atlas du spectre d'absorption de la molecule d'iode, CNRS, Paris 1978.

7. S. Gerstenkorn and P. Luc, Rev. Phys. Appl. 14, 791-794 (1979).

8. J. B. West, R. S. Bradford, Jr., J. D. Eversole, and C. R. Jones, Rev. Sci. Instrum. 46, 164-168 (1975).

9. M. S. Sorem and A. L. Schawlow, Opt. Commun. 5, 148-151 (1972).

10. P. F. Bernath, P. G. Cummins, and R. W. Field, Chem. Phys. Lett. 70, 618-620 (1980).

11. P. F. Bernath, B. Pinchemel, and R. W. Field, submitted J. Chem. Phys.

12. M. Dulick, P. F. Bernath, and R. W. Field, Can. J. Phys. 58, 703-712 (1980).

13. L. E. Berg. L. Klynning, and H. Martin, Physica Scripta 21, 173-178 (1980).

14. W. Demtröder in Case Studies in Atomic Physics, vol. 6. Edited by M.R.C. McDowell and E. W. McDaniels, North-Holland, Amsterdam, 1976.

15. C. Linton, J. Mol. Spectrosc. 69, 351-364 (1978).

16. G. Herzberg, Spectra of Diatomic Molecules, Van Nostrand, New York,1950.

17. A. J. Kotlar, R. W. Field, J. I. Steinfeld, and J. A. Coxon, J. Mol. Spectrosc. 80, 86-108 (1980).

18. C. L. Pekeris, Phys. Rev. 45, 98-103 (1934).

19. R. J. LeRoy, private communication.

20. R. N. Zare, J. Chem. Phys. 40, 1934-1944 (1964).

21. P. F. Bernath and R. W. Field, J. Mol Spectrosc. 82, 339-347 (1980).

22. L. E. Berg, L. Klynning, and H. Martin, Physica Scripta, in press (1980).

23. R. S. Mulliken and A. Christy, Phys. Rev. 38, 87-119 (1931).

24. D. E. Reisner, P. F. Bernath, and R. W. Field, unpublished results.

25. J. M. Brown and J.K.G. Watson, J. Mol. Spectrosc. 65, 65-74 (1977).

26. J. M. Brown, E. A. Colbourn, J.K.G. Watson, and F. D. Wayne, J. Mol. Spectrosc. 74, 294-318 (1979).

27. D. L. Albritton, W. J. Harrop, A. L. Schmeltekopf, and R. N. Zare, J. Mol. Spectrosc. 46, 25-36 (1973).

28. L. Veseth, J. Phys. B.: Atom. Molec. Phys. 3, 1677-1691 (1970).

29. A. J. Merer, Mol. Phys. 23, 309-315 (1972).

Footnotes

1. Present address, Herzberg Institute for Astrophysics, National Research Council of Canada, Ottawa K1A 0R6, CANADA
2. Visiting scientist at MIT.
3. Tables I and II were prepared before the microwave data were available so all residuals were obtained from fits that included only optical data. The change in observed-calculated from the combined microwave-optical fits was typically $\pm$ 0.001 $cm^{-1}$.
4. This separation of $\gamma$ and $A_D$ is supposed to yield a $\gamma$-value which contains both spin-rotation and second-order spin-orbit contributions.

Fig. 1. CaBr $B^2\Sigma^+$-$X^2\Sigma^+$ laser excitation spectrum. This figure illustrates the complexity of the B-X system. One feature, near-overlap of $R_1$ lines of the 0-0 and 1-1 bands differing by only one J unit, would make rotational assignment of a non-laser spectrum a formidable task. Trace 2 shows the spectrum obtained when total fluorescence is detected. Trace 1 shows the simplification into groups of four lines [0-0 $R_1(J)$ and 1-1 $R_1(J + 1)$ for both Br isotopes] that occurs when narrow bandpass fluorescence detection is employed.

Fig. 2. CaBr $A^2\Pi$-$X^2\Sigma^+$ laser induced fluorescence spectrum. A Fortrat diagram illustrates the structure of the 0-0 (solid lines) and 1-1 (dotted lines) bands of the A-X system. A 1 $cm^{-1}$ bandwidth laser is tuned to the region of the $Q_{12}$ and $P_1$ heads of the 1-1 band. The resulting spectrum, shown at the top of the Figure, includes a complex pattern of lines, the sources of which are indicated by the heavy portions of the Fortrat parabolae directly under the laser line.Each excitation line is accompanied by a fluorescence line [shifted by approximately $\pm$ B" (4N + 2)] originating from a common upper level. These lines appear above the heavy portions of the Fortrat parabolae for the conjugate branches. Note that the fluorescence is organized into distinct regions, each associated with a different excitation branch and band combination. This is the basis for success of the selective fluorescence detection laser excitation method.

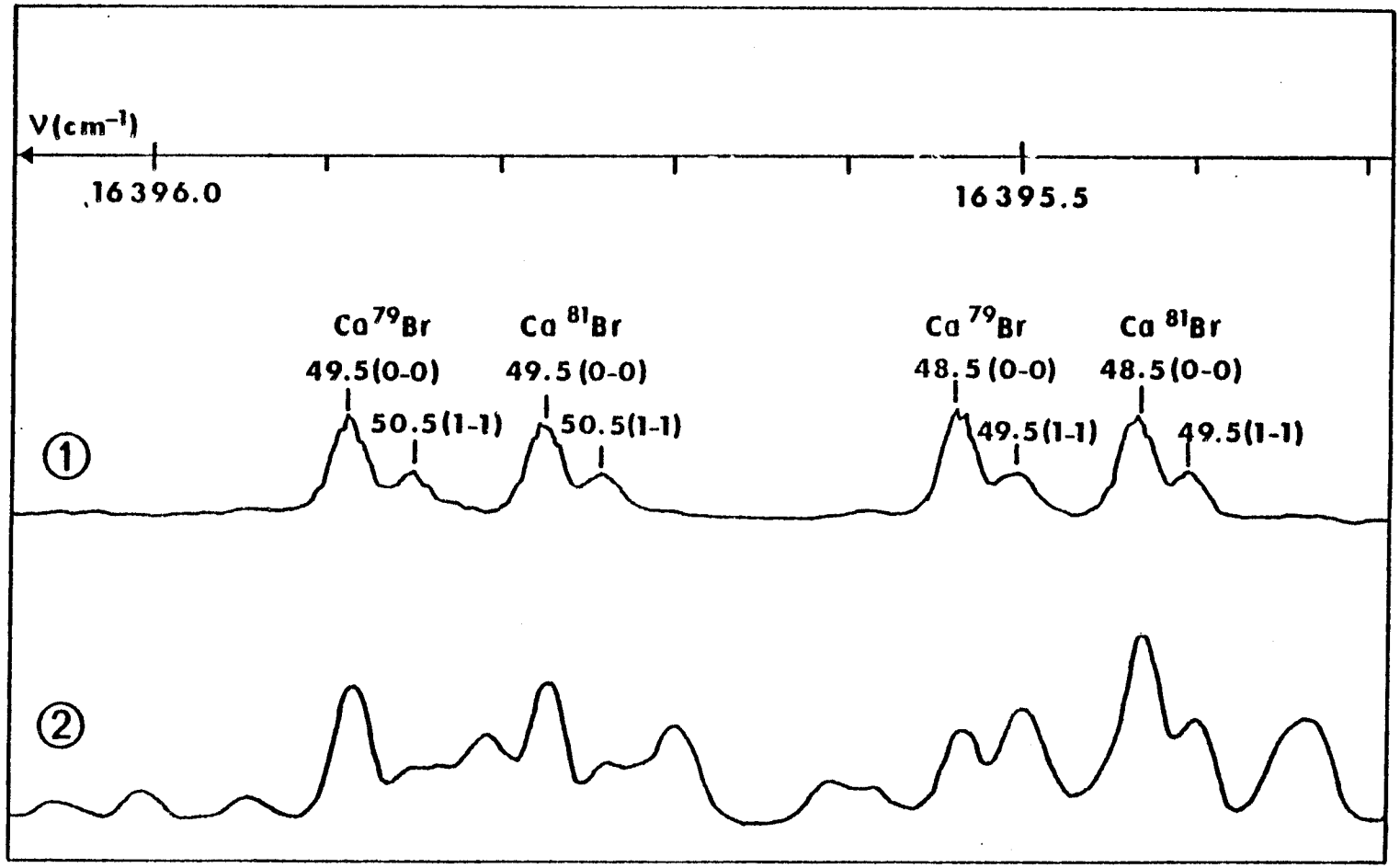


Figure I : Voir page 98.

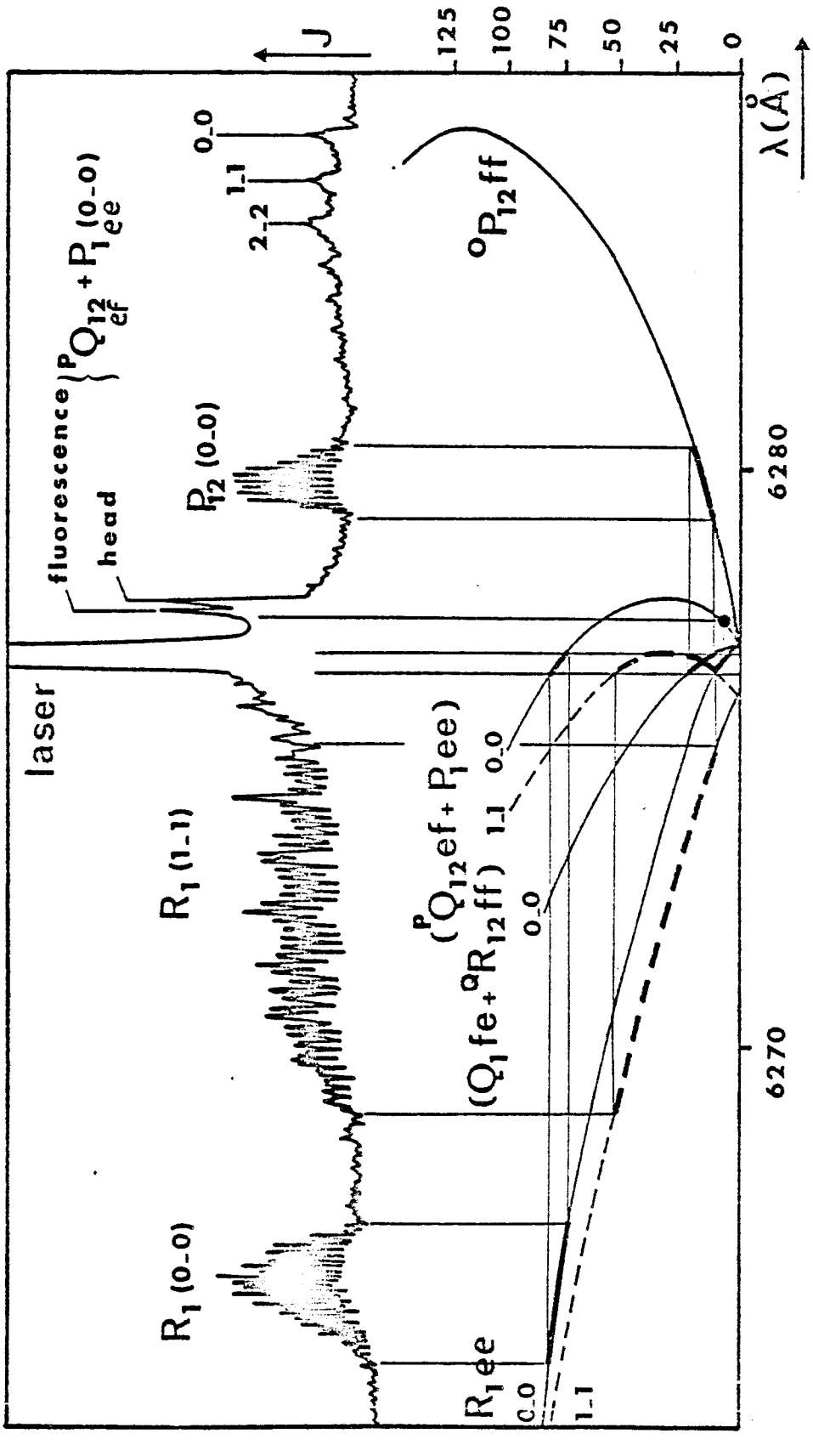


Figure II : Voir page 98

TABLE I : Measured line positions for Ca $^{79}$Br (in cm$^{-1}$)

$A^2\Pi_{1/2} - X\ ^2\Sigma^+$

| v'-v" | 0 - 0 | | | | | | | | 1 - 1 | | | | | | | |
|---|---|---|---|---|---|---|---|---|---|---|---|---|---|---|---|---|
| J | $P_{12ff}$ | Δν | $Q_{1fe}$ | Δν | $R_{12ff}$ | Δν | $R_{1ee}$ | Δν | $P_{12ff}$ | Δν | $Q_{1fe}$ | Δν | $R_{12ff}$ | Δν | $R_{1ee}$ | Δν |
| 0.5 | | | | | 15 925.091* | 4 | | | | | | | | | | |
| | | | 15 925.091* | 9 | 25.152* | -2 | | | | | | | | | | |
| | | | 25.152* | 5 | 25.219* | -4 | | | | | | | | | | |
| | | | 25.220* | 6 | 25.287* | -9 | | | | | | | | | | |
| | | | 25.287* | 5 | 25.369* | -1 | | | | | | | | | | |
| | 15 923.229 | 3 | 25.357* | 4 | 25.446* | 0 | | | | | | | | | | |
| | 22.929 | 6 | 25.428* | 1 | 25.525* | 1 | | | | | | | | | | |
| | - | | 25.501* | -1 | 25.611* | 6 | | | | | | | | | | |
| | 22.326* | 3 | 25.579* | -1 | 25.691* | 3 | | | | | | | | | | |
| | 22.027* | 0 | 25.658* | -2 | 25.775* | 2 | | | | | | | | | | |
| 10.5 | 21.736* | 2 | 25.737* | -5 | 25.866* | 5 | 15 928.708 | -4 | | | | | | | | |
| 11.5 | 21.446 | 4 | 25.819* | -7 | - | | 29.050 | -4 | | | | | | | | |
| | 21.152 | 0 | - | | - | | 29.392 | -8 | 15 922.559 * | 7 | | | | | | |
| | 20.865 | -1 | - | | - | | 29.747 | 7 | 23.272 * | 8 | | | | | | |
| | 20.581 | 1 | - | | 26.227* | -6 | 30.097 | 1 | 22.983 * | 3 | | | | | | |
| | - | | 26.177* | -9 | 26.325* | -6 | 30.448 | 1 | - | | | | | | | |
| | - | | 26.276* | -6 | 26.426* | -7 | - | | 22.417 * | 0 | | | 15 928.811* | 8 | | |
| | 19.741 | 1 | 26.374* | -6 | 26.529* | -7 | - | | 22.138 | -1 | | | 28.912* | 8 | | |
| | 19.465 | 1 | 26.476* | -4 | 26.634* | -7 | 31.514 | 1 | 21.861 | -1 | 15 928.845* | -4 | 29.014* | 7 | | |
| | 19.193 | 3 | 26.573* | -9 | 26.742* | -6 | 31.874 | 1 | 21.586 | -3 | 28.945* | -5 | 29.120* | 7 | 15 934.248 | 6 |
| 20.5 | 18.922 | 4 | 26.681* | -5 | 26.852* | -7 | 32.232 | -2 | 21.315 | -1 | 29.052 | -1 | 29.225* | 4 | 34.604 | 1 |
| 21.5 | 18.654 | 5 | 26.786* | -7 | 26.968* | -2 | 32.599 | 1 | 21.049 | 1 | 29.155 | -3 | 29.336* | 5 | 34.961 | -4 |
| | - | | 26.895* | -7 | 27.091* | 7 | 32.969 | 4 | 20.781 | 1 | 29.263 | -2 | 29.446* | 3 | 35.330 | 0 |
| | 18.122 | 3 | 27.009 | -4 | 27.203* | 2 | 33.336 | 3 | 20.517 | 1 | 29.372 | -2 | 29.559* | 2 | 35.695 | -1 |
| | 17.860 | 3 | 27.121 | -5 | 27.322* | 2 | | | 20.253 | 0 | 29.483 | -3 | - | | - | |
| | 17.600 | 3 | 27.239 | -3 | 27.445* | 5 | | | - | | 29.594 | -5 | 29.790* | -3 | - | |
| | - | | 27.360 | 0 | 27.568* | 4 | | | 19.736 | 1 | - | | 29.910* | -4 | 36.808 | 0 |
| | 17.085 | 1 | 27.478 | -3 | 27.693* | 4 | | | 19.480 | 1 | 29.826* | -7 | 30.032* | -5 | 37.182 | 0 |
| | 16.833 | 2 | 27.602 | -1 | 27.822* | 5 | | | 19.227 | 2 | 29.948* | -5 | 30.159* | -3 | 37.564 | 4 |
| | 16.582 | 2 | 27.726 | -2 | 27.949* | 2 | | | 18.973 | 0 | 30.070* | -6 | 30.283* | -6 | 37.943 | 4 |
| 30.5 | - | | 27.854 | -1 | 28.081* | 2 | | | 18.725 | 1 | 30.195* | -6 | 30.416* | -3 | - | |
| 31.5 | - | | 27.983 | -1 | 28.215* | 2 | | | 18.479 | 2 | 30.322* | -5 | 30.548* | -3 | - | |
| | 15.842 | 0 | 28.114 | -1 | - | | | | - | | 30.453* | -3 | 30.694* | 9 | 39.087 | 0 |
| | 15.598 | -2 | - | | - | | | | 17.994 | 4 | 30.582* | -6 | 30.819* | -3 | 39.474 | 0 |
| | 15.357 | -3 | - | | - | | | | 17.753 | 3 | 30.719 | -2 | 30.958* | -2 | 39.860 | -3 |
| | 15.121 | -2 | - | | 28.774* | 1 | | | 17.516 | 4 | 30.856 | -1 | 31.100* | -1 | | |
| | 14.888 | -1 | | | 28.916* | -3 | | | - | | 30.994 | -1 | | | | |
| | 14.656 | -1 | 28.806 | 0 | 29.064* | -3 | | | 17.045 | 2 | | | | | | |
| | 14.426 | 0 | 28.952 | 2 | 29.215* | -2 | | | 16.814 | 2 | | | | | | |
| | 14.199 | 0 | 29.100 | 2 | 29.365* | -4 | | | 16.585 | 2 | | | | | | |
| 40.5 | 13.975 | 2 | 29 247 | 0 | 29.519* | -5 | | | | | | | | | | |
| 41.5 | 13.751 | 0 | 29.399 | 0 | 29.674* | -7 | | | | | | | | | | |
| | - | | 29.553 | 0 | 29.834* | -6 | | | | | | | 32.148* | 1 | | |
| | 13.314 | 2 | 29.707 | -2 | 29.999* | -3 | | | | | | | 32.313* | 8 | | |
| | 13.099 | 3 | 29.867* | 0 | 30.166* | 1 | | | 15.472 | -1 | 32.174* | -2 | 32.475* | 9 | | |
| | 12.885 | 3 | 30.027* | -1 | | | | | 15.258 | -1 | 32.331* | -3 | 32.637* | 9 | | |
| | 12.672* | 1 | 30.188* | -2 | | | | | 15.046 | 1 | 32.488* | -5 | 32.800* | 7 | | |
| | 12.467 | 5 | | | | | | | 14.835 | 0 | 32.650* | -5 | 32.967* | 6 | | |
| | 12.259 | 4 | | | | | | | - | | 32.815* | -4 | 33.134* | 4 | | |
| | 12.055 | 4 | | | | | | | 14.423 | 3 | 32.977* | -9 | 33.305* | 4 | | |
| 50.5 | 11.853 | 4 | | | 31.198 | 3 | | | 14.223 | 6 | 33.147* | -7 | - | | | |
| 51.5 | 11.650 | 0 | | | 31.380 | 6 | | | 14.019 | 3 | 33.321* | -5 | 33.664* | 13 | | |
| | 11.454 | 2 | 31.213* | -2 | 31.560* | 5 | | | 13.822 | 6 | - | | 33.844* | 14 | | |
| | 11.258 | 1 | 31.393* | -1 | 31.745* | 6 | | | - | | 33.664* | -9 | 34.022* | 12 | | |
| | 11.066 | 1 | 31.570* | -4 | 31.927* | 2 | | | - | | 33.844* | -7 | 34.204* | 11 | 48.069 | 1 |
| | 10.873* | -1 | 31.753* | -5 | 32.117* | 3 | | | - | | 34.022* | -9 | 34.386* | 9 | 48.504 | 4 |
| | | | 31.933* | -9 | 32.308* | 4 | | | - | | 34.204* | -9 | 34.574* | 9 | 48.937 | 4 |
| | | | 32.125* | -6 | 32.502* | 5 | | | 12.859 | 3 | 34.386* | -11 | 34.764* | 10 | 49.365 | -3 |
| | | | 32.312* | -8 | 32.698* | 6 | 47.542 | 4 | 12.673 | 2 | 34.574* | -9 | 34.954* | 9 | 49.801 | -4 |
| | | | 32.502* | -10 | 32.893* | 3 | 47.984 | 4 | 12.491 | 3 | 34.764* | -8 | 35.146* | 7 | 50.237* | -7 |
| 60.5 | | | 32.695* | -9 | 33.096* | 6 | 48.428 | 3 | 12.311 | 3 | 34.954* | -9 | | | | |

TABLE I (continued)

| v'-v" | 0 - 0 | | | | | | | | 1 - 1 | | | | | | | |
|---|---|---|---|---|---|---|---|---|---|---|---|---|---|---|---|---|
| J | $P_{12ff}$ | Δν | $Q_{1fe}$ | Δν | $R_{12ff}$ | Δν | $R_{1ee}$ | Δν | $P_{12ff}$ | Δν | $Q_{1fe}$ | Δν | $R_{12ff}$ | Δν | $R_{1ee}$ | Δν |
| 61.5 | | | 15 932.893 * | -10 | 15 933.296 * | 5 | 15 948.875 | 4 | 15 912.134 | -9 | | | | | | |
| | | | 33.096 * | -7 | 33.499 * | 3 | 49.314 | -6 | 11.5.4 | 0 | | | | | | |
| | | | 33.296 * | -7 | 33.707 * | 5 | 49.766 | -4 | 11.784 | 4 | | | | | | |
| | | | 33.499 * | -8 | - | | 50.217 | -5 | 11.611 | 2 | | | | | | |
| | | | 33.707 * | -6 | 34.128 * | 6 | | | 11.446 | 6 | | | | | | |
| | | | - | | 34.341 * | 6 | | | 11.277 | 4 | | | | | | |
| | | | 34.128 * | -3 | 34.555 * | 4 | | | 11.110 | 1 | | | | | | |
| | | | 34.341 * | -3 | 34.772 * | 4 | | | 10.949 | 2 | | | | | | |
| | | | 34.555 * | -3 | 34.991 * | 2 | | | | | | | | | | |
| 70.5 | | | 34.772 * | -3 | 35.212 * | 2 | | | | | | | | | | |
| 71.5 | | | 34.991 * | -4 | 35.438 * | 3 | | | | | | | | | 15 955.664 | 2 |
| | | | 35.212 * | -3 | 35.665 * | 3 | | | | | | | | | 56.126 | 1 |
| | | | 35.438 * | -1 | | | | | | | | | | | 56.592 | 1 |
| | | | 35.665 * | 0 | | | | | | | | | | | 57.059 | 0 |
| | 15 907.574 * | 6 | | | | | | | | | | | | | 57.528 | -1 |
| | 7.434 * | 6 | | | | | 55.806 | 3 | | | | | | | | |
| | 7.294 * | 3 | | | | | 56.284 | 3 | | | | | | | | |
| | 7.153 * | -2 | | | | | 56.772 * | 11 | | | | | | | | |
| | 7.020 * | 3 | | | | | 57.246 | 4 | | | | | | | | |
| 80.5 | 6.892 * | 0 | | | | | 57.726 | 1 | | | | | | | | |
| 81.5 | 6.760 | -3 | | | | | 58.209 | -2 | | | | | 15 939.959 * | 0 | | |
| | 6.636 | -1 | | | | | 58.696 | -2 | | | | | 40.202 * | -1 | | |
| | 6.516 | 2 | | | | | 59.184 | -3 | | | 15 939.959 * | 0 | 40.447 * | -2 | | |
| | 6.393 | 0 | | | | | 59.679 | 1 | | | 40.202 * | -1 | 40.698 * | 0 | | |
| | 6.272 | -2 | | | | | 60.169 | -2 | | | 40.447 * | -2 | 40.951 * | 2 | | |
| | 6.157 | -1 | | | | | | | | | 40.698 * | 1 | 41.202 * | 0 | | |
| | 6.046 | 1 | | | | | | | | | 40.951 * | 4 | | | | |
| | 5.934 | 1 | | | | | | | | | 41.202 * | 2 | | | | |
| | 5.825 | 1 | | | 39.854 * | -6 | | | | | | | | | | |
| 90.5 | 5.721 | 3 | | | 40.122 * | -5 | | | | | | | | | | |
| 91.5 | 5.617 | 4 | 39.854 * | 3 | 40.393 * | -4 | | | | | | | | | | |
| | 5.515 | 3 | 40.122 * | 5 | 40.664 * | -4 | | | | | | | | | | |
| | 5.415 | 2 | 40.393 * | 7 | 40.937 * | -5 | | | | | | | | | | |
| | 5.315* | 0 | 40.664 * | 8 | | | | | | | | | | | | |
| | 5.222 | 0 | 40.937 * | 8 | | | | | | | | | | | | |
| | - | | | | | | | | | | | | | | | |
| | 5.039* | 0 | | | | | | | | | | | | | | |
| | 4.954* | 1 | | | | | | | | | | | | | | |
| | 4.870* | 2 | | | | | | | | | | | | | | |
| 100.5 | 4.791* | 5 | | | | | | | | | | | | | | |
| 101.5 | 4.709* | 4 | | | | | | | | | | | | | | |
| | 4.628 | 0 | | | | | | | | | | | | | | |
| | 4.551 | -2 | | | | | | | | | | | | | | |
| | 4.479 | -1 | | | | | | | | | | | | | | |
| | 4.406 | -4 | | | | | | | | | | | | | | |
| | 4.341 | -1 | | | | | | | | | | | | | | |
| | 4.275 | -2 | | | | | | | | | | | | | | |
| | 4.214 | 0 | | | | | | | | | | | | | | |
| | 4.158 | 4 | | | | | | | | | | | | | | |
| 110.5 | 4.098* | 2 | | | | | | | | | | | | | | |
| 111.5 | 4.038* | -2 | | | | | | | | | | | | | | |
| | 3.987* | 0 | | | | | | | | | | | | | | |
| | 3.934* | -2 | | | | | | | | | | | | | | |
| | 3.888* | 0 | | | | | | | | | | | | | | |
| | 3.841* | -1 | | | | | | | | | | | | | | |
| | 3.797* | -2 | | | | | | | | | | | | | | |
| | 3.754* | -4 | | | | | | | | | | | | | | |

TABLE I (Continued)

$A\ ^2\Pi_{3/2} - X\ ^2\Sigma^+$

| v'-v" | 0 - 0 | | | | | | | | 1 - 1 | | | | | | | |
|---|---|---|---|---|---|---|---|---|---|---|---|---|---|---|---|---|
| J' | $P_{2ff}$ | Δν | $Q_{21fe}$ | Δν | $R_{2ff}$ | Δν | $R_{21ee}$ | Δν | $P_{2ff}$ | Δν | $Q_{21fe}$ | Δν | $R_{2ff}$ | Δν | $R_{21ee}$ | Δν |
| 5.5 | 15 987.600* | 7 | | | 15 989.872* | -13 | | | | | | | | | | |
| | 87.331 | 6 | 15 989.872* | 7 | 89.989* | -10 | 15 991.294* | -4 | | | | | | | | |
| | 87.068 | 7 | 89.975* | -2 | 90.107* | -10 | 91.602 | 1 | | | | | | | 15 994.014 | 5 |
| | 86.805 | 6 | 90.090 | -1 | 90.227* | -9 | 91.909* | 2 | | | | | | | 94.311 | -2 |
| | 86.545 | 6 | 90.206 | -2 | 90.357 | -2 | 92.218 | 3 | | | | | | | 94.615 | -4 |
| 10.5 | 86.289* | 7 | 90.321 | -6 | 90.475* | -8 | 92.528* | 3 | | | | | | | 94.926 | -1 |
| | 86.033 | 6 | 90.443* | -6 | 90.601* | -10 | 92.837 | 0 | | | | | | | 95.240 | 2 |
| | 85.778 | 3 | 90.570* | -4 | 90.732* | -9 | 93.152 | -1 | | | | | | | 95.558 | 7 |
| | 85.527 | 2 | 90.695* | -5 | 90.866* | -7 | - | | | | | | | | 95.866 | -1 |
| | | | 90.823* | -6 | 91.007* | -2 | - | | | | | | | | 96.183 | -3 |
| | | | 90.961* | 0 | 91.146 | 1 | - | | | | | | | | 96.505 | -2 |
| | | | 91.097* | 1 | 91.286 | 1 | - | | | | | | | | 96.825 | -5 |
| | | | 91.234 | 1 | 91.427 | 0 | 94.770 | 2 | 15 986.988 | 4 | | | 15 993.829* | 1 | 97.153 | -3 |
| | | | 91.375 | 3 | 91.576 | 3 | 95.102 | 3 | 86.750 | 2 | 15 993.776* | 2 | 93.973* | 2 | 97.481 | -2 |
| | | | 91.515 | 2 | 91.722 | 2 | 95.434 | 2 | - | | 93.915* | 1 | 94.120* | 3 | 97.812 | -3 |
| 20.5 | | | 91.660 | 2 | 91.871 | 1 | 95.768 | 0 | 86.277 | -4 | 94.061* | 4 | 94.269* | 4 | | |
| | | | 91.806 | 1 | 92.023 | 0 | 96.109 | 4 | 86.049 | -3 | 94.203* | 1 | 94.417* | 2 | | |
| | | | 91.954 | 0 | 92.180 | 3 | 96.449 | 2 | 85.822 | -2 | 94.352* | 3 | 94.576* | 8 | | |
| | | | 92.106 | 0 | 92.335 | 1 | 96.792 | 1 | 85.596 | -4 | 94.499* | 0 | 94.725* | 2 | | |
| | | | 92.262 | 1 | 92.496 | 2 | 97.140 | 4 | 85.375 | -3 | 94.652* | 0 | 94.883* | 2 | | |
| | | | 92.419 | 1 | 92.658 | 1 | 97.486 | 2 | | | 94.807* | 0 | 95.044* | 3 | | |
| | | | 92.577 | 1 | 92.821 | 0 | 97.837 | 2 | | | 94.964* | 0 | 95.201* | 3 | | |
| | 82.301 | 2 | 92.737 | -1 | 92.989 | 1 | 98.190 | 1 | | | 95.125* | 1 | 95.371* | 3 | | |
| | 82.089 | 1 | 92.901 | -2 | 93.159* | 0 | 98.545 | 1 | | | 95.286* | 1 | 95.539* | 3 | | |
| | 81.880 | 1 | 93.069* | 0 | 93.331* | 1 | 98.904 | 1 | | | 95.450* | 0 | 95.710* | 4 | | |
| 30.5 | 81.674 | 1 | 93.239* | 1 | 93.506* | 1 | 99.260 | -3 | | | 95.617* | 0 | 95.885* | 7 | | |
| | 81.463 | -5 | 93.411* | 1 | 93.670* | -12 | 99.622 | -5 | | | 95.788* | 2 | 96.053* | 0 | 16 001.975 | 0 |
| | 81.264 | -4 | 93.583* | -1 | 93.860* | -2 | | | | | 95.953* | -5 | 96.232* | 2 | 2.342 | 5 |
| | 81.064 | -4 | 93.757* | -4 | 94.044* | 0 | | | | | 96.128* | -5 | 96.420* | 11 | 2.704 | 1 |
| | 80.867 | -5 | 93.938* | -1 | 94.227* | -2 | | | | | 96.303* | -6 | 96.602* | 11 | 3.069 | -2 |
| | 80.677 | 1 | 94.118* | -3 | - | | | | | | 96.488* | 0 | 96.785* | 10 | 3.440 | -1 |
| | - | | 94.305* | -1 | - | | | | | | 96.673* | 4 | 96.973* | 11 | - | |
| | 80.297 | -2 | - | | 94.801* | 4 | | | | | 96.853* | 0 | 97.162* | 11 | 4.192 | 4 |
| | 80.111 | -1 | 94.683* | 2 | 94.997* | 6 | 16 002.246 | 4 | | | 97.040* | 1 | | | 4.569 | 4 |
| | 79.926 | -3 | 94.875* | 3 | - | | 2.632 | 6 | 82.347 | 2 | | | | | - | |
| 40.5 | 79.745 | -3 | 95.068* | 2 | 95.389* | 2 | 3.014 | 3 | 82.163 | | | | | | 5.328 | 0 |
| | 79.566 | -3 | 95.264* | 2 | 95.589* | 0 | 3.402 | 1 | 81.984 | 1 | | | | | 5.710 | -2 |
| | 79.388 | -5 | 95.458* | -2 | 95.792* | -1 | - | | 81.807 | 1 | | | | | 6.098 | -2 |
| | 79.216 | -4 | 95.658* | -3 | 95.999* | -1 | 4.190 | 5 | 81.629 | -1 | | | | | 6.487 | -1 |
| | 79.043 | -6 | 95.859* | -6 | 96.213* | 4 | 4.587 | 5 | 81.457 | -1 | | | | | 6.878 | -3 |
| | - | | 96.067* | -4 | 96.425* | 4 | | | 81.295 | 7 | | | | | 7.275 | 0 |
| | 78.714 | 0 | 96.282* | 2 | 96.636* | 2 | 5.385 | 3 | 81.118 | -2 | | | | | | |
| | 78.547 | -4 | 96.493* | 2 | - | | 5.787 | 2 | 80.953 | -2 | | | | | | |
| | 78.388 | -2 | - | | 97.074* | 4 | 6.192 | 0 | 80.790 | -2 | | | | | | |
| | 78.228 | -3 | 96.926* | 6 | 97.290* | 0 | 6.599 | -1 | 80.633 | 1 | | | | | | |
| 50.5 | 78.073 | -3 | 97.144* | 6 | 97.512* | -2 | 7.013 | 2 | 80.476 | 1 | | | | | | |
| | - | | 97.359* | 1 | 97.735* | -2 | | | 80.321 | 1 | | | | | | |
| | 77.771 | 0 | 97.588* | 6 | 97.961* | -8 | | | 80.168 | 1 | | | | | | |
| | 77.623 | 0 | 97.806* | -1 | 98.188* | -11 | | | 80.017 | 1 | | | | | | |
| | 77.476 | -1 | 98.034* | 0 | 98.425* | -8 | | | 79.870 | 2 | | | | | | |
| | 77.334 | -1 | 98.260* | -5 | 98.630* | -4 | | | - | | | | | | | |
| | 77.193 | 0 | 98.495* | -2 | 98.901* | -5 | | | - | | | | | | | |
| | - | | - | | 99.144* | -2 | | | - | | | | | | | |
| | 76.922 | 2 | 98.969* | -1 | 99.386* | -4 | | | - | | | | | | | |
| | 76.790 | 3 | 99.208* | -2 | 99.633* | -2 | | | 79.166 | 1 | | | | | | |
| 60.5 | 76.658 | 2 | 99.447* | -5 | 99.887* | 4 | | | 79.036 | 3 | | | | | | |
| | 76.526 | 2 | 99.703* | 6 | 16 000.137* | 4 | | | 78.904 | 3 | | | | | | |
| | 76.403 | 0 | 99.948* | 4 | | | | | 78.775 | 2 | | | | | | |
| | 76.279 | 0 | 16 000.189* | -4 | | | | | 78.648 | 0 | | | | | | |
| | 76.156 | 3 | | | | | | | 78.525 | 1 | | | | | | |
| | - | | | | | | | | 78.403 | 0 | | | | | | |
| | - | | | | | | | | 78.279* | -5 | | | | | | |
| | 75.811* | -1 | | | | | | | 78.164 | -5 | | | | | | |
| | 75.703* | 1 | | | 1.962* | 12 | | | 78.051 | -4 | | | | | | |
| | 75.597* | 4 | | | 2.221 | 1 | | | 77.944 | 0 | | | | | | |
| 70.5 | 75.492* | 4 | 2.019* | 13 | 2.494 | 3 | | | 77.837* | 1 | | | | | | |
| | 15 975.390* | 5 | 16 002.277* | 2 | 16 002.767 | 2 | | | | | | | | | | |
| | 75.290* | 6 | 2.549* | 3 | 3.044 | 3 | | | | | | | | | | |
| | 75.191* | 5 | 2.823* | 4 | 3.317 | -2 | | | | | | | | | | |
| | 75.097* | 6 | 3.100* | 6 | 3.599 | -1 | | | | | | | | | | |
| | | | 3.372* | 0 | 3.884 | 1 | 16 018.101 | 1 | | | | | | | | |
| | | | 3.653* | 1 | - | | 18.574 | -2 | | | | | | | | |
| | | | 3.935* | 0 | 4.451 | -6 | 19.055 | 0 | | | | | | | | |
| | | | - | | 4.742 | -5 | 19.537 | 2 | | | | | | | | |
| | 74.653 | 3 | 4.505* | -2 | 5.038 | -2 | 20.020 | 2 | | | | | | | | |
| 80.5 | 74.570 | 0 | 4.795* | -2 | 5.335 | 0 | - | | | | | | | | | |
| | 74.491 | -1 | 5.089* | 0 | 5.633 | 1 | 20.990 | -2 | | | | | | | | |
| | 74.413 | -3 | 5.384* | 2 | 5.935 | 3 | 21.481 | -1 | | | | | | | | |
| | 74.341 | -2 | 5.684* | 5 | 6.237 | 4 | 21.974 | -1 | | | | | | | | |
| | 74.269 | -3 | 5.982* | 4 | 6.541 | 3 | 22.471 | 1 | | | | | | | | |
| | 74.202 | -2 | 6.285* | 6 | | | 22.968 | 0 | | | | | | | | |
| | 74.140 | 2 | 6.589* | 6 | | | | | | | | | | | | |
| | 74.081 | 6 | | | | | | | | | | | | | | |

## TABLE I (Continued)

### $B\ ^2\Sigma^+ - X\ ^2\Sigma^+$

| v'-v" | 0 - 0 | | | | | | | | 1 - 1 | | | | | | | |
|---|---|---|---|---|---|---|---|---|---|---|---|---|---|---|---|---|
| J | $R_1$ | Δν | $R_2$ | Δν | $P_1$ | Δν | $P_2$ | Δν | $R_1$ | Δν | $R_2$ | Δν | $P_1$ | Δν | $P_2$ | Δν |
| 1.5 | | | | | | | 16 382.672* | 1 | | | | | | | | |
| | | | | | | | 82.531* | 0 | | | | | | | 16 382.321 | 0 |
| | | | | | 16 382.276 | 0 | 82.395* | 0 | | | | | | | 82.185 | -1 |
| | | | | | 82.067 | 0 | 82.267* | 4 | | | | | | | - | |
| | 16 384.288* | -9 | | | 81.863 | 0 | 82.133* | -2 | | | | | | | 81.931 | 4 |
| | 84.471* | -11 | | | 81.659 | -4 | 82.010* | 0 | | | | | | | 81.812* | 9 |
| | 84.663* | -8 | 16 385.616* | -1 | 81.459 | -8 | | | | | | | | | | |
| | 84.854* | -10 | 85.882* | -4 | 81.273 | -2 | | | | | | | | | | |
| 10.5 | 85.054* | -7 | 86.153* | -6 | 81.089 | 2 | | | | | 16 385.923* | -10 | | | | |
| | 85.262 | 0 | 86.445* | 9 | 80.906 | 3 | | | 16 385.038* | 8 | 86.198* | -10 | 16 380.697 | 6 | | |
| | 85.464 | -3 | 86.729* | 11 | 80.728 | 5 | | | 85.242* | 9 | 86.486* | -2 | 80.513 | 2 | | |
| | 85.674 | -2 | 87.013* | 10 | 80.554 | 7 | | | 85.446* | 6 | 86.767* | -3 | 80.344 | 9 | | |
| | 85.882* | -7 | - | | 80.379 | 3 | 81.256* | 1 | 85.654* | 4 | 87.054* | -3 | - | | | |
| | 86.103 | -3 | 87.589* | 4 | 80.215 | 7 | 81.166* | 2 | 85.865 | 0 | 87.348 | 0 | - | | | |
| | 86.325 | -3 | 87.885* | 3 | - | | 81.079* | 3 | 86.080 | -4 | 87.644 | 1 | - | | | |
| | 86.553 | 0 | 88.185* | 2 | - | | 80.996* | 4 | 86.303 | -4 | 87.943 | 1 | 79.674 | 4 | 80.785 | 2 |
| | 86.783 | 1 | 88.493* | 5 | - | | 80.916* | 3 | 86.528 | -5 | 88.245 | 0 | 79.514 | 1 | 80.707 | 4 |
| | 87.017 | 1 | 88.799* | 2 | 79.579 | 1 | 80.843* | 6 | 86.757 | -7 | 88.549 | -3 | 79.360 | -1 | 80.633 | 5 |
| 20.5 | 87.253 | 0 | 89.114* | 4 | 79.432 | 1 | - | | 86.992 | -6 | 88.859 | -3 | 79.215 | 3 | | |
| | 87.497 | 2 | 89.427 | 0 | 79.290 | 2 | | | - | | 89.174 | -3 | 79.069 | 1 | | |
| | 87.735 | -5 | 89.752* | 3 | 79.150 | 2 | | | 87.481 | 2 | 89.494 | -1 | 78.918 | -9 | | |
| | 87.988 | -2 | 90.074* | 0 | 79.012 | -1 | | | 87.733 | 8 | 89.815 | -2 | 78.789* | -1 | | |
| | 88.244 | 1 | 90.405* | 2 | 78.883 | 1 | | | 87.974 | -2 | 90.143 | -1 | 78.645* | -12 | | |
| | 88.497 | -4 | 90.735 | -1 | 78.755 | -1 | | | 88.229 | -1 | 90.472 | -2 | 78.516* | -14 | | |
| | 88.761 | -2 | 91.073* | 0 | 78.635 | 3 | | | 88.487 | -1 | 90.807 | -1 | 78.402 | -3 | | |
| | 89.028 | 0 | 91.416* | 2 | 78.515 | 1 | | | 88.749 | -1 | 91.146 | 0 | 78.284 | -1 | | |
| | 89.299 | 1 | - | | 78.399 | 0 | | | 89.017 | 1 | 91.489 | 2 | 78.166 | -2 | | |
| | 89.573 | 1 | 92.105* | -3 | 78.288 | -1 | | | 89.286 | 0 | 91.832 | -1 | 78.054 | -2 | | |
| 30.5 | 89.852 | 3 | 92.456* | -5 | 78.181 | -1 | | | 89.560 | 0 | 92.180 | -2 | 77.943 | -4 | | |
| | 90.132 | 1 | | | 78.083 | 3 | | | 89.843 | 6 | 92.535 | 1 | 77.835 | -7 | | |
| | 90.420 | 3 | | | 77.981 | 0 | | | 90.117 | -2 | 92.891 | -2 | 77.739 | -3 | | |
| | 90.704 | -2 | | | 77.884 | -3 | | | 90.407 | 2 | - | | - | | | |
| | 91.001 | | | | 77.794 | -3 | | | 90.695 | 1 | 93.620 | 0 | - | | | |
| | 91.301 | 3 | | | 77.709 | -2 | | | 90.989 | 2 | 93.990 | 2 | 77.453* | -10 | | |
| | 91.604 | 4 | 94.662 | 1 | 77.627 | -2 | | | 91.291 | 6 | 94.363 | 2 | - | | | |
| | 91.908 | 2 | 95.041 | -1 | 77.547 | -4 | | | 91.586 | 1 | 94.738 | 1 | 77.295 | -2 | | |
| | 92.219 | 3 | 95.419 | -7 | 77.477 | 0 | | | 91.892 | 2 | 95.119 | 2 | 77.218 | -3 | | |
| | 92.532 | 2 | 95.809 | -6 | 77.410 | 3 | | | 92.201 | 2 | 95.494 | -7 | 77.145 | -3 | | |
| 40.5 | | | 96.204 | -3 | 77.340 | -2 | | | 92.516 | 4 | 95.887 | -2 | 77.075 | -4 | | |
| | | | 96.601 | -2 | | | | | 92.829* | 0 | 96.281 | 0 | 77.005* | -10 | | |
| | | | 96.006 | 2 | | | | | 93.150* | 0 | 96.676 | -7 | 76.947* | -7 | | |
| | | | 97.409 | 1 | | | | | 93.471* | -3 | 97.080 | 4 | 76.891* | -6 | | |
| | | | 97.811 | -5 | | | | | 93.799* | -4 | 97.483* | 4 | 76.843* | -1 | | |
| | | | 98.226 | -2 | | | | | 94.136 | 1 | 97.891* | 5 | 76.790* | -6 | | |
| | 94.842 | 4 | 98.642 | -2 | | | | | 94.471 | 0 | 98.294 | 3 | | | | |
| | 95.187 | 3 | 99.062 | -1 | | | | | 94.812 | 1 | 98.711 | -1 | | | | |
| | 95.535 | 1 | 99.486 | -1 | | | | | 95.157 | 2 | 99.129 | -1 | | | | |
| | 95.891 | 4 | 99.915 | 1 | | | | | 95.503 | 0 | 99.554 | 1 | | | | |
| 50.5 | 96.245 | 0 | | | | | | | 95.852 | -2 | 99.979 | 0 | | | | |
| | 96.608 | 1 | | | | | | | 96.214 | 4 | | | | | | |
| | 96.972 | 0 | | | | | | | 96.569 | 0 | | | | | | |
| | 97.343 | 1 | | | | | 80.660* | -4 | 96.936 | 4 | | | | | | |
| | 97.718 | 3 | | | | | 80.727* | -2 | 97.301 | 2 | | | | | | |
| | 98.091 | -2 | | | | | 80.807* | 9 | 97.674 | 4 | | | | | | |
| | 98.473 | -1 | | | | | 80.876* | 5 | 98.046 | 2 | | | | | | |
| | 98.859 | 0 | | | | | 80.954* | 6 | 98.424 | 2 | | | | | | |
| | 99.245 | -4 | | | | | 81.034* | 5 | 98.806 | 1 | | | | | | |
| | 99.639 | -3 | | | | | 81.119* | 6 | 99.190 | 0 | | | | | | |
| 60.5 | 400.035 | -5 | | | | | | | 99.583 | 2 | | | | | | |
| | | | | | | | | | 16 399.975 | 0 | | | | | | |
| | | | | | | | 16 381.706 * | 2 | | | | | | | | |
| | | | | | | | 81.820 * | 4 | | | | | | | | |
| | | | | | | | 81.937 * | 5 | | | | | | | | |
| | | | | | | | 82.054 * | 1 | | | | | | | | |
| | | | | | | | 82.189 * | 1 | | | | | | | | |
| 70.5 | | | | | | | 82.305 * | 1 | | | | | | | | |
| 71.5 | | | | | | | 82.437 * | 1 | | | | | | | | |
| | | | 16 410.811* | 5 | | | | | | | | | | | | |
| | | | 11.327* | 2 | | | | | | | | | | | | |
| | | | 11.849 | 2 | | | | | | | | | | | | |
| | | | 12.373 | 0 | | | | | | | | | | | | |
| | | | 12.898 | -6 | | | | | | | | | | | | |
| 80.5 | | | | | | | | | | | | | | | | |
| 81.5 | | | | | | | | | | | | | | | | |
| | | | | | | | | | 411.033 | -4 | | | | | | |
| | | | | | | | | | 11.530 | 3 | | | | | | |
| | | | | | | | | | 12.024 | 3 | | | | | | |
| | | | | | | | | | 12.521 | 2 | | | | | | |
| 90.5 | | | | | | | | | 13.023 | 3 | | | | | | |

TABLE I (Continued)

$B\ ^2\Sigma^+ - X\ ^2\Sigma^+$

| | 2 - 2 | | | | | | | |
|---|---|---|---|---|---|---|---|---|
| | $R_1$ | $\Delta\nu$ | $R_2$ | $\Delta\nu$ | $P_1$ | $\Delta\nu$ | $R_2$ | $\Delta\nu$ |
| 11.5 | | | | | | | | |
| | | | 16 386.305 | -5 | | | | |
| | | | 86.591 | -4 | | | | |
| | | | 86.880 | -3 | | | | |
| | 16 385.832* | -1 | | | | | | |
| | 86.056* | -2 | 87.774 | 1 | | | | |
| | 86.280* | -3 | 88.078 | 2 | | | | |
| 20.5 | | | 88.385 | 0 | | | | |
| | | | 88.697 | 1 | | | | |
| | | | 89.015 | 4 | | | | |
| | 87.481 | 2 | | | | | | |
| | 87.734 | 4 | | | | | | |
| | 87.988 | 4 | | | | | | |
| | 88.244 | 2 | | | 16 377.833* | 6 | | |
| | | | | | 77.708 | 0 | | |
| | | | | | 77.594 | 1 | | |
| 30.5 | | | | | 77.481 | -1 | | |
| | | | | | 77.377 | 1 | | |
| | 89.591 | -1 | | | 77.274 | 1 | | |
| | 89.870 | -3 | | | 77.172 | -1 | | |
| | 90.158 | 0 | | | 77.078 | 0 | | |
| | | | | | 76.989 | 2 | | |
| | 90.737 | -3 | | | 76.897 | -2 | | |
| | 91.037 | 1 | | | 76.813 | -3 | | |
| | 91.338 | 1 | | | 76.737 | 1 | | |
| | 91.643 | 2 | | | 76.658 | -2 | | |
| 40.5 | 91.951 | 2 | | | 76.581* | -7 | | |
| | 92.264 | 3 | | | 76.520* | 0 | | |
| | 92.579 | 2 | | | 76.453* | -3 | | |
| | 92.897 | 1 | | | 76.393* | -3 | | |
| | 93.213 | -6 | | | 76.340* | 1 | | |
| | 93.540 | -6 | | | 76.290* | 3 | | |
| | 93.872 | -5 | | | 76.244* | 5 | | |
| | 94.213 | 1 | | | 76.201* | 7 | | |
| | 94.552 | 2 | | | 76.161* | 8 | | |
| | 94.892 | -1 | | | | | | |
| 50.5 | 95.241 | 3 | | | | | | |
| | 95.591 | 2 | | | | | | |
| | 95.940 | -2 | | | | | | |
| | 96.299 | -1 | | | | | | |
| | 96.662 | 1 | | | | | | |
| | 97.027 | 1 | | | | | | |
| | 97.398 | 4 | | | | | | |
| | 97.765 | -2 | | | | | | |
| | 98.140 | -3 | | | | | | |
| | 98.521 | -2 | | | | | | |
| 60.5 | 98.907 | 0 | | | | | | |
| | 99.295 | 1 | | | | | | |
| | 99.686 | 1 | | | | | | |
| | 16 400.080 | 0 | | | | | | |

TABLE II Measured line positions for Ca $^{81}$Br (in cm$^{-1}$)

$A\ ^2\Pi_{1/2} - X\ ^2\Sigma^+$

| v'-v" | 0 - 0 | | | | | | | | 1 - 1 | | | | | | | |
|---|---|---|---|---|---|---|---|---|---|---|---|---|---|---|---|---|
| J | $P_{12ff}$ | Δν | $Q_{1fe}$ | Δν | $R_{12ff}$ | Δν | $R_{1ee}$ | Δν | $P_{12ff}$ | Δν | $Q_{1fe}$ | Δν | $R_{12ff}$ | Δν | $R_{1ee}$ | Δν |
| 0.5 | | | | | 15 925.091* | 10 | | | | | | | | | | |
| | | | 15 925.091* | 14 | 25.152* | 3 | | | | | | | | | | |
| | | | 25.152* | 11 | 25.220* | 2 | | | | | | | | | | |
| | | | 25.220* | 13 | 25.287* | -2 | | | | | | | | | | |
| | | | 25.287* | 11 | 25.367* | 6 | | | | | | | | | | |
| | 15 923.229* | -7 | 25.357* | 11 | 25.446* | 7 | | | | | | | | | | |
| | 22.929* | -7 | 25.428* | 9 | 25.525* | 9 | | | | | | | | | | |
| | | | 25.501* | 8 | 25.611* | 15 | | | | | | | | | | |
| | 22.335* | -6 | 25.579* | 8 | 25.691* | 13 | | | | | | | | | | |
| | 22.037 | -10 | 25.658* | 8 | 25.775* | 12 | | | | | | | | | | |
| 10.5 | 21.758 | 2 | 25.737* | 5 | 25.866* | 16 | | | | | | | | | | |
| 11.5 | 21.464 | -3 | 25.819* | 3 | | | 15 929.010 | -7 | | | | | | | | |
| | 21.177 | -3 | | | | | 29.351 | -7 | 15 923.559* | -7 | | | | | | |
| | 20.893 | -2 | | | | | | | 23.272* | -9 | | | | | | |
| | 20.611 | -1 | | | 26.227* | 8 | 30.047 | -3 | 22.994* | -5 | | | | | | |
| | | | 26.177* | 4 | 26.325* | 8 | 30.396 | -1 | | | | | | | | |
| | | | 26.276* | 8 | 26.426* | 9 | | | 22.439 | -2 | | | 15 928.774 | -2 | | |
| | 19.778 | 0 | 26.374* | 9 | 26.529* | 10 | | | 22.165 | 0 | | | 28.874 | -2 | | |
| | 19.504 | 0 | 26.476* | 12 | 26.634* | 11 | 31.451 | -4 | 21.891 | 0 | 15 928.811* | -9 | 28.979 | 0 | | |
| | 19.234 | 1 | 26.573* | 8 | 26.727 | -3 | 31.810 | -2 | 21.619 | -1 | 28.912* | -8 | 29.084 | 0 | 15 934.175 | 4 |
| 20.5 | 18.967 | 3 | 26.665 | -3 | 26.837 | -2 | 32.168 | -3 | 21.350 | 0 | 29.014* | -8 | 29.193 | 2 | 34.528 | 0 |
| 21.5 | 18.699 | 2 | 26.772 | -2 | 26.949 | -1 | 32.529 | -3 | 21.085 | 2 | 29.120* | -6 | 29.299 | -1 | 34.888 | 1 |
| | | | 26.878 | -4 | 27.061 | -2 | | | 20.820 | 1 | 29.225* | -7 | 29.411 | -1 | 35.250 | 1 |
| | 18.172 | 1 | 26.983* | -10 | 27.173 | -6 | 33.263 | 2 | 20.557 | 1 | 29.336* | -5 | 29.524 | -1 | 35.614 | 1 |
| | 17.913 | 2 | 27.091* | -14 | 27.291 | -6 | 33.630 | 2 | 20.296 | 1 | 29.446* | -5 | | | | |
| | 17.656 | 3 | 27.203* | -17 | 27.413 | -4 | | | | | 29.559* | -5 | 29.754 | -5 | | |
| | | | | | 27.536 | -3 | | | 19.784 | 2 | | | 29.876 | -3 | 36.717 | 2 |
| | 17.147 | 1 | 27.445* | -11 | 27.661 | -2 | | | 19.530 | 2 | 29.790* | -6 | 29.996 | -6 | 37.087 | -1 |
| | 16.894 | 1 | 27.568* | -10 | 27.786 | -3 | | | 19.279 | 2 | 29.910* | -6 | 30.121 | -5 | 37.462 | 1 |
| | 16.645 | 0 | 27.693* | -8 | 28.916 | -3 | | | 19.030 | 3 | 30.032* | -5 | 30.249 | -4 | 37.841 | 4 |
| 30.5 | | | 27.822* | -5 | 28.047 | -2 | | | 18.782 | 2 | 30.159* | -2 | 30.382 | 0 | | |
| 31.5 | | | 27.949* | -6 | 28.182 | -1 | | | 18.537 | 2 | 30.283* | -3 | 30.512 | -1 | | |
| | 15.912 | 0 | 28.081* | -5 | | | | | | | 30.417* | 2 | 30.646 | 0 | 38.978 | 1 |
| | 15.672 | -1 | | | | | | | 18.058 | 5 | 30.550* | 5 | 30.784 | 2 | 39.358 | -3 |
| | 15.432 | -3 | | | | | | | 17.818 | 3 | 30.684* | 6 | 30.920 | 1 | 39.745 | -3 |
| | 15.201 | 0 | | | 28.738 | -1 | | | 17.583 | 4 | 30.819* | 7 | 31.061 | 2 | | |
| | 14.966 | -2 | | | 28.884 | 0 | | | | | 30.958* | 9 | | | | |
| | 14.735 | -2 | 28.774* | 3 | 29.030 | 0 | | | 17.115 | 0 | | | | | | |
| | 14.512 | 3 | 28.916* | 2 | 29.177 | -2 | | | 16.887 | 1 | | | | | | |
| | 14.284 | 1 | 29.064* | 4 | 29.330 | 0 | | | 16.658 | -1 | | | | | | |
| 40.5 | 14.059 | 0 | 29.215* | 6 | 29.481 | -2 | | | 16.436 | 1 | | | | | | |
| 41.5 | 13.838 | 0 | 29.365* | 6 | 29.637 | -2 | | | | | | | | | | |
| | | | 29.518* | 6 | 29.794 | -3 | | | | | | | 32.104* | 6 | | |
| | 13.406 | 2 | 29.674* | 7 | 29.956 | -1 | | | | | | | 32.256* | 1 | | |
| | 13.191 | 1 | 29.824* | 1 | 30.117 | -2 | | | | | 32.120* | -1 | 32.418* | 3 | | |
| | 12.980 | 2 | 29.982* | -1 | | | | | 15.348 | 2 | 32.280* | 2 | 32.580* | 3 | | |
| | 12.770 | 2 | 30.142* | -2 | | | | | 15.136 | 0 | 32.440* | 4 | 32.745* | 4 | | |
| | | | | | | | | | 14.925 | -1 | 32.596* | -2 | 32.907* | 0 | | |
| | 12.361 | 5 | | | | | | | 14.720 | -1 | 32.755* | -6 | 33.082* | 8 | | |
| | 12.158 | 4 | | | | | | | 14.519 | 2 | 32.923* | -3 | 33.253* | 8 | | |
| 50.5 | 11.958 | 5 | | | 31.143* | 3 | | | 14.316 | 1 | 33.082* | -10 | | | | |
| 51.5 | 11.757 | 2 | | | 31.321* | 2 | | | 14.118 | 2 | 33.253* | -10 | | | | |
| | 11.564 | 4 | 31.158* | -2 | 31.492* | -6 | | | 13.919 | 1 | | | 33.775* | 6 | | |
| | 11.369 | 3 | 31.336* | -2 | 31.679* | -2 | | | 13.726 | 2 | | | 33.954* | 5 | | |
| | 11.177 | 1 | 31.518* | 1 | 31.867* | 1 | | | | | 33.775* | -9 | 34.134* | 4 | 47.887 | -2 |
| | 10.990 | 3 | 31.689* | -10 | 32.054* | 2 | | | | | 33.954* | -8 | 34.317* | 3 | 48.316 | 0 |
| | 10.804 | 3 | 31.877* | -6 | 32.250* | 8 | | | | | 34.134* | -9 | 34.502* | 3 | 48.748 | 1 |
| | | | 32.065* | -4 | 32.439* | 6 | | | | | 34.317* | -9 | 34.692* | 5 | 49.181 | 3 |
| | | | 32.250* | -7 | 32.633* | 6 | | | 12.783 | -1 | 34.502* | -9 | 34.880* | 3 | 49.605 | -6 |
| | | | 32.439* | -9 | 32.827* | 5 | 47.793 | 3 | 12.601 | -2 | 34.692* | -6 | 35.072* | 3 | 50.038* | -9 |
| 60.5 | | | 32.633* | -8 | 33.024* | 3 | 48.231 | 4 | 12.424 | 0 | 34.881* | -6 | | | | |

TABLE II (Continued)

| v'-v" | 0 - 0 | | | | | | | | 1 - 1 | | | | | | | |
|---|---|---|---|---|---|---|---|---|---|---|---|---|---|---|---|---|
| J | $P_{12ff}$ | Δν | $Q_{1fe}$ | Δν | $R_{12ff}$ | Δν | $R_{1ee}$ | Δν | $P_{12ff}$ | Δν | $Q_{1fe}$ | Δν | $R_{12ff}$ | Δν | $R_{1ee}$ | Δν |
| 61.5 | | | 32.827* | -9 | 33.226* | 5 | 48.679 | 5 | 12.248 | 0 | 35.072 | -6 | | | | |
| | | | 33.024* | -10 | 33.428* | 4 | 49.123 | 4 | 12.078 | 4 | | | | | | |
| | | | 33.226* | -7 | 33.632* | 3 | 49.570 | 3 | 11.907 | 4 | | | | | | |
| | | | 33.428* | -7 | 33.840* | 4 | 50.010 | -4 | 11.737 | 5 | | | | | | |
| | | | 33.632* | -7 | 34.050* | 5 | 50.461 | -5 | 11.565 | -1 | | | | | | |
| | | | 33.840* | -5 | 34.265* | 8 | | | 11.397 | -3 | | | | | | |
| | | | 34.050* | -4 | 34.478* | 8 | | | 11.237 | -1 | | | | | | |
| | | | 34.265* | 0 | 34.694* | 8 | | | 11.072 | -6 | | | | | | |
| | | | 34.478* | 0 | | | | | 10.915 | -5 | | | | | | |
| 70.5 | | | 34.694* | 1 | 35.127* | 2 | | | | | | | | | | |
| 71.5 | | | | | 35.349* | 1 | | | | | | | | | | |
| | | | 35.127* | -3 | 35.575* | 3 | | | | | | | | | 55.884 * | 3 |
| | | | 35.349* | -3 | 35.803* | 3 | | | | | | | | | 56.345 * | 2 |
| | | | 35.575* | -1 | | | | | | | | | | | 56.804 * | -4 |
| | | | 35.803* | 1 | | | | | | | | | | | 57.274 * | 1 |
| | | | | | | | 56.028 | 1 | | | | | | | | |
| | 7.293* | -7 | | | | | 56.508 | 6 | | | | | | | | |
| | 7.165* | -4 | | | | | 56.983 | 3 | | | | | | | | |
| 80.5 | 7.034* | -5 | | | | | 57.464 | 4 | | | | | | | | |
| 81.5 | 6.909* | -3 | | | | | 57.938 | -4 | | | | | 39.845 * | -6 | | |
| | 6.784 | -4 | | | | | 58.421 | -4 | | | | | 40.088 * | -6 | | |
| | 6.663 | -3 | | | | | 58.907 | -4 | | | 39.946 * | 3 | 40.332 * | -7 | | |
| | 6.545 | 0 | | | | | 59.396 | -2 | | | 40.088 * | 4 | 40.578 * | -7 | | |
| | 6.429 | 0 | | | | | 59.886 | -5 | | | 40.332 * | 4 | 40.832 * | -3 | | |
| | 6.311 | -2 | | | | | 60.375 | -2 | | | 40.578 * | 4 | 41.082 * | -4 | | |
| | 6.199 | -2 | | | | | | | | | 40.832 * | 9 | 41.335 * | -5 | | |
| | 6.089 | -2 | | | | | | | | | 41.082 * | 9 | | | | |
| | 5.984 | 1 | | | | | | | | | 41.335 * | 9 | | | | |
| 90.5 | 5.882 | 4 | | | 40.000 * | -4 | | | | | | | | | | |
| 91.5 | 5.775 | 1 | | | 40.264 * | -7 | | | | | | | | | | |
| | 5.677 | 3 | 40.000 * | 6 | 40.535 * | -6 | | | | | | | | | | |
| | 5.579 | 3 | 40.264 * | 4 | 40.807 * | -5 | | | | | | | | | | |
| | 5.484 | 4 | 40.535 * | 6 | 41.081 * | -6 | | | | | | | | | | |
| | 5.390 | 3 | 40.807 * | 7 | | | | | | | | | | | | |
| | 5.305 * | 9 | 41.081* | 7 | | | | | | | | | | | | |
| | 5.213 * | 5 | | | | | | | | | | | | | | |
| | 5.039 * | 2 | | | | | | | | | | | | | | |
| 100.5 | 4.954 * | -2 | | | | | | | | | | | | | | |
| 101.5 | 4.870 * | -7 | | | | | | | | | | | | | | |
| | 4.791 * | -10 | | | | | | | | | | | | | | |
| | 4.720 * | -6 | | | | | | | | | | | | | | |
| | 4.650 * | -5 | | | | | | | | | | | | | | |
| | 4.581 * | -5 | | | | | | | | | | | | | | |
| | 4.513 * | -6 | | | | | | | | | | | | | | |
| | 4.452 * | -3 | | | | | | | | | | | | | | |
| 110.5 | | | | | | | | | | | | | | | | |

## TABLE II (Continued)

### $A\ ^2\Pi_{3/2} - X\ ^2\Sigma^+$

| v'-v" | 0 - 0 | | | | | | | | 1 - 1 | | | | | |
|---|---|---|---|---|---|---|---|---|---|---|---|---|---|---|
| J | $P_{2ff}$ | Δν | $Q_{21fe}$ | Δν | $R_{2ff}$ | Δν | $R_{21ee}$ | Δν | $P_{2ff}$ | Δν | $Q_{21fe}$ | Δν | $R_{2ff}$ | Δν | $R_{21ee}$ | Δν |
| 5.5 | 15 987.600* | -2 | | | 15 989.872* | 3 | | | | | | | | | | |
| | 87.331* | -5 | 15 989.872* | 16 | 89.989* | 0 | 15 991.280* | 3 | | | | | | | | |
| | 87.068* | -5 | 89.975* | 9 | 90.107* | 2 | 91.580 | 3 | | | | | | | 15 993.974 | 0 |
| | 86.805* | -9 | 90.090* | 10 | 90.227* | 3 | 91.880 | 0 | | | | | | | 94.273 | -2 |
| | 86.545* | -11 | 90.206* | 11 | 90.357* | 11 | 92.184 | -1 | | | | | | | 94.575 | -3 |
| 10.5 | 86.289* | -12 | 90.321* | 7 | 90.475* | 6 | 92.493 | 0 | | | | | | | 94.883 | 0 |
| 11.5 | 86.046* | -3 | 90.443* | 8 | 90.601* | 6 | 92.800 | -3 | | | | | | | 95.194 | 1 |
| | 85.790* | -8 | 90.570* | 12 | 90.732* | 8 | 93.115 | -1 | | | | | | | 95.506 | 0 |
| | 85.547* | -3 | 90.695* | 12 | 90.866* | 11 | | | | | | | | | 95.823 | 7 |
| | | | 90.823* | 11 | 90.994* | 5 | | | | | | | | | 96.131 | -1 |
| | | | 90.950* | 8 | 91.130* | 4 | | | | | | | | | 96.451 | 0 |
| | | | 91.080* | 4 | 91.268* | 4 | | | | | | | | | 96.770 | -1 |
| | | | 91.214* | 3 | 91.408 | 3 | | | 15 987.008 | 2 | | | 15 993.792* | -3 | 97.093 | -1 |
| | | | 91.353 | 4 | 91.553 | 5 | 95.048 | 2 | 86.769 | -2 | | | 93.936* | -1 | 97.419 | -1 |
| | | | 91.495 | 5 | 91.698 | 3 | 95.377 | 0 | | | 15 993.882 | 3 | 94.081 | -1 | 97.747 | -1 |
| 20.5 | | | 91.636 | 3 | 91.845 | 2 | 95.707 | -3 | 86.305 | -4 | 94.023 | 3 | 94.230 | 1 | | |
| 21.5 | | | 91.780 | 1 | 91.994 | 0 | 96.046 | 1 | 86.071 | -10 | 94.167 | 3 | 94.379 | 1 | | |
| | | | 91.929 | 2 | 92.149 | 1 | 96.384 | 1 | 85.856 | -1 | 94.313 | 2 | 94.531 | 1 | | |
| | | | 92.079 | 1 | 92.303 | -1 | 96.727 | 4 | 85.632 | -2 | 94.461 | 2 | 94.685 | 1 | | |
| | | | 92.232 | 1 | 92.462 | -1 | 97.069 | 3 | 85.413 | -1 | 94.612 | 1 | 94.841 | 5 | | |
| | | | 92.387 | 1 | 92.621 | -2 | 97.412 | 0 | | | 94.765 | 1 | 95.002 | 2 | | |
| | | | 92.542 | -2 | 92.787 | 0 | 97.760 | 0 | | | 94.921 | 1 | 95.163 | 2 | | |
| | 82.352 | 1 | 92.702 | -2 | 92.951 | -1 | 98.111 | 1 | | | | | 95.326 | 1 | | |
| | 82.143 | 2 | 92.866 | -1 | 93.120 | -1 | 98.462 | -1 | | | 95.240 | 1 | 95.492 | 1 | | |
| | 81.936 | 3 | 93.031 | -1 | 93.295 | -2 | 98.819 | 1 | | | 95.403 | 1 | 95.663 | 3 | | |
| 30.5 | 81.731 | 2 | 93.199 | -1 | 93.465 | -1 | 99.172 | -5 | | | 95.569 | 2 | 95.829 | -2 | | |
| 31.5 | | | 93.370 | -1 | 93.638 | -2 | 99.531 | -6 | | | 95.738 | 2 | 95.998 | -6 | | |
| | 81.323 | -4 | 93.540 | -3 | 93.816 | -3 | | | | | 95.897 | *-9 | 96.176 | -4 | 16 002.237 | 3 |
| | 81.126 | -4 | 93.715 | -3 | 93.996 | -3 | | | | | 96.071 | *-8 | 96.354 | -3 | 2.602 | 6 |
| | 80.931 | -4 | 93.893 | -3 | 94.180 | -2 | | | | | 96.246 | *-8 | 96.540 | 2 | 2.960 | -1 |
| | 80.737 | -6 | 94.073 | -3 | 94.372 | 4 | | | | | 96.433 | * 1 | 96.725 | 4 | 3.324 | -4 |
| | | | 94.255 | -3 | 94.560 | 4 | | | | | 96.613 | * 2 | 96.908 | 1 | | |
| | 80.362 | -4 | 94.445* | 2 | 94.748 | 2 | | | | | 96.785 | *-8 | 97.094 | 0 | 4.073 | 3 |
| | 80.180 | -2 | 94.628* | -2 | 94.944 | 5 | | | | | 96.973 | *-5 | | | 4.448 | 5 |
| | 79.998 | -1 | 94.818* | -2 | 95.137 | 3 | 16 002.514 | 4 | 82.407 | 0 | | | | | | |
| 40.5 | 79.817 | -3 | 94.999* | -13 | 95.335 | 3 | 2.895 | 2 | 82.227 | 1 | | | | | 5.198 | -1 |
| 41.5 | 79.641 | -2 | 95.197* | -10 | 95.533 | 1 | 3.279 | 0 | 82.048 | 0 | | | | | 5.582 | 1 |
| | 79.464 | -4 | 95.397* | -7 | 95.734 | 0 | | | 81.871 | -1 | | | | | 5.964 | -1 |
| | 79.292 | -4 | 95.597* | -6 | | | 4.060 | 4 | 81.697 | -2 | | | | | 6.350 | -1 |
| | 79.122 | -5 | | | 96.146 | 0 | 4.452 | 2 | | | | | | | 6.738 | -1 |
| | 78.955 | -5 | 96.005* | -5 | 96.356 | 0 | | | 81.358 | -2 | | | | | 7.130 | -1 |
| | 78.794 | 0 | 96.213* | -4 | 96.568 | 0 | 5.243 | 0 | 81.190 | -3 | | | | | | |
| | 78.633 | 0 | 96.425* | -1 | | | 5.642 | -1 | 81.028 | -2 | | | | | | |
| | 78.471 | -2 | 96.636* | -1 | 97.005 | 5 | 6.046 | 0 | 80.857 | -1 | | | | | | |
| | 78.315 | -1 | | | 97.217 | -2 | 6.450 | -2 | 80.708 | -3 | | | | | | |
| 50.5 | 78.161 | -1 | 97.074* | +6 | 97.438 | -3 | 6.856 | -3 | 80.554 | 0 | | | | | | |
| 51.5 | 78.005* | -4 | 97.286* | 0 | 97.664 | -1 | 7.269 | 0 | 80.401 | 1 | | | | | | |
| | 77.858 | -2 | 97.509* | 1 | 97.888 | -4 | | | 80.247 | -1 | | | | | | |
| | 77.712 | -1 | 97.736* | 5 | 98.115 | *-6 | | | 80.100 | 0 | | | | | | |
| | 77.567 | -1 | 97.964* | 6 | 98.344 | *-9 | | | 79.953 | -1 | | | | | | |
| | 77.425 | -1 | 98.188* | 2 | 98.580 | *-6 | | | | | | | | | | |
| | 77.285 | -2 | 98.425* | 9 | 98.818 | *-4 | | | | | | | | | | |
| | 77.149 | -1 | | | 99.057 | *-4 | | | | | | | | | | |
| | | | 98.887* | 2 | 99.298 | *-3 | | | | | | | | | | |
| | 76.885* | 2 | 99.124* | 1 | 99.549 | 4 | | | | | | | | | | |
| 60.5 | 76.760* | 6 | 99.365* | 2 | 99.795 | 5 | | | 79.125 | 0 | | | | | | |
| 61.5 | 76.632* | 5 | 99.611* | 5 | 16 000.046 | 7 | | | 78.994 | -2 | | | | | | |
| | 76.512* | 10 | 99.856* | 5 | | | | | 78.867 | -2 | | | | | | |
| | 76.387* | 6 | 16 000.101* | 2 | | | | | 78.745 | 0 | | | | | | |
| | 76.266* | 5 | | | | | | | 78.624 | 1 | | | | | | |
| | 76.156* | 12 | | | | | | | 78.506 | 3 | | | | | | |
| | | | | | | | | | 78.387 | 1 | | | | | | |
| | 75.811* | 3 | | | | | | | 78.279* | 8 | | | | | | |
| | 75.703* | 2 | | | 2.109 | 1 | | | 78.164* | 5 | | | | | | |
| 70.5 | 75.597* | 1 | 1.909* | 12 | 2.378 | 0 | | | 78.051* | 2 | | | | | | |
| | | | | | | | | | 77.944* | 3 | | | | | | |
| 71.5 | 75.492* | -2 | 2.165* | 1 | 2.652 | 3 | | | 77.837* | 0 | | | | | | |
| | 75.390* | -4 | 2.436* | 4 | 2.925 | 1 | | | | | | | | | | |
| | 75.290* | -7 | 2.705* | 2 | 3.205 | 5 | | | | | | | | | | |
| | 75.198* | -5 | 2.980* | 4 | 3.475 | -3 | | | | | | | | | | |
| | 75.105* | -6 | 3.255* | 3 | 3.758 | -2 | 17.854 | 0 | | | | | | | | |
| | 75.019* | -3 | 3.528* | -2 | 4.042 | -1 | 18.326 | -1 | | | | | | | | |
| | | | 3.812* | 1 | 4.330 | 1 | 18.799 | -2 | | | | | | | | |
| | | | | | 4.610 | -7 | | | | | | | | | | |
| | | | 4.374* | -5 | 4.904 | -4 | 19.759 | 3 | | | | | | | | |
| 80.5 | | | 4.561* | -5 | | | 20.240 | 3 | | | | | | | | |
| 81.5 | 74.610* | 0 | 4.952* | -4 | 5.494 | -1 | 20.722 | 1 | | | | | | | | |
| | 74.535* | 0 | 5.248* | 1 | 5.793 | 1 | 21.205 | -2 | | | | | | | | |
| | 74.464* | 0 | 5.542* | 0 | 6.092 | 0 | 21.697 | 1 | | | | | | | | |
| | 74.400* | 6 | 5.839* | 1 | 6.396 | 2 | 22.186 | -2 | | | | | | | | |
| | 74.332* | 6 | 6.139* | 2 | 6.700 | 2 | 22.682 | 1 | | | | | | | | |
| | 74.269* | 8 | 6.441* | 2 | | | 23.178 | 1 | | | | | | | | |
| | 74.202* | 3 | | | | | | | | | | | | | | |
| | 74.140* | 1 | | | | | | | | | | | | | | |
| | 74.081* | 0 | | | | | | | | | | | | | | |
| 90.5 | | | | | | | | | | | | | | | | |

## TABLE II (Continued)

### $B\ ^2\Sigma^+ - X\ ^2\Sigma^+$

| v'-v" | 0 - 0 | | | | | | | | 1 - 1 | | | | | | | |
|---|---|---|---|---|---|---|---|---|---|---|---|---|---|---|---|---|
| J | $R_1$ | Δν | $R_2$ | Δν | $P_1$ | Δν | $P_2$ | Δν | $R_1$ | Δν | $R_2$ | Δν | $P_1$ | Δν | $P_2$ | Δν |
| 0.5 | | | | | | | 16 382.672 | 5 | | | | | | | | |
| | | | | | | | 82.531 | 3 | | | | | | | 16 382.321 | 2 |
| | | | | | 16 382.276 | 1 | 82.395 | 2 | | | | | | | 82.185 | 5 |
| | | | | | 82.067 | -2 | 82.267 | 5 | | | | | | | | |
| | 16 384.288 | 7 | | | 81.863 | -3 | 82.133 | -2 | | | | | | | 81.931 | 4 |
| | 84.471 | 7 | | | 81.659 | -9 | 82.010 | -1 | | | | | | | 81.812 | 8 |
| | 84.663 | 11 | 16 385.593 | 4 | 81.459 | -14 | 81.906 | 13 | | | | | | | | |
| | 84.853 | 9 | 85.855 | -1 | 81.273 | -10 | | | | | | | | | | |
| 10.5 | 85.052 | 13 | 86.124 | -2 | 81.089 | -8 | | | | | | | | | | |
| 11.5 | 85.247 | 9 | 86.401 | 0 | 80.912 | -2 | | | | | | | 16 380.697 | -7 | | |
| | 85.457 | 15 | 86.681 | 0 | 80.728 | -8 | | | | | 16 386.445 | -5 | 80.520 | -5 | | |
| | 85.654 | 5 | 86.965 | 2 | 80.554 | -7 | | | 16 381.419 | 4 | 86.729 | -2 | 80.350 | 0 | | |
| | 85.864 | 4 | | | 80.383 | -8 | 81.256 | -6 | 85.630 | 6 | 87.013 | -3 | 80.180 | 1 | | |
| | 86.082 | 6 | 87.542 | 1 | 80.215 | -6 | 81.166 | -5 | 85.841 | 4 | | | 80.006 | -7 | | |
| | 86.302 | 5 | 87.838 | 3 | | | 81.079 | -6 | 86.054 | 0 | 87.589 | -8 | | | | |
| | 86.524 | 5 | 88.136 | 2 | | | 80.996 | -6 | 86.278 | 3 | 87.885 | -8 | 79.695 | 4 | 80.785 | -7 |
| | 86.751 | 4 | 88.437 | 0 | | | 80.916 | -7 | 86.499 | -1 | 88.185 | -9 | 79.541 | 5 | 80.709 | -4 |
| | 86.985 | 6 | 88.744 | 1 | 79.592 | -9 | 80.843 | -5 | 86.725 | -4 | 88.492 | -5 | 79.388 | 4 | 80.633 | -4 |
| 20.5 | 87.225 | 11 | 89.053 | -1 | 79.454 | -1 | | | 86.960 | -2 | 88.798 | -7 | 79.237 | -1 | 80.564 | -1 |
| 21.5 | 87.442 | 12 | 89.369 | 1 | 79.312 | -1 | 80.709 | -1 | | | 89.112 | -5 | 79.093 | -1 | | |
| | 87.690 | -7 | 89.687 | 1 | 79.175 | -1 | | | 87 442 | 3 | 89.427 | -6 | 78.951 | -4 | | |
| | 87.939 | -6 | 90.010 | 1 | 79.040 | -2 | | | 8..690 | 8 | 89.750 | -3 | 78.820 | 1 | | |
| | 88.193 | -4 | 90.336 | 1 | 78.915 | 3 | | | | | 90.074 | -2 | 78.680 | -8 | | |
| | 88.449 | -4 | 90.666 | 0 | 78.739 | 2 | | | | | 90.404 | 0 | 78.546 | -15 | | |
| | 88.711 | -1 | 91.001 | 1 | 78.666 | 1 | | | | | 90.735 | -1 | 78.434 | -3 | | |
| | 88.976 | 0 | 91.341 | 2 | 78.554 | 7 | | | | | 91.073 | 2 | 78.318 | 1 | | |
| | 89.245 | 2 | 91.684 | 3 | 78.437 | 3 | | | | | 91.416 | 6 | 78.197 | -5 | | |
| | 89.514 | -1 | 92.027 | 0 | 78.325 | 1 | | | | | 91.753 | 1 | 78.080 | -10 | | |
| 30.5 | 89.791 | 0 | 92.376 | -1 | 78.219 | 0 | | | 89.502 | -1 | 92.104 | 5 | 77.984 | 1 | | |
| 31.5 | 90.070 | 1 | | | 78.116 | 0 | | | 89.781 | 3 | 92.456 | 6 | 77.877 | -2 | | |
| | 90.352 | -1 | | | 78.014 | -5 | | | 90.063 | 6 | 92.813 | 8 | 77.779 | 0 | | |
| | 90.637 | -4 | | | 77.922 | -4 | | | | | | | | | | |
| | 90.932 | 0 | | | 77.836 | 0 | | | 90.628 | 0 | 93.530 | 6 | | | | |
| | 91.229 | 1 | | | 77.749 | -1 | | | 90.919 | 0 | 93.896 | 6 | | | | |
| | 91.529 | 3 | | | 77.669 | 0 | | | 91.217 | 3 | 94.263 | 4 | | | | |
| | 91.831 | 0 | 94.941 | 3 | 77.591 | -1 | | | 91.518 | 5 | 94.639 | 6 | | | | |
| | 92.140 | 2 | 95.321 | 2 | 77.520 | 1 | | | 91.817 | 2 | 95.015 | 4 | | | | |
| | 92.454 | 5 | 95.700 | -4 | 77.453 | 3 | | | 92.124 | 3 | 95.393 | 1 | | | | |
| 40.5 | | | 96.091 | -3 | | | | | 92.434 | 2 | 95.777 | 0 | | | | |
| 41.5 | | | 96.487 | 0 | | | | | 92.745 | -1 | 96.163 | -2 | 77.070 | 12 | | |
| | | | 96.885 | 1 | | | | | 93.065 | 1 | 96.558 | 0 | 77.005 | 7 | | |
| | | | 97.283 | -1 | | | | | 93.380 | -6 | 96.959 | 4 | 76.947 | 6 | | |
| | | | 97.693 | 4 | | | | | 93.708 | -3 | 97.356 | 1 | 76.891 | 2 | | |
| | | | 98.095 | -3 | | | | | | | 97.763 | 4 | 76.843 | 3 | | |
| | 94.740 | 2 | 98.507 | -3 | | | | | 94.374 | 0 | 98.164 | -2 | 76.790 | -6 | | |
| | 95.082 | 1 | 98.924 | -2 | | | | | 94.711 | 0 | 98.576 | -2 | | | | |
| | 95.428 | 1 | 99.345 | -1 | | | | | 95.050 | -3 | 98.990 | -3 | | | | |
| | 95.778 | 0 | 99.769 | -1 | | | | | 95.396 | -1 | 99.409 | -3 | | | | |
| 50.5 | 96.132 | 0 | 400.197 | -1 | | | | | 95.743 | -3 | 99.834 | -1 | | | | |
| 51.5 | 96.490 | -1 | | | | | | | 96.096 | -2 | | | | | | |
| | 96.856 | 3 | | | | | | | 96.454 | 0 | | | | | | |
| | 97.220 | 1 | | | | | | | 96.813 | -1 | | | | | | |
| | 97.591 | 2 | | | | | | | 97.179 | 1 | | | | | | |
| | 97.965 | 2 | | | | | 80.807 | -2 | 97.546 | 1 | | | | | | |
| | 98.340 | -1 | | | | | 80.876 | -6 | 97.918 | 0 | | | | | | |
| | 98.723 | 0 | | | | | 80.954 | -4 | 98.295 | 2 | | | | | | |
| | 99.106 | -3 | | | | | 81.034 | -4 | 98.670 | -1 | | | | | | |
| | 99.496 | -2 | | | | | 81.119 | -2 | 99.053 | -1 | | | | | | |
| 60.5 | 99.888 | -3 | | | | | | | 99.437 | -3 | | | | | | |
| 61.5 | | | | | | | | | 99.830 | -1 | | | | | | |
| | | | | | | | 81.706* | -1 | | | | | | | | |
| | | | | | | | 81.820* | 2 | | | | | | | | |
| | | | | | | | 81.937* | 4 | | | | | | | | |
| | | | | | | | 82.058* | 6 | | | | | | | | |
| | | | | | | | 82.189* | 14 | | | | | | | | |
| 70.5 | | | | | | | 82.305* | 4 | | | | | | | | |
| 71.5 | | | | | | | 82.437* | 6 | | | | | | | | |
| | | | 410.572 | 6 | | | | | | | | | | | | |
| | | | 11.082 | 1 | | | | | | | | | | | | |
| | | | 11.596 | -2 | | | | | | | | | | | | |
| | | | 12.115 | -4 | | | | | | | | | | | | |
| | | | 12.638 | -7 | | | | | | | | | | | | |
| 80.5 | | | | | | | | | | | | | | | | |
| 81.5 | | | | | | | | | | | | | | | | |
| | | | | | | | | | 410.799 | 1 | | | | | | |
| | | | | | | | | | 11.284 | -1 | | | | | | |
| | | | | | | | | | 11.775 | 0 | | | | | | |
| | | | | | | | | | 12.268 | 0 | | | | | | |
| 90.5 | | | | | | | | | 12.766 | 0 | | | | | | |
| 91.5 | | | | | | | | | 13.268 | 2 | | | | | | |

TABLE II (Continued)

| | 2-2 | | | | | | | |
|---|---|---|---|---|---|---|---|---|
| J | $R_1$ | Δν | $R_2$ | Δν | $P_1$ | Δν | $P_2$ | Δν |
| 1.5 | | | | | | | | |
| 10.5 | | | | | | | | |
| | | | 16 386.281 | 1 | | | | |
| | | | 86.559 | -3 | | | | |
| | | | 86.846 | -2 | | | | |
| | 16 385.805 | -2 | | | | | | |
| | 86.028 | -1 | 87.732 | 1 | | | | |
| | 86.257 | 2 | 88.032 | 0 | | | | |
| 20.5 | | | 88.336 | -2 | | | | |
| 21.5 | | | 88.646 | -1 | | | | |
| | | | 88.964 | 5 | | | | |
| | 87.444 | 2 | | | | | | |
| | 87.692 | 2 | | | | | | |
| | 87.946 | 3 | | | | | | |
| | 88.197 | | | | | | | |
| | | | | | 16 377.746 | -3 | | |
| | | | | | 377.636 | 0 | | |
| 30.5 | | | | | 377.522 | 0 | | |
| 31.5 | | | | | 377.417 | -2 | | |
| | 89.534 | 0 | | | 377.320 | 2 | | |
| | 89.817 | 0 | | | 377.220 | 1 | | |
| | 90.099 | 0 | | | 377.124 | -1 | | |
| | | | | | 377.034 | 1 | | |
| | 90.679 | 2 | | | 376.947 | 0 | | |
| | 90.980* | 9 | | | 376.861 | -4 | | |
| | 91.275* | 5 | | | 376.789 | 4 | | |
| | 91.570* | -1 | | | 376.713 | 3 | | |
| 40.5 | 91.881* | 4 | | | 376.639 | 1 | | |
| 41.5 | 92.190* | 4 | | | 376.574* | 3 | | |
| | 92.504* | 5 | | | 376.516* | 9 | | |
| | | | | | 376.453* | 5 | | |
| | | | | | 376.393* | 1 | | |
| | | | | | 376.340* | 1 | | |
| | | | | | 376.290* | -1 | | |
| | | | | | 376.244* | -3 | | |
| | | | | | 376.201* | -5 | | |
| | | | | | 376.161* | -8 | | |
| 50.5 | 95.136* | -2 | | | | | | |
| 51.5 | 95.486* | 1 | | | | | | |
| | 95.832* | -2 | | | | | | |
| | 96.189* | 0 | | | | | | |
| | 96.544* | -2 | | | | | | |
| | 96.905* | -2 | | | | | | |
| | 97.272 | -1 | | | | | | |
| | 97.637 | -4 | | | | | | |
| | 98.009 | -5 | | | | | | |
| | 98.388 | -2 | | | | | | |
| 60.5 | 98.770 | 0 | | | | | | |
| 61.5 | 99.155 | 0 | | | | | | |
| | 99.546 | 5 | | | | | | |
| | 99.936 | 3 | | | | | | |

| | v | $B_v$ | $D_v \times 10^8$ | $A_v$ | $A_{D_v} \times 10^5$ | $p_v$ | $p_{D_v} \times 10^7$ | $q_v \times 10^4$ | $o_v$[a] | $\gamma_v$ | $\gamma_{D_v} \times 10^7$ |
|---|---|---|---|---|---|---|---|---|---|---|---|
| | 2 | 0.09539098(203) | 4.350(38) | | | | | | | -0.069922(62) | 2.58[b] |
| $Ca^{79}Br$ | 1 | 0.09584311(50) | 4.451(13) | | | | | | | -0.069544(42) | 2.56(22) |
| | 0 | 0.09629057(71) | 4.398(15) | | | | | | | -0.068988(38) | 2.58(14) |
| $B^2\Sigma^+$ | | | | | | | | | | | |
| | 2 | 0.09460563(227) | 4.344(44) | | | | | | | -0.069309(62) | 2.40[b] |
| $Ca^{81}Br$ | 1 | 0.09505133(63) | 4.364(17) | | | | | | | -0.068738(65) | 1.64(29) |
| | 0 | 0.09549450(84) | 4.385(18) | | | | | | | -0.068359(37) | 2.40(14) |
| | 1 | 0.09508517(252) | 4.2132(82) | 59.067(1) | -3.646(53) | -0.068379(37) | 1.799(145) | -1.2766(478) | -5.310 | | |
| $Ca^{79}Br$ | 0 | 0.09551790(47) | 4.2142(29) | 59.139(1) | -3.091(15) | -0.067349(31) | 1.552(55) | -1.3189(79) | -5.212 | | |
| $A^2\Pi$ | | | | | | | | | | | |
| | 1 | 0.09429751(238) | 4.1580(81) | 59.065(1) | -3.540(48) | -0.067838(37) | 1.957(155) | -1.2061(453) | -5.311 | | |
| $Ca^{81}Br$ | 0 | 0.09472437(55) | 4.1341(37) | 59.136(1) | -3.002(16) | -0.066815(34) | 1.580(58) | -1.2826(85) | -5.214 | | |
| | 2 | 0.093460329(86) | 4.13247(171) | | | | | | | 0.00295781(56) | |
| $Ca^{79}Br$ | 1 | 0.093861918(19) | 4.13136(38) | | | | | | | 0.00298013(55) | |
| | 0 | 0.094264488(18) | 4.13028(38) | | | | | | | 0.00300355(49) | |
| $X^2\Sigma^+$ | | | | | | | | | | | |
| | 2 | 0.092688896(71) | 4.0670[c] | | | | | | | 0.0029312[c] | |
| $Ca^{81}Br$ | 1 | 0.093085456(25) | 4.06503(52) | | | | | | | 0.00295515(73) | |
| | 0 | 0.093482984(13) | 4.06300(28) | | | | | | | 0.00297907(53) | |

Numbers in parentheses are 1σ uncertainties.

[a] Calculated from unique perturber relationship $o_v = \frac{A_v p_v}{8B_v}$. (Ref. 4)

[b] Fixed at value for v = 0.

[c] Fixed at values linearly extrapolated from v = 0 and 1.

Table III. Spectroscopic Constants of CaBr (in $cm^{-1}$)

$Ca^{79}Br$

| | 0-1 | 1-2 | 1-0 | 2-1 |
|---|---|---|---|---|
| J | $P_1$ | $P_1$ | $R_1$ | $R_1$ |
| 17.5 | | 16 097.423 0 | | 16 668.504 0 |
| | | 97.281 0 | | 68.720 0 |
| | | 97.154 9 | | |
| 20.5 | | 97.001 -1 | | |
| 21.5 | | 96.882 -2 | | 68.938 1 |
| | | 96.757 -4 | | 69.159 0 |
| | | 96.637 -6 | | 69.376 -8 |
| | | | | 69.619 7 |
| | | | | 69.839 -3 |
| | | 96.317 -1 | | 70.075 0 |
| | 16 094.766 0 | 96.217 -2 | | 70.304 -8 |
| | 94.674 0 | 96.116 -8 | | 70.551 -1 |
| | 94.587 0 | 96.036 0 | | 70.802 7 |
| 30.5 | 94.504 -1 | 95.952 1 | | 71.043 2 |
| 31.5 | 94.427 0 | 95.873 1 | | |
| | 94.355 0 | 95.797 -1 | | |
| | 94.288 0 | 95.724 -2 | | |
| | 94.225 1 | 95.663 2 | | |
| | 94.167 0 | 95.603 2 | 16 677.504 -2 | |
| | 94.114 0 | 95.548 4 | 77.849 0 | |
| | 94.066 1 | 95.499 5 | 78.197 0 | |
| | 94.023 1 | 95.448 1 | 78.543 1 | |
| | 93.984 0 | | 78.896 0 | |
| 40.5 | 93.950 0 | | 78.250 -1 | |
| 41.5 | 93.922 1 | | 79.609 1 | |
| | | | 79.970 1 | |
| | | | 80.334 0 | |
| | | | 80.698 -2 | |
| | | | 81.072 1 | |
| 52.5 | 93.928 0 | | | |
| | 93.958 1 | | | |
| | 93.993 1 | | | |
| | 94.032 1 | | | |
| | 94.077 1 | | | |
| | 94.126 1 | | | |
| | 94.180 1 | | | |
| | 94.239 1 | | | 79.474 1 |
| 60.5 | 94.302 0 | | | 79.808 -1 |
| 61.5 | 94.370 1 | | | 80.148 0 |
| | 94.443 0 | | | 80.491 3 |
| | 94.522 -1 | | | 80.831 -2 |
| | 94.605 -1 | | | 80.182 -2 |
| | 94.693 -1 | | | |
| | 94.785 -1 | | | |

Numbers following each line position are obs.-calc. in units of $10^{-3}cm^{-1}$

$Ca^{81}Br$

| | 0-1 | 1-0 | 2-1 |
|---|---|---|---|
| J | $P_1$ | $R_1$ | $R_1$ |
| 39.5 | 16 095.199 -1 | 16 677.621 -1 | |
| 40.5 | 95.167 2 | 77.974 -1 | |
| 41.5 | 95.136 -2 | 79.688 0 | |
| | | 79.049 -1 | |
| | | 79.412 2 | |
| | | 79.782 0 | |
| | | 80.154 2 | |
| | | 80.524 -1 | |
| | | 80.900 2 | |
| 48.5 | | 81.283 2 | |
| 57.5 | | | 16 677.541 1 |
| | | | 77.867 0 |
| | | | 78.198 2 |
| | | | 78.524 -4 |
| 60.5 | | | |
| 61.5 | | | 78.864 0 |
| | | | - |
| | | | 79.543 -1 |
| | | | 79.888 0 |
| | | | 80.236 1 |
| | | | 80.581 -3 |
| | | | 80.940 3 |
| | | | 81.293 1 |

Numbers following each line position are obs.-calc. in units of $10^{-3}cm^{-1}$.



Table IV : Measured Line Positions of $\Delta V \neq 0$ Bands of B $^2\Sigma^+$ - X $^2\Sigma^+$ Transition (in $cm^{-1}$).

## $B^2\Sigma^+ - X^2\Sigma^+$

| | $Ca^{79}Br$ | | $Ca^{81}Br$ | |
|---|---|---|---|---|
| v'-v" | $P_1$ | $P_2$ | $P_1$ | $P_2$ |
| 0-1 | 6 211.830 | 6 210.762 | 6 211.364 | 6 210.308 |
| 1-2 | 6 211.297 | 6 210.204 | 6 210.832 | 6 209.748 |
| 2-3 | 6 210.846 | 6 209.734 | 6 210.390 | 6 209.284 |
| 3-4 | - | 6 209.368 | - | 6 208.910 |
| 0-0 | 6 104.862 | 6 103.246 | 6 104.848 | 6 103.246 |
| 1-1 | 6 104.613 | 6 103.337 | 6 104.593 | 6 103.337 |
| 2-2 | 6 104.820 | 6 103.510 | 6 104.800 | 6 103.510 |
| 3-3 | 6 105.112 | 6 103.777 | 6 105.092 | 6 103.766 |
| 4-4 | 6 105.485 | 6 104.125 | 6 105.460 | 6 104.110 |
| 1-0 | 6 001.133 | 5 999.585 | 6 001.530 | 5 999.996 |
| 2-1 | 6 001.966 | 6 000.370 | 6 002.356 | 6 000.776 |
| 3-2 | - | 6 001.237 | - | 6 001.635 |
| 4-3 | - | 6 001.823 | - | - |

The accuracy of heads is 0.004Å

## $A^2\Pi - X^2\Sigma^+$

### $Ca^{79}Br$

| | $^2\Pi_{1/2}-{}^2\Sigma^+$ | | | $^2\Pi_{3/2}-{}^2\Sigma^+$ | | |
|---|---|---|---|---|---|---|
| v'-v" | $P_{1ee}$ | $Q_{12ef}$ | $P_{12ff}$ | $P_{21ee}$ | $Q_{2ef}$ | $P_{2ff}$ |
| 0-0 | 6 278.057 | 6 278.026 | 6 286.210 | 6 253.208 | 6 253.165 | 6 258.707 |
| 1-1 | 6 277.112 | 6 277.079 | - | 6 252.274 | 6 252.233 | - |

### $Ca^{81}Br$

| | $^2\Pi_{1/2}-{}^2\Sigma^+$ | | | $^2\Pi_{3/2}-{}^2\Sigma^+$ | | |
|---|---|---|---|---|---|---|
| | $P_{1ee}$ | $Q_{12ef}$ | $P_{12ff}$ | $P_{21ee}$ | $Q_{2ef}$ | $P_{2ff}$ |
| 0-0 | 6 278.057 | 6 278.026 | 6 286.138 | 6 253.208 | 6 253.165 | 6 258.653 |
| 1-1 | 6 277.112 | 6 277.079 | - | 6 252.274 | 6 252.233 | - |

The accuracy of heads is 0.004Å.



Table V : Measured CaBr Band Heads (in Å)

| | $B^2\Sigma^+-X^2\Sigma^+$ | | $A^2\Pi-X^2\Sigma^+$ | |
|---|---|---|---|---|
| v'v" | $Ca^{79}Br$ | $Ca^{81}Br$ | $Ca^{79}Br$ | $Ca^{81}Br$ |
| 0-1 | 16 099.066(5) | 16 100.237(2) | | |
| 1-2 | 16 100.533(6) | | | |
| 0-0 | 16 383.114(1) | 16 383.108(1) | 15 959.774(1) | 15 959.770(1) |
| 1-1 | 16 382.901(1) | 16 382.895(1) | 15 962.230(1) | 15 962.213(1) |
| 2-2 | 16 382.462(1) | 16 382.464(1) | | |
| 1-0 | 16 666.956(1) | 16 665.777(2) | | |
| 2-1 | 16 664.835(5) | 16 663.674(2) | | |

Numbers in parentheses are 1σ uncertainties.

Table VI : CaBr Band Origins (in $cm^{-1}$)

| | $X^2\Sigma^+$ | | $A^2\Pi$ | | $B^2\Sigma^+$ | |
|---|---|---|---|---|---|---|
| | $Ca^{79}Br$ | $Ca^{81}Br$ | $Ca^{79}Br$ | $Ca^{81}Br$ | $Ca^{79}Br$ | $Ca^{81}Br$ |
| $T_e$ | 0 | 0 | 15 958.41(10)[c,d] | 15 958.41(10)[c,d] | 16 383.137(6) | 16 383.133(8) |
| $\omega_e$ | 285.7315(92) | 284.5430(135) | 288.56(20)[c,d] | 287.35(20)[c,d] | 285.7465(92) | 284.5491(143) |
| $\omega_e x_e$ | 0.8400(39) | 0.8333(48) | - | - | 0.9540(39) | 0.9428(50) |
| $\omega_e x_e$ (Pekeris) | 0.9480(2) | 0.9315(4) | 1.024(9) | 1.014(14) | 1.046(8) | 1.040(4) |
| $B_e$ | 0.094466141(32) | 0.093682111(68) | 0.0957343(20) | 0.0949378(20) | 0.0965151(20) | 0.0957166(11) |
| $\alpha_e$ | 0.000403551(38) | 0.000398496(80) | 0.0004327(20) | 0.0004269(29) | 0.0004483(15) | 0.0004437(8) |
| $\gamma_e \times 10^7$ | 4.91(38) | 4.84(80) | - | - | - | - |
| $D_e \times 10^8$ | 4.129737(90) | 4.06199(68) | 4.2142(29)[b] | 4.1341(37)[b] | 4.398(15)[b] | 4.385(18)[b] |
| $D_e \times 10^8$ f (calc.) | 4.1271(1) | - | 4.213(3) | - | 4.4013(2) | - |
| $D_e \times 10^8$ (Kratzer) | 4.1303(2) | 4.0619(4) | 4.215(7) | 4.145(6) | 4.4043(6) | 4.3322(4) |
| $\beta_e \times 10^{11}$ | 1.084(76) | 2.03(80) | - | - | - | - |
| $\beta_e \times 10^{11}$ f (calc.) | 1.88(7) | - | 14.4(2) | - | 5.7(1) | - |
| $\gamma_e$ (spin-rotation) | 0.00301484(50) | 0.00299103(116) | - | - | -0.068767(79) | -0.068115(63) |
| $\alpha_\gamma \times 10^4$ a | -0.2289(31) | -0.2392(126) | - | - | -4.84(55) | -4.64(45) |
| $p_e$ | - | - | -0.066834(64) | -0.066304(70) | - | - |
| $\alpha_p$ a | - | - | -0.001030(68) | -0.001023(71) | - | - |
| $A_e$ | - | - | 59.175(1)[d] | 59.172(1)[d] | - | - |
| $\alpha_A$ a | - | - | -0.072(1)[d] | -0.071(1)[d] | - | - |
| $R_e$(Å) | 2.593585(1) | 2.593584(1) | 2.5764(1) | 2.5764(1) | 2.56769(3)[e] | 2.56759(2)[e] |

Numbers in parentheses are 1σ uncertainties.



Table VII. Equilibrium Constants (in $cm^{-1}$)

footnotes for Table VII

[a]Our α's (except $\alpha_e$) are defined by $X_v = X_e + \alpha_X(v + \frac{1}{2})$ with X = γ, p, A.

[b]$D_o$ not $D_e$.

[c]Only 0-0 and 1-1 A-X bands were analyzed so the $\omega_e x_e$ used to obtain $T_e$ and $\omega_e$ came from the Pekeris relationship. This relationship seems to work to about 10% accuracy in the other CaBr states. The uncertainties of $T_e$ and $\omega_e$ reflect this fact.

[d]The o parameter used in our fit is completely correlated with the band origin and the spin-orbit constant. Thus this parameter affects the values of $T_e$, $\omega_e$, $A_e$ and $\alpha_A$ given in this table.

[e]The values for $R_e$ were computed from the $B_e$ values by correcting for $q^\Sigma$. The unique perturber model predicts $q^\Sigma = -q^\Pi$ so $B_e^\Sigma = B_e + q^\Pi$ (4).

$B^2\Sigma^+ - X^2\Sigma^+$

| v' \ v" | 0 | 1 | 2 | 3 | 4 | 5 |
|---|---|---|---|---|---|---|
| 0 | 0.919 | 0.075 | 0.006 | - | - | - |
| 1 | 0.080 | 0.774 | 0.129 | 0.016 | 0.002 | - |
| 2 | 0.001 | 0.148 | 0.652 | 0.167 | 0.030 | 0.004 |
| 3 | - | 0.003 | 0.207 | 0.551 | 0.193 | 0.040 |
| 4 | - | - | 0.006 | 0.257 | 0.466 | 0.208 |
| 5 | - | - | - | 0.009 | 0.300 | 0.395 |

$A^2\Pi - X^2\Sigma^+$

| v' \ v" | 0 | 1 | 2 | 3 | 4 | 5 |
|---|---|---|---|---|---|---|
| 0 | 0.968 | 0.031 | 0.001 | - | - | - |
| 1 | 0.032 | 0.907 | 0.058 | 0.003 | - | - |
| 2 | - | 0.062 | 0.851 | 0.080 | 0.006 | - |
| 3 | - | - | 0.089 | 0.801 | 0.099 | 0.009 |
| 4 | - | - | 0.001 | 0.114 | 0.756 | 0.115 |
| 5 | - | - | - | 0.001 | 0.137 | 0.715 |

Only values greater than 0.001 are listed.

Table VIII : Equilibrium Constants (in $cm^{-1}$)

# THE HYPERFINE STRUCTURE OF THE CALCIUM MONOHALIDES

P. F. Bernath*, B. Pinchemel†, and R. W. Field
Spectroscopy Laboratory and Department of Chemistry
Massachusetts Institute of Technology
Cambridge, Massachusetts 02139

Submitted to the Journal of Chemical Physics November 1, 1980

* Present address: Herzberg Institute for Astrophysics, National Research Council of Canada, Ottawa, CANADA K1A 0R6

† Visiting scientist at MIT from: Laboratoire de Spectroscopie des Molécules Diatomiques, Université des Sciences et Techniques, U.E.R. de Physique Fondamentale, 59655 Villeneuve d'Ascq, FRANCE

19 Pages

2 Figures

4 Tables

ABSTRACT

Intermodulated fluorescence spectra of the $A^2\Pi$-$X^2\Sigma^+$ and $B^2\Sigma^+$-$X^2\Sigma^+$ systems of $Ca^{79}Br$, $Ca^{81}Br$, and CaI have been recorded. $^{79}Br$, $^{81}Br$, and $^{127}I$ magnetic and electric quadrupole hyperfine structure was observed. The following parameters were determined (in MHz, 1σ uncertainties in parentheses):

| | $Ca^{79}Br$ | $Ca^{81}Br$ | CaI |
|---|---|---|---|
| $X^2\Sigma^+$ b | 90 (1) | 98 (1) | 116 (1) |
| $B^2\Sigma^+$ b | 7 (1) | -- | 18 (1) |
| $B^2\Sigma^+$ eQq | <3 | -- | -66 (3) |
| $A^2\Pi$ eQq | 31 (1) | 28 (2) | -55 (1) |

with eQq set equal to zero in all $X^2\Sigma^+$ states. The observed hyperfine structure of CaF, CaCl, CaBr, and CaI may be interpreted in terms of halide orbital polarization rather than ionic-covalent mixing of $M^+X^-$ and MX configurations.

## I. Introduction

The first application of the technique of intermodulated fluorescence spectroscopy (IFS) to a diatomic molecular electronic transition was on isolated lines of the $I_2$ $BO_u^+$-$X^1\Sigma_g^+$ system.[1] Since this initial demonstration, IFS has been applied to such molecules as $NH_2$ [2], $BO_2$ [3], CaCl [4], CaF [5], and VO.[6] We report here some results on the intermodulation spectra of the CaBr and CaI radicals.

Hyperfine structure of the $A^2\Pi$-$X^2\Sigma^+$ and $B^2\Sigma^+$-$X^2\Sigma^+$ transitions has been observed for $^{40}Ca^{79}Br$, $^{40}Ca^{81}Br$, and $^{40}Ca^{127}I$. Hyperfine interactions within the X, A, and B electronic states were fit simultaneously in order to minimize correlations between molecular parameters for upper and lower electronic states. The addition of A-X data to the fit allowed determination of a magnetic hyperfine parameter for the $B^2\Sigma^+$ state of both CaBr and CaI. In this paper, the Frosch and Foley[7] a, b, and c magnetic hyperfine parameters are used.

The alkaline earth monohalides are a family of highly ionic molecules with the special attribute that all but one electron reside in filled shells. Thus it is tempting to interpret all observable properties (electronic energy levels, spin-orbit constants, Λ-doubling and spin-rotation splittings, hfs, and transition intensities) in terms of the properties of the single occupied, open-shell, mostly non-bonding, formally metal-centered orbital. The present hfs results probe the density and the gradient of the density of this metal-centered orbital at the halogen nucleus. Constrained by knowledge of other calcium monohalide molecular parameters, the hfs results permit estimates to be made of $Ca^+$ s/p/d hybridization and $X^-$ s and p polarization.

## II. Experiment

The experimental arrangement was identical to that used for IFS of the

CaF $A^2\Pi$-$X^2\Sigma^+$ system.[5] Calcium, entrained in argon, was reacted in a Broida-type flow system[8] with $CH_3Br$ or $CH_3CH_2I$ to form CaBr or CaI. Typical operating pressures were 0.5 torr Ar to which <1% oxidant was added via a concentric injector, just outside of the calcium oven.

The tunable, 1 MHz bandwidth laser used was a Coherent 699-21 ring dye laser pumped by 6-8 W of 514 nm radiation from a CR 18 argon ion laser. A dye mixture consisting of equal amounts of Rhodamine 101 and 6G covered the 610-650 nm spectral region at output power levels of 100-300 mW. The dye laser output was divided by a beam splitter into two beams of approximately equal intensity. One beam was mechanically chopped at 20 Hz, the other at 1 kHz by a separate chopper. The two counter-propagating beams were directed, unfocussed, through irises and, in a horizontal plane, through the vertical CaX flame. The power density of each beam in the fluorescence excitation and detection region was on the order of 100 mW $cm^{-2}$.

Fluorescence was detected, through 10 nm bandpass interference filter centered at the laser wavelength, by a photomultiplier. The filters partly discriminated against weak chemiluminescence. Scattered laser light plus chemiluminscence amounted to typically 1% of the detected fluorescence intensity. Oxidants were selected to minimize chemiluminescence.

The fluorescence signal was input into two phase sensitive detectors, in series, as described for IFS on CaF.[5] The first (1 kHz) lock-in was operated at 10 ms time constant, the second (20 Hz) at 1s and the resultant IFS signal corresponded to typically 0.1% of the detected fluorescence intensity.

The hyperfine linewidths were 25-40 MHz, due mainly to power broadening. The natural linewidth is about 4 MHz for these molecules[9] and the onset of power broadening, calculated from

$$\frac{\mu E}{h} = (2\pi\tau)^{-1}$$

occurs near 20 mW $cm^{-2}$. At 0.5 torr Ar, pressure broadening probably contributes 10 MHz. Stray magnetic fields from the 30A AC current through the tungsten basket heater situated 6 cm from the fluorescence zone also broaden the IFS lines.

Absolute frequency calibration ($\pm$ 0.003 $cm^{-1}$) was made by simultaneously recording CaX and $I_2$ excitation spectra.[10] A 300 MHz semi-confocal Fabry-Perot etalon provided relative frequency calibration (to $\pm$ 3 MHz for hyperfine components within a rotational line). Rotational assignments were made with reference to previous analyses of CaBr[11] and CaI[12] spectra.

## III. Results

For CaBr, the nuclear spin of $^{79}Br$ or $^{81}Br$ is 3/2, thus 4 strong $\Delta F = \Delta J$ hyperfine lines are expected for each $J \geq 3/2$ rotational line. Figure 1 shows the hfs pattern observed for the $P_{12}$ (64.5) line of the $A^2\Pi$-$X^2\Sigma^+$ 0-0 band. At such high J one would expect 4 equidistant lines if the only significant contribution to hfs were magnetic hyperfine in the $X^2\Sigma^+$ state. The $A^2\Pi$ state should follow Hund's case $a_\beta$ coupling, so its magnetic hfs decreases as 1/J and ought to be negligible[5] at J = 63.5. The Hund's $b_{\beta J}$ coupling[13] of $X^2\Sigma^+$ would result in a constant hfs splitting of b/2 at high J. In fact, the hfs components are not equally spaced; this indicates the presence of electric quadrupole contributions to X and/or A state hfs.

This effect is more pronounced in the CaI $A^2\Pi$-$X^2\Sigma^+$ 0-0 $P_2$ (51.5) line illustrated by Figure 2. The $^{127}I$ nucleus has spin of 5/2, so there are 6 strong hfs lines. However, the electric quadrupole moment of $^{127}I$ is about a factor of two larger and has opposite sign than for $^{79}Br$ and $^{81}Br$.[14] As a result, the hfs of CaI exhibits larger deviations (and in the opposite sense) from equidistant spacing than CaBr.

The spectra of CaBr and CaI are extremely congested due to overlapping sequences and branches and the presence of two approximately equally abundant Br isotopes. This means that, even with sub-Doppler resolution, only a few branches could be examined for hfs. These branches are: $A^2\Pi_{1/2}$-$X^2\Sigma^+$ 0-0 and 1-1 $P_{12}(J)$ ($Ca^{81}Br$, 14 lines; $Ca^{79}Br$, 11 lines; CaI, 9 lines), $A^2\Pi_{3/2}$-$X^2\Sigma^+$ 0-0 and 1-1 $P_2(J)$ ($Ca^{81}Br$, 9 lines; $Ca^{79}Br$, 10 lines; CaI, 9 lines), $B^2\Sigma^+$-$X^2\Sigma^+$ 0-0 and 0-1 $P_1(N)$ ($Ca^{79}Br$, 14 lines; CaI, 5 lines). Table I contains all of the splittings for lines of the A-X and B-X transitions that were examined for hfs in CaBr, while Table II lists the CaI results. The splittings are tabulated as differences between adjacent components, starting from the red and progressing to higher frequency. In the case of the $B^2\Sigma^+$-$X^2\Sigma^+$ $P_1(N")$ branch, the differences D0 to D4 and D$\Sigma$ are:

$$D0 = E'(F'=N"+1) - E'(N"+2) + E"(F"=N"+3) - E"(N"+2) \quad (1a)$$

$$D1 = E'(N") - E'(N"+1) + E"(N"+2) - E"(N"+1) \quad (1b)$$

$$D2 = E'(N"-1) - E'(N") + E"(N"+1) - E"(N") \quad (1c)$$

$$D3 = E'(N"-2) - E'(N"-1) + E"(N") - E"(N"-1) \quad (1d)$$

$$D4 = E'(N"-3) - E'(N"-2) + E"(N"-1) + E"(N"-2) \quad (1e)$$

$$D\Sigma = \Sigma\bar{D}i = E'(F'_{min}) - E'(F'_{max}) + E"(F"_{max}) - E"(F"_{min}) \quad (1f)$$

For the $A^2\Pi$-$X^2\Sigma^+$ transition, the $P_{12}$ ($J" = N" - \frac{1}{2}$) and $P_2(J" = N" - \frac{1}{2})$ branches originate from the f parity component of the $X^2\Sigma^+$ state, so the order of the F quantum numbers is reversed[13]:

$$D0 = E'(F'=N"-4) - E'(N"-3) + E"(F'=N"-2) - E"(N"-3) \quad (2a)$$

$$D1 = E'(N"-3) - E'(N"-2) + E"(N"-1) - E"(N"-2) \quad (2b)$$

$$D2 = E'(N"-2) - E'(N"-1) + E"(N") - E"(N"-1) \quad (2c)$$

$$D3 = E'(N"-1) - E'(N") + E"(N"+1) - E"(N") \quad (2d)$$

$$D4 = E'(N") - E'(N"+1) + E"(N"+2) - E"(N"+1) \quad (2e)$$

$$D\Sigma = E'(F'_{min}) - E'(F'_{max}) + E"(F"_{max}) - E"(F"_{min}) \quad (2f)$$

In taking differences of adjacent hfs components, the extreme red and blue components of a rotational line are used only once. Their measured difference, $D\Sigma$, was included in the fit so that <u>each</u> component would be used twice in the measured differences.

The model used to fit the results is based on the Frosch and Foley[7] Hamiltonian.

$$H_{hfs} = a\Lambda\underset{\sim}{I}\cdot\underset{\sim}{k} + b\underset{\sim}{I}\cdot\underset{\sim}{S} + c(\underset{\sim}{I}\cdot\underset{\sim}{k})(\underset{\sim}{S}\cdot\underset{\sim}{k}) + eQq[3I_z^2-I(I+1)]/4I(2I-1). \qquad (3)$$

In the case of $^2\Sigma$ states, it is possible to derive exact analytical expressions for the hyperfine splittings.[15] For the $X^2\Sigma^+$ state it is necessary to use these expressions since there is a transition from case $b_{\beta S}$ to $b_{\beta J}$ as N increases.[5] The hyperfine Hamiltonian matrix shown in Table III is very similar to Radford's.[15] The off-diagonal electric quadrupole term is too small to affect the energy levels of CaBr and CaI so it has been eliminated. The resultant 2 x 2 matrix is exactly diagonalized and the resultant energy level expressions used without further algebraic simplification.

In the CaBr and CaI $B^2\Sigma^+$ states the spin-rotation constants are much larger than in $X^2\Sigma^+$ (see Table IV). The separation between electron-spin components ($J = N \pm 1/2$) is always at least 10 times larger than hfs splittings and $\Delta J = \pm 1$ interaction terms (case $b_{\beta J}$), thus only the diagonal elements ($\Delta J = 0$) of the hyperfine matrix were used in the least-squares fits.

The $A^2\Pi$ states were assumed to obey $a_\beta$ type coupling, with hyperfine energy levels described by[13]

$$E_{a_\beta}(J,\Omega,\Sigma,F) = [a+(b+c)\Sigma]\Omega C(F,I,J)/2J(J+1) \qquad (4)$$

where $C(F,I,J)$ is defined in Table III. The electric quadrupole hfs is given by

$$W_Q = -eQqY(F,J,I)[1-3\Omega^2/J(J+1)] \qquad (5)$$

where Y(F,J,I) is Casimir's function.[14]

The splittings listed in Tables I and II were input to nonlinear, least-squares fits. All hfs splittings for both A-X and B-X systems were fit simultaneously. Lines from 0-0, 1-1, and 0-1 vibrational bands were included since no vibrational dependence of hfs parameters could be detected at the precision ($\pm$ 3 MHz) of the present IFS spectra. Childs and Goodman[16] found that the magnetic hfs of CaF $X^2\Sigma^+$ decreased by 0.85% as v increased by one. A similar hfs variation for CaBr or CaI would have been undetectable here. The precision of the radiofrequency measurements[17] was 3 x $10^3$ higher than the present IFS results.

In all, the hyperfine Hamiltonian for the X, A, and B states involves 11 independent parameters: b, c, eQq, and $\gamma$ for both the X and B states; a, (b+c) and eQq for the A state. The present data set is inadequate in both precision and extent to determine all 11 parameters. Some of these parameters, such as c in the $B^2\Sigma^+$ state should be undetectably small[5]; others, such as the three eQq parameters should be partly correlated, even if data from more than one branch were available.[18] The contribution of the c parameter to the X and B state hfs varies as $N^{-1}$, and, since low-N data was unobtainable, was fixed at zero in the fits. The a and (b+c) parameters for $A^2\Pi$ were set to zero for the same reason. The correlation of eQq parameters was artificially broken by setting eQq" = 0 for the $X^2\Sigma^+$ states. This means, in effect, that the parameters $\Delta$eQq(A-X) and $\Delta$eQq(B-X) are being determined. The remaining parameters, b in the $^2\Sigma^+$ states and eQq in the $A^2\Pi$ and $B^2\Sigma^+$ states were determined and their values are listed in Table IV. The values of $\gamma$ for the X and B states were fixed at their known values.[11,12] The previously determined CaF[17] and CaCl[19] constants are included for comparison.

As a check of the parameters obtained, the $Ca^{81}Br$ constants can be predicted from those of $Ca^{79}Br$ using the known ratio of nuclear moments.[14] For the $X^2\Sigma^+$ state, the predicted and observed values are 97(1) MHz and 98(1) MHz, respectively. For eQq (actually $\Delta eQq$) of the $A^2\Pi$ state, the predicted and observed $Ca^{81}Br$ values are 26(1) MHz and 28(2) MHz.

## IV. Discussion

In this section, the observed hfs parameters will be used to construct a simple model for the electronic structure of the calcium monohalides. The unique feature of these highly ionic molecules is that, in zeroth order, only one electron resides outside of filled $Ca^+$ and $X^-$ shells. All known CaX electronic transitions correspond to promotions of this electron between nonbonding, metal-centered orbitals. Since virtually all observable properties of CaX molecules should be predominantly determined by the form of the occupied nonbonding orbital, one has an unusual opportunity to characterize such orbitals.

The halide nuclear spin acts as a probe of the size and shape of the unpaired spin-density present at the halide nucleus. The strongest indication that the CaX molecules are nearly perfectly $M^+X^-$ ionic is that the magnitudes of the magnetic hyperfine parameters (b's) are less than 1% of the values calculated for neutral halogen atoms.[20] This is consistent with almost complete localization of the unpaired spin density on the $Ca^+$.

The hfs of such highly ionic molecules can be viewed as arising via two distinct mechanisms: (1) a small amount of covalent character is present by $Ca^+X^- \sim CaX$ configuration interaction, (2) the $X^-$ orbitals are polarized by the unpaired electron on $Ca^+$ (spin-polarization).[21] Mechanism (1) requires net formal electron transfer from $X^-$ to $Ca^+$, while (2) preserves the formally

closed-shell character of $X^-$. A convenient feature of mechanism (2) is that all relevant matrix elements may be estimated using $M^+$ and $X^-$ atomic orbitals. It will be shown that mechanism (2) accounts for the major part of the CaX hfs.

The b parameter (Fermi contact term) is related to the spin-density at the halide nucleus through the equation[7]

$$b = g_I \mu_0 \mu_N \left[ \frac{16\pi}{3} |\psi(0)|^2 - \left\langle \frac{3\cos^2\chi - 1}{r^3} \right\rangle \right] \qquad (6)$$

where $g_I$ is the X nuclear magnetic moment, $\mu_0$ and $\mu_N$ are the electron and nuclear magneton, $\psi(0)$ is the amplitude of the electron spin-density at the X nucleus, r is the $e^-$ to X -nuclear separation, $\chi$ is the angle between $\underset{\sim}{r}$ and the $M^+$-$X^-$ axis, and < > implies expectation value. The first problem is to separate out the $\psi(0)$ part of b. If the c parameter were known

$$c = 3g_I \mu_0 \mu_N \langle (3\cos^2\chi - 1)/r^3 \rangle , \qquad (7a)$$

then one could define

$$b_{iso} = b + c/3, \qquad (7b)$$

where $b_{iso}$ is directly proportional to $|\psi(0)|^2$. For CaF $X^2\Sigma^+$, the known value[16] of c allows calculation of

$$b_{iso} = 121.6 \text{ MHz}.$$

In this case b and $b_{iso}$ differ by only 12%. Fortunately, one expects the c constant to be sufficiently small for all of the CaX molecules that

$$b_{iso} \tilde{\approx} b$$

will give a good approximation to $|\psi(0)|^2$. Table IV lists known values of $b/g_I$ for the X, A, and B states of CaF, $Ca^{35}Cl$, $Ca^{79}Br$, $Ca^{81}Br$, and CaI so that spin-densities may be directly compared. It will be suggested below that the fivefold increase in $|\psi(0)|^2$ for $X^2\Sigma^+$ from CaF to CaI results from mainly the increasing

spin polarization of the halogen, not from an increase in covalent character.

The model used here to explain the magnetic hfs in the $B^2\Sigma^+$ and $X^2\Sigma^+$ states is a generalization of one used by Dagdigian, Cruse, and Zare[9] and by Knight et al.[22] It combines the idea of s/p/d mixing of $Ca^+$ orbitals[9,22] with a (zero free parameter) renormalization effect discussed by Freeman and Watson[21] which mixes in a small amount of $X^-$ ns character into the singly-occupied open-shell molecular orbital.

One starts by writing the CaX molecular orbitals in terms of linear combinations of $Ca^+$ atomic orbitals. The $X^-$ ion provides a ligand field which mixes atomic orbitals of different $n\ell$ values and also splits these orbitals into the $\sigma$, $\pi$,$\delta$ forms appropriate to the $C_{\infty v}$ point group. One obtains for molecular orbital shapes:

$$\psi(B^2\Sigma^+) = e\,|4p\sigma(Ca^+)\rangle - (1-e^2)^{1/2}|3d\sigma(Ca^+)\rangle \qquad (8a)$$

$$\psi(A^2\Pi\ ) = f\,|4p\pi\ Ca^+)\rangle - (1-f^2)^{1/2}|3d^{\pi}(Ca^+)\rangle \qquad (8b)$$

$$\psi(X^2\Sigma^+) = g\,|4s\sigma(Ca^+)\rangle - (1-g^2)^{1/2}|4p\sigma(Ca^+)\rangle\ . \qquad (8c)$$

Note that $4s\sigma$ and $3d\sigma$, respectively, are artificially (but inconsequentially) excluded from B and X state wavefunctions. The e, f, and g mixing coefficients are to be determined from measured molecular parameters such as radiative lifetimes, $\Lambda$-doubling, spin-rotation, spin-orbit, and hfs constants.

It is easy to show that Eq. (8c) is inadequate to explain the magnetic hyperfine structure. Representing each atomic orbital by a single Slater type orbital, with the exponents chosen by Burns' rules,[23] one can calculate $|\psi(r_\chi)|^2$. Burns' rules were formulated to reproduce Hartree-Fock moments of r (orbital shapes) rather than minimize the total orbital energy. Using Eq. 6, the predicted magnetic hfs is more than a factor of 10 too small for all $X^2\Sigma^+$ states.

Following Freeman and Watson[21], the molecular wavefunctions are now augmented by a small amount of ns halide character $-(S+\lambda)|nsX^-\rangle$. Although Freeman and Watson show that halide orbitals in addition to the valence halide orbitals should be included, for simplicity inner orbital contributions will be neglected. The coefficient $\lambda$ is interpreted as a covalency parameter while S is a measure of halide spin-orbital polarization. The S contribution can be considered to originate solely from the non-orthogonality of the atomic $Ca^+$ and $X^-$ basis orbitals. A reasonable estimate for S is thus the orbital overlap integral between the $Ca^+$ and $X^-$ basis functions.[21] Orbital overlap integrals for Slater-type functions are tabulated.[24] Burns' rules[23] were used to determine the orbital exponents for the single-$\zeta$ , Slater-type basis functions for valence $Ca^+$ and $X^-$ orbitals.

The covalency parameter $\lambda$ must also be estimated. It is reasonable to set $\lambda = 0$ for the entire CaX series. This may seem surprising in reference to the traditional ionicity index,[25] $R_e/R_x$. $R_e$ and $R_x$ are, respectively, the equilibrium internuclear distance and the hypothetical internuclear distance at which the bound ionic potential curve crosses the non-bonding neutral curve. When $1.5 < R_e/R_x < 2$, as it is only for CaI (1.67), bonding is expected to be mostly ionic, but with some covalent character.

The following facts suggest that $\lambda$ is negligibly small, even for CaI: (1) The Rittner ionic model[26] accurately reproduces the $X^2\Sigma^+$ state dissociation energies[27] of the calcium monohalides. (2) The spin-orbit constant, A, of $A^2\Pi$ changes monotonically from 71.45 $cm^{-1}$ in CaF[28] to 45.8 $cm^{-1}$ for CaI[12] (These A-values are corrected using unique perturber estimates of the $o$ parameter.[29] Without this correction, A ranges from 72.60 $cm^{-1}$ for CaF to 60.12 $cm^{-1}$ for CaI.) About half of the change in A can be accounted for by the increasing d-character

(F→I) of the molecular orbital. The remainder is consistent with $\lambda \tilde{\sim} 0.05$ (about 0.25% covalent character), a value that is nearly independent of halide. This argument depends on the assumption that the X, A, and B states all have similar $\lambda$-values. The small differences in $R_e$ and $\omega_e$ values between these states[28] supports this assumption. (3) The conventional correlation between ionicity and electronegativity differences (p. 582, Ref. 14) suggests 11% covalent character ($\lambda \tilde{\sim} 0.33$) for the CaI $X^2\Sigma^+$ state. This would imply, if $\lambda$ were identical for the $A^2\Pi$ state, a spin-orbit constant $A = -500\ cm^{-1}$!

The above arguments demonstrate that $\lambda$ is small. It will now be shown that even a small value of $\lambda$ leads to contradictory interpretations of the magnetic and electric quadrupole hfs. The decrease, by almost an order of magnitude, of the magnetic hyperfine b parameter from the $X^2\Sigma^+$ to the $B^2\Sigma^+$ state of CaBr, would normally be explained by a <u>decrease</u> in $\lambda$. In contrast, the value of eQq is the same in the B and X states of CaBr and actually larger in absolute magnitude in the B vs. X state of CaI, thus suggesting[14] either no change or an <u>increase</u> in $\lambda$. The simplest way out of this quandary is to set $\lambda = 0$ and attempt to explain the hfs entirely by spin-polarization.

It is not surprising that the usual correlation[14] between eQq and the $\lambda$ ionicity parameter breaks down for the alkaline earth monohalides. These molecules are unique in that they have an odd total number of electrons and that the odd electron is located predominantly on the nucleus without spin. This means that hfs is determined by a delicate balance of weakly-sampled large effects, in contrast to the more usual situation when valence orbitals all contain an even number of electrons or the odd electron is formally associated with the $I > 1/2$ nucleus.

The first step in explaining the hfs in terms of the spin-polarization model

is to use the magnetic hfs to obtain an estimate of S, the overlap integral of the unique $Ca^+$ centered orbital with one of the filled-shell $X^-$ orbitals. Eqs. (6), (8), and the suggested[21] admixed $-S|nsX^-\rangle$ ns halide character lead to

$$b/g_I \doteq 800\ S^2|\phi_{nsX^-}(0)|^2 \qquad (9)$$

where $|\phi_{nsX^-}(0)|^2$ is the charge density (in atomic units) of the halide ns-orbital at the halide nucleus and $b/g_I$ is in MHz. The overlap integrals, S, for the $X^2\Sigma^+$ and $B^2\Sigma^+$ states are:

$$S_X = gS[4s\sigma(Ca^+),ns\sigma(X^-)] - (1-g^2)^{1/2}S[4p\sigma(Ca^+),ns\sigma(X^-)] \qquad (10a)$$

$$S_B = eS[4p\sigma(Ca^+),ns\sigma(X^-)] - (1-e^2)^{1/2}S[3d\sigma(Ca^+),ns\sigma(X^-)]. \qquad (10b)$$

Values of $|\phi_{nsX^-}(0)|^2$ were taken from Hartree-Fock calculations of Froese-Fischer[30] (on neutral atoms). Equations 10 were then solved for the mixing coefficients, g and e, using overlap integrals between $Ca^+$ and $X^-$ atomic orbitals for which Burns' rule $\zeta$-values were selected. The mixing fractions obtained are listed in Table V.

The magnetic hfs of the $X^2\Sigma^+$ state for the CaX molecules suggests that 25-35% $4p\sigma$ $(Ca^+)$ character is admixed with $4s\sigma$ $(Ca^+)$ into the lowest energy CaX molecular orbital. This conclusion is qualitatively supported by population analyses of two independent Hartree-Fock calculations which give 13%[16] and 18%[31] $4p\sigma$ character for the $X^2\Sigma^+$ state of CaF. Knight et al.[22] made similar s/p mixing conclusions for the $X^2\Sigma^+$ states of SrF and BaF. This latter result, however, was obtained from magnetic hfs associated with the $^{87}Sr$ and $^{137}Ba$ nuclei.

The CaBr and CaI $B^2\Sigma^+$ state mixing fractions (65-55% $4p\sigma$, 35-45% $3d\sigma$) are consistent with an independent estimate[32] of $e^2$, based on radiative lifetime data,[9] $\Lambda$-doubling of the $A^2\Pi$ state, and the spin-rotation constant of the $B^2\Sigma^+$ state.

Hartree-Fock calculations for CaF $B^2\Sigma^+$ give 38% 4pσ, 54% 3dσ[17] or 45% 4pσ, 48% 3dσ.[31] The Hartree-Fock calculations also indicate that the $B^2\Sigma^+$ state contains less than 7% 4sσ and the $X^2\Sigma^+$ state has less than 3% 3dσ, justifying their exclusion from equations 8a, c.

The smaller magnetic hfs in the B than X states is explained by a simple cancellation effect. The 4pσ and 3dσ mixing coefficients are nearly equal in magnitude but opposite in sign, thus the p and d oribtal contributions to the hfs almost cancel. This is reasonable since the 4dσ orbital has a lobe that points directly at the halide, so it should be more heavily mixed. The negative signs for the mixing coefficients in Eqs. (8) are essential to enable the non-bonding $Ca^+$ orbital to distort so that it avoids the negatively charged $X^-$. The increase in spin density at the halide nucleus in the $X^2\Sigma^+$ states of the CaF to CaI series is due to an increase in the atomic orbital density $|\phi_{nsX^-}(0)|^2$ (from 11.4 a.u. for F to 22.9 for I[30]) and an increase in the overlap integral [from $S(4s\sigma(Ca^+), 2s\sigma(F^-)) = 0.219$ to $S(4s\sigma(Ca^+), 5s\sigma(I^-)) = 0.352$].

Additional support for this interpretation comes from comparison with CaF, SrF, and BaF, where there is no question of covalent mixing. In this series, $b/g_I$ is 20, 18, and 11 MHz.[22] The decrease in spin-density from CaF to BaF is caused by decreasing spin-polarization as measured by the metal-halide overlap integral [$S(5s\sigma(Sr^+), 2s\sigma(F^-)) = 0.113$ and $S(6s\sigma(Ba^+), 2s\sigma(F^-)) = 0.039$]. The calculated mixing fractions for the $X^2\Sigma^+$ states are 37% admixed 5pσ for SrF and only 4% 6pσ admixed for BaF. It seems likely that the small admixture of 6pσ in BaF is a reflection of inability to calculate the small overlap integral accurately rather than a dramatic increase in the orbital purity of the ground state.

The electric quadrupole hyperfine structure can be rationalized similarly. The model is expected to work less well, however, since eQq values depend on the gradient of the charge density at the nucleus rather than simply on its magnitude.

It is the distortion of np halide orbitals by the presence of the unpaired $Ca^+$ electron that is important. Calculation of overlap integrals demonstrates that $4p\pi$ and $3d\pi$ $Ca^+$ orbitals have much greater overlap with halide np orbitals than $4s\sigma$, $4p\sigma$, or $3d\sigma$ $Ca^+$ orbitals. Thus, this qualitative picture predicts eQq for the $A^2\Pi$ state should have a larger absolute value than those for $X^2\Sigma^+$ and $B^2\Sigma^+$. This is the case for CaBr and CaI (Table IV).

It is clear, however, that the model gives an unsatisfactory explanation of the electric quadrupole hfs except for possibly the ground $X^2\Sigma^+$ state. The $X^2\Sigma^+$ state is a reasonably pure $4s\sigma$ state. Using the mixing coefficients from the magnetic hfs, overlap integrals calculated as described above and $eQq_{n\ell m}$ values (p. 579, Ref. 14) for $\ell = 1$, $m = 0$, the eQq" values are predicted to be 2 MHz for CaCl, 10 MHz for CaBr and -150 MHz for CaI. Calculations using this simple model for the excited states predict very small eQq ($\sim$ 1 MHz) for both $A^2\Pi$ and $B^2\Sigma^+$ states of CaBr,mainly due to cancellation by 4p and 3d terms. These estimates are at variance with experimental $\Delta eQq$ values of Table IV.

The size of $\Delta eQq(B-X)$ in CaBr and CaI is particularly puzzling. For CaBr, the eQq value of the B state is identical, within experimental error,to that of the ground state. In CaI, however, eQq of the B state is almost the same as that of the $A^2\Pi$ state. We can offer no reasonable explanation for this behaviour. More sophisticated calculations are required to explain the electric quadrupole hfs for the excited states of the calcium halides.

## V. Conclusion

The intermodulated fluorescence spectra of CaBr and CaI have provided some insight into the electronic structure of the calcium monohalide radicals. The data suggest that bonding is completely ionic for the CaX series. A simple model built from a small number of atomic orbitals has provided an explanation for the

magnetic hyperfine structure. It is hoped that this work will encourage more accurate determinations of hyperfine structure in these molecules (particularly the Frosch and Foley[7] c parameters and eQq for the $X^2\Sigma^+$ states) by radiofrequency methods.[17] Accurate molecular calculations of electronic properties of the alkaline earth halides would also be valuable. The hyperfine structure serves as a useful test of computed molecular wavefunctions.

Acknowledgment

P.F.B. was supported, in part, by a Natural Sciences and Engineering Research Council of Canada postgraduate fellowship. This research was supported by the following grants: AFOSR-76-3056, NSF CHE-78-18427, NSF CHE-78-10178, and NATO 1177.

References


1. M.S. Sorem and A.L. Schawlow, Opt. Commun. 5, 148 (1972).

2. A. Muirhead, K.V.L.N. Sastry, R.F. Curl, Jr., J. Cook, and F.K. Tittel, Chem. Phys. Lett. 24, 208 (1974).

3. R.S. Lowe, H. Gerhardt, W. Dillenschneider, R.F. Curl, Jr., and F.K. Tittel, J. Chem. Phys. 70, 42 (1979).

4. J.M. Brown, H. Martin,and F.D. Wayne, Chem. Phys. Lett. 55, 67 (1978).

5. P.F. Bernath, P.G. Cummins,and R.W. Field, Chem. Phys. Lett. 70, 618 (1980).

6. A.S-C. Cheung, R.C. Hansen, A.M. Lyyra,and A.J. Merer, private communication.

7. R.A. Frosch and H.M. Foley, Phys. Rev. 88, 1337 (1952).

8. J.B. West, R.S. Bradford, J.D. Eversole,and C.R. Jones, Rev. Sci. Instr. 46, 164 (1975).

9. P.J. Dagdigian, H.W. Cruse,and R.N. Zare, J. Chem. Phys. 60, 2330 (1974).

10. S. Gerstenkorn and P. Luc, Atlas du spectre d'absorption de la molecule d'iode (CNRS, Paris, 1978).

11. P.F. Bernath, R.W. Field, B. Pinchemel, Y. Lefebvre,and J. Schamps, unpublished work.

12. D.E. Reisner, P.F. Bernath,and R.W. Field, unpublished results.

13. T.M. Dunn in Molecular Spectroscopy: Modern Research ed. K.N. Rao and C.W. Mathews (Academic Press, N.Y. 1972). p. 231.

14. W. Gordy and R.L. Cook, Microwave Molecular Spectra part II of Chemical Application of Spectroscopy ed. W. West (Wiley, N.Y., 1970).

15. H.E. Radford, Phys. Rev. 136, 1571 (1964). Note there are several factor of 2 errors in his expression for hfs in $^2\Sigma$ states. Those relevant to this paper are:the definition of q should have (3 cos $^2\chi_i$-1)/2 and $W_Q$ should have a term 3C(C+1)/4.

16. W.J. Childs, G.L. Goodman,and L.S. Goodman, J. Mol. Spectrosc. 00, 000 (1981).

17. W.J. Childs and L.S. Goodman, Phys. Rev. Lett. 44, 316 (1980).

18. A. Yokozeki and J.S. Muenter, J. Chem. Phys. 72, 3796 (1980).

19. J.V. Martinez de Pinillos and W. Weltner, Jr., J. Chem. Phys. 65, 4256 (1976).

20. P.B. Ayscough, Electron Spin Resonance in Chemistry (Methuen,London,1967) p. 438.

21. A.J. Freeman and R.E. Watson, Phys. Rev. Lett. 6, 343 (1961).

22. L.B. Knight, Jr., W.C. Easley, W. Weltner, Jr., and M. Wilson, J. Chem. Phys. 54, 322 (1971).

23. G. Burns, J. Chem. Phys. 41, 1521 (1964).

24. E.A. Boudreaux, L.C. Cusachs and L. Dureaux, Numerical Tables of Two-Centre Overlap Integrals (Benjamin, N.Y., 1970).

25. G. Herzberg, Spectra of Diatomic Molecules (Van Nostrand, Princeton, N.J., 1950) p. 374.

26. E.S. Rittner, J. Chem. Phys. 19, 1030 (1951).

27. P.D. Kleinschmidt and D.L. Hildenbrand, J. Chem. Phys. 68, 2819 (1978).

28. P.F. Bernath and R.W. Field, J.Mol. Spectrosc. 82, 339 (1980).

29. R.N. Zare, A.L. Schmeltekopf, W.J. Harrop, and D.L. Albritton, J. Mol. Spectrosc. 46, 37 (1973).

30. C. Froese-Fischer, Atomic Data 4, 301 (1972).

31. B. Pouilly and J. Schamps, private communication.

32. P. Bernath, Ph.D. thesis 1980.

Table IA.

$B^2\Sigma^+$-$X^2\Sigma^+$ $Ca^{79}Br$ Hyperfine Splittings (in MHz)[a]

| Band | Assignment | D1 | D2 | D3 | DΣ |
|---|---|---|---|---|---|
| 0-1 | $P_1(25)$ | 41(0) | 44(-3) | 41(1) | 126(-2) |
| 0-1 | $P_1(27)$ | 41(0) | 41(0) | 39(3) | 121(3) |
| 0-1 | $P_1(28)$ | 42(-1) | 41(0) | 39(3) | 122(2) |
| 0-1 | $P_1(32)$ | 39(2) | 46(-4) | 42(0) | 127(-2) |
| 0-1 | $P_1(33)$ | 42(-1) | 43(-1) | 39(3) | 124(1) |
| 0-1 | $P_1(34)$ | 43(-2) | 40(2) | 43(-1) | 126(-1) |
| 0-1 | $P_1(35)$ | 43(-2) | 42(0) | 43(-1) | 128(-3) |
| 0-1 | $P_1(58)$ | 43(-2) | 40(2) | 44(-2) | 127(-2) |
| 0-1 | $P_1(59)$ | 42(-1) | 43(-1) | 40(2) | 125(0) |
| 0-1 | $P_1(60)$ | 42(-1) | 43(-1) | 43(-1) | 128(-3) |
| 0-1 | $P_1(61)$ | 44(-3) | 40(2) | 40(2) | 124(-1) |
| 0-1 | $P_1(65)$ | 40(2) | 41(1) | 42(0) | 123(3) |
| 0-1 | $P_1(66)$ | 40(2) | 41(1) | 39(3) | 120(6) |
| 0-1 | $P_1(68)$ | 42(0) | 45(-3) | 38(4) | 125(1) |
| | $A^2\Pi_{1/2}$-$X^2\Sigma^+$ $Ca^{79}Br$ | | | | |
| 0-0 | $P_{12}(5.5)$ | 50(-3) | 48(1) | 31(-5) | 129(-7) |
| 0-0 | $P_{12}(7.5)$ | 54(1) | 47(1) | 30(-6) | 131(-4) |
| 0-0 | $P_{12}(9.5)$ | 52(-1) | 44(-2) | 34(-3) | 130(-6) |
| 1-1 | $P_{12}(15.5)$ | 54(1) | 41(-5) | 35(-2) | 130(-6) |
| 0-0 | $P_{12}(18.5)$ | 52(-1) | 46(1) | 33(-4) | 131(-4) |
| 0-0 | $P_{12}(24.5)$ | 49(-4) | 45(0) | 34(-3) | 128(-7) |
| 0-0 | $P_{12}(25.5)$ | 55(2) | 47(2) | 41(4) | 143(8) |
| 1-1 | $P_{12}(27.5)$ | 50(-3) | 41(-4) | 36(-1) | 127(-8) |
| 0-0 | $P_{12}(59.5)$ | 51(-2) | 46(1) | 36(-1) | 133(-2) |
| 0-0 | $P_{12}(63.5)$ | 52(-1) | 45(0) | 39(2) | 136(1) |
| 0-0 | $P_{12}(69.5)$ | 48(-5) | 44(-1) | 35(-2) | 127(-8) |

Table IA (Continued)

$A^2\Pi_{3/2}$-$X^2\Sigma^+$ $Ca^{79}Br$

| Band | Assignment | D1 | D2 | D3 | DΣ |
|---|---|---|---|---|---|
| 0-0 | $P_2(13.5)$ | 52(0) | 45(-1) | 37(0) | 134(-1) |
| 0-0 | $P_2(18.5)$ | 53(0) | 45(0) | 34(-3) | 132(-3) |
| 0-0 | $P_2(24.5)$ | 53(0) | 49(4) | 38(1) | 140(5) |
| 0-0 | $P_2(25.5)$ | 53(0) | 49(4) | 36(-1) | 138(3) |
| 0-0 | $P_2(34.5)$ | 53(0) | 50(5) | 44(7) | 147(12) |
| 0-0 | $P_2(46.5)$ | 54(1) | 43(-2) | 38(1) | 135(-1) |
| 0-0 | $P_2(58.5)$ | 58(5) | 50(5) | 37(0) | 145(10) |
| 0-0 | $P_2(59.5)$ | 56(3) | 43(-2) | 42(5) | 141(6) |
| 0-0 | $P_2(76.5)$ | 50(-3) | 47(2) | 40(3) | 137(2) |
| 0-0 | $P_2(77.5)$ | 51(-2) | 49(4) | 41(4) | 141(6) |

[a]Obs-calc in parentheses.

Table IB.

$A^2\Pi_{1/2}$-$X^2\Sigma^+$ $Ca^{81}Br$ Hyperfine Splittings

| Band | Assignment | D1 | D2 | D3 | DΣ |
|---|---|---|---|---|---|
| 0-0 | $P_{12}(3.5)$ | 57(0) | 47(-2) | 39(2) | 143(0) |
| 0-0 | $P_{12}(4.5)$ | 57(-1) | 47(-3) | 38(-1) | 142(-5) |
| 0-0 | $P_{12}(5.5)$ | 57(-1) | 58(8) | 33(-7) | 142(0) |
| 0-0 | $P_{12}(7.5)$ | 62(5) | 48(-2) | 31(-10) | 153(13) |
| 0-0 | $P_{12}(9.5)$ | 62(5) | 49(-1) | 36(-5) | 147(-1) |
| 0-0 | $P_{12}(12.5)$ | 55(-2) | 52(2) | 40(-1) | 147(-1) |
| 1-1 | $P_{12}(15.5)$ | 56(-1) | 48(-2) | 38(-3) | 142(-6) |
| 0-0 | $P_{12}(18.5)$ | 56(0) | 51(1) | 41(-1) | 148(0) |
| 0-0 | $P_{12}(24.5)$ | 51(-5) | 48(-2) | 42(0) | 141(-7) |
| 0-0 | $P_{12}(25.5)$ | 57(1) | 49(0) | 42(0) | 148(1) |
| 1-1 | $P_{12}(27.5)$ | 55(-1) | 45(-4) | 40(-2) | 140(-7) |
| 0-0 | $P_{12}(64.5)$ | 56(0) | 49(0) | 43(1) | 148(1) |
| 0-0 | $P_{12}(70.5)$ | 56(0) | 48(-1) | 41(-1) | 145(-2) |
| 0-0 | $O_{12}(84.5)$ | 57(1) | 53(4) | 42(0) | 152(5) |
| | $A^2\Pi_{3/2}$-$X^2\Sigma^+$ $Ca^{81}Br$ | | | | |
| 0-0 | $P_2(13.5)$ | 60(4) | 47(-3) | 43(1) | 150(2) |
| 0-0 | $P_2(24.5)$ | 60(4) | 50(1) | 43(1) | 153(6) |
| 0-0 | $P_2(34.5)$ | 56(0) | 48(-1) | 45(3) | 149(2) |
| 0-0 | $P_2(47.5)$ | 56(0) | 51(2) | 49(7) | 156(9) |
| 0-0 | $P_2(48.5)$ | 54(-2) | 48(-1) | 44(2) | 146(-1) |
| 0-0 | $P_2(59.5)$ | 56(0) | 49(0) | 44(2) | 149(2) |
| 0-0 | $P_2(60.5)$ | 55(-1) | 49(0) | 43(1) | 147(0) |
| 0-0 | $P_2(77.5)$ | 53(-3) | 51(2) | 49(7) | 153(6) |
| 0-0 | $P_2(78.5)$ | 57(1) | 50(1) | 42(0) | 149(2) |

Table II.

CaI $B^2\Sigma^+$-$X^2\Sigma^+$ Hyperfine Splittings[a]

| Band | Assignment | D0 | D1 | D2 | D3 | D4 | DΣ |
|---|---|---|---|---|---|---|---|
| 0-1 | $P_1(24)$ | 41(-2) | 44(1) | 49(1) | 55(-1) | 49(-1) | 238(-2) |
| 0-1 | $P_1(53)$ | 40(-1) | 44(0) | 52(-3) | 53(1) | 57(1) | 246(-2) |
| 0-1 | $P_1(54)$ | 42(-4) | 44(0) | 48(1) | 54(0) | 57(1) | 245(-2) |
| 0-0 | $P_1(62)$ | 39(0) | 44(0) | 48(1) | 53(1) | 59(-1) | 243(1) |
| 0-0 | $P_1(65)$ | 42(-3) | 46(-2) | 49(0) | 59(-5) | 65(-7) | 261(-17) |
| $A^2\Pi_{1/2}$-$X^2\Sigma^+$ | | | | | | | |
| 0-0 | $P_{12}(15.5)$ | 52(4) | 58(-4) | 55(-2) | 61(-1) | 66(-2) | 292(-5) |
| 0-0 | $P_{12}(17.5)$ | 49(-1) | 56(4) | 51(-6) | 66(4) | 66(-2) | 288(-1) |
| 0-0 | $P_{12}(26.5)$ | 48(-1) | 54(1) | 57(0) | 63(1) | 65(-3) | 287(-2) |
| 0-0 | $P_{12}(27.5)$ | 48(-1) | 53(0) | 59(2) | 62(0) | 65(-3) | 287(-2) |
| 0-0 | $P_{12}(46.5)$ | 48(1) | 51(-3) | 59(-2) | 64(-1) | 69(2) | 291(-3) |
| 0-0 | $P_{12}(51.5)$ | 46(-3) | 50(-3) | 58(0) | 57(-5) | 68(1) | 279(-10) |
| 0-0 | $P_{12}(56.5)$ | 48(-1) | 52(-1) | 56(-2) | 61(-1) | 68(1) | 285(-4) |
| 0-0 | $P_{12}(58.5)$ | 49(0) | 49(-4) | 57(-1) | 61(-1) | 66(-1) | 282(-7) |
| 0-0 | $P_{12}(61.5)$ | 52(3) | 58(5) | 60(2) | 60(-2) | 78(11) | 308(19) |
| $A^2\Pi_{3/2}$-$X^2\Sigma^+$ | | | | | | | |
| 0-0 | $P_2(8.5)$ | 49(2) | 49(2) | 59(3) | 63(2) | 64(-4) | 284(5) |
| 0-0 | $P_2(9.5)$ | 50(3) | 52(1) | 58(2) | 63(2) | 69(1) | 292(9) |
| 0-0 | $P_2(19.5)$ | 56(8) | 53(1) | 58(1) | 65(3) | 66(-2) | 298(11) |
| 0-0 | $P_2(30.5)$ | 55(7) | 48(-5) | 59(2) | 63(1) | 68(1) | 293(6) |
| 1-1 | $P_2(38.5)$ | 47(-2) | 53(0) | 58(1) | 61(-1) | 67(0) | 286(-2) |
| 0-0 | $P_2(40.5)$ | 46(-3) | 56(3) | 57(0) | 61(-1) | 68(1) | 288(0) |
| 0-0 | $P_2(51.5)$ | 48(-1) | 56(3) | 58(1) | 63(1) | 69(2) | 294(6) |
| 0-0 | $P_2(55.5)$ | 44(-5) | 53(0) | 57(-1) | 62(0) | 65(-2) | 281(-8) |
| 1-1 | $P_2(68.5)$ | 49(1) | 50(-3) | 58(0) | 62(0) | 70(3) | 289(1) |

[a]. Obs.-calc. in parentheses.

Table III.

Hyperfine Hamiltonian for the $F_1(e)$ and $F_2(f)$ Components of a Given N of a $^2\Sigma^+$ State.

| | $e\ (J = N + \frac{1}{2})$ | $f\ (J = N - \frac{1}{2})$ |
|---|---|---|
| e | $\left[b + \frac{c}{2N+3}\right] \frac{C(F,I,J)}{2(2N+1)}$ $+ W_Q + \frac{\gamma N}{2}$ | $\left[b + \frac{c}{2}\right] \frac{E(F,I,N)}{2(2N+1)}$ |
| f | sym | $\left[-b + \frac{c}{2N-1}\right] \frac{C(F,I,J)}{2(2N+1)}$ $+ W_Q - \frac{\gamma(N+1)}{2}$ |

$$C(F,I,J) = F(F+1) - I(I+1) - J(J+1)$$

$$E(F,I,N) = [(F+N-I+1/2)(F-N+I+1/2)(F+N+I+3/2)(-F+N+I+1/2)]^{1/2}$$

$$W_Q = -eQq\frac{[3C(C+1)/4 - I(I+1)J(J+1)]}{8I(2I-1)J(J+1)}$$

Table IV.

Fine and Hyperfine Structure of Calcium Halides for v = 0 (in MHz)

| | | $CaF^a$ | $Ca^{35}Cl$ | $Ca^{79}Br$ | $Ca^{81}Br$ | CaI |
|---|---|---|---|---|---|---|
| $X^2\Sigma^+$ | $\gamma$ | 39.505 | 41(2)[b] | 90.1[e] | 89.4[e] | 168(1)[f] |
| | b | 108.491 | 30[c] | 90(1) | 98(1) | 116(1) |
| | c | 39.476 | --- | ---[d] | ---[d] | ---[d] |
| | $b/g_I$ | 20.635 | 55 | 64(1) | 65(1) | 103(1) |
| $B^2\Sigma^+$ | $\gamma$ | -1374(1)[g] | -1965(2)[h] | -2069(1)[e] | -2052(1)[e] | -4202(10)[f] |
| | b | --- | --- | 7(1) | --- | 18(1) |
| | $eQq^i$ | --- | --- | 0(<3MHz) | --- | -66(3) |
| | $b/g_I$ | --- | --- | 5(1) | --- | 16(1) |
| $A^2\Pi$ | $eQq^i$ | --- | --- | 31(1) | 28(2) | -55(1) |

a. Ref. 16. One $\sigma$ uncertainties in parentheses.

b. P.J. Domaille, T.C. Steimle, and D.O. Harris, J. Mol. Spectrosc. 66, 503 (1977).

c. Ref. 19.

d. Set to zero in the fits.

e. Ref. 11.

f. Ref. 12.

g. M. Dulick, P.F. Bernath and R.W. Field, Can. J. Phys. 58, 703 (1980).

h. L.E. Berg, L. Klynning, and H. Martin, Physica Scripta,to be published.

i. "eQq" of $X^2\Sigma^+$ set to zero in the fits. Constants given are actually $\Delta eQq(B-X)$ and $\Delta eQq(A-X)$.

Table V.

Mixing Fractions from Magnetic hfs

| | CaF | CaCl | CaBr | CaI |
|---|---|---|---|---|
| $g^2(X^2\Sigma^+)^a$ | 0.65 | 0.75 | 0.77 | 0.76 |
| $e^2(B^2\Sigma^+)^b$ | - | - | 0.66 | 0.55 |

a. $g^2$ is fractional $4s\sigma$ character in $X^2\Sigma^+$; $(1-g^2)$ is $4p\sigma$.

b. $e^2$ is fractional $4p\sigma$ character in $B^2\Sigma^+$; $(1-e^2)$ is $3d\sigma$.

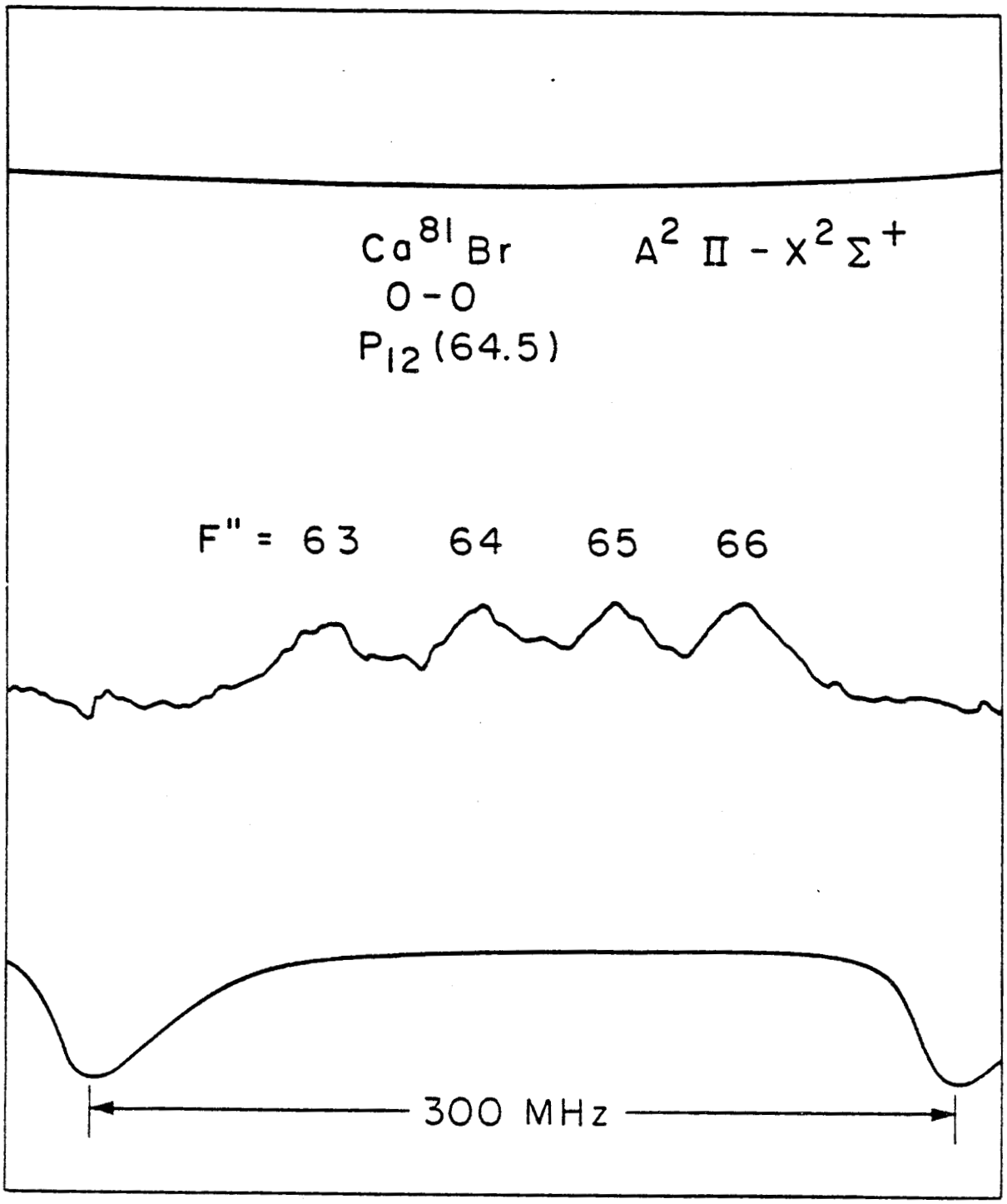


Figure 1. Intermodulated Fluorescence Spectrum of the $Ca^{81}Br$ $A^2\Pi$-$X^2\Sigma^+$ 0-0 $P_{12}$ (64.5) line. Top trace is part of the Doppler-broadened line, middle trace is the Doppler-Free Spectrum, and bottom trace shows frequency markers from a 300 MHz Fabry-Perot interferometer.

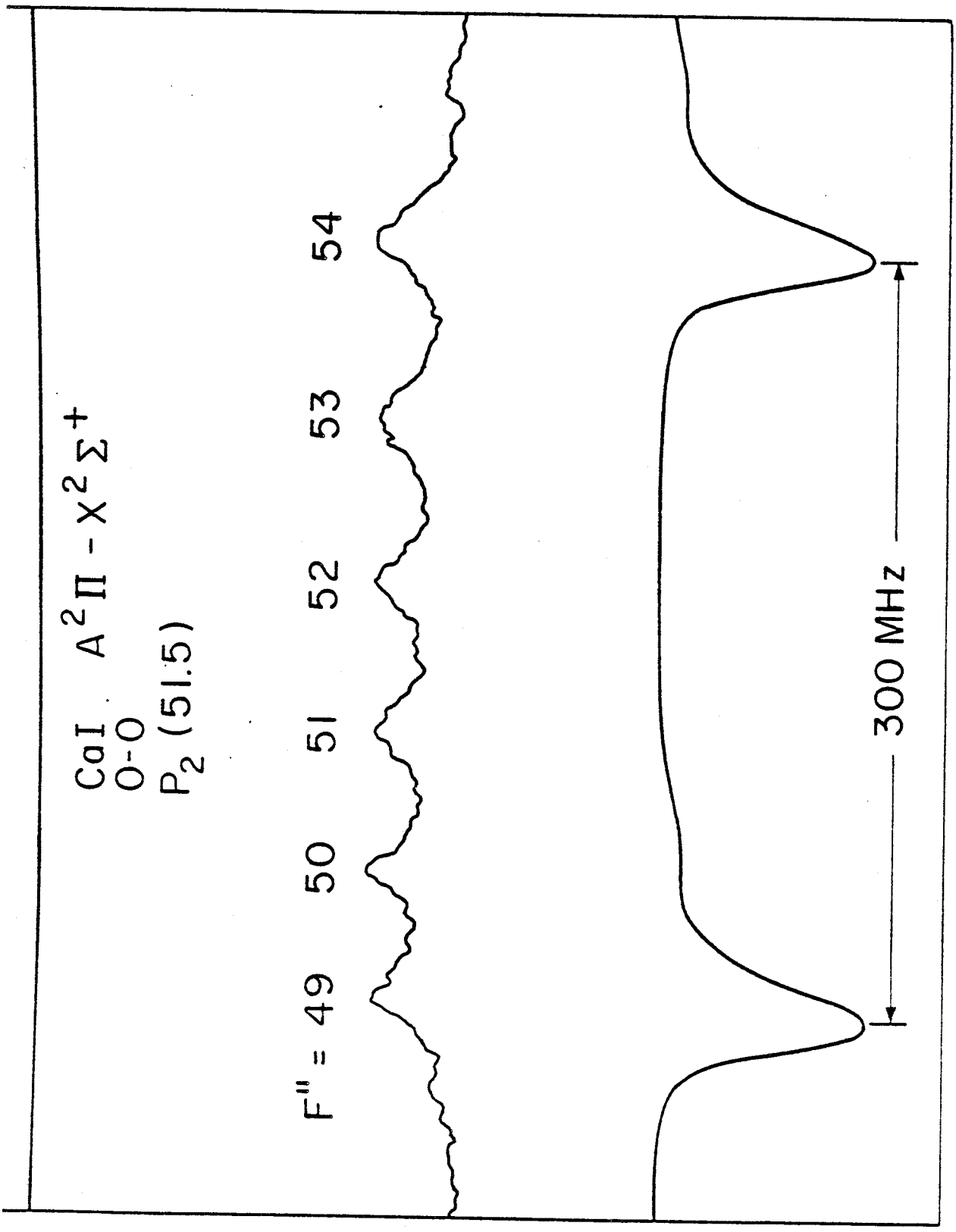


Figure 2. Intermodulated Fluorescence Spectrum of the CaI $A^2\Pi$-$X^2\Sigma^+$ 0-0 $P_2$ (51.5) line. The asymmetry produced by the quadrupole interaction is more evident than in Figure 1.

# Combined Fitting of Optical and Millimeter Wave Data: The Linked $A^2\Pi$-$X^2\Sigma^+$ and $B^2\Sigma^+$-$X^2\Sigma^+$ Systems of $Ca^{79}Br$ and $Ca^{81}Br$

P. F. Bernath[1], B. Pinchemel[2], and R. W. Field

Department of Chemistry and Spectroscopy Laboratory

Massachusetts Institute of Technology
Cambridge, Massachusetts 02139

and

K. Möller and T. Törring
Institut für Molekül Physik
Fachbereich Physik
Freie Universität Berlin
1000 Berlin 33, WEST GERMANY

5 Pages

2 Tables

0 Figures

In this note we illustrate the effects of combining, in a statistically rigorous procedure (1,2), two large and highly precise data sets from millimeter wave (3) and laser excitation spectroscopy (4). The former set consists of 40 lines, at 40 kHz accuracy ($1.3\times10^{-6}$ $cm^{-1}$), from the N~15 and N~50 regions of $X^2\Sigma^+$ v=0-2 for both $^{40}Ca^{79}Br$ and $^{40}Ca^{81}Br$; the latter, more than 2000 lines, at 0.003 $cm^{-1}$ accuracy, from the 0-0, 1-1, and 2-2 bands of the $B^2\Sigma^+$-$X^2\Sigma^+$ and 0-0 and 1-1 bands of the $A^2\Pi$-$X^2\Sigma^+$ electronic transitions for $0<N<117$ of both isotopic species.

Our reasons for illustrating what should by now be an obvious result are:

(1) The extent and precision of the optical data set are unusual. Inclusion of two linked electronic transitions with totally distinct branch structure would be expected to break correlations between upper and lower state parameters.

(2) The extent and precision of the millimeter wave data set are remarkable, but the transitions sampled do not span a continuous range of N-levels. Such disjoint sampling can lead to artifacts in fitted, high-order constants.

(3) A large number of small and highly correlated parameters are required to fit the energy levels of $^2\Pi$ and $^2\Sigma^+$ states, in marked contrast to the situation for $^1\Sigma$ states.

(4) Two useful internal consistency tests were available to us, isotope relations and predictions of lines in $\Delta v\neq0$ bands using rotational constants derived from $\Delta v=0$ bands.

Table 1 displays several correlations between parameters and the effects of adding first the A-X optical and then the X state mm-wave data to the B-X data set. It is well known that correlation between upper and lower

state parameters is the main difficulty in reducing electronic band spectra to molecular constants (2). Some of these correlations may be broken by fitting simultaneously two electronic transitions which share a common state. For instance, our fit to the 0-0 bands of the CaBr A-X and B-X systems reduced the correlation coefficient between spin-rotation constants ($\gamma$) for the B and X states from 0.999 (separate B-X fit) to 0.35 (combined fit). However, the ($B_0'$, $B_0''$), ($D_0'$, $D_0''$), and ($B_0''$, $D_0''$) correlation coefficients decrease only slightly. Introduction of the mm-wave data (with inverse-uncertainty-squared relative weighting) breaks the remaining upper state-lower state correlations: ($B_0'$, $B_0''$) and ($D_0'$, $D_0''$) both decrease to 0.02, but the ($B_0''$, $D_0''$) correlation within $X^2\Sigma^+$ increases from 0.79 to 0.989, which is identical to that found for the mm-wave data set alone. The failure of the optical data to reduce the ($B_0''$, $D_0''$) correlation reflects the $10^2$ greater sensitivity of $B_0''$ and $D_0''$ to the millimeter wave data. Because $D_0''$ is $2 \times 10^6$ smaller than $B_0''$, the large ($B_0''$, $B_0''$) correlation causes a larger error in the value of $D_0''$ than in $B_0''$.

The $B_0''$ values from mm-wave alone and combined B-X, A-X optical data differ by 6 times the standard deviation for the optical value. This is another example of the misleadingly small uncertainities that are often obtained when correlations are severe (5). The X state B, D, and $\gamma$ values obtained from mm-wave alone and from B-X, A-X, mm-wave combined data are identical, but with two to three times smaller uncertainties than those from the combined fit. This is simply a reflection of the larger number of degrees of freedom (data points) in the combined fit, despite the fact that each optical transition is weighted $10^{-6}$ as heavily as a mm-wave transition. The agreement between the mm-wave only and combined fits shows

that no artifacts result from the disjoint nature of the mm-wave data set. $B_0'$ and $D_0'$ constants for the $B^2\Sigma^+$ state are changed by 6σ when the mm-wave data are added to the A-X, B-X set, and these constants remain about 10 times less precisely determined than those of $X^2\Sigma^+$. Only part of the mm-wave precision is propagated into the upper states of the electronic transitions. Note that, as expected, ΔB changes by less than $6\times10^{-7}cm^{-1}$ for the three fits.

The effects of (B', B'') correlations in the optical data are manifest when rotational constants determined from fits to 0-0 and 1-1 bands were used in limited fits to a few high and low N lines of 1-0 and 0-1 bands. When lines were fitted by varying only the band origin, systematic residuals were observed. These residuals became random when, instead, fixed values of the rotational constants obtained from the combined mm-wave, optical fits were used.

Use of combined fit parameters also eliminated a systematic but trivial misassignment of the $Ca^{79}Br$ B-X 0-1 band $P_1$ branch near its band head. High and low N lines overlap to within their Doppler width near the head. These lines were resolved using intermodulated fluorescence spectroscopy (6), but the correct high vs. low N assignment of each high-N, low-N pair was not obvious. When the combined mm-wave, A-X, B-X constants were used, these line pairs could be unambiguously assigned and the residuals from N=27 to 66 were smaller than 0.001 $cm^{-1}$ in a fit with the band origin as the only variable parameter.

Satisfaction of the usual isotope relationships (7,8) between small parameters is the final, and perhaps most stringent test of the fits to various data sets. Table 2 gives the percentage agreement [(exp.ratio-calc.ratio)/calc. ratiox100)] between experimental and theoretical isotopic ratios. The agreement for the small parameters of the optical data fitted alone is rather poor, but

falls within the estimated experimental uncertainty. The addition of mm-wave data dramatically improves the agreement between experiment and theory. This implies that the combined optical-mm-wave fitted constants are superior estimates of the "true" molecular parameters.

Acknowledgments

P.F.B. was supported, in part, by a Natural Sciences and Engineering Research Council of Canada Postgraduate Scholarship. The MIT portion of this research was supported by the grants: AFOSR-76-3056, NSF CHE78-18427, CHE78-10178, and NATO 1177.

Footnotes

1. Present address: Herzberg Institute of Astrophysics, National Research Council of Canada, K1A 0R6, Ottawa, Ontario, CANADA.

2. Visiting scientist at MIT. Present address: Laboratoire de Spectroscopie des Molécules Diatomiques, E.R.A. 303, Université des Sciences et Techniques de Lille, Bât. P5, 59655 Villeneuve d'Ascq, FRANCE.

References

1. R. N. Zare, A. L. Schmeltekopf, W. J. Harrop, and D. L. Albritton, J. Mol. Spectrosc. 46, 37-66 (1973).

2. D. L. Albritton, A. L. Schmeltekopf, and R. N. Zare, "An Introduction to the Least-Squares Fitting of Spectroscopic Data," Modern Spectroscopy, Modern Research, vol. 2, p.1-67 (K. N. Rao, editor), Academic Press, New York, 1976.

3. K. Möller and T. Törring, unpublished.

4. P. F. Bernath, R. W. Field, B. Pinchemel, Y. Lefebvre, and J. Schamps, J. Mol. Spectrosc. (submitted).

5. D. L. Albritton, W. J. Harrop, A. L. Schmeltekopf, and R. N. Zare J. Mol. Spectrosc. 46, 103-118 (1973).

6. P. F. Bernath and B. Pinchemel, unpublished.

7. G. Herzberg, Spectra of Diatomic Molecules, Van Nostrand, New York, 1950.

8. J. M. Brown and J. K. G. Watson, J. Mol. Spectrosc. 65, 65-74 (1977).

| Data Set | $X^2\Sigma^+$ | | | $B^2\Sigma^+$ | | | | | $(B_0', B_0'')$ | $(D_0', D_0'')$ | $(B_0'', D_0'')$ | $(\gamma_0', \gamma_0'')$ | $(D_0'', \gamma_0'')$ | Degrees of Freedom | Variance |
|---|---|---|---|---|---|---|---|---|---|---|---|---|---|---|---|
| | $B_0'' \times 10^2$ | $D_0'' \times 10^8$ | $\gamma_0'' \times 10^3$ | $\nu_0$ | $B_0' \times 10^2$ | $D_0' \times 10^8$ | $\gamma_0' \times 10^2$ | $\gamma_{D_0}' \times 10^7$ | | | | | | | |
| mm-wave | 9.426 448 8(44) | 4.130 28(91) | 3.003 42(118) | --- | ---- | ---- | ---- | ---- | ---- | ---- | 0.989 | ---- | $0.8 \times 10^{-7}$ | 7 | 2.0 |
| $B^2\Sigma^+$-$X^2\Sigma^+$ only | 9.424 86(131) | 4.206(220) | 2.902(976) | 16 383.115(1) | 9.627 46(128) | 4.458(209) | -6.913 5(955) | 2.80(14) | 0.999 | 0.997 | 0.927 | 0.999 | -0.749 | 141 | 0.31 |
| $B^2\Sigma^+$-$X^2\Sigma^+$ and $A^2\Pi$-$X^2\Sigma^+$ | 9.424 36(33) | 3.971(30) | 3.024(11) | 16 383.108(1) | 9.627 01(33) | 4.241(33) | -6.900 5(39) | 2.72(14) | 0.978 | 0.882 | 0.793 | 0.352 | 0.109 | 613 | 0.32 |
| Combined A-X B-X, and mm-wave | 9.426 448 8(18) | 4.130 28(38) | 3.003 55(49) | 16 383.114(1) | 9.629 057(71) | 4.398(15) | -6.898 8(38) | 2.58(14) | 0.025 | 0.023 | 0.989 | 0.013 | -0.0004 | 623 | 0.34 |

Table I: Summary of parameter values and correlation coefficients for $Ca^{79}Br$ v'=v"=0

Table 2

$Ca^{81}Br/Ca^{79}Br$ Isotope Ratios for $B^2\Sigma^+$ and $X^2\Sigma^+$ States

| Parameter | Percentage Deviation from Theoretical Ratio | | |
|---|---|---|---|
| | mm-wave | A-X and B-X Optical Data | Combined Optical and mm-wave data |
| $B_e(X^2\Sigma^+)$ | | 0.014(10)% | -0.000068(106) |
| $B_e(B^2\Sigma^+)$ | | 0.016(10) | 0.0028(31) |
| $\alpha_e(X)$ | | -1.8(20) | -0.010(30) |
| $\alpha_e(B)$ | | -1.7(20) | 0.22(50) |
| $D_e(X)$ | | 2.4(15) | 0.013(17) |
| $D_e(B)$ | | 3.8(16) | 1.4(8) |
| $\gamma_e(X)$ [a] | | 0.17(67) | 0.041(58) |
| $\gamma_e(B)$ [a] | | -0.17(35) | -0.12(18) |
| $\gamma_D(B)$ | | -9.2(11) | -5.4(12) |

1σ uncertaintities are in parentheses.

a. Spin-rotation constant.

# COMPLEMENT AUX ARTICLES

# SUR CaBr et CaI (ARTICLES 7 ET 8)

Nous développerons dans ce complément les techniques expérimentales utilisées dans l'étude de CaBr et de CaI. Nous insisterons particulièrement sur la spectroscopie d'absorption saturée qui a permis d'étudier la structure hyperfine de ces molécules.

## I - SPECTROSCOPIE DE FLUORESCENCE INDUITE PAR LASER

Cette technique se rapproche de la spectroscopie classique dans la mesure où elle fait appel à un spectrographe comme appareil dispersif. La qualité des résultats est donc liée à celle du spectrographe et en particulier à son pouvoir de résolution.

Le principe est extrêmement simple puisqu'on se contente d'enregistrer la fluorescence issue d'un niveau rotationnel excité de la molécule, peuplé par absorption de la raie laser lorsque la fréquence de cette dernière correspond à une fréquence de résonance.

En pratique il n'est pas toujours possible de disposer d'une raie laser suffisamment fine pour n'exciter qu'une seule raie du spectre. Dans ce cas un nombre plus ou moins important de raies fluoresceront simultanément.

Cet inconvénient peut parfois se transformer en avantage, il est en effet possible de gagner beaucoup de temps en travaillant avec une raie large ($1cm^{-1}$) et en plaçant celle-ci sur une branche dont

les raies sont très serrées. On peut alors enregistrer en une seule fois la fluorescence d'un grand nombre de raies d'une même bande et extraire ainsi cette bande d'une structure vibrationnelle très complexe (voir par exemple la figure 2 de l'article 7 relatif à CaBr).

L'observation directe de la fluorescence est très utile car on peut observer l'évolution de cette fluorescence en balayant le spectre par la raie laser. On peut par exemple effectuer cette observation à l'aide d'une lunette placée à la sortie du spectrographe.

L'utilisation d'un étalon intra-cavité permet de réduire la largeur de la raie du laser à environ 0,03 $cm^{-1}$. Ceci permet d'exciter les raies du spectre une à une. Connaissant ainsi la position de la raie laser et les raies qui fluorescent à partir du niveau supérieur de la transition excitée par le laser, le calcul des relations de combinaison donne immédiatement la numérotation absolue des branches. Ceci d'autant plus facilement que l'on travaille au voisinage de l'origine, puisqu'aux basses valeurs de J, une variation d'une unité de la numérotation entraîne un changement très sensible dans le résultat donné par la relation de combinaison (figure C1).

Les limites de cette technique sont liées à la résolution du spectrographe, ainsi il n'a pas été possible par exemple, de résoudre le dédoublement $\gamma$ provenant de l'état inférieur de la transition $A^2\Pi - X^2\Sigma^+$ de CaBr.

## II - SPECTROSCOPIE D'EXCITATION

### A - Principe de la spectroscopie d'excitation.

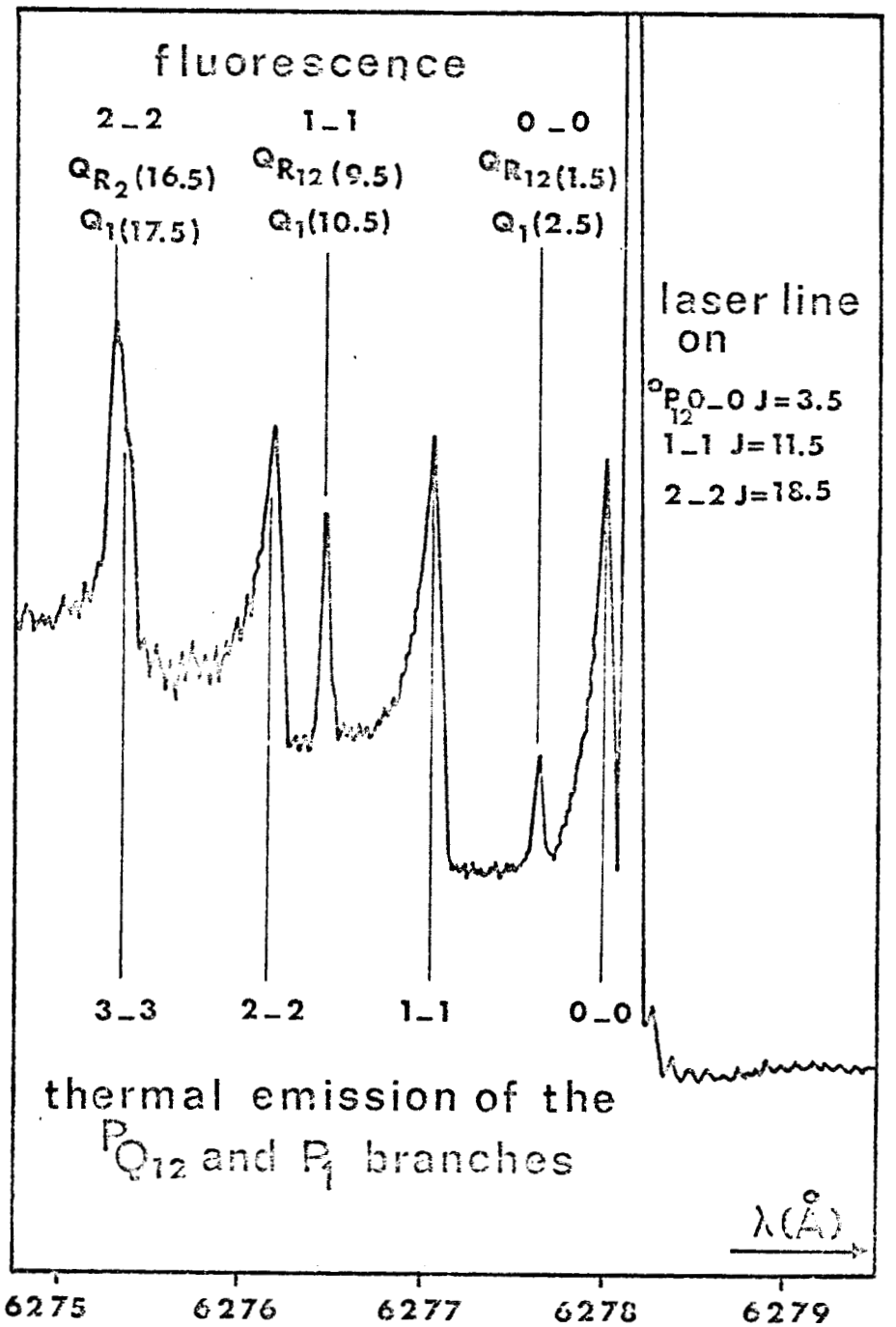


Fig C1 : spectre de fluorescence obtenu avec un étalon intracavité

(sous-système $A^2\Pi_{1/2} - X^2\Sigma^+$)

La mise au point des lasers continus monomodes, balayables en fréquence, a profondément modifié les techniques de la spectroscopie puisqu'ils ne nécessitent pas d'appareil dispersif performant.

En isolant un mode axial de la cavité laser et en faisant varier sa fréquence continûment, en modifiant la largeur de la cavité, on obtient une raie laser très étroite (1 MHz) pouvant balayer une zone de fréquence appréciable ($1cm^{-1}$).

L'excitation des molécules par la raie donne lieu à une fluorescence qui est localisée directement sur un photomultiplicateur sans passer par un spectrographe. On obtient ainsi un enregistrement de l'intensité de la fluorescence obtenue au cours du déplacement de la raie laser.

Comme à un instant donné, cette fluorescence est proportionnelle à l'intensité de la raie moléculaire excitée par la raie laser l'enregistrement obtenu reconstitue la partie du spectre balayée par la raie laser au cours de son déplacement en fréquence.

Il est bien sûr indispensable de ne travailler qu'avec un seul mode axial du laser pour éviter d'enregistrer les fluorescences provenant de deux ou plusieurs zones spectrales différentes.

Un spectre d'excitation est donc la reproduction fidèle du spectre d'émission avec bien sûr une résolution qui n'est limitée que par l'élargissement Doppler des raies.

## B : Dispositif expérimental utilisé pour l'étude de CaBr et CaI

Nous ne reviendrons pas sur les conditions de fonctionnement du laser ni sur la détection du signal qui sont décrits dans les articles 7 et 8.

1°) La source

Cette source, dite de Broida, est maintenant bien connue, elle a été décrite par Johnson (1) et elle a été utilisée avec succès pour l'étude de nombreuses molécules. West et al. (2) ont décrit les diverses modifications qui lui ont été apportées pour répondre à des conditions de travail diverses.

Rappelons brièvement les qualités. Elle permet d'obtenir des molécules à une température peu élevée donc dans un état d'excitation thermique bas. Elle crée une très bonne concentration des produits mis en réaction. De plus, elle favorise la formation des molécules diatomiques au détriment des composés polyatomiques et ne donne pas d'émission de raies atomiques. Enfin, elle est d'une grande stabilité puisqu'elle peut fonctionner plusieurs heures sans aucune variation des conditions de travail.

Le principe (figure C2) consiste à chauffer sous basse pression (1 torr environ) le métal intervenant dans la réaction et à faire transporter les vapeurs produites par un gaz porteur inerte (argon) dans la zone de réaction située au-dessus du brûleur par lequel arrive un oxydant gazeux ($CH_3Br$ dans le cas de CaBr). Une pompe primaire mécanique à deux étages permet de maintenir une pression constante dans l'enceinte.

2°) Utilisation du monochromateur (les deux figures citées sont celles de l'article 7)

Nous avons vu qu'un spectre d'excitation enregistré directement permet de reconstituer le spectre d'émission classique en améliorant fortement la résolution. Cependant les difficultés qui existent dans l'analyse d'un spectre par des techniques classiques ne sont pas toujours

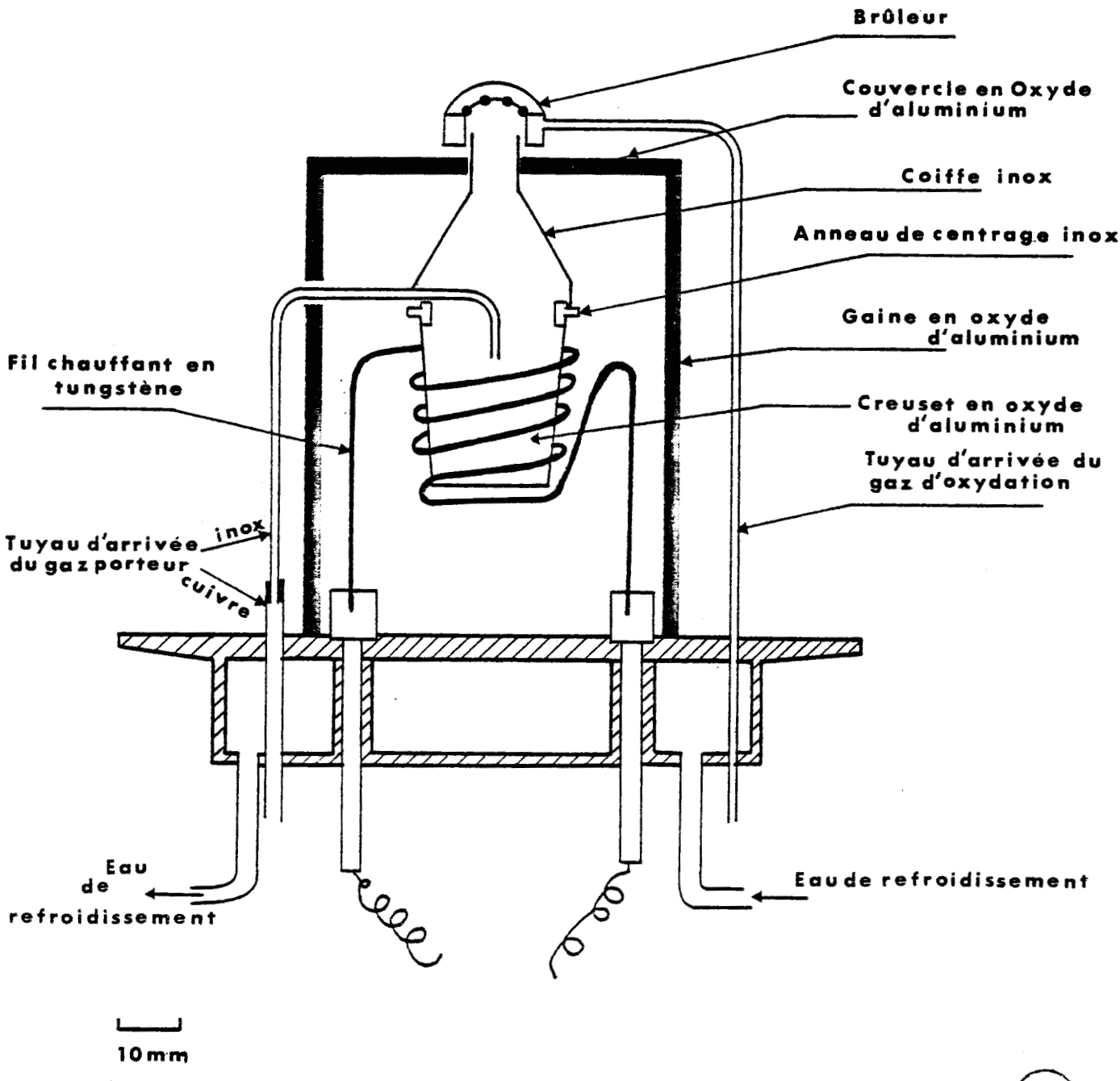




Figure $C_2$ : Schéma de principe de la source de Broida

éliminées, l'augmentation de la résolution ne supprimant pas les recouvrements entre les branches (trace n° 2 de la figure 1).

Le spectre de fluorescence de la figure 2 montre bien le parti que l'on peut tirer de l'utilisation d'un monochromateur utilisé comme filtre à bande passante étroite.

Sur cette figure les diverses branches qui fluorescent correspondent chacune à l'excitation par le laser de raies d'une des branches des bandes 0-0 et 1-1 superposées dans la région balayée par le laser. Sans même tenir compte des bandes provenant de niveaux de vibration supérieurs à 1, plus de douze branches sont excitées par le laser.

En sélectionnant, grace au monochromateur, une zone de fluorescence particulière, il est possible de ne reconstituer que les raies de la branche qui a donné lieu à la fluorescence sélectionnée. Par exemple en isolant avec le monochromateur les raies $R_{1ee}$ qui fluorescent dans la bande 0-0 on enregistrera les raies des branches $Q_{12ef}$ et $P_{1ee}$ qui ont donné lieu à cette fluorescence (puisque ces trois branches proviennent toutes d'un niveau supérieur de symétrie e). En plaçant le monochromateur "devant" une autre fluorescence $^{O}P_{12ff}$ par exemple on enregistrera les branches $Q_{1fe}$ et $^{Q}R_{12ff}$.

On reconstitue ainsi une par une, ou deux par deux éventuellement, toutes les branches qui, superposées dans la même région rendaient le spectre incompréhensible.

Comme on le voit sur la figure 2, les fluorescences sont plus ou moins étendues il est donc nécessaire de tenir compte pour régler l'ouverture de la fente du monochromateur de façon à ce que toutes les raies de fluorescence passent par la fente de sortie. Cette ouverture sera d'autant plus grande que la distance entre les raies qui fluorescent sera elle-même plus grande.

En pratique il n'est pas toujours possible ni utile d'isoler chaque branche : ce n'est pas possible lorsque, par exemple pour les faibles valeurs de J, les fluorescences des raies des branches de même nature des bandes 0-0 et 1-1 sont trop proches. De même dans les séquences principales nous n'avons jamais pu enregistrer séparément les deux isotopes. Ceci permet parfois de gagner du temps lorsqu'il n'y a pas d'ambigüité sur la nature des branches enregistrées simultanément. La trace n° 1 de la figure 1 donne un bon exemple d'un tel enregistrement. Le seul problème est alors le recouvrement fortuit des branches enregistrées.

La différence d'intensité entre les raies provenant de bandes différentes est parfois trompeuse car elle peut n'être due qu'à un meilleur centrage du monochromateur sur la fluorescence d'une bande au détriment de l'autre.

## III - DISPOSITIF EXPERIMENTAL UTILISE POUR LA SPECTROSCOPIE D'ABSORPTION SATUREE DE CaBr et CaI

Ce bref rappel qualitatif sur le principe de la technique d'absorption saturée ne se veut pas théorique ; l'étude théorique est complexe et a été exposée en détail par exemple par B. Couillaud et A. Ducasse (3). Il faut noter que notre analyse de la structure hyperfine ne nécessite que la connaissance aussi précise que possible de la position des raies. Nous n'attachons pas d'importance au profil de ces raies ni à leur intensité (4). De telles études nécessiteraient l'analyse de phénomènes tels que l'influence de la qualité et de la géométrie des faisceaux, l'élargissement par saturation, les inhomogéneités de saturation...

Dans nos expériences de spectroscopie d'absorption saturée, le faisceau laser est partagé en deux par une lame semi-réfléchissante

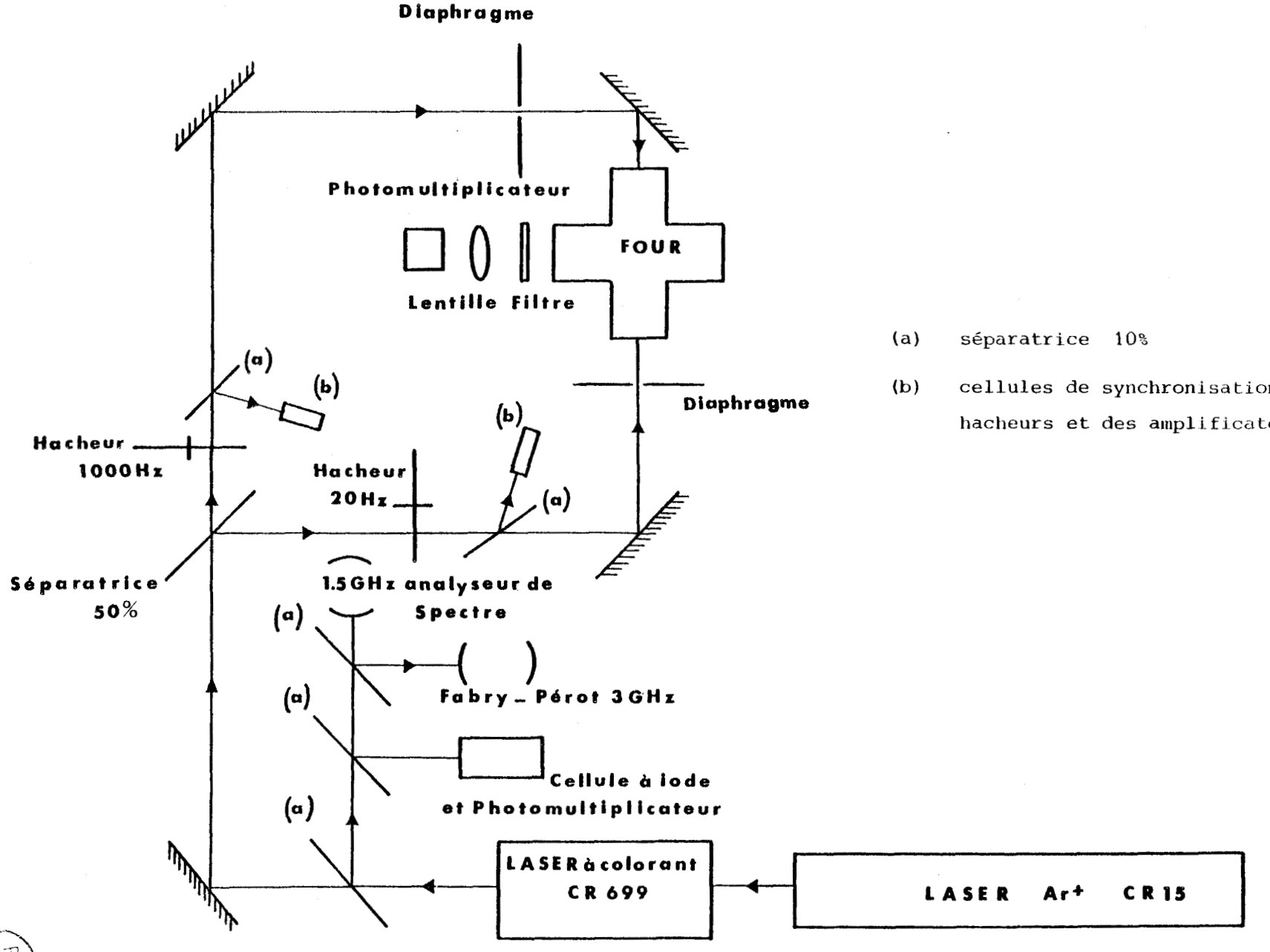


(a) séparatrice 10%

(b) cellules de synchronisation des hacheurs et des amplificateurs synchrones





Figure $C_3$ Dispositif expérimental utilisé pour les expériences de spectroscopie d'absorption saturée

(figure C3) et les deux faisceaux résultants pénètrent dans la source suivant une même direction, perpendiculaire à l'axe d'observation, mais en sens opposés. Pour mettre en évidence le phénomène d'absorption saturée on module mécaniquement l'un des deux faisceaux (que nous appelerons faisceau sonde) à une fréquence élevée (1000 Hz par exemple) et on détecte la fluorescence créée par ce faisceau au moyen d'un photomultiplicateur relié à un amplificateur synchrone.

Supposons que la fréquence de la raie laser corresponde à la fréquence de l'aile du profil d'une raie du spectre moléculaire étudié, on observe un signal en tous points semblable à celui d'un spectre d'excitation classique (paragraphe II de ce complément). Le second faisceau laser (faisceau saturant) n'influe **pas** sur les molécules touchées par le faisceau sonde puisqu'il est "vu" par ces molécules à une autre fréquence du fait même de l'effet Doppler. Ce faisceau saturant excite les molécules se déplaçant dans une direction symétrique de la direction des molécules touchées par le faisceau sonde, par rapport au plan perpendiculaire aux deux faisceaux laser. Mais la fluorescence qui en résulte n'est pas détectée puisqu'elle est produite par le faisceau saturant qui n'est pas modulé à 1 000 Hz. Lorsque la fréquence de la raie laser atteint le maximum de la raie moléculaire, qui correspond à l'excitation des molécules se déplaçant suivant l'axe d'observation, il y a résonance puisque la même molécule peut être excitée par les deux faisceaux laser.

Le nombre de molécules succeptibles d'être excitées par le faisceau sonde diminue brusquement puisqu'un certain nombre d'entre elles sont excitées par le faisceau saturant. Ceci se traduit sur l'enregistrement par un creux très étroit correspondant à la largeur

de la raie en l'absence d'effet Doppler. Il ne s'agit pas en fait exactement de la largeur naturelle de la raie car il est impossible de travailler avec deux faisceaux parfaitement colinéaires sans renvoyer le rayonnement dans le laser ce qui entraînerait une perturbation dans le fonctionnement monomode de ce dernier. Il est donc nécessaire de créer un léger angle (inférieur à un degré) entre les deux faisceaux ce qui laisse subsister un très faible élargissement Doppler. De plus, il se produit généralement un élargissement dû à la pression régnant dans la source et à la puissance du rayonnement et du laser (élargissement par saturation).

Pour éliminer les ailes du profil Doppler on module le faisceau saturant à une fréquence assez basse (20 Hz par exemple). Ceci se traduit par une modulation de l'amplitude du signal provenant du faisceau-sonde puisqu'en effet l'absorption saturée ne peut se produire que pendant la demi-période de passage du faisceau saturant. On envoie le signal de sortie du premier amplificateur synchrone sur un second calé sur la fréquence de modulation du faisceau saturant.

Rappelons que nous enregistrons uniquement le signal créé par le faisceau sonde modulé à 1 000 Hz. Si l'on se trouve hors de la résonance des deux faisceaux, c'est à dire dans l'aile d'une raie, il ne se passe rien puisque le signal modulé à 1 000 Hz, qui est détecté par le premier amplificateur synchrone, est éliminé par le second, l'aile de la raie est donc assimilable à un bruit et ne peut être enregistrée.

Au maximum de la raie l'amplitude du phénomène d'absorption saturée est modulée à 20 Hz, à la sortie du 1er amplificateur on obtient donc un signal modulé à 20 Hz qui est détecté et amplifié par la seconde détection synchrone.

Ce type de détection suppose un choix approprié des constantes de temps des deux amplificateurs, il faut en particulier que le premier amplificateur synchrone puisse effectuer au moins quelques intégrations pendant la demi-période de passage du faisceau saturant. Avec le choix fait pour les fréquences (1 000 Hz pour le faisceau sonde et 20 Hz pour le faisceau saturant) la constante de temps du premier amplificateur doit être de l'ordre de 5 ms ce qui donne effectivement quatre ou cinq intégrations complètes par demi-périodes (0,025s) de passage du faisceau saturant. La constante de temps du second amplificateur synchrone est nettement plus longue, elle dépend principalement de la vitesse de défilement de la fréquence du laser, elle sera de l'ordre de 0,3s pour un défilement rapide et pourra être de 1s pour un défilement lent.

En effet, la résolution dépend beaucoup de la vitesse du défilement de la fréquence de la raie laser. Les figures C4 et C5 donnent deux exemples d'enregistrement de raies de CaBr par spectroscopie d'absorption saturée. Le premier éffectué rapidement ne donne que peu d'information supplémentaire par rapport au spectre d'excitation puisqu'un profil, résultant de la composition de deux raies, large de 0,04 $cm^{-1}$ est assez mal résolu. La figure C5 enregistrée à une vitesse dix fois plus lente montre que des profils de largeur inférieure à 0,02 $cm^{-1}$ sont parfaitement résolus, on observe même assez distinctement les quatre composantes de la structure hyperfine de chaque raie. Enfin les figures de l'article 8 montrent deux exemples caractéristiques de la résolution obtenue en réduisant encore la vitesse de défilement de la longueur d'onde du laser. Il faut cependant noter que le bruit est assez important ; il est dû principalement aux fluctuations du laser et à la lumière parasite provenant de réflexions de la lumière du

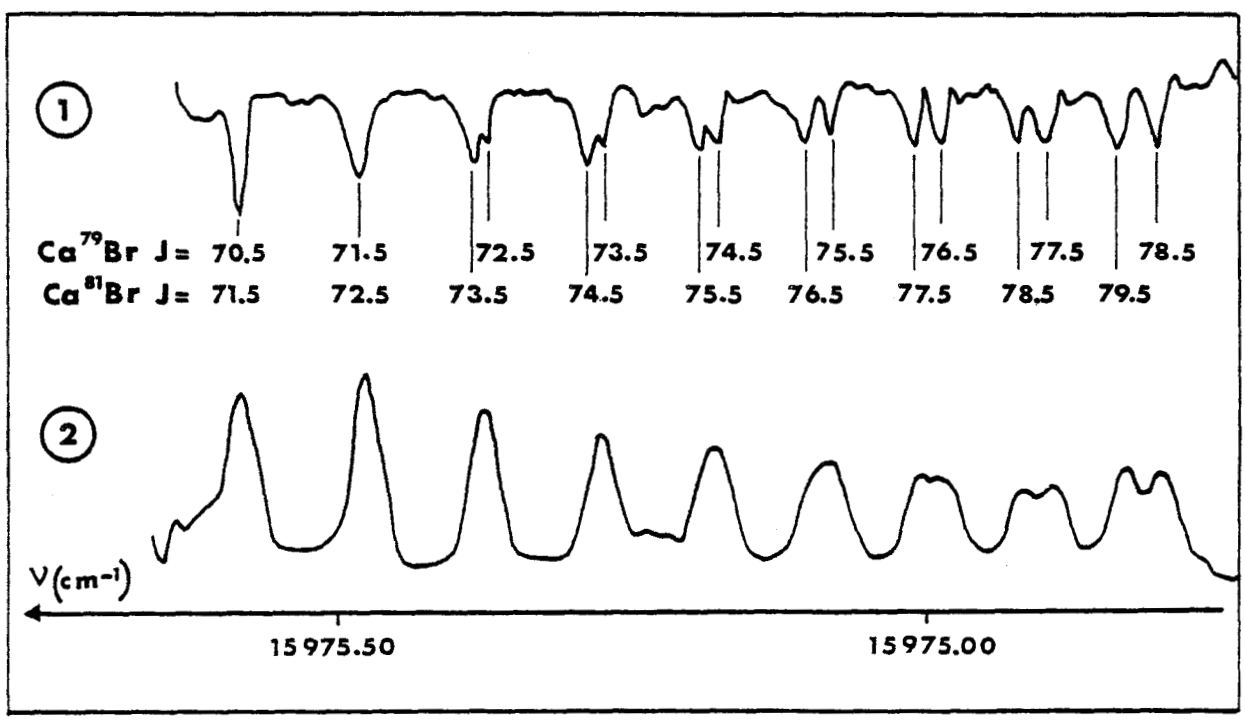


Figure $C_4$ : exemple d'enregistrement rapide d'un spectre d'absorption saturée
CaBr $A^2\Pi_{3/2} - X^2\Sigma^+$ bande O-O branche $P_{2ff}$
trace 1 : spectre d'absorption saturée
trace 2 : spectre d'excitation

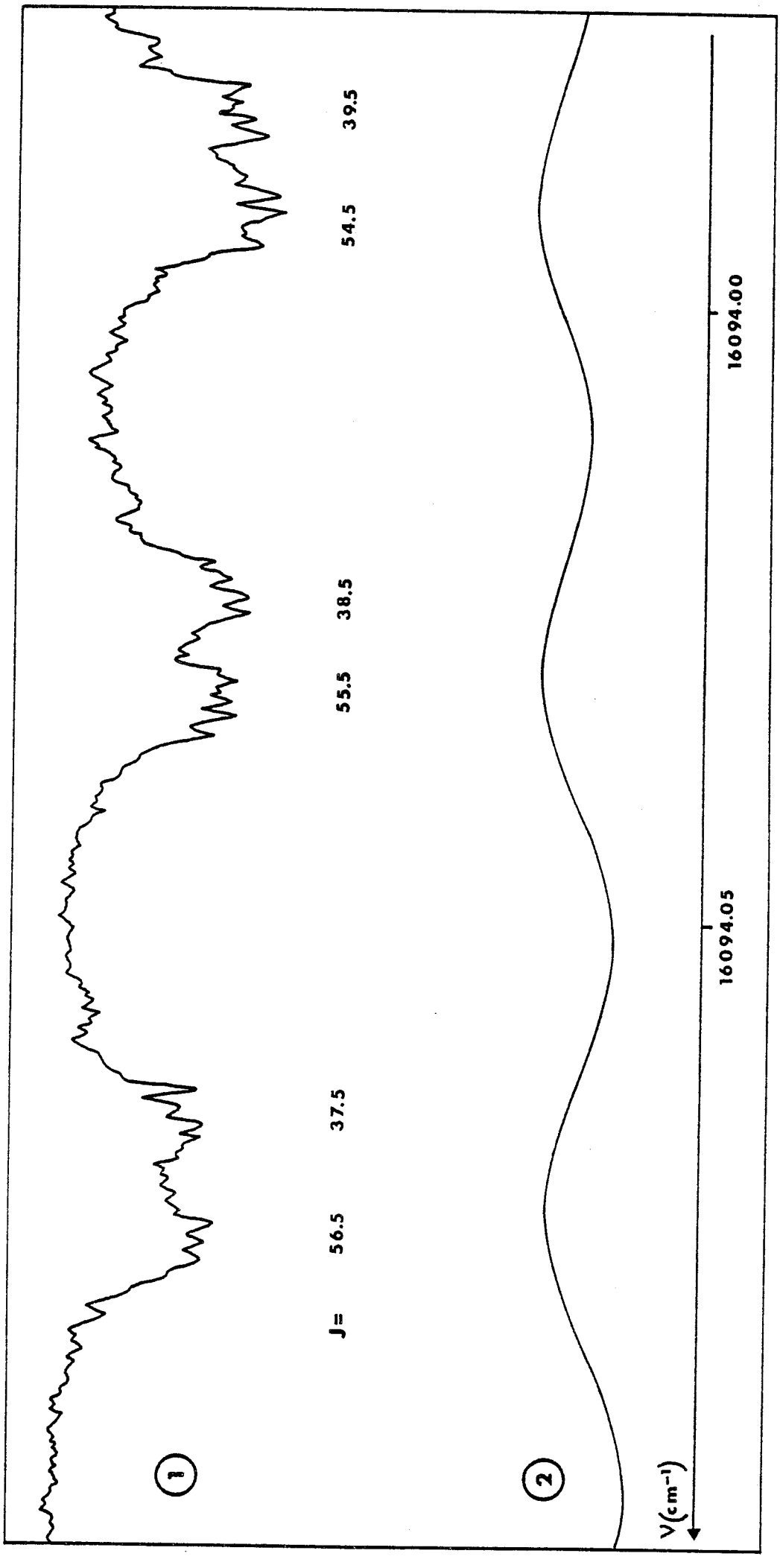


Figure $C_5$ : CaBr transition $B^2\Sigma^+ - X^2\Sigma^+$ bande 0-1 branche $P_1$

trace 1 : spectre d'absorption saturée

trace 2 : spectre d'excitation

laser sur des particules solides émises par le four. Il a été nécessaire d'enregistrer deux fois chaque raie et de prendre la moyenne des mesures pour réduire les erreurs dues à ce bruit.

Il aurait été intéressant de réaliser des spectres d'absorption saturée en passant par le monochromateur pour nous affranchir des recouvrements entre les raies, en particulier pour des basses valeurs de J.

Nous avons constaté en essayant cette technique une augmentation très sensible du bruit rendant inexploitables les enregistrements; nous n'avons pas été capables d'éliminer ce bruit qui pourrait provenir des vibrations de la source créées par la pompe mécanique.

## IV - COMPLEMENT A L'ARTICLE 8

L'article 8 relatif à la structure hyperfine de CaBr et de CaI ne donne que très peu d'explications sur les calculs utilisés pour la détermination des constantes de structure hyperfine. Nous allons détailler ici un exemple qui montrera en outre comment se traduit dans chaque état l'effet des paramètres sur les niveaux hyperfins.

Nous prendrons l'exemple de la raie J = 5,5 de la branche $P_{12ff}$ de la transition $A^2\Pi_{1/2} - X^2\Sigma^+$ de $Ca^{79}Br$. Cette transition est en effet plus intéressante que la transition $B^2\Sigma^+ - X^2\Sigma^+$ car la structure de l'état supérieur provient essentiellement du moment quadripolaire électrique alors que c'est la structure hyperfine d'origine magnétique qui domine dans l'état fondamental puisqu'il provient de la configuration

$$4s^{}_{Ca^+}(\sigma) + 4p^6_{Br^-}(\pi^4\sigma^2)$$

Rappelons que nous avons utilisé dans cet article les notations de Frosch et Foley (5) et de Townes et Schawlow (6). La forme du

hamiltonien d'interaction magnétique pour une molécule diatomique

est $H = a\,\Lambda I.k + b\ I.S + c\ (I.k)\ (S.k)$

où I est le spin nucléaire ($I = \frac{3}{2}$ pour le brome)

$\Lambda$ est le moment angulaire orbital électronique

k est le vecteur unitaire sur l'axe intermoléculaire

S est le spin électronique

Nous savons que, pour un état $^2\Sigma^+$ $\Lambda$ est nul ; d'autre part la configuration dominante de caractère $4s\sigma$ pour l'état fondamental de CaBr rend nul le paramètre c pour des raisons de symétrie de la distribution électronique des charges. Seul le terme bI.S subsiste.

Il représente le terme de contact de Fermi. Dans l'état fondamental la valeur de la constante de couplage spin-rotation est faible $\gamma = 0{,}003\ cm^{-1}$ (90 MHz), il est donc nécessaire, surtout aux basses valeurs de N, de tenir compte des termes non diagonaux en J du hamiltonien b I.S qui couplent les niveaux $e(N=J-\frac{1}{2})$ et $f(N=J+\frac{1}{2})$. Nous nous plaçons dans la base du cas $b_{\beta J}$ de Hund et nous négligeons les interactions entre niveaux correspondant à des valeurs de N différentes puisque la séparation entre niveaux de rotation est grande devant les effets hyperfins.

Rappelons ces éléments de matrice en les réduisant à la partie qui nous intéresse.

$$\langle N, \begin{matrix} e \\ f \end{matrix} \mid b\ I.S \mid N, \begin{matrix} e \\ f \end{matrix} \rangle = \pm \frac{bC}{2(2N+1)}$$

avec $C = F(F+1) - I(I+1) - J(J+1)$

$$\langle N, \begin{matrix} e \\ f \end{matrix} \mid b\ I.S \mid N, \begin{matrix} f \\ e \end{matrix} \rangle = \frac{b\,E}{2(2N+1)}$$

avec $E = \left[ (F+N-I+\frac{1}{2})\ (F+I-K+\frac{1}{2})\ (F+K+I+\frac{3}{2})\ (K+I-F+\frac{1}{2}) \right]^{1/2}$

F étant le moment angulaire orbital total incluant le spin nucléaire.

Si dans nos calculs nous avons utilisé une méthode de moindre carré non linéaire pour calculer les paramètres, nous utiliserons ici la méthode de perturbation du second ordre qui traduit assez correctement le spectre expérimental même aux faibles valeurs de N.

Nos calculs ont donné b = 90 MHz. Par rapport à la position de la raie en l'absence de structure hyperfine les niveaux sont décalés des valeurs suivantes lorsqu'on ne tient compte que des termes diagonaux :

| niveaux f(N=6, J=5,5) | | niveaux e(N=6, J=6,5) | |
|---|---|---|---|
| F=4 | 67,5 MHz | F=5 | -77,8 MHz |
| F=5 | 32,9 MHz | F=6 | -36,3 MHz |
| F=6 | - 8,7 MHz | F=7 | 12,1 MHz |
| F=7 | -57,1 MHz | F=8 | 67,5 MHz |

Les termes non diagonaux déplacent les niveaux f des quantités suivantes :

| | |
|---|---|
| F=4 | 0 MHz |
| F=5 | -10,6 MHz |
| F=6 | -14,2 MHz |
| F=7 | -10,5 MHz |

Dans l'état supérieur $^2\Pi_{1/2}$ la configuration dominante $4p_{Ca^+}(\pi) + 4p^6_{Br^-}(\pi^4\sigma^2)$ favorise la structure hyperfine d'origine quadripolaire électrique.

L'énergie correspondante est donnée par la relation

$$W_Q = \frac{eqQ\left[3\frac{\Omega^2}{J(J+1)} - 1\right]}{2I(2I-1)(2J-1)(2J+3)}\left[\frac{3}{4}C(C+1) - I(I+1)J(J+1)\right]$$

e est la charge du proton

Q est le moment quadripolaire nucléaire

$q = \left(\frac{\partial^2 V}{\partial z^2}\right)_{moy.}$ est le gradient du champ électrique produit par les électrons suivant l'axe internucléaire.

$\Omega$ est la projection sur l'axe internucléaire du moment angulaire total $\vec{J}$ ($\frac{1}{2}$ pour l'état $^2\Pi_{1/2}$)

Avec la valeur trouvée pour eqQ = 31 MHz les niveaux d'énergie hyperfins se trouvent déplacés de la façon suivante par rapport au niveau de rotation J=4,5 obtenu en l'absence de structure hyperfine :

| | |
|---|---|
| F=3 | -5,2 MHz |
| F=4 | +2,3 MHz |
| F=5 | +4,5 MHz |
| F=6 | -2,7 MHz |

La figure C6 regroupe tous ces résultats et permet de calculer les écarts entre deux raies consécutives de la structure hyperfine et de faire la comparaison avec les mesures expérimentales:

nous obtenons ainsi

| | écart calculé | écart mesuré |
|---|---|---|
| raies F"=4 et F"=5 | 53 MHz | 50 MHz |
| raies F"=5 et F"=6 | 47 MHz | 48 MHz |
| raies F"=6 et F"=7 | 37 MHz | 31 MHz |

Notre calcul traduit donc bien le spectre expérimental malgré l'imprécision qu'entraîne l'utilisation de la méthode des perturbations du second ordre aux basses valeurs de J. On constate bien que l'évolution entre les écarts provient de l'état supérieur de la transition et donc de l'interaction quadripolaire électrique puisque en son absence les valeurs des écarts seraient pratiquement identiques entre elles comme le montre la figure C6.

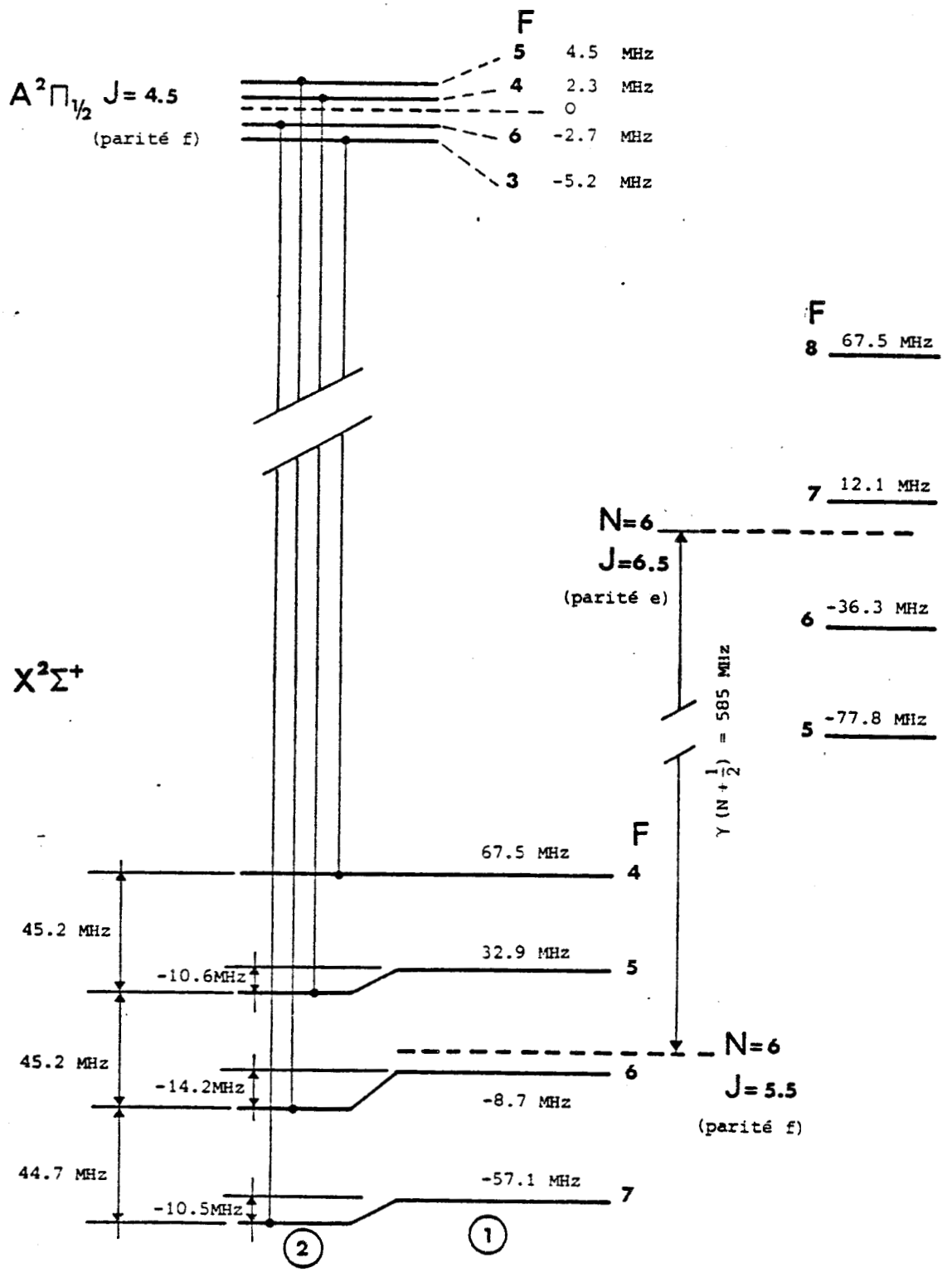


(1) positions des raies données par les termes diagonaux de la matrice

(2) décalage apporté par les termes non diagonaux de la matrice



Figure C6 : Position des niveaux d'énergie hyperfins correspondant à la transition entre les niveaux de rotation v'=0, J'=4,5 de l'état A $^2\Pi_{1/2}$ et v"=0, N"=6, J"=5,5 de l'état X $^2\Sigma^+$ de Ca $^{79}$Br.

# BIBLIOGRAPHIE

1 - S.E. Johnson J. Chem Phys 56, 149 (1972)

2 - J.B. West, R.S. Bradford Jr., J.D. Eversole et C.R. Jones, Rev. Sci. Instrum. 46, 164 (1975)

3 - B. Couillaud et A. Ducasse Thèse de doctorat Bordeaux (1978)

4 - J. Bordé et Ch. J. Bordé J. Mol. Spectrosc. 78 353 (1979)

5 - R.A. Frosch et H.M. Foley, Phys Rev 88 1337 (1952)

6 - C.H. Townes et A.L. Schawlow, Modern Spectroscopy Dover Publications New-York (1975)

# CONCLUSION

Notre étude permet de tirer un certain nombre d'enseignements et de perspectives dans le domaine de la spectroscopie moléculaire diatomique.

Sur le plan expérimental, il nous semble prématuré de reléguer les techniques de spectroscopie classique en prenant pretexte de l'apparition des lasers à colorant continus monomodes. Dans de nombreux cas, à condition d'utiliser une source bien adaptée au problème, ces méthodes, peu onéreuses sur le plan du matériel, donnent rapidement des spectres de très bonne qualité. En effet malgré les progrès spectaculaires des techniques lasers, et en particulier des colorants, certaines régions spectrales sont encore difficiles d'accès et supposent l'utilisation de lasers ioniques de grande puissance pour pomper les colorants correspondants.

Il nous parait raisonnable de réserver l'usage du laser aux cas particuliers des structures très complexes. Dans de telles situations, il se révèle être un instrument incomparable pour clarifier des spectres très confus.

Les lasers continus monomodes doivent nous permettre d'aborder des domaines nouveaux, la double excitation ou la spectroscopie d'absorption saturée par exemple ou même les réactions chimiques assistées par laser. Cependant ces études nécessiteront toujours une bonne connaissance des structures électroniques, vibrationnelles et rotationnelles des molécules, qui sera obtenue, le cas échéant, par des moyens plus classiques (nous incluons dans ces moyens la spectroscopie d'excitation).

Des molécules comme CuO ou les halogénures de calcium qui possèdent des spectres intenses dans la région voisine de 6000 Å se prêtent bien à de telles expériences même avec des lasers de

faible puissance. Dans ce sens notre travail nous donne une excellente base de départ pour aborder de nouveaux domaines d'étude.

En parallèle la spectroscopie d'absorption saturée, encore peu utilisée jusqu'à présent en spectroscopie des molécules diatomiques (si on fait exception de l'iode) ouvre un certain nombre de perspectives. Associées à des études théoriques elles permettront de compléter les connaissances sur ce type de molécules. Ainsi nous avons vu qu'il existe des liens très étroits entre la structure hyperfine et la structure électronique moléculaire.

Il est intéressant aussi de noter l'apport que présente la confrontation des résultats obtenus par différentes techniques développées par des équipes travaillant dans des domaines spectraux très éloignés; l'exemple de CaBr est instructif à cet égard.

Sur le plan théorique, un gros travail reste à faire pour obtenir une vue d'ensemble précise et détaillée des lois qui régissent la liaison chimique dans les composés d'éléments de transition. Nous connaissons maintenant bien deux composés de haute multiplicité : MnO et FeF ; CuO fait actuellement l'objet d'une étude détaillée; enfin CuF, NiF et TiO seront très prochainement abordés par notre équipe.

# TABLE DES MATIERES